Contributions to the Neoproterozoic Geobiology

Bing Shen

Dissertation submitted to the faculty of the Virginia Polytechnic Institute and State University in partial fulfillment of the requirements for the degree of

Doctor of Philosophy
In
Department of Geosciences

Shuhai Xiao (Chair)
Robert Bodnar
Michal Kowalewski
J. Fred Read

November 29, 2007
Blacksburg, Virginia

Key words: Neoproterozoic, Ediacaran, Ediacara fossils, China, Disparity, Sulfur isotope, Carbon isotope

Copyright 2007, Bing Shen

Contributions to the Neoproterozoic Geobiology

Bing Shen

Abstract

This thesis makes several contributions to improve our understanding of the Neoproterozoic Paleobiology. In chapter 1, a comprehensive quantitative analysis of the Ediacara fossils indicates that the oldest Ediacara assemblage—the Avalon assemblage—already encompassed the full range of Ediacara morphospace. A comparable morphospace range was occupied by the subsequent White Sea and Nama assemblages, although it was populated differently. In contrast, taxonomic richness increased in the White Sea assemblage and declined in the Nama assemblage. The Avalon morphospace expansion mirrors the Cambrian explosion, and both may reflect similar underlying mechanisms.

Chapter 2 describes problematic macrofossils collected from the Neoproterozoic slate of the upper Zhengmuguan Formation in North China and sandstone of the Zhoujieshan Formation in Chaidam. Some of these fossils were previously interpreted as animal traces. Our study of these fossils recognizes four genera and five species. None of these taxa can be interpreted as animal traces. Instead, they are problematic body fossils of unresolved phylogenetic affinities.

Chapter 3 reports stable isotopes of the Zhamoketi cap dolostone atop the Tereeken diamictite in the Quruqtagh area, eastern Chinese Tianshan. Our new data indicate that carbonate associated sulfate (CAS) abundance decreases rapidly in the basal cap dolostone and $\delta^{34}S_{CAS}$ composition varies between +9‰ and +15‰ in the lower 2.5 m. In the overlying interval, CAS abundance remains low while $\delta^{34}S_{CAS}$ rises ~5‰ and varies more widely between +10‰ and +21‰. $\delta^{34}S_{py}$ is typically greater than $\delta^{34}S_{CAS}$ measured from the same samples. We propose that CAS and pyrite were derived from two isotopically distinct reservoirs in a chemically stratified basin.

Chapter 4 studies $\delta^{13}C$, $\delta^{18}O$, $\delta^{34}S_{CAS}$, and $\delta^{34}S_{py}$ of the Zhoujieshan cap carbonate that overlies the Ediacaran Hongtiegou glaciation. The Zhoujieshan cap dolostone shows positive $\delta^{13}C$ values (0 –1.7‰). $\delta^{34}S_{CAS}$ shows rapid stratigraphic variations from +13.9 to +24.1‰, probably due to relatively low oceanic sulfate concentrations. $\delta^{34}S_{py}$ shows a steady stratigraphic trend. Thus, the $\delta^{34}S_{CAS}$ and $\delta^{34}S_{py}$ trends are decoupled from each other. The decoupling of $\delta^{34}S_{CAS}$ and $\delta^{34}S_{py}$ trends suggests that CAS and pyrite were derived from different sulfur pools, which were probably due to the postglacial basin stratification.

Acknowledgments

This work would not have been possible without the efforts and dedication of my advisor, Shuhai Xiao. I thank Shuhai for introducing me to this fascinating field of Neoproterozoic geobiology, spending numerous hours discussing fossils, geochemistry, and various other questions with me, and being patient in correcting my naïve grammatical errors. Many thanks to my committee members: Bob Bodnar, Michal Kowalewski, and J. Fred Read, for providing continuous support and inspiration.

I also thank Juan Liu and Nizhou Han and Kathleen McFadden for helping me with geochemistry laboratory experiments. Clayton Loehn, James Schiffbauer, and Viktoras Liogys helped me in sample preparation, scanning electron microscopy, and elemental mapping. Rich Krause, John Huntley, Ying Zhang, and Zhengrong Li provided valuable suggestions in writing SAS codes. Susan Barbour Wood, Jen Stempien, Peter Voice, Matthew Bychowski, Troy Dexter, Yurena Yanes, Jing Zhao, Fang Lin, and many other fellow graduate students, have always been helpful whenever I need their expertise.

I would also like to thank Chuanming Zhou, Xunlai Yuan, Guoxiang Li, Zhe Chen, Yaosong Xue, Leiming Yin, Jinlong Wang, Jie Hu, Guwei Xie, and Fanwei Meng, from Nanjing Institute of Geology and Palaeontology, Yunshan Wang from Geological Survey of Qinghai Province, Luyi Zhang from Xi'an Institute of Geology They assisted me in my field work in China and made my trips much more enjoyable. My data collection would not have gone as smoothly without their help.

I want to thank my parents for their love, understanding, and morale support for such a long time. Finally, special thanks to my wife, Lin Dong, for her useful comments, discussions, arguments, and suggestions on my research, and for all of her love and support in the past four years.

TABLE OF CONTENTS

Abstract ……..ii
Table of Contents ……..iii
List of Figures ……...vi
List of Tables ……..viii
Introduction and Overview of the Research ……ix
Acknowledgements ……xvi
Chapter 1
The Avalon Explosion: Evolution of Ediacara Morphospace
Abstract ……1
1. Introduction ……1
2. Materials and Methods ……2
2.1. Data Acquisition ……..……3
2.1.1. Morphological data ……...….3
2.1.2. Abundance and preservational quality ……...5
2.2. Data Analysis……6
2.2.1. Taxonomic diversity ……...6
2.2.2. Morphological analysis ……...7
2.3. Potential Bias ……10
2.3.1. Temporal resolution ……10
2.3.2. Spatial resolution ……10
2.3.3. Paleogeographic map ……...11
3. Discussion ……11
4. Conclusions ……...14
References ……..15
Chapter 2
Problematic Macrofossils from Ediacaran Successions in the North China and Chaidam Blocks: Implications for Their Evolutionary Roots and Biostratigraphic Significance ……34
Abstract ……..34
1. Introduction ……...34
2. Geological Settings ……...36
2.1. Suyukou Section ……36
2.2. Quanjishan Section ……37
2.3. Interpretation and Correlation of Diamictite ……...38
3. Systematic Paleontology ……...39
Genus HELANOICHNUS Yang *in* Yang and Zheng, 1985 ……39
Genus HORODYSKIA Yochelson and Fedonkin, 2000 ……42

Genus PALAEOPASCICHNUS Palij, 1976 ……44
Genus SHAANXILITHES Xing, Yue, and Zhang *in* Xing et al., 1984...49
4. Taphonomy ……...52
5. Interpretations and Affinities ……53
5.1. *Helanoichnus helanensis* ……..……...53
5.2. *Horodyskia* ……...53
5.3. *Palaeopascichnus* ……..54
5.4. *Shaanxilithes* ……55
6. Implications for Regional Correlation ……..56
7. Conclusions ……...57
References ……..57
Chapter 3
Stratification and Mixing of a Post-glacial Neoproterozoic Ocean: Evidence from Carbon and Sulfur Isotopes in a Cap Dolostone from Northwest China ……82
Abstract ……..82
1. Introduction ……...83
2. Geological Background ……84
3. Methods ……86
3.1. Carbon and Oxygen Isotopes ……...86
3.2. Sulfur Isotopes ……..87
3.3. Elemental Geochemistry ……88
4. Results ……...89
4.1. Carbon and Oxygen Isotopes ……...89
4.2. Sulfur Isotopes ……..89
4.3. Elemental Geochemistry ……90
5. Validity of CAS Concentration, $\delta^{34}S_{CAS}$, and $\delta^{34}S_{py}$ Data ……90
5.1. Pyrite oxidation during laboratory preparation or outcrop weathering ……90
5.2. Diagenetic alteration of CAS concentration and $\delta^{34}S_{CAS}$ ……...91
5.3. Using $\delta^{34}S_{CAS}$ as a proxy for seawater sulfate ……92
5.4. Evaluation of $\delta^{34}S_{py}$ values ……..93
6. Implications for Sulfur Cycling in the Quruqtagh Basin ……..94
6.1. Oceanic stratification model ……95
6.2. Sulfate minimum zone model ……..99
7. Conclusions ……100
References ……101
Chapter 4

The Neoproterozoic Quanji Group in the Chaidam Basin, carbon and sulfur isotopes of a cap carbonate associated with an Ediacaran glaciation ……..124
Abstract ……124
1. Introduction ……125
2. Regional Geology ……...126
3. Litho- and Biostratigraphy of the Quanji Group ……126
3.1. The Mahuanggou Formation ……..127
3.2. The Kubaimu Formation ……...127
3.3. The Shiyingliang Formation ……..128
3.4. The Hongzaoshan Formation ……128
3.5. The Heitupo Formation ……129
3.6. The Hongtiegou Formation ……129
3.7. The Zhoujieshan Formation ……...130
4. Methods ……...130
4.1. Carbon and Oxygen Isotopes ……131
4.2. Sulfur Isotopes ……131
4.3. Elemental Geochemistry ……...133
5. Results ……133
5.1. $\delta^{13}C$ and $\delta^{18}O$ ……..133
5.2. $\delta^{34}S_{CAS}$ and $\delta^{34}S_{py}$ **……...134**
5.3. Elemental Geochemistry ……...134
6. Discussions ……134
6.1. Diagenetic alteration of $\delta^{13}C$ values ……134
6.2. Fidelity of sulfur isotope signatures ……135
6.3. Age of the Hongtiegou Glaciation ……..136
6.4. Geochemical Cycle after the Hongtiegou Glaciation ……..138
6.4.1. Interpretation of $\delta^{13}C$ in the Zhoujieshan Cap Dolostone ……138
6.4.2. Interpretation of Sulfur Isotope ……139
7. Conclusions ……142
References ……143
Vita……163

LIST OF FIGURES

Fig. 1.1. Ediacaran paleogeographic map and fossil localities. ……20
Fig. 1.2. Taxonomic and morphology diversity of Ediacara fossils. ……21
Fig. 1.3. Results of MDS analysis using three-dimensional ordination. ……..…...23

Fig. 2.1. Geographic map, showing the location of the North China Block, South China Block, Tarim Block, and Chaidam Block. … ……67
Fig. 2.2. Stratigraphic columns of upper Neoproterozoic successions in (from left to right) the Helanshan area, North China; Quanjishan area, Chaidam; Ningqiang area, South China; and Yangtze Gorge area, South China……..68
Fig. 2.3. Field photographs of the Quanjishan and Suyukou sections. ……69
Fig. 2.4. *Helanoichnus helanensis* Yang *in* Yang and Zheng, 1985, from the Zhengmuguan and Zhoujieshan formations, and *Horodyskia moniliformis*? Yochelson and Fedonkin, 2000, from the Zhengmuguan Formation. ……...70
Fig. 2.5. Measurements of 25 *Helanoichnus helanensis* specimens from the Zhengmuguan Formation. ……..72
Fig. 2.6. Measurements of 5 *Horodyskia moniliformis*? specimens from the Zhengmuguan Formation. ……..73
Fig. 2.7. Cartoon showing the descriptive terminology of *Palaeopascichnus* Palij, 1976. ……...74
Fig. 2.8. *Palaeopascichnus minimus* n. sp.; *Palaeopascichnus meniscatus* n. sp.; and *Shaanxilithes* cf. *ningqiangensis* Xing, Yue, and Zhang *in* Xing et al., 1984. ..75
Fig. 2.9. Log plot, showing the correlation between segment width and segment thickness of *Palaeopascichnus*. ……77
Fig. 2.10. Thin sections and elemental geochemistry of *Helanoichnus helanensis* from the Zhoujieshan Formation and Zhengmuguan Formation ……..78

Fig. 3.1. Geographic location of the Tarim Block and Quruqtagh area. ……113
Fig. 3.2. Stratigraphic column of Neoproterozoic Quruqtagh Group. ……114
Fig. 3.3. Field photograph and SEM photomicrography of the Zhamoketi cap carbonate. ……115
Fig. 3.4. Isotopic and elemental geochemistry profiles of the Zhamoketi cap dolostone at the Yukkengol section. ……116
Fig. 3.5. Isotope and elemental cross-plots ……117
Fig. 3.6. Basin stratification model ……118
Fig. 3.7. Mass balance calculation of basin stratification model. ……...119
Fig. 3.8. Sulfate minimum zone model. ……..120
Fig. 3.9. Comparison of $\delta^{34}S_{CAS}$ profiles of supposedly equivalent cap carbonate following the Marinoan glaciation. ……..121

Fig. 4.1. Geological map and localities of Quanji Group in the Chaidam Basin. ……...149
Fig. 4.2. Stratigraphic columns of the Quanji Group and the Zhoujieshan cap dolostone. ……150
Fig. 4.3. Field photographs of the lower Quanji Group. ……151

Fig. 4.4. Field photographs of the upper Quanji Group ……..153
Fig. 4.5. Carbon and oxygen isotope profiles of the Hongzaoshan Formation and the Zhoujieshan cap dolostone ……...155
Fig. 4.6. Isotopic and elemental geochemistry profiles of the Zhoujieshan cap dolostone at section B. …….156
Fig. 4.7. Isotope and element crossplots. ……157

LIST OF TABLES

Table 1.1. Summary of the literature data. ……24
Table 1.2. Number of genera, species occurrences, morphotypes, specimens, and preservational quality, with data grouped by sedimentary basins or biotas. ……25
Table 1.3. Number of genera, species occurrences, morphotypes, specimens, and preservation quality, with data grouped into assemblages. ……26
Table 1.4. Character coding of Ediacara fossils ……...27
Table 1.5. Mahalanobis distances between the centroids of the three Ediacara assemblages. ……...32
Table 1.6. Classificatory error rates based on the discriminant analysis for the three Ediacara assemblages. ……33

Table 2.1. Comparison of *Palaeopascichnus* species and *Palaeopascichnus*-like fossils. ……80

Table 3.1. Geochemical data of the Zhamoketi cap carbonate at the Yukkengol. …….122

Table 4.1. $\delta^{13}C$ and $\delta^{18}O$ data of the Quanjishan carbonate samples from section A and the Hongzaoshan dolostone from section B in the Quanjishan area. ……...158
Table 4.2. Geochemical data of the Zhoujieshan cap carbonate at section B in the Quanjishan area. ……...162

INTRODUCTION AND OVERVIEW OF THE RESEARCH

The Ediacaran Period (635–543 Ma) bridges the Cryogenian (750–635 Ma) snowball Earth (Hoffman et al., 1998) and the Cambrian explosion (Briggs et al., 1994; Gould, 1989), and represents one of the most critical period during Earth history (Knoll et al., 2006). It witnessed the dramatic changes in atmosphere, hydrosphere, and biosphere, which finally led to the transition from the Proterozoic Earth system to the Phanerozoic Earth system. The Ediacaran atmosphere experienced an episodic oxygenation event, which may have played a key role in remodeling global biogeochemical cycles and triggering the evolution of macroscopic organisms (Canfield et al., 2007; Fike et al., 2006; Narbonne and Gehling, 2003). Ediacaran oceans also experienced an irreversible transition from H_2S enriched to oxygen enriched (Canfield, 1998). In addition, at least one glaciation may have occurred in the Ediacaran Period. Compared with the Cryogenian snowball Earth, the Ediacaran glaciation (e.g. the Gaskiers glaciation in Newfoundland) was much shorter, and probably not global in extent (Bowring et al., 2003; Xiao et al., 2004). The Ediacaran biosphere is characterized by the first appearance of macroscopic, complex organisms, the Ediacara biota (Narbonne, 1998; Narbonne, 2005). In addition, the earliest animals can be traced back in the Ediacaran Period, e.g. the putative animal embryos and bilaterians from the Ediacaran Doushantuo Formation (Xiao et al., 2000; Xiao et al., 1998). Finally, animal biomineralization, although became widespread in the early Cambrian, first appeared in the late Ediacaran Period (Bengtson and Conway Morris, 1992; Hua et al., 2005).

This dissertation focuses on both the paleobiology and biogeochemistry of the Ediacaran Period. The first two chapters devote to the Ediacaran fossil record. The third and fourth chapters focus on geochemical cycles in Ediacaran basins.

In chapter one, I present results of an analysis of the morphological and taxonomical diversity of Ediacara fossils. The Ediacara fossils, representing the most ancient, enigmatic and controversial macroscopic life forms, have been discovered from more than 30 localities with a worldwide distribution (Narbonne, 1998; Narbonne, 2005).

With very few exceptions (Xiao et al., 2005), Ediacara fossils are preserved as casts and molds in siliciclastic rocks without internal anatomical structures (Gehling, 1999; Narbonne, 2005). Although the cast-and-mold preservation of Ediacara fossils impedes morphological reconstruction of anatomical structures, the large fossil collections allow us to apply quantitative methods to synthesize the evolutionary patterns of Ediacara organisms. A cluster analysis based on the taxonomic similarities recognized three Ediacara assemblages, in chronological order, the Avalon, White Sea and Nama (Waggoner, 1999; Waggoner, 2003). In this project, I used morphometric analysis to quantify Ediacara morphospace and evaluated the morphological and taxonomic evolution of Ediacara biotas. The analysis shows that the earliest Ediacara assemblage (Avalon) had realized more than 80% of total Ediacara morphospace, in spite of its low taxonomic diversity. The subsequent diversification in the White Sea assemblage was not associated with morphospace expansion or shift. This pattern echoes the diversity-disparity pattern of the Cambrian explosion (Davidson and Erwin, 2006; Gould, 1989). The parallel diversity-disparity evolution of Ediacara and Cambrian biotas implies the similar evolutionary mechanisms underlying both evolutionary events.

An important line of evidence for animal life in the Ediacaran Period comes from trace fossils. Some paleontologists believe that the trace fossil record can be traced back to Palaeoproterozoic (Bengtson et al., 2007; Seilacher et al., 1998), while others argue that animal traces first occurred in the Ediacaran Period (Droser et al., 2005; Jensen et al., 2006). The interpretation of trace-like fossils as animal traces is far from straightforward (Jensen, 2003; Jensen et al., 2006). In chapter two, we reexamined some purported trace fossils from Ediacaran successions in the North China and Chaidam blocks (Wang et al., 1980; Xing et al., 1984; Yang and Zheng, 1985). Our study recognizes four genera and five species: *Helanoichnus helanensis* Yang *in* Yang and Zheng, 1985; *Palaeopascichnus minimus* new species; *Palaeopascichnus meniscatus* new species; *Horodyskia moniliformis*? Yochelson and Fedonkin, 2000; and *Shaanxilithes* cf. *ningqiangensis* Xing et al., 1984. Our careful investigation suggests that none of these taxa can be interpreted as animal traces. Instead, they are likely body fossils with uncertain phylogenetic affinities. Among these fossils, *Palaeopascichnus* and *Shaanxilithes* are common late

Ediacaran members, and may have implication in regional biostratigraphic correlations. *Horodyskia* can be traced back into the Mesoproterozoic, suggesting that at least some Ediacaran organisms may have a deep evolutionary root (Fedonkin and Yochelson, 2002; Grey and Williams, 1990; Martin, 2004; Yochelson and Fedonkin, 2000).

Ediacaran biological evolution occurred in geochemical and environmental contexts. To characterized Ediacaran geochemical and environmental conditions, I studied stable isotope geochemistry of two postglacial cap carbonates that overlie two Neoproterozoic glacial deposits in northwest China, and the results are presented in chapter 3 and 4. The purposes of these projects are to reconstruct the global carbon and sulfur cycles, and paleoceonography after Neoproterozoic glaciations. I measured the carbon isotopes of carbonate and organic carbon to reconstruct the carbon cycle. I also analyzed sulfur isotopes carbonate associated sulfate (CAS) and pyrite to understand sulfur cycle.

In chapter three, we report the stable isotopes of the Zhamoketi cap dolostone that directly overlies the Tereeken diamictite in the Quruqtagh area, northwest China (Gao and Zhu, 1984; Xiao et al., 2004). Radiometric dating and chemostratigraphic correlation suggest that the Tereeken diamictite can be correlated with the Marinoan glaciation that terminated at 635 Ma (Condon et al., 2005; Xiao et al., 2004). The Zhamoketi cap dolostone is characterized by inverse sulfur isotopic fractionation between $\delta^{34}S_{CAS}$ and $\delta^{34}S_{pyrite}$ ($\delta^{34}S_{CAS} < \delta^{34}S_{pyrite}$). Combined with sedimentological evidence, sulfur isotopes of the Zhamoketi cap dolostone imply basin stratification after the Tereeken glaciation. In this stratified basin, fresh and warm surface water mass derived from melting ice overlaid saline and cold sea water relict from the Tereeken glaciation. In this stratified basin, CAS in cap carbonate was derived from surface water, whereas pyrite was precipitated from bottom water.

Chapter four presents and carbon and sulfur isotopic data from the Quanji Group, a Neoproterozoic succession in the Chaidam basin (Wang et al., 1980). The Quanji Group is a siliciclastic dominated sequence with two carbonate units, the Hongzaoshan dolostone and the Zhoujieshan cap dolostone. The Zhoujieshan cap dolostone overlies the

Hongtiegou diamictite. Although the depositional age of the Quanji Group is poorly constrained (Lu, 2002), paleontological and chemostratigraphic evidence suggest that the Hongtiegou glaciation may represent an Ediacaran glaciation (Shen et al., 2007). Unlike other Neoproterozoic postglacial cap carbonate, $\delta^{13}C$ of the Zhoujieshan cap dolostone is positive. The positive $\delta^{13}C$ values are distinct from the typically negative $\delta^{13}C$ values of Neoproterozoic cap carbonates. $\delta^{34}S_{CAS}$ and $\delta^{34}S_{pyrite}$ values of the Zhoujieshan cap carbonateare decoupled from each other. $\delta^{34}S_{CAS}$ varies between +14‰ and +24‰, whereas $\delta^{34}S_{pyrite}$ steadily increases by 13‰ within the 3.8-m Zhoujieshan cap dolostone. The upper part of the Zhoujieshan cap carbonate is characterized by inverse fractionations between CAS and pyrite. The decoupling of $\delta^{34}S_{CAS}$ and $\delta^{34}S_{pyrite}$ suggest that CAS and pyrite were not derived from the same sulfur pool. Separation of CAS and pyrite sulfur pools can be achieved by the postglacial stratification model described in chapter 3.

REFERENCES

Bengtson, S. and Conway Morris, S., 1992. Early radiation of biomineralizing phyla. In: J.H. Lipps and P.W. Signor (Editors), Origin and early evolution of the Metazoa. Topics in Geobiology. Plenum, New York, United States, pp. 447-481.

Bengtson, S., Rasmussen, B. and Krapež, B., 2007. The Paleoproterozoic megascopic Stirling biota. Paleobiology, 33: 351-381.

Bowring, S., Myrow, P., Landing, E., Ramezani, J. and Grotzinger, J., 2003. Geochronological constraints on terminal Neoproterozoic events and the rise of metazoans. Geophysical Research Abstracts, 5: 13219.

Briggs, D.E.G., Erwin, D.H. and Collier, F.J., 1994. The Fossils of the Burgess Shale. Smithsonian Institution Press, Washington, 238 pp.

Canfield, D.E., 1998. A new model for Proterozoic ocean chemistry. Nature, 396: 450-453.

Canfield, D.E., Poulton, S.W. and Narbonne, G.M., 2007. Late-Neoproterozoic Deep-Ocean Oxygenation and the Rise of Animal Life. Science, 315: 92-95.

Condon, D., Zhu, M., Bowring, S., Wang, W., Yang, A. and Jin, Y., 2005. U-Pb Ages from the Neoproterozoic Doushantuo Formation, China. Science, 308: 95-98.

Davidson, E.H. and Erwin, D.H., 2006. Gene regulatory networks and the evolution of animal body plans. Science, 311: 796-800.

Droser, M.L., Gehling, J.G. and Jensen, S., 2005. Ediacaran trace fossils: true and false. In: D.E.G. Briggs (Editor), Evolving Form and Function: Fossils and Development. Yale Peabody Museum Publications, New Haven, pp. 125-138.

Fedonkin, M.A. and Yochelson, E.L., 2002. Middle Proterozoic (1.5 Ga) *Horodyskia moniliformis* Yochelson and Fedonkin, the oldest known tissue-grade colonial eucaryote. Smithsonian Contributions to Paleobiology, 94: 1-29.

Fike, D.A., Grotzinger, J.P., Pratt, L.M. and Summons, R.E., 2006. Oxidation of the Ediacaran ocean. Nature, 444: 744-747.

Gao, Z. and Zhu, S., 1984. Precambrian Geology in Xinjiang, China. Xinjiang People's Publishing House, Urumuqi, China, 151 pp.

Gehling, J.G., 1999. Microbial mats in terminal Proterozoic siliciclastics: Ediacaran death masks. Palaios, 14: 40-57.

Gould, S.J., 1989. Wonderful Life: The Burgess Shale and the Nature of History. Norton, New York, 347 pp.

Grey, K. and Williams, I.R., 1990. Problematic bedding-plane markings from the Middle Proterozoic Manganese Subgroup, Bangemall Basin, Western Australia. Precambrian Research, 46: 307-328.

Hoffman, P.F., Kaufman, A.J., Halverson, G.P. and Schrag, D.P., 1998. A Neoproterozoic snowball Earth. Science, 281: 1342-1346.

Hua, H., Chen, Z., Yuan, X., Zhang, L. and Xiao, S., 2005. Skeletogenesis and asexual reproduction in the earliest biomineralizing animal *Cloudina*. Geology, 33: 277-280.

Jensen, S., 2003. The Proterozoic and Earliest Cambrian trace fossil record: patterns, problems and perspectives. Integrative and Comparative Biology, 43: 219-228.

Jensen, S., Droser, M.L. and Gehling, J.G., 2006. A critical look at the Ediacaran trace fossil record. In: S. Xiao and A.J. Kaufman (Editors), Neoproterozoic Geobiology and Paleobiology. Springer, Dordrecht, Netherlands, pp. 116-159.

Knoll, A., Walter, M., Narbonne, G. and Christie-Blick, N., 2006. The Ediacaran Period: a new addition to the geologic time scale. Lethaia, 39: 13-30.

Lu, S., 2002. The Precambrian geology of Northern Tibet. Geological Publishing House, Beijing, 125 pp.

Martin, D.M., 2004. Depositional environment and taphonomy of the 'strings of beads': Mesoproterozoic multicellular fossils in the Bangemall Supergroup, Western Australia. Australian Journal of Earth Sciences, 51: 555-561.

Narbonne, G.M., 1998. The Ediacara Biota: A terminal Neoproterozoic experiment in the evolution of life. GSA Today, 8: 1-6.

Narbonne, G.M., 2005. The Ediacara Biota: Neoproterozoic origin of animals and their ecosystem. Annual Review of Earth and Planetary Sciences, 33: 421-442.

Narbonne, G.M. and Gehling, J.G., 2003. Life after snowball: The oldest complex Ediacaran fossils. Geology, 31: 27-30.

Seilacher, A., Bose, P.K. and Pflüger, F., 1998. Triploblastic animals more than one billion years ago: trace fossil evidence from India. Science, 282: 80-83.

Shen, B., Xiao, S., Dong, L., Zhou, C. and Liu, J., 2007. Problematic macrofossils from Ediacaran successions in the North China and Chaidam blocks: implications for there evolutionary root and biostratigraphic significance. Journal of Paleontology, 81: 1396-1411.

Waggoner, B., 1999. Biogeographic analyses of the Ediacara biota; a conflict with paleotectonic reconstructions. Paleobiology, 25: 440-458.

Waggoner, B., 2003. The Ediacaran Biotas in Space and Time. Integrative and Comparative Biology, 43: 104-113.

Wang, Y., Zhuang, Q., Shi, C., Liu, J. and Zheng, L., 1980. Quanji Group along the northern border of Chaidamu Basin. In: Tianjin Institute of Geology and Mineral Resources (Editor), Research on Precambrian Geology Sinian Suberathem in China, Tianjin, pp. 214-230.

Xiao, S., Bao, H., Wang, H., Kaufman, A.J., Zhou, C., Li, G., Yuan, X. and Ling, H., 2004. The Neoproterozoic Quruqtagh Group in eastern Chinese Tianshan: Evidence for a post-Marinoan glaciation. Precambrian Research, 130: 1-26.

Xiao, S., Shen, B., Zhou, C., Xie, G. and Yuan, X., 2005. A uniquely preserved Ediacaran fossil with direct evidence for a quilted bodyplan. Proceeding of the National Academy of Sciences of the United State of America, 102: 10227-10232.

Xiao, S., Yuan, X. and Knoll, A.H., 2000. Eumetazoan fossils in terminal Proterozoic phosphorites? Proceedings of the National Academy of Sciences, USA, 97: 13684-13689.

Xiao, S., Zhang, Y. and Knoll, A.H., 1998. Three-dimensional preservation of algae and animal embryos in a Neoproterozoic phosphorite. Nature, 391: 553-558.

Xing, Y., Ding, Q., Luo, H., He, T. and Wang, Y., 1984. The Sinian-Cambrian boundary of China. Bulletin of the Institute of Geology, Chinese Academy of Geological Sciences: 1-262.

Yang, S. and Zheng, Z., 1985. The Sinian trace fossils from Zhengmuguan Formation of Helanshan Mountain, Ningxia. Earth Science - Journal of Wuhan College of Geology, 10.

Yochelson, E.L. and Fedonkin, M.A., 2000. A new tissue-grade organism 1.5 billion years old from Montana. Proceedings of the Biological Society of Washington, 113: 843-847.

Chapter 1

The Avalon Explosion: Evolution of Ediacara Morphospace[1]

Abstract

Ediacara fossils (575–542 Ma) represent Earth's oldest known complex macroscopic life forms, but their morphological history is poorly understood. A comprehensive quantitative analysis of these fossils indicates that the oldest Ediacara assemblage—the Avalon assemblage (575–565 Ma)—already encompassed the full range of Ediacara morphospace. A comparable morphospace range was occupied by the subsequent White Sea (560–550 Ma) and Nama (550–542 Ma) assemblages, although it was populated differently. In contrast, taxonomic richness increased in the White Sea assemblage and declined in the Nama assemblage. These diversity changes, occurring while morphospace range remained relatively constant, led to inverse shifts in morphological variance. The Avalon morphospace expansion mirrors the Cambrian explosion, and both may reflect similar underlying mechanisms.

1. INTRODUCTION

The evolutionary history of macroscopic organisms in the late Ediacaran Period (ca. 575–542 Ma) is regarded as a prelude to the Cambrian Explosion (Narbonne, 2005). There are >270 described Ediacara species occurrences from >30 localities on several major continents (Fig. 1.1; Table 1.1–1.3), providing an adequate dataset for a quantitative analysis of Ediacara taxonomic and morphological evolution. Using cluster analysis of taxonomic composition, Waggoner recognized three Ediacara assemblages: Avalon, White Sea and Nama (Waggoner, 2003). The Avalon assemblage (575–565 Ma) (Narbonne and Gehling, 2003) is restricted to deep-water environments in the Avalon Province and represents an early evolutionary stage with relatively low taxonomic richness. The subsequent White Sea assemblage (560–550 Ma) shows a substantial diversity increase and a significant geographic expansion into Baltica (Winter Coast and adjacent area, Podolia, Finnmark, Urals) (Farmer et al., 1992; Sokolov and Iwanowski,

[1] Article published by Shen, B., Dong, L., Xiao, S. and Kowalewski, M. (2008) The Avalon Explosion: Evolution of Ediacara Morphospace. Science. 319: 81-84. (American Association for the Advancement of Science)

1990), Australia (Gehling et al., 2005), Siberia (Sokolov and Iwanowski, 1990), and Laurentia (Narbonne and Hofmann, 1987). Diversity drops again in the Nama assemblage (549–542 Ma) (Amthor et al., 2003; Grotzinger et al., 1995), which includes fossils from the Kalahari Craton (Grazhdankin and Seilacher, 2002), Yangtze Platform (Sun, 1986; Xiao et al., 2005), Laurentia (Hagadorn and Waggoner, 2000; Hofmann et al., 1991), and Carolina Terrace (Gibson et al., 1984; Weaver et al., 2006).

Waggoner (Waggoner, 2003) discussed three possible interpretations of the Ediacara assemblages: they may represent different evolutionary stages, biogeographic provinces, or environmental-ecological associations. These interpretations need not be mutually exclusive, because evolutionary changes could be driven by biogeographic, ecological, and environmental factors. Grazhdankin (Grazhdankin, 2004) argued that these assemblages represent environmental-ecological associations with little biogeographic provinciality or evolutionary change, although available geochronological data (Amthor et al., 2003; Bowring et al., 1993; Grotzinger et al., 1995; Martin et al., 2000; Narbonne, 2005) indicate that the assemblages may indeed differ in age.

Previous work on the Ediacara assemblages focused on taxonomic data. Here, we test whether morphological patterns mirror taxonomic trends and whether there are any temporal, geographic, and environmental effects on Ediacara morphological patterns.

2. MATERIALS AND METHODS

We recorded the presence or absence of 50 morphological characters for 272 occurrences of Ediacara species (or unnamed forms) from 60 publications and one unpublished museum sample (Table 1.4). To maintain taphonomic uniformity, we focused on classical Ediacara assemblages and excluded possible Ediacara fossils preserved as carbonaceous compressions (Xiao et al., 2002). Although the coded characters are not exhaustive and exclude some inferred anatomical structures such as gonads and intestine of some dickinsoniid fossils (Dzik, 2003), they represent the overall shape, first-order symmetry (e.g., unipolar bilateral symmetry in *Charniodiscus*), and central-peripheral differentiation (e.g., central stalk and primary side branches in Ediacara fronds). They also include such important features as stems and discoidal holdfasts. The chosen characters are easily recognizable and less likely to be altered beyond

recognition by taphonomic processes, an important factor considering that most Ediacara fossils are preserved as casts and molds. A coded character may not be phylogenetically homologous or functionally analogous among different taxa, but we focus on morphological evolution and make no inference on the phylogenetic homology and functional biology of the coded characters.

2.1 Data Acquisition

In this research, all data were collected from published literature, except one unpublished specimen reposited at Yale University Peabody Museum (Table 1.1). An extensive literature review covered most of the English-language literature and some publications in German and Russian. The database includes species description compiled from 60 publications, totaling 272 species occurrences from 13 localities on 6 continents (Table 1.1–1.4). Of these, 259 species occurrences were assigned to the three assemblages (Avalon, White Sea, and Nama), as recognized by Waggoner (Waggoner, 2003). The remaining 13 species occurrences are from the Mackenzie Mountains (Hofmann, 1981; Narbonne, 1994; Narbonne and Aitken, 1990), and they were not assigned to any of the three assemblages according to Waggoner (Waggoner, 2003).

2.1.1. Morphological data.

In our analysis, we focused on classical Ediacara fossils that are preserved as casts and molds, although some fossils from the White Sea assemblage are somewhat flattened. We did not include possible Ediacara fossils preserved as carbonaceous compressions, e.g., in the Ediacaran Miaohe biota (Xiao et al., 2002). Thus, the taphonomy is more or less uniform across the assemblages. In addition, the preservational quality of the three Ediacara assemblages (Table 1.3) is comparable, so that the impact of unequal preservational quality is minimized.

We identified 50 morphological characters to quantify the symmetry and geometric morphology of Ediacara fossils. Each species occurrence was coded for the presence or absence of all characters, based on careful examination of original descriptions, reconstructions, and illustrations. Each species occurrence was only counted once for each locality. However, if two or more specimens of different morphologies were assigned to one species by the original authors, they were coded separately as distinct morphotypes.

These 50 morphological characters describe the overall shape and symmetry, important structures observed in central, intermediate, and peripheral zones of the body, and accessory structures such as stem, holdfast, aperture, and spines. To maintain objectivity of character

codings, we used as much as possible descriptive terms (e.g., side branches in *Spriggina*; concentric grooves in *Aspidella*) rather than interpretive terms [e.g., parapodia, arthropod-type segmentation, concentric muscles; in (Glaessner, 1984)]. Ecological interpretations (e.g., mobility, filter feeding, and deposit feeding) were not included in our coding. In addition, our coding did not include inferred anatomical structures [e.g., basement membrane, gonads, intestine of dickinsoniid; in (Dzik, 2003)] that are not preserved or are only ambiguously supported by preserved morphologies. Such labile structures—important as they are—are expected to occur only in a few best preserved specimens, and the inclusion of such labile structures would introduce preservational bias to our database. Thus, the morphological trends identified in our analysis are pertinent to characters that were included in our codings. Furthermore, because the majority of Ediacara fossils are preserved as casts and molds, their three-dimensional morphologies are sometimes uncertain. For example, there is no consensus on the number of vanes in some frondose fossils (Dzik, 2002; Dzik, 2003; Grazhdankin and Seilacher, 2005; Jenkins, 1985; Jenkins, 1992; Jenkins and Gehling, 1978; LaFlamme et al., 2004), although it is clear that some Ediacara fossils [e.g., *Swartpuntia* (Narbonne et al., 1997), *Ventogyrus* (Ivantsov and Grazhdankin, 1997), and *Pteridinium* (Grazhdankin and Seilacher, 2002)] are likely multifoliate whereas others [e.g., *Charnia* (LaFlamme and Narbonne, 2007; Laflamme et al., 2007)] are bifoliate. To avoid such uncertainties, we primarily focused on preserved two-dimensional morphologies.

The focus of this study was on morphospace occupation, which can be achieved convergently through independent evolution. Thus, the selected morphological characters do not necessarily imply homology. Rather, they were chosen because they represent basic aspects of Ediacara morphologies that are fossilizable and easily recognizable. These morphological characters have wide distribution among Ediacara fossils from different localities and with different preservational quality, maximizing the statistical power of the analysis.

The morphological characters are listed below. Abbreviations used in the coding system and exemplary Ediacara taxa are given in the parentheses. The complete codings are given in Table 1.4.

a. Overall Shape: Circular (C, *Aspidella*); Fan-shaped (F, *Parvancorina minchami*); Oval (O, *Dickinsonia*); Angular/Triangular/Polygonal (A, *Thectardis*); Lobate (L, *Triforillonia*); Spindle (S, *Fractofusus misrai*).

b. Symmetry: Radial (Rd, *Aspidella*); Bilaterial and unipolar (Up, *Charniodiscus*); Bilateral and bipolar (Bp, *Dickinsonia*); Tri-radial (Tr, *Tribrachidium*); Tetra-radial (Te, *Conomedusa*); Penta-radial (Pe, *Arkarus*); Fractal-branching modules (Md, *Rangea*).
c. Structures in the central region: Tubercle (Ctu, *Skinnera*); Smooth (Csm, *Mawsonites*); Central boss (Cbo, *Ediacara*); Central groove (Cgr, *Dickinsonia*); Central ridge (Cri, *Vendia*); Lateral ridge (Clr, *Parvancorina*); Segmented central ridge (Csr, *Swartpuntia*); Tapering central ridge (Ctr, *Charniodiscus procerus*); Transverse groove (Ctv, *Chondroplon*); Concentric groove (Cco, *Aspidella*); Dichotomous radial groove (Cdr, *Rugoconites*); Straight radial groove (Cra, *Eoporpita*); Spiral ridge (Csp, *Tribrachidium*); Straight tapering radial groove (Cta, *Albumares*); Smooth interzone (Cis, *Tribrachidium*); Dichotomous groove in interzone (Cid, *Anfesta*); Parallel primary branch (Pp, *Vendia*); Primary branch curved toward one end (P1, *Paravendia*); Primary branch curved toward both ends (P2, *Dickinsonia*); Secondary branch on one side of primary branch (S1, *Charnia*); Secondary branch on both sides of primary branch (S2, *Rangea*); Primary branches organized in two ranks in terms of length (Sec, *Ventogyrus*); Primary branches organized in three ranks (Ter, *Ventogyrus*).
d. Structures in the intermediate region: Frontal area (Mfa, *Parvancorina*); Smooth (Msm, *Parvacorina*); Straight radial groove (Mra, *Kimberella*); Dichotomous radial groove (Mdr, *Solza*); Multiple radial groove (Mmr, *Eoporpita*?); Concentric groove (Mco, *Aspidella*); Tubercle (Mtu, *Skinnera*).
e. Structures in the peripheral region: Smooth (Psm, *Kimberella quadrata* from South Australia); Radial furrows (Pra, *Mawsonites*); Concentric furrows (Pco, *Kimberella* from Russia).
f. Other structures: Stem (Sk, *Swartpuntia*); Discoidal holdfast (Dh, *Charniodiscus*); Sternal chamber (Sc, *Ventogyrus*?); Terminal spine (Sp, *Charniodiscus spinosus*).

2.1.2. Abundance and preservational quality.

The abundance and preservational quality data were also recorded from the literature. The abundance data were needed to perform specimen-level rarefaction analysis (Fig. 1.2B) and

diversity standardization (Fig. 1.2A). The exact numbers of specimens were recorded whenever reported. Often, only qualitative description was given or no abundance data were given at all. In these cases, we arbitrarily assigned an abundance value according to the following scheme: abundant = 200, several dozen = 24, dozen = 12, several = 5, not mentioned = 5.

The preservational quality was used as an index to evaluate potential taphonomic control on the observed taxonomic diversity trend (Fig. 1.2A). Typically, a taxonomic classification based on better preserved specimens would allow the recognition of a greater number of lower-level taxa than one based on poorly preserved specimens. If preservation has a major control on taxonomic diversity, then these two parameters are expected to be correlated with each other. Preservational quality was evaluated as follows. Each genus was assigned into one of four preservation grades on the basis of description and illustrations: well preserved, variably preserved, fairly preserved, and poorly preserved, in the order of decreasing preservational quality. If the preservational quality was not mentioned in the description and there were no illustrations for evaluation, then the preservational quality of this genus was regarded as poorly preserved. The preservational quality of a bin (e.g., an assemblage or a biota) was calculated as the percentage of genera characterized by fair or better preservation (Table 1.2, 1.3).

2.2 Data Analysis

2.2.1. Taxonomic diversity.

The taxonomic diversity of each Ediacara assemblages (Avalon, White Sea, and Nama) was evaluated at the genus level. This is justified because most Ediacara genera (~80%) are monospecific and genus-level taxonomy is more stable and thus more robust against taxonomic inconsistencies among different researchers. The raw genus-level diversity was calculated by counting the total number of genera in each assemblage (Fig. 1.2A, green line). To test the possible effect of sampling intensity on genus-level diversity, we carried out a rarefaction analysis to characterize the relationship between the number of specimens sampled and the number of genera observed. The rarefaction analysis was based on 1000 independent iterations (Fig. 1.2B, solid symbols). The standardized genus-level diversity is reported as the mean diversity estimated by 1000 iterations standardized at n=400 specimens. The 95% confidence intervals are estimated using the 2.5 and 97.5 percentiles of diversity estimates obtained in 1000 iteration runs (Fig. 1.2A, red line).

In calculating the genus-level diversity, we adopted the most recent taxonomic revisions of Ediacara fossils, although the taxonomic diversity is expected to vary because of synonymy and taxonomic inconsistencies. To evaluate the effect of synonymy, we carried out an independent classification of all fossil occurrences based on our morphological coding, so that specimens characterized by a distinct set of morphological characters were interpreted as unique morphotypes. Using the same protocol as described above, the morphotype data were also rarefied (1000 independent iterations) and standardized at n=400 specimens (Fig. 1.2A, blue line; Fig. 1.2B, hollow symbols) in order to compare the morphotype estimates with those based on formally named genera. It is clear that the standardized morphotype diversity trend mirrors the standardized genus diversity trend (Fig. 1.2A), indicating that taxonomic synonymy does not mask the diversity pattern and no additional bias was introduced during coding.

Percentage shared genera among the three Ediacara assemblages (Fig. 1.2D, green line) were calculated using the Sorensen's Index $(SI)_{A\text{-}B} = 2 \times G_o / (G_A + G_B)$, where G_A, G_B, and G_o represent the number of genera in assemblage A, in assemblage B, and shared by A and B, respectively.

2.2.2. Morphological analysis.

The nature of our morphological data matrix allowed us to employ multiple analytical approaches to investigate the morphological history in Ediacara fossils. In order to more fully understand morphological history of Ediacara fossils, both the total range of morphospace (an overall morphospace size) and the morphological disparity (morphological distance among taxa) were estimated using multiple approaches (Ciampaglio et al., 2001; Foote, 1997).

Non-parametric multidimensional scaling (MDS) was used to simplify the multidimensional data matrix, creating a two-dimensional ordination from the original 50 characters of all 259 species occurrences. This gradient analysis technique method is particularly attractive for morphological data that are based on discrete characters and include missing values (Marcus, 1990; Roy, 1994). Principal coordinate analysis, commonly used in disparity analyses, is not designed to handle missing values and was not used in this study. The MDS procedure was predefined to reduce the data matrix to two dimensions, so that the position of each species occurrence can be defined by two MDS scores (dimensions 1 and 2), and plotted using x-y ordination plots. A convex hull was constructed for each bin (e.g., each of the three assemblages),

and the area of the convex hull was calculated. This area was used as a proxy for morphospace size (Fig. 1.2C). Percentage shared morphospace among the three Ediacara assemblages (Fig. 1.2D, red line) were calculated using the Sorensen's Index $(SI)_{A\text{-}B} = 2 \times S_o / (S_A + S_B)$, where S_A, S_B, and S_o represent the area of assemblage A convex hull, of assemblage B convex hull, and the overlapping area of the two convex hulls, respectively.

Because the *a priori* choice of the number of dimensions is arbitrary and results may change if MDS ordinations are derived by reducing original data matrices into more than two dimensions, we repeated the MDS analysis using three dimensions. The outcome of the three-dimensional MDS is displayed in two cross plots (Fig. 1.3A, 1.3B). Although there are some subtle differences in location of individual species occurrences (compare Fig. 1.2C and Fig. 1.3), the overall ordination pattern is remarkably consistent with two-dimensional MDS ordination (Fig. 1.2C). In both cases, morphospaces of the three assemblages show nearly complete overlap and comparable sizes.

To determine whether the three Ediacara assemblages differ in the position of their centroids (i.e., an estimate of the average morphological shape), discriminant analysis and MANOVA of MDS scores were carried out to evaluate if the three assemblages are statistically distinct. Multivariate analyses based on ordination scores have been widely employed in both morphometric and ecological studies, including MANOVA tests of scores derived from non-parametric ordination techniques such as MDS and correspondence analysis (McCoy et al., 1999; van Zyll de Jong and Cowx, 2005). Because the MDS scores obtained in our analysis do not differ statistically from normally distributed data (Kolmogorov Smirnov $D<0.2$, Bonferroni-corrected $p>0.05$ for all three assemblages for both Dim1 and Dim2) and do not include any notable outliers, the approach should be reasonably robust. The results show that Mahalanobis distances between the centroids of the three assemblages are relatively small. However, these distances are statistically significant in the case of Avalon-Nama and Avalon-White Sea comparisons (Table 1.5). Despite these statistically significant but distance-wise subtle shifts in centroid location, the discriminant analysis highlights a very strong overlap of the three morphospaces, as demonstrated by a very high error rate (~60%) in *a posteriori* classification of species occurrences (Table 1.6). Discriminant analysis and MANOVA were performed using PROC DISCRIM (SAS 9.1). The classification errors were estimated using jackknife-corrected cross-validation approach (option CROSSVALIDATE in PROC DISCRIM).

Similar analyses (MDS ordination, discriminant analysis, and MANOVA; Fig. 1.2E, 1.2G, Table 1.5, 1.6) were also carried out for the four biotas of the White Sea assemblage (Baltica, Flinders Ranges, Siberia, and Wernecke biotas; Fig. 1.2E) and the three biotas representing different depositional environments (Newfoundland biota of the Avalon assemblage, Flinders Ranges biota of the White Sea assemblage, and Namibia biota of the Nama assemblage; Fig. 1.2G). In these analyses, MDS scores were independently calculated based on the morphological data in question rather than the entire database.

When sample size (number of species occurrences) is small, it may affect morphospace size. To investigate how sample size of the four biotas in the White Sea assemblage would affect their morphospace size, we carried out a rarefaction analysis on the MDS scores independently calculated from the White Sea assemblage data (Fig. 1.2E). White Sea species occurrences were randomly subsampled without replacement and their original MDS scores for DIM1 and DIM2 were retained. Morphospace size of a resulting subset of White Sea specimens was estimated as the product of maximum ranges along the two MDS axes. Mean and 95% confidence interval were estimated from 100 rarefaction runs (Fig. 1.2F).

We used MDS variance, total character variance, and mean dissimilarity coefficient (MDC) to evaluate morphological disparity (Fig. 1.2H). MDS variance was calculated as the sum variance along the two dimensions (MDS dim1 and dim2; Fig. 1.2H) or three dimensions (MDS dim1, dim2, and dim3; Fig. 1.3C). In addition, to test possible sampling-related biases, we run a randomization test with 1000 iterations performed on the MDS scores. In each iteration, we randomly reassigned each species occurrences to one of the three assemblages such that the sampling structure was preserved (i.e., 33, 202, and 24 species occurrences in the Avalon, White Sea, and Nama assemblages, respectively). The MDS variance was calculated for each iteration and the 95% confidence intervals (defined by the 2.5% and 97.5% percentiles) were calculated from all iterations combined. The resulting curve can be understood as a null model of a homogenous morphospace where all three assemblages were simply random samples drawn from the same underlying statistical population. Consequently, the resulting confidence intervals provide a null estimate for an expected variation if all three assemblages were the same and their differences in MDS variance were merely a result of random uneven sampling of the same underlying population. Note that 2-D MDS variances for two (Avalon and White Sea) of the three assemblages (Fig. 1.2H) lie outside the 95% confidence intervals of the null model

predicted from the randomization, indicating that the observed MDS variance pattern cannot be explained by sampling alone.

Total character variance was calculated as the sum of univariate variances computed separately for each assemblage using all 50 variables. The results (Fig. 1.3D) are similar to those obtained using MDS variances.

MDC was calculated as the fraction of morphological characters that are different, averaged across all pairwise comparisons of species occurrences in each assemblage (Fig. 1.2H). The 95% confidence intervals were estimated using 500 balanced bootstrapping iterations (Huntley et al., 2006; Kowalewski et al., 1998). A similar MDC analysis was also carried out using pairwise comparisons of species (rather than species occurrences) as analytical units. The pattern observed for species occurrences (lower MDC estimate obtained for the White Sea assemblage compared to higher MDC estimates obtained for the Avalon and Nama assemblages; Fig. 1.2H) was retained when species were used as analytical units (results not shown).

Codes for bootstrap, randomization, and rarefaction simulations were written in SAS/IML (SAS 9.1). Confidence intervals were estimated using 2.5 and 97.5 percentiles of sampling distributions generated in simulations [“naïve bootstrap” sensu Efron (Efron, 1981)].

2.3 Potential biases

2.3.1. Temporal resolution.

The temporal resolution is rather low, due to the lack of precise radiometric dates in most localities. Although the stratigraphic occurrence of most Ediacara fossils has been documented precisely (often at the level of formations), stratigraphic correlation among different localities is often uncertain. In this analysis, we adopted Waggoner’s (Waggoner, 2003) analysis to classify Ediacara fossils into three temporal bins, in chronological order, the Avalon, White Sea, and Nama assemblages. The binning is consistent with available radiometric dates and chemostratigraphic correlation (Amthor et al., 2003; Benus, 1988; Bowring et al., 2003; Bowring et al., 1993; Condon et al., 2005; Grazhdankin, 2004; Grotzinger et al., 1995; Martin et al., 2000), and is supported by differences and similarities in taxonomic composition.

2.3.2. Spatial resolution.

Each species occurrence was assigned to a sedimentary basin (or biota) according to its precise location recorded in the literature. Considering the poor temporal resolution and the relatively small number of species occurrences in the temporal bins, we regard the spatial resolution at the basin level as appropriate in order to maintain reasonable sample size in each bin.

2.3.3. Paleogeographic map.

The paleogeographic reconstruction of the Ediacaran Period is uncertain. The purpose of using paleogeographic map in this study was to illustrate the wide geographic distribution of Ediacara fossils. We adopted the paleogeographic map published by Smith (Smith, 2001).

3. DISCUSSION

Our raw diversity estimates (Fig. 1.2A; Table 1.3)—20, 77, and 15 genera in the Avalon, White Sea, and Nama assemblages, respectively—are broadly similar to Waggoner's estimate. To correct for uneven sampling, we used rarefaction to standardize taxonomic richness estimates. The diversity pattern observed for raw data persisted after rarefaction (Fig. 1.2A, 1.2B). To further test whether taxonomic synonymy had an impact on the observed diversity pattern, we reclassified all taxa in our database on the basis of unique morphotypes using our character coding system and then conducted rarefaction analysis. Again, the richness pattern remained unchanged (Fig. 1.2A, 1.2B), indicating minimal impact of taxonomic synonymy. Furthermore, because the quality of fossil preservation is comparable in the three assemblages (Table 1.3), the significant differences in taxonomic diversity and morphospace are unlikely to have been an artifact of differential preservation of the assemblages.

To compare the realized morphospaces of the three Ediacara assemblages, we first used the non-parametric multidimensional scaling (MDS) method to ordinate the pooled multivariate dataset into two dimensions (MDS Dim1 and Dim2) so that each species occurrence can be represented by two MDS scores rather than 50 characters. The morphospace of each assemblage can then be visualized as a convex hull in a scatter plot of the two-dimensional MDS scores (Huntley et al., 2006). Our results show that all three assemblages share similar morphospaces of comparable size (Fig. 1.2C), and this pattern persisted when the MDS ordination was fitted into

three dimensions (Fig. 1.3A, 1.3B). Shared morphospace calculated as overlapping area between convex hulls is on average 81.9% (Avalon–White Sea: 81.9%; Nama–White Sea: 84.1%; Avalon–Nama: 79.7%; Fig. 1.2D), compared with 12.3% shared genera (Avalon–White Sea: 10.3%; Nama–White Sea: 15.2%; Avalon–Nama: 11.4%; Fig. 1.2D). Thus, despite substantial changes in taxonomic diversity throughout the Ediacara history, the overall size and position of the Ediacara morphospace remained remarkably static.

Although the morphospace range (Fig. 1.2C, 1.3A, 1.3B) is comparable across the three assemblages, the group centroids are statistically distinct for Avalon-White Sea and Avalon-Nama comparisons (Table 1.5). Thus, the typical (average) morphology of the Avalon assemblage may differ from those of the two subsequent assemblages, perhaps reflecting the intuitive perception that the Avalon assemblage was somewhat distinct. However, the difference is minor—all pairwise distances between centroids are small (Table 1.5) and discriminant analysis misclassifies 59.2% of species occurrences into incorrect assemblages (Table 1.6). These results are consistent with a substantial overlap among the three morphospaces observed on ordination plots (Figs. 1.2C, 1.3A, 1.3B).

To test whether Ediacara biotas of similar age from different biogeographic provinces or paleolatitudes have distinct morphospaces, we focused on the White Sea assemblage—the only assemblage with sufficient geographic coverage—and used MDS to ordinate the Baltica, Flinders Ranges, Siberia, and Wernecke biotas (Fig. 1.2E; Table 1.2). The Baltica and Flinders Ranges biotas, likely coeval (Waggoner, 2003) but from different paleolatitudes (Smith, 2001), share similar morphospaces (90.2% shared morphospace vs. 41.3% shared genera) that are comparable to the morphospace of the entire White Sea assemblage (shared morphospace: Baltica–White Sea 86.9%, Flinders Ranges–White Sea 91.9%; shared genera: Baltica–White Sea 75.3%, Flinders Ranges–White Sea 44.2%). In contrast, the Siberia and Wernecke biotas occupy smaller morphospaces. However, these smaller morphospaces may reflect inadequate sampling, as these two biotas are represented by 10 and 13 species occurrences only. Indeed, rarefaction analysis of the White Sea assemblage suggests that at least ~30 species occurrences are required to retain its morphospace size (Fig. 1.2F). In sum, the comparable morphospaces of the adequately sampled Flinders Ranges and Baltica biotas, the small distances between centroids (Table 1.5), and poor classificatory performance of discriminant analysis (Table 1.6), all suggest that the Ediacara morphospace may have been decoupled from paleobiogeography.

It has been argued that the distribution of Ediacara taxa was primarily controlled by paleoenvironments (Grazhdankin, 2004): Avalon-type biotas occur in deep marine habitats, Flinders Ranges-type biotas in shallow marine prodeltaic settings, and Nama-type biotas in distributary-mouth bar shoals. According to Grazhdankin (Grazhdankin, 2004), these three biotas represent an environmental-ecological gradient involving little evolutionary change or biogeographic provinciality. We recalculated MDS scores of the Newfoundland, Flinders Ranges, and Namibia biotas that represent these three paleoenvironments (Table 1.2). There are significant taxonomical differences among the three biotas (shared genera: Flinders Ranges–Newfoundland 11.8%, Newfoundland–Namibia 6.7%, Namibia–Flinders Ranges 12.8%). However, the percentage of shared morphospace is high (Fig. 1.2G; Flinders Ranges–Newfoundland 86.3%, Newfoundland–Namibia 91.7%, Namibia–Flinders Ranges 89.6%) and discriminant analysis suggests (Tables 1.5, 1.6) that the three groups are indistinguishable or strongly overlapping, indicating that paleoenvironments were not a major factor controlling the extent of Ediacara morphospace.

Although evolutionary change, biogeographic provinciality, and paleoenvironments might have played a role in Ediacara taxonomic evolution, they do not seem to have controlled the overall range of the realized morphospace, which appears invariant to notable taxonomic differences. Thus, changes in taxonomic diversity that occurred through time while morphospace range remained relatively constant should affect the internal structure of morphospace. Because of its greater taxonomic diversity, the White Sea assemblage should have a more crowded morphospace. Consequently, the morphological disparity (average morphological distances between taxa) of the White Sea assemblage should be smaller than the disparities of the Avalon and Nama assemblages.

We used three metrics, MDS variance, total character variance, and mean dissimilarity coefficient (MDC) (Foote, 1992; Foote, 1993; Foote, 1994), to quantify morphological disparity. The MDS variance was estimated by summing the variances of MDS scores along the two MDS dimensions. As expected, sum MDS variance is lower in the White Sea assemblage than in the other two (Fig. 1.2H). Results were similar when scores based on the 3-D MDS ordination were used (Fig. 1.3C). The total character variance, calculated by summing up variances of the original 50 variables, shows a comparable outcome (Fig. 1.3D). For binary characters, MDC of an assemblage can be calculated as the fraction of dissimilar characters averaged across all

pairwise comparisons. The MDC results are remarkably consistent with those based on variances, although the difference between White Sea and Nama is statistically insignificant (Fig. 1.2H), perhaps due to low statistical power associated with small sample size of the Nama assemblage (Table 1.3). The inverse relation between taxonomic diversity (Fig. 1.2A) and morphological disparity, observed for all applied metrics (Fig. 1.2H, 1.3C, 1.3D), reflects morphospace saturation: an increase in diversity within the confines of a static morphospace inevitably reduces the average morphological distance between taxa.

4. CONCLUSIONS

In summary, although the three Ediacara assemblages differ in taxonomic composition, their morphospaces overlap strongly and are comparable in size. Ediacara morphospace reached its maximum range already in the Avalon assemblage and was subsequently maintained in the White Sea and Nama assemblages. The morphospace was filled sparsely in the low-diversity, high-disparity Avalon and Nama assemblages, but densely in the high-diversity, low-disparity White Sea assemblage. Furthermore, the Ediacara morphospace ranges do not appear to have been controlled by paleobiogeography or paleoenvironments.

What might have led to the rapid morphospace expansion in the Avalon assemblage and what might have constrained the Ediacara morphospace from further expansion or shift in the subsequent White Sea and Nama assemblages? We consider a long, undocumented period of Ediacara history before the Avalon assemblage to be unlikely. The rapid increase of morphospace at the beginning of Ediacara evolution parallels the disparity patterns of the Cambrian explosion (Briggs et al., 1992; Foote et al., 1992; Gould, 1991): a rapid evolution of body plans followed by taxonomic diversification within the limits of a predefined morphospace. Various environmental, ecological, and developmental factors have been proposed to explain the rapid evolution of animal body plans during the Cambrian explosion as well as post-Cambrian constraints on modifications of these basic body plans despite taxonomic diversification (Marshal, 2006). In principle, these explanations may also be applied to the Avalon radiation. Future research should combine paleoecological, paleoenvironmental, developmental, and morphometric data to test whether the Gaskiers glaciation (Narbonne and Gehling, 2003), Ediacaran oxygenation (Canfield et al., 2007; Fike et al., 2006), establishment of a regulatory

developmental system (Davidson and Erwin, 2006), or sophisticated ecological interactions (Peterson and Butterfield, 2005) might have been the underlying drivers for the early morphological diversification of Ediacara organisms, and whether the ecological saturation or developmental entrenchment might have constrained Ediacara morphospaces. Regardless of the veracity of these causative explanations, the remarkable parallels between the Cambrian and Avalon explosions suggest that the decoupling of taxonomic and morphological evolution is not unique and that the Avalon explosion represents an independent, failed experiment with an evolutionary pattern similar to that of the Cambrian explosion.

REFERENCES

Amthor, J.E., Grotzinger, J.P., Schröder, S., Bowring, S.A., Ramezani, J., Martin, M.W. and Matter, A., 2003. Extinction of *Cloudina* and *Namacalathus* at the Precambrian-Cambrian boundary in Oman. Geology, 31: 431-434.

Benus, A.P., 1988. Sedimentological context of a deep-water Ediacaran fauna (Mistaken Point Formation, Avalon Zone, eastern Newfoundland). In: E. Landing, G.M. Narbonne and P. Myrow (Editors), Trace Fossils, Small Shelly Fossils and the Precambrian-Cambrian Boundary, Bulletin of the New York State Museum, pp. 8-9.

Bowring, S., Myrow, P., Landing, E., Ramezani, J. and Grotzinger, J., 2003. Geochronological constraints on terminal Neoproterozoic events and the rise of metazoans. Geophysical Research Abstracts, 5: 13219.

Bowring, S.A., Grotzinger, J.P., Isachsen, C.E., Knoll, A.H., Pelechaty, S.M. and Kolosov, P., 1993. Calibrating rates of Early Cambrian evolution. Science, 261: 1293-1298.

Briggs, D.E.G., Fortey, R.A. and Wills, M.A., 1992. Morphological disparity in the Cambrian. Science, 256: 1670-1673.

Canfield, D.E., Poulton, S.W. and Narbonne, G.M., 2007. Late Neoproterozoic deep-ocean oxygenation and the rise of animal life. Science, 315: 92-95.

Ciampaglio, C.N., Kemp, M. and McShea, D.W., 2001. Detecting changes in morphospace occupation patterns in the fossil record: characterization and analysis of measures of disparity. Paleobiology, 27: 695-715.

Condon, D., Zhu, M., Bowring, S., Wang, W., Yang, A. and Jin, Y., 2005. U-Pb ages from the Neoproterozoic Doushantuo Formation, China. Science, 308: 95-98.

Davidson, E.H. and Erwin, D.H., 2006. Gene regulatory networks and the evolution of animal body plans. Science, 311: 796-800.

Dzik, J., 2002. Possible Ctenophoran affinities of the Precambrian "sea-pen" *Rangea*. Journal of Morphology, 252: 315-334.

Dzik, J., 2003. Anatomical information content in the Ediacaran fossils and their possible zoological affinities. Integrative and Comparative Biology, 43: 114-126.

Efron, B., 1981. Nonparametric standard errors and confidence intervals. Canadian Journal of Statistics, 9: 139-172.

Farmer, J., Vidal, G., Moczydlowska, M., Strauss, H., Ahlberg, P. and Siedlecka, A., 1992. Ediacaran fossils from the Innerelv Member (late Proterozoic) of the Tanafjorden area, northeastern Finnmark. Geological Magazine, 129: 181-195.

Fike, D.A., Grotzinger, J.P., Pratt, L.M. and Summons, R.E., 2006. Oxidation of the Ediacaran ocean. Nature, 444: 744-747.

Foote, M., 1992. Paleozoic record of morphologica diversity in blastozoan echinoderms. Proceedings of the National Academy of Sciences of the United States of America, 89: 7325-7329.

Foote, M., 1993. Discordance and Concordance Between Morphological and Taxonomic Diversity. Paleobiology, 19: 185-204.

Foote, M., 1994. Morphological disparity in Ordovician-Devonian crinoids and the early saturation of morphological space. Paleobiology, 20: 320-344.

Foote, M., 1997. Sampling, Taxonomic Description, and Our Evolving Knowledge of Morphological Diversity. Paleobiology, 23: 181-206.

Foote, M., Gould, S.J., Lee, M.S.Y., Briggs, D.E.G., Fortey, R.A. and Wills, M.A., 1992. Cambrian and Recent morphological disparity. Science, 258: 1816-1818.

Gehling, J.G., Droser, M.L., Jensen, S.R. and Runnegar, B.N., 2005. Ediacara organisms: relating form to function. In: D.E.G. Briggs (Editor), Evolving Form and Function: Fossils and Development. Yale Peabody Museum Publications, New Haven, pp. 43-66.

Gibson, G.G., Teeter, S.A. and Fedonkin, M.A., 1984. Ediacarian fossils from the Carolina slate belt, Stanly County, North Carolina. Geology, 12: 387-390.

Glaessner, M.F., 1984. The dawn of animal life: a biohistorical study. Cambridge Univ. Press, Cambridge, United Kingdom, 244 pp.

Gould, S.J., 1991. The disparity of the Burgess Shale arthropod fauna and the limits of cladistic analysis: Why we must strive to quantify morphospace. Paleobiology, 17: 411-423.

Grazhdankin, D., 2004. Patterns of distribution in the Ediacaran biotas: facies versus biogeography and evolution. Paleobiology, 30: 203–221.

Grazhdankin, D. and Seilacher, A., 2002. Underground Vendobionta from Namibia. Palaeontology, 45: 57-78.

Grazhdankin, D. and Seilacher, A., 2005. A re-examination of the Nama-type Vendian organism *Rangea schneiderhoehni*. Geological Magazine, 142: 571-582 (doi:10.1017/S0016756805000920).

Grotzinger, J.P., Bowring, S.A., Saylor, B.Z. and Kaufman, A.J., 1995. Biostratigraphic and geochronologic constraints on early animal evolution. Science, 270: 598-604.

Hagadorn, J.W. and Waggoner, B.M., 2000. Ediacaran fossils from the southwestern Great Basin, United States. Journal of Paleontology, 74: 349-359.

Hofmann, H.J., 1981. First record of a Late Proterozoic faunal assemblage in the North American Cordillera. Lethaia, 14: 303-310.

Hofmann, H.J., Mountjoy, E.W. and Teitz, M.W., 1991. Ediacaran fossils and dubiofossils, Miette Group of Mount Fitzwilliam area, British Columbia. canadian Journal of Earth Sciences, 28: 1541-1552.

Huntley, J.W., Xiao, S. and Kowalewski, M., 2006. 1.3 billion years of acritarch history: An empirical morphospace approach. Precambrian Research, 144: 52-68.

Ivantsov, A.Y. and Grazhdankin, D., 1997. A new representative of the Petalonamae from the upper Vendian of the Arkhangelsk Region. Paleontological Journal (English Translation), 31: 1-16.

Jenkins, R.J.F., 1985. The enigmatic Ediacaran (Late Precambrian) genus *Rangea* and related forms. Paleobiology, 11: 336-355.

Jenkins, R.J.F., 1992. Functional and ecological aspects of Ediacaran assemblages. In: J.H. Lipps and P.W. Signor (Editors), Origin and Early Evolution of Metazoa. Plenum Press, New York, pp. 131-176.

Jenkins, R.J.F. and Gehling, J.G., 1978. A review of the frond-like fossils of the Ediacara assemblage. Record of South Australia Museum, 17: 347-359.

Kowalewski, M., Goodfriend, G.A. and Flessa, K.W., 1998. High resolution estimates of temporal mixing within shell beds: the evils and virtues of time-averaging. Paleobiology, 24: 287–304.

LaFlamme, M. and Narbonne, G.M., 2007. Ediacaran fronds. Palaeogeography Palaeoclimatology Palaeoecology, in press.

LaFlamme, M., Narbonne, G.M. and Anderson, M.M., 2004. Morphometric analysis of the Ediacaran frond Charniodiscus from the Mistaken Point Formation, Newfoundland. Journal of Paleontology, 78: 827-837.

Laflamme, M., Narbonne, G.M., Greentree, C. and Anderson, M.M., 2007. Morphology and taphonomy of an Ediacaran frond: *Charnia* from the Avalon Peninsula of

Newfoundland. Geological Society of London Special Publication, 286: in press.

Marcus, L.F., 1990. Traditional morphometrics. In: F.J. Rohlf and F.L. Bookstein (Editors), Proceedings of the Michigan Morphometrics Workshop (Special Publication Number 2). The University of Michigan Museum of Zoology, Ann Arbor, pp. 77-122.

Marshal, C.R., 2006. Explaining the Cambrian “explosion” of animals. Annual Review of Earth and Planetary Sciences, 34: 355-384.

Martin, M.W., Grazhdankin, D.V., Bowring, S.A., Evans, D.A.D., Fedonkin, M.A. and Kirschvink, J.L., 2000. Age of Neoproterozoic bilaterian body and trace fossils, White Sea, Russia: Implications for metazoan evolution. Science, 288: 841-845.

McCoy, S., Jaffré, T., Rigault, F. and Ash, J.E., 1999. Fire and succession in the ultramafic maquis of New Caledonia. Journal of Biogeography, 26: 579-594.

Narbonne, G.M., 1994. New Ediacaran fossils from the Mackenzie Mountains, northwestern Canada. Journal of Paleontology, 68: 411-416.

Narbonne, G.M., 2005. The Ediacara Biota: Neoproterozoic origin of animals and their ecosystems. Annual Review of Earth and Planetary Sciences, 33: 421-442.

Narbonne, G.M. and Aitken, J.D., 1990. Ediacaran fossils from the Sekwi Brook area, Mackenzie Mountains, northwestern Canada. Palaeontology, 33: 945-980.

Narbonne, G.M. and Gehling, J.G., 2003. Life after snowball: The oldest complex Ediacaran fossils. Geology, 31: 27-30.

Narbonne, G.M. and Hofmann, H.J., 1987. Ediacaran biota of the Wernecke Mountains, Yukon, Canada. Palaeontology, 30: 647-676.

Narbonne, G.M., Saylor, B.Z. and Grotzinger, J.P., 1997. The youngest Ediacaran fossils from southern Africa. Journal of Paleontology, 71: 953-967.

Peterson, K.J. and Butterfield, N.J., 2005. Origin of the Eumetazoa: Testing ecological predictions of molecular clocks against the Proterozoic fossil record. Proceedings of the National Academy of Sciences of the United States of America, 102: 9547-9552.

Roy, K., 1994. Effects of the Mesozoic Marine Revolution on the taxonomic, morphologic, and biogeographic evolution of a group:Aporrhaid gastropods during Mesozoic. Paleobiology, 20: 274-296.

Smith, A.G., 2001. Paleomagnetically and tectonically based global maps for Vendian to Mid-Ordovician time. In: A.Y. Zhuravlev and R. Riding (Editors), The Ecology of the Cambrian Radiation. Columbia University Press, New York, pp. 11-46.

Sokolov, B.S. and Iwanowski, A.B., 1990. The Vendian System, Volume 1: Paleontology. Springer-Verlag, Heidelberg, 383 pp.

Sun, W., 1986. Late Precambrian pennatulids (sea pens) from the eastern Yangtze Gorge, China: *Paracharnia* gen. nov. Precambrian Research, 31: 361-375.

van Zyll de Jong, M.C. and Cowx, I.G., 2005. Association between biogeographical factors and boreal lake fish assemblages. Fisheries Management and Ecology, 12: 189-199.

Waggoner, B., 2003. The Ediacaran biotas in space and time. Integrative and Comparative Biology, 43: 104-113.

Weaver, P.G., McMenamin, M.A.S. and Tacker, R.C., 2006. Paleoenvironmental and paleobiogeographic implications of a new Ediacaran body fossil from the Neoproterozoic Carolina Terrane, Stanly County, North Carolina. Precambrian Research, 150: 123-135.

Xiao, S., Shen, B., Zhou, C., Xie, G. and Yuan, X., 2005. A uniquely preserved Ediacaran fossil with direct evidence for a quilted bodyplan. Proceedings National Academy of Sciences, USA, 102: 10227-10232.

Xiao, S., Yuan, X., Steiner, M. and Knoll, A.H., 2002. Macroscopic carbonaceous compressions in a terminal Proterozoic shale: A systematic reassessment of the Miaohe biota, South China. Journal of Paleontology, 76: 345-374.

Figure 1.1 Ediacaran paleogeographic map and fossil localities. Modified from Waggoner (*1*). **Avalon assemblage** (stars): 1, Charnwood Forest, England; 2, Avalon Peninsula, Newfoundland. **White Sea assemblage** (squares): 3, Winter Coast and adjacent area, Russia; 4, Podolia, Ukraine; 5, Urals, Russia; 6, Finnmark, Norway; 7, Olenëk Uplift, Siberia; 8, Flinders Ranges, Australia; 9, Central Australia; 10, Wernecke Mountains, Canada; **Nama assemblage** (circles): 11, British Columbia, Canada; 12, Great Basin, United States; 13, southern Namibia. Baltica biota refers to Ediacara fossils of White Sea assemblage from four localities: Winter Coast and adjacent area, Russia; Podolia, Ukraine; Urals; and Finnmark, Norway.

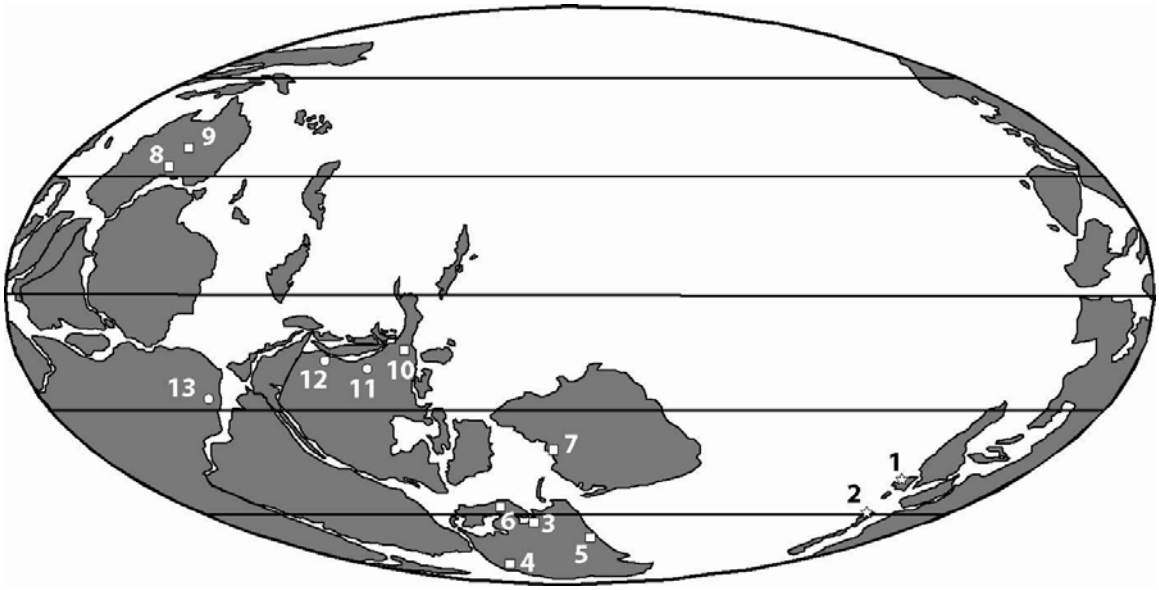

Figure 1.2 Taxonomic and morphology diversity of Ediacara fossils. (**A**) Taxonomic richness measured as number of genera from raw data, genus-level richness standardized at 400 specimens, and number of morphotypes standardized at 400 specimens. Bars represent 95% confidence intervals, each estimated using 1000 independent rarefaction runs. (**B**) Rarefaction analysis showing relation between sampling intensity and diversity. Mean genus-level diversity and mean morphotype diversity estimated using 1000 independent rarefaction runs. (**C**) MDS ordination plot with convex hulls delineating the morphospace range realized by the three Ediacara assemblages. (**D**) Percentage of shared morphospace or genera among the three Ediacara assemblages. (**E**) MDS ordination plot and convex hulls of four Ediacara biotas within the White Sea assemblage—the Baltica, Flinders Ranges, Siberia, and Wernecke biotas. (**F**) Rarefaction analysis showing the effect of sampling intensity (number of species occurrences) on realized morphospace of the White Sea assemblage. Morphospace size (black) and 95% confidence interval (red) estimated from 100 independent rarefaction runs. (**G**) MDS ordination plot and convex hulls of the Newfoundland biota of the Avalon assemblage, the Flinders Ranges biota of the White Sea assemblage, and the Namibia biota of the Nama assemblage. (**H**) MDS variance (solid red line) compared against predictions of the constant-disparity null model estimated using a Monte Carlo simulation that calculates expected variation in MDS scores if the disparity of the three assemblages were identical (dashed red lines are the 95% confidence intervals of the null model estimated using 1000 randomization runs). Note that two of the three assemblages are located outside the 95% confidence intervals predicted by the null model of time-invariant morphospace. MDC estimates (blue line) with 95% confidence intervals (brackets; estimated separately for each of the three Ediacara assemblages using 500 balanced-bootstrap iterations).

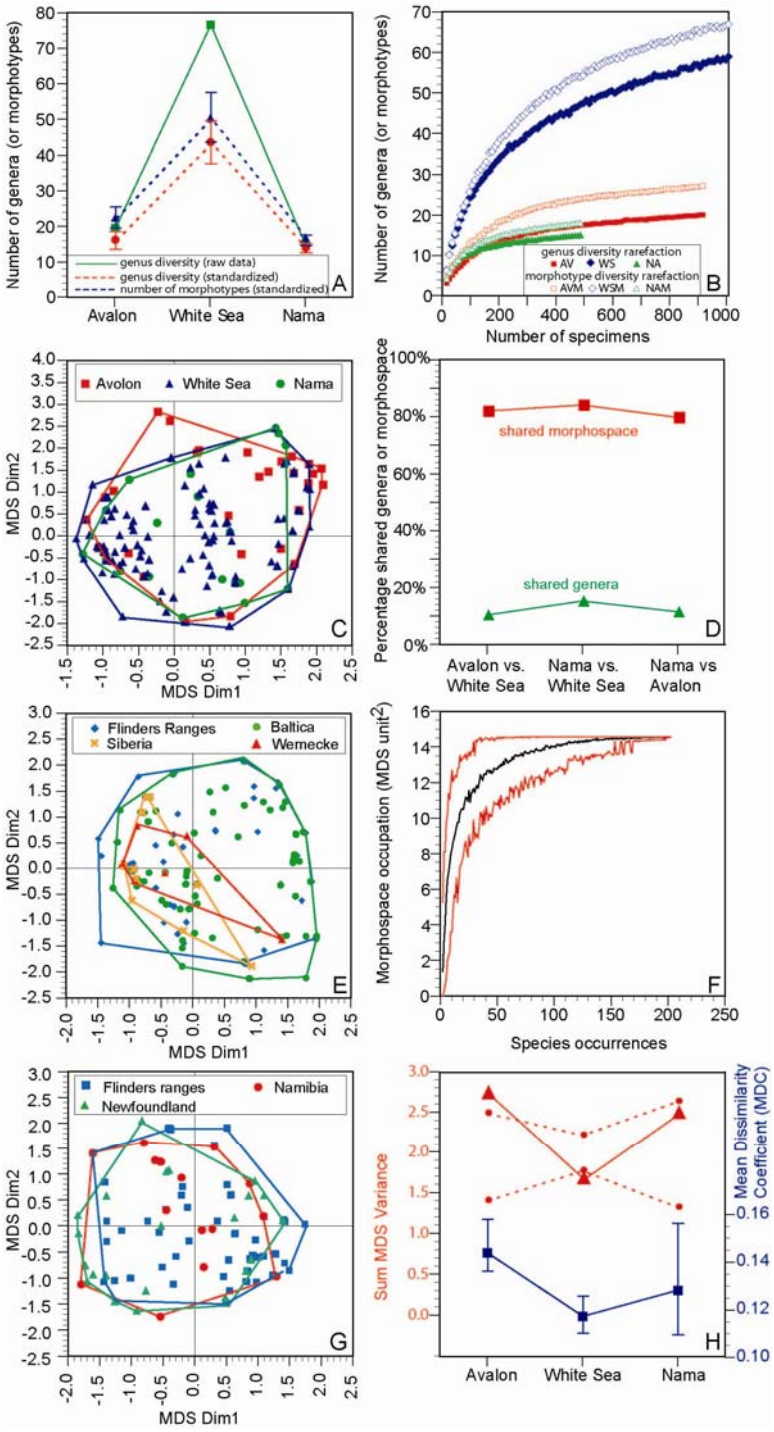
Number of genera (or morphotypes)
genus diversity (raw data)
genus diversity (standardized)
number of morphotypes (standardized)
A
Avalon
White Sea
Nama
Number of genera (or morphotypes)
genus diversity rarefaction
AV WS NA
morphotype diversity rarefaction
AVM WSM NAM
B
Number of specimens
Avalon
White Sea
Nama
MDS Dim2
MDS Dim1
C
Percentage shared genera or morphospace
shared morphospace
shared genera
D
Avalon vs. White Sea
Nama vs. White Sea
Nama vs Avalon
Flinders Ranges
Siberia
Baltica
Wernecke
MDS Dim2
MDS Dim1
E
Morphospace occupation (MDS unit²)
F
Species occurrences
Flinders ranges
Newfoundland
Namibia
MDS Dim2
MDS Dim1
G
Sum MDS Variance
Mean Dissimilarity Coefficient (MDC)
H
Avalon
White Sea
Nama

Figure 1.3 Results of MDS analysis using three-dimensional ordination. (**A-B**) MDS ordination plots and convex hulls of the three Ediacara assemblages. (**C**) Sum MDS variances from two-dimensional and three-dimensional ordinations. (**D**) Total character variances and MDC (95% confidence intervals based on 500 balanced bootstrap iterations) of the three Ediacara assemblages.

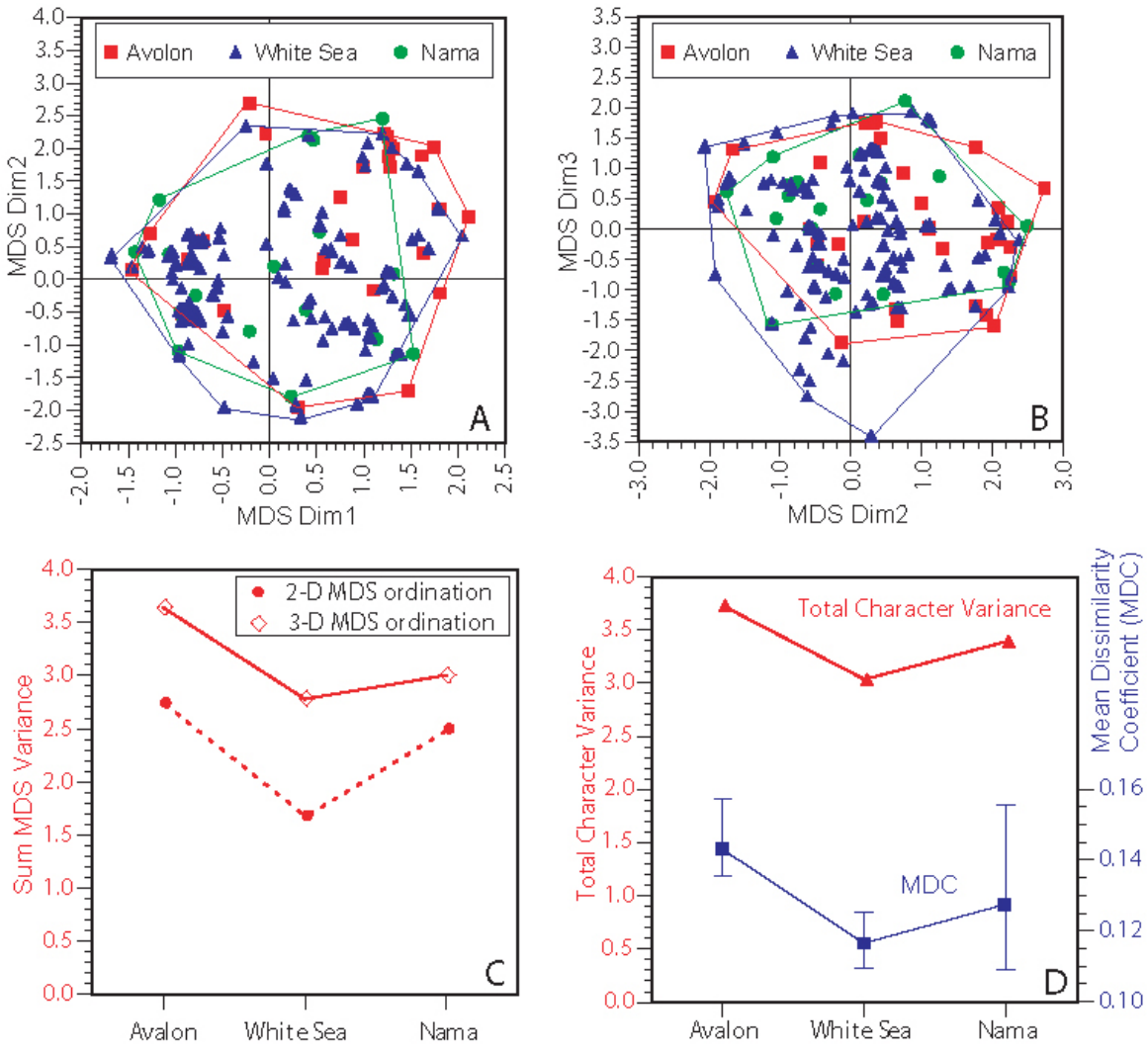

Table 1.1 Summary of the literature data. Localities were assigned to continents and assemblages. Number of morphotype refers to the total number of unique morphotypes that could be distinguished using our coding of 50 morphological characters. Assignment of localities to assemblages followed Waggoner (*S1*). Flinders Ranges data were based on 18 publications and one unpublished specimen reposited at Yale University Peabody Museum (YPM-204511).

Assemblage	Continent	Basin or Locality	Species occurrences	No. Morphotypes	No. Ref.
White Sea	Baltica	Winter Coast and adjacent areas (White Sea)	69	45	10
		Podolia	26	13	2
		Ural	11	7	2
		Finnmark	6	5	1
	Siberia	Olenëk Uplift	10	7	3
	Australia	Flinders Ranges and Mt. Skinner, Northern Territory	67	42	18 plus YPM-204511
	Laurentia	Wernecke	13	6	1
Nama	Kalahari	Namibia (Nama)	16	14	11
	Laurentia	Great Basin	2	2	1
		British Columbia	6	5	2
Avalon	Avalon	Newfoundland	23	21	8
		Charnwood	10	8	3
N/A	Laurentia	Mackenzie Mts.	13	9	3

Table 1.2 Number of genera, species occurrences, morphotypes, specimens, and preservational quality, with data grouped by sedimentary basins or biotas. The preservational quality of each continent was estimated as the number (or percentage; in brackets) of genera that were characterized by fair or better preservation. Siberia specimens were coded on the basis of description only, so the preservational quality data are not available.

Sedimentary Basins or biotas	No. Genera	No. Species occurrences	No. Morphotypes	Estimated No. specimens	Preservational quality
Newfoundland	16	23	21	888	15 (94%)
Baltica	58	112	49	1670	47 (81%)
Flinders Ranges	34	67	42	1190	25 (74%)
Siberia	6	10	7	454	not available
Wernecke	6	13	6	476	1 (17%)
Namibia	12	16	14	453	11 (92%)

Table 1.3 Number of genera, species occurrences, morphotypes, specimens, and preservation quality, with data grouped into assemblages. The preservational quality of each assemblage was estimated as the number (or percentage; in brackets) of genera that were characterized by fair or better preservation.

Assemblage	No. Genera	No. Species occurrences	No. Morphotypes	No. Specimens	Preservational quality
Avalon	20	33	27	918	16 (80%)
White Sea	77	202	81	3790	64 (80%)
Nama	15	24	18	485	12 (80%)

Table 1.4. Character codings for Ediacara fossils.

AS	CO	BT	Rf	Genus	Species	Figures	C	F	O	A	L	S	Rd	Up	Bp	Md	Tr	Te	Pe	Ctu	Csm	Cbo	Cgr	Cri	Clr	Csr	Ctr	Ctv	Cco	Cdr	Cra	Csp	Cta	Cis	Cid	Pp	P1	P2	S1	S2	Sec	Ter	Mfa	Msm	Mra	Mdr	Mmr	Mco	Mtu	Psm	Pra	Pco	Sk	Dh	Sc	Sp
AV	AV	NF	(1)	*Charniodiscus*	*procerus*	F3.1-3.4	0	0	0	0	0	1	0	1	0	0	0	0	0	0	0	0	0	0	0	0	1	0	0	0	0	0	0	0	0	1	0	0	1	0	0	0	0	0	0	0	0	0	0	0	0	0	1	1	0	0
AV	AV	NF	(1)	*Charniodiscus*	*spinosus*	F2.1,3.1,4.1-4.4	0	0	0	0	0	1	0	1	0	0	0	0	0	0	0	0	0	1	0	0	0	0	0	0	0	0	0	0	0	1	0	0	1	0	0	0	0	0	0	0	0	0	0	0	0	0	1	1	0	1
AV	AV	NF	(1)	*Charniodiscus*	*arboreus*	F4.5	0	0	0	0	0	1	0	1	0	0	0	0	0	0	0	0	0	1	0	0	0	0	0	0	0	0	0	0	0	1	0	0	0	0	0	0	0	0	0	0	0	0	0	0	0	0	1	1	0	0
AV	AV	NF	(2)	*Charnia*	*masoni*	P1-I	0	0	0	0	0	1	0	1	0	1	0	0	0	0	0	0	0	0	0	0	1	0	0	0	0	0	0	0	0	1	0	0	1	0	0	0	0	0	0	0	0	0	0	0	0	0	0	0	0	0
AV	AV	NF	(3)	*Charnia*	*wardi*	F3	0	0	0	0	0	1	0	1	0	1	0	0	0	0	0	0	0	0	0	0	1	0	0	0	0	0	0	0	0	1	0	0	1	0	0	1	0	0	0	0	0	0	0	0	0	0	0	0	0	0
AV	AV	NF	(4)	Rangeomorph-frondlet	frondlet-B	F2A,B	0	0	0	0	0	1	0	1	0	1	0	0	0	0	0	0	0	0	0	0	1	0	0	0	0	0	0	0	0	1	0	0	0	1	0	0	0	0	0	0	0	0	0	0	0	0	1	0	0	0
AV	AV	NF	(4)	Rangeomorph-plumose	plumose	F2C,D	0	0	1	0	0	0	0	1	0	1	0	0	0	0	0	0	1	0	0	0	0	0	0	0	0	0	0	0	0	1	0	0	0	1	0	0	0	0	0	0	0	0	0	0	0	0	0	0	0	0
AV	AV	NF	(4)	Rangeomorph-spindle	spindle	F3F	0	0	0	0	0	1	0	0	1	1	0	0	0	0	0	0	1	0	0	0	0	0	0	0	0	0	0	0	0	1	0	0	0	1	0	0	0	0	0	0	0	0	0	0	0	0	0	0	0	0
AV	AV	NF	(4)	Rangeomorph-bush	bush	F3E	0	1	0	0	0	0	0	1	0	1	0	0	0	0	0	0	0	0	0	0	0	0	0	0	1	0	0	0	0	0	0	0	0	1	0	0	0	0	0	0	0	0	0	0	0	0	0	0	0	0
AV	AV	NF	(2)	Pizza Disc		F3G	1	0	0	0	0	0	1	0	0	0	0	0	0	1	0	0	0	0	0	0	0	0	0	0	0	0	0	0	0	0	0	0	0	0	0	0	0	0	0	0	0	0	0	0	0	0	0	0	0	0
AV	AV	NF	(2)	Rangeomorph-spindle	spindle-A	P1-B	0	0	0	0	0	1	0	1	0	1	0	0	0	0	0	0	1	0	0	0	0	0	0	0	0	0	0	0	0	0	1	0	0	1	0	0	0	0	0	0	0	0	0	0	0	0	0	0	0	0
AV	AV	NF	(2)	Rangeomorph-comb	comb	P1-E	0	0	0	1	0	0	0	1	0	1	0	0	0	0	0	0	0	0	0	0	0	0	0	0	0	0	0	0	0	1	0	0	0	1	0	0	0	0	0	0	0	0	0	0	0	0	0	0	0	0
AV	AV	NF	(2)	Rangeomorph-network	network	P1-F	0	0	1	0	0	0	0	0	1	1	0	0	0	0	0	0	1	0	0	0	0	0	0	0	0	0	0	0	0	0	0	1	0	1	0	0	0	0	0	0	0	0	0	0	0	0	0	0	0	0
AV	AV	NF	(2)	*Hiemalora*	sp.	P1-H	1	0	0	0	0	0	1	0	0	0	0	0	0	0	1	0	0	0	0	0	0	0	0	0	0	0	0	0	0	0	0	0	0	0	0	0	0	0	1	0	0	0	0	0	0	0	0	0	0	0
AV	AV	NF	(5)	*Aspidella*	*terranovica*	F6A	1	0	0	0	0	0	1	0	0	0	0	0	0	0	0	1	0	0	0	0	0	0	0	0	1	0	0	0	0	0	0	0	0	0	0	0	0	1	0	0	0	0	0	0	0	0	0	0	0	0
AV	AV	NF	(5)	*Ediacaria*	sp.	F6E	1	0	0	0	0	0	1	0	0	0	0	0	0	0	0	1	0	0	0	0	0	0	1	0	0	0	0	0	0	0	0	0	0	0	0	0	0	0	0	0	0	0	0	0	0	0	0	0	0	0
AV	AV	NF	(5)	*Spriggia*	sp.	F6J	1	0	0	0	0	0	1	0	0	0	0	0	0	0	0	?	0	0	0	0	0	0	1	0	0	0	0	0	0	0	0	0	0	0	0	0	0	0	0	0	0	0	0	0	0	0	0	0	0	0
AV	AV	NF	(5)	*Triforillonia*	*costellae*	F17-A-H	0	0	0	0	1	0	0	0	0	0	1	0	0	0	0	?	0	0	0	0	0	0	0	0	1	0	0	0	0	0	0	0	0	0	0	0	0	0	0	0	0	0	0	0	0	0	0	0	0	0
AV	AV	NF	(6)	Bush-like form		F5A	0	0	0	0	0	1	0	1	0	0	0	0	0	0	0	0	0	0	0	0	1	0	0	0	0	0	0	0	0	1	0	0	0	1	0	1	0	0	0	0	0	0	0	0	0	0	0	?	0	0
AV	AV	NF	(6)	Ladder-like form		F4B	0	0	0	1	0	0	0	0	1	0	0	0	0	0	0	0	0	0	0	0	0	1	0	0	0	0	0	0	0	0	0	0	0	0	0	0	0	0	0	0	0	0	0	0	0	0	0	0	0	0
AV	AV	NF	(7)	*Thectardis*	*avalonensis*	F2,3	0	0	0	1	0	0	0	0	0	0	1	0	0	0	1	0	0	0	0	0	0	0	0	0	0	0	0	0	0	0	0	0	0	0	0	0	0	0	0	0	0	0	0	0	0	0	0	0	0	0
AV	AV	NF	(2)	*Bradgatia*	*linfordensis*	P1.D	0	1	0	0	0	0	0	1	0	1	0	0	0	0	0	0	0	0	0	0	0	0	0	0	1	0	0	0	0	0	0	0	0	1	0	?	0	0	0	0	0	0	0	0	0	0	0	?	0	0
AV	AV	NF	(8)	Star-Shaped form		F3	1	0	0	0	0	0	1	0	0	0	0	0	0	0	1	0	0	0	0	0	0	0	0	0	0	0	0	0	0	0	0	0	0	0	0	0	0	0	0	1	0	0	0	0	0	0	0	0	0	0
AV	AV	CF	(9)	*Charnia*	*masoni*	F1	0	0	0	0	0	1	0	1	0	1	0	0	0	0	0	0	1	0	0	0	0	0	0	0	0	0	0	0	0	1	0	0	1	0	0	0	0	0	0	0	0	0	0	0	0	0	0	0	0	0
AV	AV	CF	(9)	*Charniodiscus*	*concentricus*	F2	0	0	0	0	0	1	0	1	0	0	0	0	0	0	0	0	0	1	0	0	0	0	0	0	0	0	0	0	0	1	0	0	1	0	0	0	0	0	0	0	0	0	0	0	0	0	1	1	0	0
AV	AV	CF	(9)	*Charnia*	*grandis*	F3	0	0	0	0	0	1	0	1	0	1	0	0	0	0	0	0	1	0	0	0	0	0	0	0	0	0	0	0	0	1	0	0	1	0	0	0	0	0	0	0	0	0	0	0	0	0	0	0	0	0
AV	AV	CF	(10)	*Bradgatia*	*linfordensis*	F3,4	0	1	0	0	0	0	0	1	0	1	0	0	0	0	0	0	0	0	0	0	0	0	0	0	1	0	0	0	0	0	0	0	0	1	0	?	0	0	0	0	0	0	0	0	0	0	0	?	0	0
AV	AV	CF	(10)	*Ivesia*	*lobata*	F12, 13	0	0	1	0	0	0	0	0	1	0	0	0	0	0	0	0	0	0	0	0	0	1	0	0	0	0	0	0	0	0	0	0	0	0	0	0	0	0	0	0	0	0	0	0	0	0	0	0	0	0
AV	AV	CF	(10)	*Cyclomedusa*	*cliffi*	F14	1	0	0	0	0	0	1	0	0	0	0	0	0	0	0	0	0	0	0	0	0	0	1	0	0	0	0	0	0	0	0	0	0	0	0	0	0	0	0	0	0	0	0	0	0	0	0	0	0	0
AV	AV	CF	(10)	*Shepshedia*	*palmata*	F16	0	0	0	0	0	1	0	1	0	0	0	0	0	0	0	0	0	0	0	0	0	0	0	0	0	0	0	0	0	0	0	0	0	0	0	0	0	0	0	0	0	0	0	0	0	0	0	0	0	0
AV	AV	CF	(10)	*Blackbrookia*	*oaksi*	F17	0	0	0	1	0	0	0	0	0	0	0	1	0	0	1	0	0	0	0	0	0	0	0	0	0	0	0	0	0	0	0	0	0	0	0	0	0	0	0	0	0	0	0	0	0	0	0	0	0	0
AV	AV	CF	(9)	*Cyclomedusa*	*davidi*	F6	1	0	0	0	0	0	1	0	0	0	0	0	0	0	0	0	0	0	0	0	0	0	1	0	0	0	0	0	0	0	0	0	0	0	0	0	0	0	0	0	0	0	0	0	0	0	0	0	0	0
AV	AV	CF	(11)	*Pseudovendia*	*charnwoodensis*	P20	0	0	1	0	0	0	0	1	0	0	0	0	0	0	0	0	0	1	0	0	0	0	0	0	0	0	0	0	0	1	0	0	0	0	0	0	1	0	0	0	0	0	0	0	0	0	0	0	0	0
WS	AU	FR	(12)	*Nemiana*	*simplex*	N/A	1	0	0	0	0	0	1	0	0	0	0	0	0	0	1	0	0	0	0	0	0	0	0	0	0	0	0	0	0	0	0	0	0	0	0	0	0	0	0	0	0	0	0	0	0	0	0	0	0	0
WS	AU	FR	(13)	*Cyclomedusa*	*radiata*	P42-2	1	0	0	0	0	0	1	0	0	0	0	0	0	0	0	0	0	0	0	0	0	0	1	0	0	0	0	0	0	0	0	0	0	0	0	0	0	0	1	0	0	0	0	0	0	0	0	0	0	0
WS	AU	FR	(13)	*Cyclomedusa*	*radiata*	P42-1	1	0	0	0	0	0	1	0	0	0	0	0	0	0	0	?	0	0	0	0	0	0	1	0	1	0	0	0	0	0	0	0	0	0	0	0	0	0	0	0	0	0	0	0	0	0	0	0	0	0
WS	AU	FR	(14)	*Ediacaria*	*flindersi*	P99-6	1	0	0	0	0	0	1	0	0	0	0	0	0	0	0	0	0	0	0	0	0	0	1	0	0	0	0	0	0	0	0	0	0	0	0	0	0	0	0	0	0	0	0	0	0	0	0	0	0	0
WS	AU	FR	(13)	*Ediacaria*	*flindersi*	P43-1	1	0	0	0	0	0	1	0	0	0	0	0	0	0	0	1	0	0	0	0	0	0	?	0	0	0	0	0	0	0	0	0	0	0	0	0	0	0	1	0	0	0	0	0	0	0	0	0	0	0
WS	AU	FR	(14)	*Ovatoscutum*	*concentricum*	P97-8	0	0	1	0	0	0	1	0	0	0	0	0	0	0	0	0	0	0	0	0	0	0	1	0	0	0	0	0	0	0	0	0	0	0	0	0	0	0	0	0	0	1	0	0	0	0	0	0	0	0
WS	AU	FR	(14)	*Tribrachidium*	*heraldicum*	P97-9; P99-5; P101-5	1	0	0	0	0	0	0	0	0	0	1	0	0	0	0	0	0	0	0	0	0	0	0	0	0	1	0	1	0	0	0	0	0	0	0	0	0	0	1	0	0	0	0	0	0	0	0	0	0	0
WS	AU	FR	(14)	*Dickinsonia*	*costata*	P101-4	0	0	1	0	0	0	0	0	1	0	0	0	0	0	0	0	1	0	0	0	0	0	0	0	0	0	0	0	0	0	0	1	0	0	0	0	0	0	0	0	0	0	0	0	0	0	0	0	0	0
WS	AU	FR	(15)	*Dickinsonia*	*lissa*	P6-6; P7-1,4	0	0	1	0	0	0	0	0	1	0	0	0	0	0	0	0	1	0	0	0	0	0	0	0	0	0	0	0	0	0	0	1	0	0	0	0	0	0	0	0	0	0	0	0	0	0	0	0	0	0
WS	AU	FR	(14)	*Pseudorhizostomites*	*howchini*	P103-2-4	1	0	0	0	0	0	1	0	0	0	0	0	0	0	0	?	0	0	0	0	0	0	0	0	1	0	0	0	0	0	0	0	0	0	0	0	0	0	0	0	0	0	0	0	0	0	0	0	0	0
WS	AU	FR	(14)	*Beltanella*	*gilesi*	N/A	1	0	0	0	0	0	1	0	0	0	0	0	0	0	0	1	0	0	0	0	0	0	0	0	0	0	0	0	0	0	0	0	0	0	0	0	0	1	0	0	0	0	0	0	0	0	0	0	0	0
WS	AU	FR	(14)	*Medusinites*	*asteroides*	P97-1-4	1	0	0	0	0	0	1	0	0	0	0	0	0	0	0	0	0	0	0	0	0	0	1	0	0	0	0	0	0	0	0	0	0	0	0	0	0	0	0	0	0	0	0	0	0	0	0	0	0	0
WS	AU	FR	(14)	*Medusinites*	*asteroides*	P97-5	1	0	0	0	0	0	1	0	0	0	0	0	0	0	1	0	0	0	0	0	0	0	0	0	0	0	0	0	0	0	0	0	0	0	0	0	0	0	1	0	0	0	0	0	0	0	0	0	0	0
WS	AU	FR	(14)	*Cyclomedusa*	*plana*	P98-1-3	1	0	0	0	0	0	1	0	0	0	0	0	0	0	0	?	0	0	0	0	0	0	1	0	0	0	0	0	0	0	0	0	0	0	0	0	0	0	?	0	0	0	0	0	0	0	0	0	0	0
WS	AU	FR	(14)	*Mawsonites*	*spriggi*	P99-1	1	0	0	0	0	0	1	0	0	0	0	0	0	0	1	0	0	0	0	0	0	0	0	0	0	0	0	0	0	0	0	0	0	0	0	0	0	0	1	0	0	1	0	0	1	0	0	0	0	0
WS	AU	FR	(14)	*Mawsonites*	*spriggi*	P99-2	1	0	0	0	0	0	1	0	0	0	0	0	0	0	1	0	0	0	0	0	0	0	0	0	0	0	0	0	0	0	0	0	0	0	0	0	0	0	1	0	0	0	0	0	0	0	0	0	0	0
WS	AU	FR	(14, 16)	*Conomedusa*	*lobatus*	P99-3-4	0	0	0	1	0	0	0	0	0	0	0	1	0	0	0	1	0	0	0	0	0	0	0	0	0	0	0	1	0	0	0	0	0	0	0	0	0	0	1	0	0	0	0	0	0	0	0	0	0	0
WS	AU	FR	(14)	*Lorenzinites*	*rarus*	P100-1	1	0	0	0	0	0	1	0	0	0	0	0	0	0	0	1	0	0	0	0	0	0	0	0	0	0	0	0	0	0	0	0	0	0	0	0	0	0	1	0	0	0	0	0	0	0	0	0	0	0
WS	AU	FR	(14)	*Rugoconites*	*enigmaticus*	P100-2-3	1	0	0	0	0	0	1	0	0	0	0	0	0	0	0	?	0	0	0	0	0	0	0	1	0	0	0	0	0	0	0	0	0	0	0	0	0	0	0	0	0	0	0	0	0	0	0	0	0	0
WS	AU	FR	(13)	*Eoporpita*	*medusa*	P40-1-6; P41-6a,b	1	0	0	0	0	0	1	0	0	0	0	0	0	0	0	0	0	0	0	0	0	0	1	0	0	0	0	0	0	0	0	0	0	0	0	0	0	0	1	0	0	0	0	0	0	0	0	0	0	0
WS	AU	FR	(14)	*Kimberia*	*quadrata*	P97-6	0	0	1	0	0	0	0	0	1	0	0	0	0	0	0	0	?	0	0	0	0	1	0	0	0	0	0	0	0	0	0	0	0	0	0	0	0	0	1	0	0	0	0	1	0	0	0	0	0	0
WS	AU	FR	(14)	*Rangea*	*longa*	P100-4	0	0	0	0	0	1	0	1	0	1	0	0	0	0	0	0	0	1	0	0	0	0	0	0	0	0	0	0	0	1	0	0	1	0	0	0	0	0	0	0	0	0	0	0	0	0	?	?	0	0
WS	AU	FR	(14)	*Rangea*	*grandis*	P100-5	0	0	0	0	0	1	0	1	0	1	0	0	0	0	0	0	1	0	0	0	0	0	0	0	0	0	0	0	0	1	0	0	1	0	0	0	0	0	0	0	0	0	0	0	0	0	0	0	0	0
WS	AU	FR	(14)	*Pteridinium*	*simplex*	P101-1-3	0	0	0	0	0	1	0	0	1	0	0	0	0	0	0	0	1	0	0	0	0	0	0	0	0	0	0	0	0	1	0	0	0	0	0	0	0	0	0	0	0	0	0	0	0	0	0	0	0	0
WS	AU	FR	(14)	*Arborea*	*arborea*	P102-1,2	0	0	0	0	0	1	0	1	0	1	0	0	0	0	0	0	0	1	0	0	0	0	0	0	0	0	0	0	0	1	0	0	1	0	0	0	0	0	0	0	0	0	0	0	0	0	?	?	0	0
WS	AU	FR	(14)	*Dickinsonia*	*elongata*	P102-3	0	0	1	0	0	0	0	0	1	0	0	0	0	0	0	0	1	0	0	0	0	0	0	0	0	0	0	0	0	0	0	1	0	0	0	0	0	0	0	0	0	0	0	0	0	0	0	0	0	0
WS	AU	FR	(14)	*Dickinsonia*	*tenuis*	P103-1	0	0	1	0	0	0	0	0	1	0	0	0	0	0	0	0	1	0	0	0	0	0	0	0	0	0	0	0	0	0	0	1	0	0	0	0	0	0	0	0	0	0	0	0	0	0	0	0	0	0
WS	AU	FR	(14)	*Spriggina*	*ovata*	P98-4	0	0	1	0	0	0	0	1	0	0	0	0	0	0	0	0	1	0	0	0	0	0	0	0	0	0	0	0	0	1	0	0	0	0	0	0	1	0	0	0	0	0	0	0	0	0	0	0	0	0
WS	AU	FR	(17)	*Spriggina*	*ovata*	P1-1-3	0	0	0	0	0	1	0	1	0	0	0	0	0	0	0	0	1	0	0	0	0	0	0	0	0	0	0	0	0	1	0	0	0	0	0	0	1	0	0	0	0	0	0	0	0	0	0	0	0	0
WS	AU	FR	(18)	*Praecambridium*	*sigillum*	P102-4	0	0	1	0	0	0	0	1	0	0	0	0	0	0	0	0	0	1	0	0	0	0	0	0	0	0	0	0	0	?	1	0	0	0	0	0	1	1	0	0	0	0	0	0	0	0	0	0	0	0
WS	AU	FR	(19)	*Parvancorina*	*minchami*	N/A	0	1	0	0	0	0	0	1	0	0	0	0	0	0	0	0	0	1	1	0	0	0	0	0	0	0	0	0	0	0	0	0	0	0	0	0	1	1	0	0	0	0	0	0	0	0	0	0	0	0
WS	AU	FR	(13)	*Cyclomedusa*	*davidi*	P41-1,2,5	1	0	0	0	0	0	1	0	0	0	0	0	0	0	0	1	0	0	0	0	0	0	1	0	0	0	0	0	0	0	0	0	0	0	0	0	0	0	0	0	0	0	0	0	0	0	0	0	0	0
WS	AU	FR	(13)	*Cyclomedusa*	*davidi*	P41-3	1	0	0	0	0	0	1	0	0	0	0	0	0	0	0	1	0	0	0	0	0	0	1	0	0	0	0	0	0	0	0	0	0	0	0	0	0	0	1	0	0	1	0	0	0	0	0	0	0	0
WS	AU	FR	(13)	*Brachina*	*delicata*	P42-3-5	1	0	0	0	0	0	1	0	0	0	0	0	0	0	0	0	0	0	0	0	0	0	1	0	0	0	0	0	0	0	0	0	0	0	0	0	0	0	1	0	0	0	0	0	0	0	0	0	0	0
WS	AU	FR	(13)	*Kimberia*	*quadrata*	P43-2a,b; 6	0	0	1	0	0	0	0	0	1	0	0	0	0	0	0	0	?	0	0	0	0	1	0	0	0	0	0	0	0	0	0	0	0	0	0	0	0	0	1	0	0	0	0	1	0	0	0	0	0	0
WS	AU	FR	(13)	*Rugoconites*	*tenuirugosus*	P43-5-7	1	0	0	0	0	0	1	0	0	0	0	0	0	1	0	0	0	0	0	0	0	0	0	0	0	0	0	0	0	0	0	0	0	0	0	0	0	0	0	1	0	0	0	0	0	0	0	0	0	0
WS	AU	FR	(15)	*Dickinsonia*	*brachina*	P6-5	0	0	1	0	0	0	0	0	1	0	0	0	0	0	0	0	1	0	0	0	0	0	0	0	0	0	0	0	0	0	0	1	0	0	0	0	0	0	0	0	0	0	0	0	0	0	0	0	0	0
WS	AU	CA	(20)	*Hallidaya*	*brueri*	P68-1,3-6; P69-1-5	1	0	0	0	0	0	1	0	0	0	0	0	0	1	0	0	0	0	0	0	0	0	0	0	0	0	0	0	0	0	0	0	0	0	0	0	0	0	0	1	0	0	0	0	0	0	0	0	0	0
WS	AU	CA	(20)	*Skinnera*	*brooksi*	P69-8-12	1	0	0	0	0	0	0	0	0	0	1	0	0	1	0	?	0	0	0	0	0	0	0	0	0	0	0	1	0	0	0	0	0	0	0	0	0	0	0	0	0	0	1	0	0	0	0	0	0	0
WS	AU	FR	(21)	*Inaria*	*karli*	F6A	1	0	0	0	0	0	0	1	0	0	0	0	0	0	0	0	0	0	0	0	0	1	0	0	0	0	0	0	0	0	0	0	0	0	0	0	0	0	0	0	0	0	0	0	0	0	0	0	0	0
WS	AU	FR	(21)	*Inaria*	*karli*	F6F	1	0	0	0	0	0	1	0	0	0	0	0	0	0	1	0	0	0	0	0	0	0	0	0	0	0	0	0	0	0	0	0	0	0	0	0	0	0	1	0	0	0	0	0	0	0	0	0	0	0

WS AU FR (21)	*Inaria*	*karli*	F6G	1	0	0	0	0	0	1	0	0	0	0	0	0	0	0	1	0	0	0	0	0	0	0	0	1	0	0	0	0	0	0	0	0	0	0	0	0	0	0	0	0	0	0	0	0	0	0	0	0	0
WS AU FR (22)	*Arkarua*	*adami*	F3-6	1	0	0	0	0	0	0	0	0	0	0	0	1	0	0	?	0	0	0	0	0	0	0	0	1	0	0	1	0	0	0	0	0	0	0	0	0	0	1	0	0	0	0	0	0	0	0	0	0	0
WS AU FR (23)	*Marywadea*	*ovata*	F1	0	0	1	0	0	0	0	1	0	0	0	0	0	0	0	0	1	0	0	0	0	0	0	0	0	0	0	0	0	1	0	0	0	0	0	0	1	0	0	0	0	0	0	0	0	0	0	0	0	0
WS AU FR (24)	*Palaeophragmodictya*	*reticulata*	F4-6	1	0	0	0	0	0	1	0	0	0	0	0	0	0	0	1	0	0	0	0	0	0	1	0	1	0	0	0	0	0	0	0	0	0	0	0	0	0	1	0	0	0	0	0	0	0	0	0	0	0
WS AU FR (25)	*Glaessnerina*	sp.	N/A	0	0	0	0	0	1	0	1	0	0	0	0	0	0	0	0	0	0	0	0	1	0	0	0	0	0	0	0	0	1	0	0	1	0	0	0	0	0	0	0	0	0	0	0	0	0	0	0	0	0
WS AU FR (25)	*Phylozoa*	*hanseni*	F7	0	0	0	0	0	1	0	1	?	0	0	0	0	0	0	0	1	0	0	0	0	0	0	0	0	0	0	0	0	1	0	0	0	0	0	0	0	0	0	0	0	0	0	0	0	0	0	0	0	0
WS AU FR (26, 27)	*Chondroplon*	*bilobatum*	N/A	0	0	1	0	0	0	0	1	?	0	0	0	0	0	0	0	?	0	0	0	0	1	0	0	0	0	0	0	0	0	?	0	0	0	0	0	0	0	0	0	0	0	0	0	0	0	0	0	0	0
WS AU FR (25)	*Charniodiscus*	*oppositus*	F5,6	0	0	0	0	0	1	0	1	0	0	0	0	0	0	0	0	0	0	0	0	1	0	0	0	0	0	0	0	0	1	0	0	1	0	0	0	0	0	0	0	0	0	0	0	0	0	1	1	0	0
WS AU FR (28)	*Mawsonites*	*randellensis*	F1,2	1	0	0	0	0	0	1	0	0	0	0	0	0	0	0	0	0	0	0	0	0	0	1	0	?	0	0	0	0	0	0	0	0	0	0	0	0	0	1	0	0	1	0	0	1	0	0	0	0	0
WS AU FR (12)	*Yorgia*	sp.	N/A	0	0	1	0	0	0	0	1	0	0	0	0	0	0	0	0	1	0	0	0	0	0	0	0	0	0	0	0	0	0	1	0	0	0	0	0	1	0	0	0	0	0	0	0	0	0	0	0	0	0
WS AU FR (12)	*Hiemalora*	sp.	N/A	1	0	0	0	0	0	1	0	0	0	0	0	0	0	1	0	0	0	0	0	0	0	0	0	0	0	0	0	0	0	0	0	0	0	0	0	0	0	1	0	0	0	0	0	0	0	0	0	0	0
WS AU FR (12)	*Anfesta*	sp.	N/A	1	0	0	0	0	0	0	0	0	0	1	0	0	0	0	0	0	0	0	0	0	0	0	0	1	0	0	0	1	0	0	0	0	0	0	0	0	0	0	0	0	0	0	0	0	0	0	0	0	0
WS AU FR (12)	*Vaveliksia*	*vana*	N/A	0	0	1	0	0	0	0	1	0	0	0	0	0	0	1	0	0	0	0	0	0	0	0	0	0	0	0	0	0	0	0	0	0	0	0	0	0	0	0	0	0	0	0	0	0	0	0	1	0	0
WS AU FR (12)	*Ivesheadia*	sp.	N/A	0	0	1	0	0	0	0	0	1	0	0	0	0	0	0	0	0	0	0	0	0	1	0	0	0	0	0	0	0	0	0	0	0	0	0	0	0	0	0	0	0	0	0	0	0	0	0	0	0	0
WS AU FR (12)	*Archaeaspis*	*fedonkini*	N/A	0	0	1	0	0	0	0	1	0	0	0	0	0	0	0	0	1	0	0	0	0	0	0	0	0	0	0	0	0	0	1	0	0	0	0	0	1	0	0	0	0	0	0	0	0	0	0	0	0	0
WS AU FR (29)	*Protoniobia*	*wadea*	PIX-1, F2	1	0	0	0	0	0	1	0	0	0	0	0	0	0	0	?	0	0	0	0	0	0	1	0	0	0	0	0	0	0	0	0	0	0	0	0	0	0	0	0	0	0	0	0	0	0	0	0	0	0
WS AU FR (29)	*Protodipleurosoma*	*wardi*	PIX-2; F3	1	0	0	0	0	0	1	0	0	0	0	0	0	0	0	0	0	0	0	0	0	0	1	0	?	0	0	0	0	0	0	0	0	0	0	0	0	0	0	0	0	0	0	0	0	0	0	0	0	0
WS AU FR (29)	*Tateana*	*inflata*	PXI-1,2	1	0	0	0	0	0	1	0	0	0	0	0	0	0	0	?	0	0	0	0	0	0	1	0	1	0	0	0	0	0	0	0	0	0	0	0	0	0	0	0	0	0	0	0	0	0	0	0	0	0
WS AU FR (29)	*Pseudorhopilema*	*chapmani*	PXII-2, F6E	1	0	0	0	0	0	1	0	0	0	0	0	0	0	0	?	0	0	0	0	0	0	0	1	0	0	0	0	0	0	0	0	0	0	0	0	0	0	0	0	0	0	0	0	0	0	0	0	0	0
WS AU FR (29)	*Medusina*	*mawsoni*	PXIII-4; F7B	1	0	0	0	0	0	1	0	0	0	0	0	0	0	0	0	0	0	0	0	0	0	1	0	0	0	0	0	0	0	0	0	0	0	0	0	0	0	0	0	0	0	0	0	0	0	0	0	0	0
WS AU FR (29)	*Medusina*	*asteroides*	PXIII-3; F7C	1	0	0	0	0	0	1	0	0	0	0	0	0	0	0	1	0	0	0	0	0	0	0	0	1	0	0	0	0	0	0	0	0	0	0	0	0	1	0	0	0	0	0	0	0	0	0	0	0	0
WS AU FR (29)	*Medusina*	*filamentus*	PXIII- 1; F7D	1	0	0	0	0	0	1	0	0	0	0	0	0	0	1	0	0	0	0	0	0	0	0	0	0	0	0	0	0	0	0	0	0	0	0	0	0	0	1	0	0	0	0	0	0	0	0	0	0	0
WS AU FR (29)	*Cyclomedusa*	*gigantea*	PXV-2; F8E	1	0	0	0	0	0	1	0	0	0	0	0	0	0	0	0	0	0	0	0	0	0	1	0	0	0	0	0	0	0	0	0	0	0	0	0	0	0	1	0	0	1	0	0	0	0	0	0	0	0
WS AU FR (29)	*Madigania*	*annulata*	PXVI-1,2; PXVII-1,2	1	0	0	0	0	0	1	0	0	0	0	0	0	0	0	1	0	0	0	0	0	0	1	0	0	0	0	0	0	0	0	0	0	0	0	0	0	0	0	0	0	0	0	0	0	0	0	0	0	0
WS AU FR (29)	*Dickinsonia*	*minima*	PXXI-1-4; F9,10E,F	0	0	1	0	0	0	0	0	1	0	0	0	0	0	0	0	1	0	0	0	0	0	0	0	0	0	0	0	0	0	0	1	0	0	0	0	0	0	0	0	0	0	0	0	0	0	0	0	0	0
WS AU FR (30)	*Mandelbrotia*	sp.	YPM208026, 204511	0	0	0	0	0	1	0	1	0	0	0	0	0	0	0	0	0	0	0	0	1	0	0	0	0	0	0	0	0	1	0	0	0	1	0	0	0	0	0	0	0	0	0	0	0	0	1	0	0	0
WS BA WC (31)	*Nemiana*	*simplex*	N/A	1	0	0	0	0	0	1	0	0	0	0	0	0	0	1	0	0	0	0	0	0	0	0	0	0	0	0	0	0	0	0	0	0	0	0	0	0	0	0	0	0	0	0	0	0	0	0	0	0	0
WS BA PD (31)	*Nemiana*	*simplex*	N/A	1	0	0	0	0	0	1	0	0	0	0	0	0	0	1	0	0	0	0	0	0	0	0	0	0	0	0	0	0	0	0	0	0	0	0	0	0	0	0	0	0	0	0	0	0	0	0	0	0	0
WS BA WC (31)	*Beltanelliformis*	*brunsae*	P4-2,3; 5-2	1	0	0	0	0	0	1	0	0	0	0	0	0	0	1	0	0	0	0	0	0	0	0	0	0	0	0	0	0	0	0	0	0	0	0	0	0	0	0	0	0	0	0	0	0	0	0	0	0	0
WS BA WC (31)	*Cyclomedusa*	*davidi*	P1-3	1	0	0	0	0	0	1	0	0	0	0	0	0	0	0	?	0	0	0	0	0	0	1	0	0	0	0	0	0	0	0	0	0	0	0	0	0	0	0	0	0	0	0	0	0	0	0	0	0	0
WS BA UR (31)	*Cyclomedusa*	*davidi*	N/A	1	0	0	0	0	0	1	0	0	0	0	0	0	0	0	?	0	0	0	0	0	0	1	0	0	0	0	0	0	0	0	0	0	0	0	0	0	0	0	0	0	0	0	0	0	0	0	0	0	0
WS BA WC (31)	*Cyclomedusa*	*plana*	P2-5; 5-7	1	0	0	0	0	0	1	0	0	0	0	0	0	0	0	?	0	0	0	0	0	0	1	0	0	0	0	0	0	0	0	0	0	0	0	0	0	0	0	0	0	0	0	0	0	0	0	0	0	0
WS BA PD (31)	*Cyclomedusa*	*plana*	N/A	1	0	0	0	0	0	1	0	0	0	0	0	0	0	0	?	0	0	0	0	0	0	1	0	0	0	0	0	0	0	0	0	0	0	0	0	0	0	0	0	0	0	0	0	0	0	0	0	0	0
WS BA WC (31)	*Cyclomedusa*	*plana*	P2-3	1	0	0	0	0	0	1	0	0	0	0	0	0	0	0	1	0	0	0	0	0	0	0	0	1	0	0	0	0	0	0	0	0	0	0	0	0	0	1	0	0	0	0	0	0	0	0	0	0	0
WS BA WC (31)	*Cyclomedusa*	*radiata*	P1-7	1	0	0	0	0	0	1	0	0	0	0	0	0	0	1	0	0	0	0	0	0	0	0	0	0	0	0	0	0	0	0	0	0	0	0	0	0	0	1	0	0	0	0	0	0	0	0	0	0	0
WS BA WC (31)	*Cyclomedusa*	*minuta*	PVIII-4	1	0	0	0	0	0	1	0	0	0	0	0	0	0	0	1	0	0	0	0	0	0	1	0	0	0	0	0	0	0	0	0	0	0	0	0	0	0	0	0	0	0	0	0	0	0	0	0	0	0
WS BA WC (31)	*Cyclomedusa*	*delicata*	P1-4	1	0	0	0	0	0	1	0	0	0	0	0	0	0	0	?	0	0	0	0	0	0	1	0	0	0	0	0	0	0	0	0	0	0	0	0	0	0	0	0	0	0	0	0	0	0	0	0	0	0
WS BA PD (31)	*Tirasiana*	*disciformis*	N/A	1	0	0	0	0	0	1	0	0	0	0	0	0	0	0	?	0	0	0	0	0	0	1	0	0	0	0	0	0	0	0	0	0	0	0	0	0	0	0	0	0	0	0	0	0	0	0	0	0	0
WS BA WC (31)	*Tirasiana*	*disciformis*	N/A	1	0	0	0	0	0	1	0	0	0	0	0	0	0	0	?	0	0	0	0	0	0	1	0	0	0	0	0	0	0	0	0	0	0	0	0	0	0	0	0	0	0	0	0	0	0	0	0	0	0
WS BA UR (31)	*Tirasiana*	*disciformis*	P29-1	1	0	0	0	0	0	1	0	0	0	0	0	0	0	0	?	0	0	0	0	0	0	1	0	0	0	0	0	0	0	0	0	0	0	0	0	0	0	0	0	0	0	0	0	0	0	0	0	0	0
WS BA WC (31)	*Paliella*	*patelliformis*	N/A	1	0	0	0	0	0	1	0	0	0	0	0	0	0	1	?	0	0	0	0	0	0	0	0	0	0	0	0	0	0	0	0	0	0	0	0	0	0	0	0	0	0	0	0	0	0	0	0	0	0
WS BA PD (31)	*Paliella*	*patelliformis*	P3-3,4,9; P10-5	1	0	0	0	0	0	1	0	0	0	0	0	0	0	1	?	0	0	0	0	0	0	0	0	0	0	0	0	0	0	0	0	0	0	0	0	0	0	0	0	0	0	0	0	0	0	0	0	0	0
WS BA UR (31)	*Paliella*	*patelliformis*	P89-4	1	0	0	0	0	0	1	0	0	0	0	0	0	0	1	0	0	0	0	0	0	0	0	0	0	0	0	0	0	0	0	0	0	0	0	0	0	0	1	0	0	0	0	0	0	0	0	0	0	0
WS BA WC (31)	*Ediacaria*	*flindersi*	P1-2,5	1	0	0	0	0	0	1	0	0	0	0	0	0	0	0	1	0	0	0	0	0	0	1	0	0	0	0	0	0	0	0	0	0	0	0	0	0	0	0	0	0	0	0	0	0	0	0	0	0	0
WS BA PD (31)	*Ediacaria*	*flindersi*	P1-1; P2-4; P7-5	1	0	0	0	0	0	1	0	0	0	0	0	0	0	0	1	0	0	0	0	0	0	1	0	0	0	0	0	0	0	0	0	0	0	0	0	0	0	0	0	0	0	0	0	0	0	0	0	0	0
WS BA WC (31)	*Nimbia*	*occlusa*	N/A	1	0	0	0	0	0	1	0	0	0	0	0	0	0	0	?	0	0	0	0	0	0	1	0	0	0	0	0	0	0	0	0	0	0	0	0	0	0	0	0	0	0	0	0	0	0	0	0	0	0
WS BA PD (31)	*Nimbia*	*occlusa*	P3-1,6,7	1	0	0	0	0	0	1	0	0	0	0	0	0	0	0	?	0	0	0	0	0	0	1	0	0	0	0	0	0	0	0	0	0	0	0	0	0	0	0	0	0	0	0	0	0	0	0	0	0	0
WS BA PD (31)	*Nimbia*	*dniesteri*	P3-2,8	1	0	0	0	0	0	1	0	0	0	0	0	0	0	0	0	0	0	0	0	0	0	1	0	0	0	0	0	0	0	0	0	0	0	0	0	0	1	0	0	0	0	0	0	0	0	0	0	0	0
WS BA WC (31)	*Protodipleurosoma*	*rugulosum*	P5-4,5,6	0	0	1	0	0	0	0	0	1	0	0	0	0	0	0	0	1	0	0	0	0	0	0	0	0	0	0	0	0	0	0	1	0	0	0	0	0	1	0	0	0	0	0	0	0	0	0	0	0	0
WS BA PD (31)	*Protodipleurosoma*	*rugulosum*	N/A	0	0	1	0	0	0	0	0	1	0	0	0	0	0	0	0	1	0	0	0	0	0	0	0	0	0	0	0	0	0	0	1	0	0	0	0	0	1	0	0	0	0	0	0	0	0	0	0	0	0
WS BA WC (31)	*Chondroplon*	sp.	P6-4	0	0	1	0	0	0	0	0	1	0	0	0	0	0	0	0	0	0	0	0	0	1	0	0	0	0	0	0	0	0	0	0	0	0	0	0	0	0	0	0	0	0	0	0	0	0	0	0	0	0
WS BA WC (31)	*Ovatoscutum*	*concentricum*	P6-1,2,3	?	0	1	0	0	0	?	0	1	0	0	0	0	0	0	0	0	0	0	0	0	0	1	0	0	0	0	0	0	0	0	0	0	0	0	0	0	0	0	0	0	0	0	0	0	0	0	0	0	0
WS BA WC (31)	*Eoporpita*	*medusa*	P6-5	1	0	0	0	0	0	1	0	0	0	0	0	0	0	?	1	0	0	0	0	0	0	0	0	1	0	0	0	0	0	0	0	0	0	0	0	0	0	0	0	?	0	0	0	0	0	0	0	0	0
WS BA WC (31)	*Kaisalia*	*mensae*	P6-6	1	0	0	0	0	0	1	0	0	0	0	0	0	0	0	0	0	0	0	0	0	0	1	0	0	0	0	0	0	0	0	0	0	0	0	0	0	0	0	0	0	0	0	0	0	0	0	0	0	0
WS BA PD (31)	*Irridinitus*	*multiradiatus*	P8-5	1	0	0	0	0	0	1	0	0	0	0	0	0	0	0	1	0	0	0	0	0	0	0	0	1	0	0	0	0	0	0	0	0	0	0	0	0	0	0	0	0	0	0	0	0	0	0	0	0	0
WS BA PD (31)	*Irridinitus*	*multiradiatus*	P8-6	1	0	0	0	0	0	1	0	0	0	0	0	0	0	0	1	0	0	0	0	0	0	0	0	1	0	0	0	0	0	0	0	0	0	0	0	0	1	0	0	0	0	0	0	0	0	0	0	0	0
WS BA WC (31)	*Irridinitus*	*multiradiatus*	P8-5	1	0	0	0	0	0	1	0	0	0	0	0	0	0	0	1	0	0	0	0	0	0	0	0	1	0	0	0	0	0	0	0	0	0	0	0	0	0	0	0	0	0	0	0	0	0	0	0	0	0
WS BA WC (31)	*Irridinitus*	*multiradiatus*	P8-6	1	0	0	0	0	0	1	0	0	0	0	0	0	0	0	1	0	0	0	0	0	0	0	0	1	0	0	0	0	0	0	0	0	0	0	0	0	1	0	0	0	0	0	0	0	0	0	0	0	0
WS BA WC (31)	*Veprina*	*undosa*	P4-6	0	0	1	0	0	0	0	0	1	0	0	0	0	0	?	0	0	0	0	0	0	0	0	0	0	0	0	0	0	0	0	0	0	0	0	0	0	0	1	0	0	0	0	0	0	0	0	0	0	0
WS BA WC (31)	*Armillifera*	*parva*	P7-3	1	0	0	0	0	0	1	0	0	0	0	0	0	0	0	?	0	0	0	0	0	0	0	0	1	0	0	0	0	0	0	0	0	0	0	0	0	1	0	0	0	0	0	0	0	0	0	0	0	0
WS BA WC (31)	*Bonata*	*septata*	P8-4	1	0	0	0	0	0	1	0	0	0	0	0	0	0	0	?	0	0	0	0	0	0	0	0	1	0	0	0	0	0	0	0	0	0	0	0	0	1	0	0	0	0	0	0	0	0	0	0	0	0
WS BA WC (31)	*Hiemalora*	*stellaris*	P7-1,6	1	0	0	0	0	0	1	0	0	0	0	0	0	0	1	0	0	0	0	0	0	0	0	0	0	0	0	0	0	0	0	0	0	0	0	0	0	0	1	0	0	0	0	0	0	0	0	0	0	0
WS BA PD (31)	*Hiemalora*	*stellaris*	N/A	1	0	0	0	0	0	1	0	0	0	0	0	0	0	1	0	0	0	0	0	0	0	0	0	0	0	0	0	0	0	0	0	0	0	0	0	0	0	1	0	0	0	0	0	0	0	0	0	0	0
WS BA WC (31)	*Evmiaksia*	*aksionovi*	P20-2	1	0	0	0	0	0	1	0	0	0	0	0	0	0	0	1	0	0	0	0	0	0	0	0	1	0	0	0	0	0	0	0	0	0	0	0	0	?	0	0	0	1	0	0	0	0	0	0	0	0
WS BA WC (31)	*Albumares*	*brunsae*	P9-1,4	1	0	0	0	0	0	0	0	0	0	1	0	0	0	0	0	0	0	0	0	0	0	0	0	0	0	1	0	1	0	0	0	0	0	0	0	0	0	0	0	0	0	0	0	0	0	0	0	0	0
WS BA WC (31)	*Anfesta*	*stankovskii*	P9-2	1	0	0	0	0	0	0	0	0	0	1	0	0	0	0	0	0	0	0	0	0	0	0	0	1	0	0	0	1	0	0	0	0	0	0	0	0	0	0	0	0	0	0	0	0	0	0	0	0	0
WS BA WC (31)	*Tribrachidium*	*heraldicum*	P9-5,6	1	0	0	0	0	0	0	0	0	0	1	0	0	0	0	0	0	0	0	0	0	0	0	0	0	0	1	0	1	0	0	0	0	0	0	0	0	0	1	0	0	0	0	0	0	0	0	0	0	0
WS BA PD (31)	*Tribrachidium*	*heraldicum*	P9-3	1	0	0	0	0	0	0	0	0	0	1	0	0	0	0	0	0	0	0	0	0	0	0	0	0	0	1	0	1	0	0	0	0	0	0	0	0	0	1	0	0	0	0	0	0	0	0	0	0	0
WS BA PD (31)	*Conomedusa*	*lobatus*	P8-1	0	0	0	1	0	0	0	0	0	0	0	1	0	0	0	1	0	0	0	0	0	0	0	0	0	0	0	0	0	0	0	0	0	0	0	0	0	0	1	0	0	0	0	0	0	0	0	0	0	0
WS BA WC (31)	*Conomedusa*	*lobatus*	N/A	0	0	0	1	0	0	0	0	0	0	0	1	0	0	0	1	0	0	0	0	0	0	0	0	0	0	0	0	0	0	0	0	0	0	0	0	0	0	1	0	0	0	0	0	0	0	0	0	0	0
WS BA WC (31)	*Stauridinia*	*crucicula*	P4-1,5	1	0	0	0	0	0	0	0	0	0	0	1	0	0	0	0	0	0	0	0	0	0	0	0	0	0	1	1	0	0	0	0	0	0	0	0	0	0	0	0	0	0	0	0	0	0	0	0	0	0
WS BA WC (31)	*Pomoria*	*corolliformis*	P7-2	0	0	1	0	0	0	0	0	1	0	0	0	0	0	?	0	0	0	0	0	0	0	0	0	0	0	0	0	0	0	0	0	0	0	0	0	0	0	1	0	0	0	0	0	0	0	0	0	0	0
WS BA WC (31)	*Platypholinia*	*pholiata*	P19-5,6	0	0	0	0	0	1	0	?	1	0	0	0	0	0	1	0	0	0	0	0	0	0	0	0	0	0	0	0	0	0	0	0	0	0	0	0	0	0	0	0	0	0	0	0	0	0	0	0	0	0
WS BA WC (31)	*Vladimissa*	*missarzhevskii*	P19-7	0	0	0	0	0	1	0	?	1	0	0	0	0	?	1	0	0	0	0	0	0	0	0	0	0	0	0	0	0	0	0	0	0	0	0	0	0	0	0	0	0	0	0	0	0	0	0	0	0	0
WS BA WC (31)	*Palaeoplatoda*	*segmentata*	P16-1,3,6	0	0	?	0	0	1	0	0	1	0	0	0	0	0	0	0	1	0	0	0	0	0	0	0	0	0	0	0	0	1	0	0	0	0	0	0	0	0	0	0	0	0	0	0	0	0	0	0	0	0
WS BA WC (31)	*Dickinsonia*	*costata*	P16-2; 17-1,2,5,6,7	0	0	1	0	0	0	0	0	1	0	0	0	0	0	0	0	1	0	0	0	0	0	0	0	0	0	0	0	0	0	0	1	0	0	0	0	0	0	0	0	0	0	0	0	0	0	0	0	0	0
WS BA PD (31)	*Dickinsonia*	*costata*	N/A	0	0	1	0	0	0	0	0	1	0	0	0	0	0	0	0	1	0	0	0	0	0	0	0	0	0	0	0	0	0	0	1	0	0	0	0	0	0	0	0	0	0	0	0	0	0	0	0	0	0
WS BA WC (31)	*Dickinsonia*	*tenuis*	P16-3	0	0	1	0	0	0	0	0	1	0	0	0	0	0	0	0	1	0	0	0	0	0	0	0	0	0	0	0	0	0	0	1	0	0	0	0	0	0	0	0	0	0	0	0	0	0	0	0	0	0

WS BA WC (31)	*Dickinsonia*	*lissa*	P16-5,7; P17-3	0	0	0	0	0	1	0	?	1	0	0	0	0	0	0	0	1	0	0	0	0	0	0	0	0	0	0	0	0	0	0	1	0	0	0	0	0	0	0	0	0	0	0	0	0	0	0	0	0	0
WS BA WC (31)	*Onega*	*stepanovi*	P19-1,2,4,8,9	0	0	1	0	0	?	0	1	0	0	0	0	0	0	0	0	1	0	0	0	0	0	0	0	0	0	0	0	0	1	0	0	0	0	0	0	1	1	0	0	0	0	0	0	0	0	0	0	0	0
WS BA WC (31)	*Vendomia*	*menneri*	P21-7	0	0	1	0	0	0	0	1	0	0	0	0	0	0	0	0	1	0	0	0	0	0	0	0	0	0	0	0	0	0	1	0	0	0	0	0	1	0	0	0	0	0	0	0	0	0	0	0	0	0
WS BA WC (31)	*Vendia*	*sokolovi*	P21-1	0	0	1	0	0	0	0	1	0	0	0	0	0	0	0	0	1	0	0	0	0	0	0	0	0	0	0	0	0	1	0	0	0	0	0	0	1	0	0	0	0	0	0	0	0	0	0	0	0	0
WS BA WC (31)	*Bomakellia*	*kelleri*	P21-6	0	0	1	0	0	0	0	1	?	0	0	0	0	?	0	0	0	0	0	0	1	0	0	0	0	0	0	0	0	1	0	0	0	0	0	0	?	0	0	0	0	0	0	0	0	0	0	0	0	0
WS BA WC (31)	*Mialsemia*	*semichatovi*	P21-2,3	0	0	1	0	0	0	0	0	1	0	0	0	0	0	0	0	0	0	0	1	1	0	0	0	0	0	0	0	0	1	0	0	0	0	0	0	0	0	0	0	0	0	0	0	0	0	0	0	0	0
WS BA WC (31)	*Spriggina*	*borealis*	P21-5	0	0	0	0	0	1	0	1	0	0	0	0	0	0	0	0	1	0	0	0	0	0	0	0	0	0	0	0	0	1	0	0	0	0	0	0	1	0	0	0	0	0	0	0	0	0	0	0	0	0
WS BA WC (31)	*Pseudorhizostomites*	*howchini*	P10-2,3	1	0	0	0	0	0	1	0	0	0	0	0	0	0	0	?	0	0	0	0	0	0	0	0	1	0	0	0	0	0	0	0	0	0	0	0	0	0	0	0	0	0	0	0	0	0	0	0	0	0
WS BA PD (31)	*Pseudorhizostomites*	*howchini*	N/A	1	0	0	0	0	0	1	0	0	0	0	0	0	0	0	?	0	0	0	0	0	0	0	0	1	0	0	0	0	0	0	0	0	0	0	0	0	0	0	0	0	0	0	0	0	0	0	0	0	0
WS BA UR (31)	*Pseudorhizostomites*	*howchini*	P89-2	1	0	0	0	0	0	1	0	0	0	0	0	0	0	0	?	0	0	0	0	0	0	0	0	1	0	0	0	0	0	0	0	0	0	0	0	0	0	0	0	0	0	0	0	0	0	0	0	0	0
WS BA WC (31)	*Charnia*	*masoni*	P12-4; P13-2,3,4	0	0	0	0	0	1	0	1	0	1	0	0	0	0	0	0	1	0	0	0	0	0	0	0	0	0	0	0	0	1	0	0	1	0	0	0	0	0	0	0	0	0	0	0	0	0	0	0	0	0
WS BA WC (31)	*Pteridinium*	*nenoxa*	P11-1,2,3,4	0	0	0	0	0	1	0	0	1	0	0	0	0	0	0	0	1	0	0	0	0	0	0	0	0	0	0	0	0	1	0	0	0	0	0	0	0	0	0	0	0	0	0	0	0	0	0	0	0	0
WS BA PD (31)	*Pteridinium*	*nenoxa*	N/A	0	0	0	0	0	1	0	0	1	0	0	0	0	0	0	0	1	0	0	0	0	0	0	0	0	0	0	0	0	1	0	0	0	0	0	0	0	0	0	0	0	0	0	0	0	0	0	0	0	0
WS BA WC (31)	*Inkrylovia*	*lata*	P12-3,5	0	0	0	0	0	1	0	0	1	0	0	0	0	0	0	0	1	0	0	0	0	0	0	0	0	0	0	0	0	1	0	0	0	0	0	0	0	0	0	0	0	0	0	0	0	0	0	0	0	0
WS BA WC (31)	*Archangelia*	*valdaica*	P11-5	0	0	1	0	0	?	0	0	1	0	0	0	0	0	0	0	1	?	0	0	0	0	0	0	0	0	0	0	0	1	0	0	0	0	0	0	0	0	0	0	0	0	0	0	0	0	0	0	0	0
WS BA WC (31)	*Ramellina*	*pennata*	P14-1	0	0	0	0	0	1	0	0	1	0	0	0	0	0	0	0	1	0	0	0	0	0	0	0	0	0	0	0	0	1	0	0	0	0	0	0	0	0	0	0	0	0	0	0	0	0	0	0	0	0
WS BA WC (31)	*Zolotytsia*	*biserialis*	P12-6; P14-2	0	0	1	0	0	0	0	0	1	0	0	0	0	0	0	0	1	0	0	0	0	0	0	0	0	0	0	0	0	1	0	0	0	0	0	0	0	0	0	0	0	0	0	0	0	0	0	0	0	0
WS BA PD (31)	*Zolotytsia*	*biserialis*	N/A	0	0	1	0	0	0	0	0	1	0	0	0	0	0	0	0	1	0	0	0	0	0	0	0	0	0	0	0	0	1	0	0	0	0	0	0	0	0	0	0	0	0	0	0	0	0	0	0	0	0
WS BA WC (31)	*Vaizitsina*	*sophia*	P14-3,4,6	0	0	0	0	0	1	0	1	0	0	0	0	0	0	0	0	0	1	0	0	0	0	0	0	0	0	0	0	0	1	0	0	0	0	0	0	0	0	0	0	0	0	0	0	0	0	1	1	0	0
WS BA PD (32)	*Cyclomedusa*	*serebrina*	PXLVIII-4	1	0	0	0	0	0	1	0	0	0	0	0	0	0	0	1	0	0	0	0	0	0	1	0	0	0	0	0	0	0	0	0	0	0	0	0	0	0	0	0	0	0	0	0	0	0	0	0	0	0
WS BA WC (33)	*Vendia*	*rachiata*	P1-10-13	0	0	1	0	0	0	0	1	0	0	0	0	0	0	0	0	0	1	0	0	0	0	0	0	0	0	0	0	0	1	0	0	0	0	0	0	1	1	0	0	0	0	0	0	0	0	0	0	0	0
WS BA WC (33)	*Cyanorus*	*singularis*	P1-1-6	0	0	1	0	0	0	0	1	0	0	0	0	0	0	0	0	0	1	0	0	0	0	0	0	0	0	0	0	0	0	0	1	?	0	0	0	0	0	0	0	0	0	0	0	0	0	0	0	0	0
WS BA WC (33)	*Paravendia*	*janae*	P1-9	0	0	1	0	0	0	0	1	0	0	0	0	0	0	0	0	0	1	0	0	0	0	0	0	0	0	0	0	0	0	1	0	0	0	0	0	1	0	0	0	0	0	0	0	0	0	0	0	0	0
WS BA WC (34)	*Parvancorina*	*sagitta*	P1-5-8	0	0	1	0	0	0	0	1	0	0	0	0	0	0	0	0	0	1	1	0	0	0	0	0	0	0	0	0	0	0	0	0	0	0	0	0	1	1	0	0	0	0	0	0	0	0	0	0	0	0
WS BA WC (34)	*Parvancorina*	*minchami*	P1-9-12	0	1	0	0	0	0	0	1	0	0	0	0	0	0	0	0	0	1	1	0	0	0	0	0	0	0	0	0	0	0	0	0	0	0	0	0	1	1	0	0	0	0	0	0	0	0	0	0	0	0
WS BA WC (34)	*Temnoxa*	*molliuscula*	P2-1,2	0	0	1	0	0	0	0	1	0	0	0	0	0	0	0	0	0	1	1	0	0	0	0	0	0	0	0	0	0	0	0	0	0	0	0	0	0	0	0	0	0	0	0	0	0	0	0	0	0	0
WS BA WC (34)	*Solza*	*margarita*	P1-1-4	0	0	1	0	0	0	0	0	1	0	0	0	0	1	0	0	0	0	0	0	0	0	0	0	0	0	0	0	0	0	0	0	0	0	0	0	0	0	0	1	0	0	0	0	0	0	0	0	0	0
WS BA WC (34)	*Karakhtia*	*nessovi*	P1-13, 14	1	0	0	0	0	0	0	0	1	0	0	0	0	0	0	0	1	0	0	0	0	0	0	0	0	0	0	0	0	1	0	0	0	0	0	0	0	?	1	0	0	0	0	0	0	0	0	0	0	0
WS BA WC (34)	*Vaveliksia*	*vana*	P2-3-10	0	0	1	0	0	?	0	1	0	0	0	0	0	0	1	0	0	0	0	0	0	0	0	0	0	0	0	0	0	0	0	0	0	0	0	0	0	0	0	0	0	0	0	0	0	0	0	1	0	0
WS BA WC (35)	*Ventogyrus*	*chistyakovi*	P1-1-5; P2-1-5	0	0	0	0	0	1	0	1	0	0	0	0	0	0	0	0	1	0	0	0	0	0	0	0	0	0	0	0	0	1	0	0	0	0	1	1	0	0	0	0	0	0	0	0	0	0	0	0	?	0
WS BA WC (35)	*Pteridinium*	*nenoxa*	P2-6-8	0	0	0	0	0	1	0	0	1	0	0	0	0	0	0	0	1	0	0	0	0	0	0	0	0	0	0	0	0	1	0	0	0	0	0	0	0	0	0	0	0	0	0	0	0	0	0	0	0	0
WS BA WC (36)	*Inaria*	*karli*	F1-7	1	0	0	0	0	0	1	0	0	0	0	0	0	0	?	0	0	0	0	0	0	0	0	0	0	0	0	0	0	0	0	0	0	0	0	0	0	1	0	0	0	0	0	0	0	0	0	0	0	0
WS BA WC (37)	*Yorgia*	*waggoneri*	F1	0	0	1	0	0	0	0	1	0	0	0	0	0	0	0	0	1	0	0	0	0	0	0	0	0	0	0	0	0	1	0	0	0	0	0	0	1	0	0	0	0	0	0	0	0	0	0	0	0	0
WS BA WC (38)	*Kimberella*	*quadrata*	F1	0	0	1	0	0	0	0	0	1	0	0	0	0	0	0	0	1	0	0	0	0	0	0	0	0	0	0	0	0	1	0	0	0	0	0	0	0	1	0	0	0	0	0	0	1	0	0	0	0	0
WS BA WC (39)	*Rangea*	*schneiderboehni*	N/A	0	0	0	0	0	1	0	1	0	1	0	0	0	0	0	0	0	0	0	0	1	0	0	0	0	0	0	0	0	1	0	0	0	1	0	0	0	?	0	0	0	0	0	0	0	0	?	?	0	0
WS BA WC (39)	*Ausia*	*fenestrata*	N/A	0	1	0	0	0	0	0	1	0	0	0	0	0	1	0	0	0	0	0	0	0	0	0	0	0	0	0	0	0	0	0	0	0	0	0	0	0	0	0	0	0	0	0	0	0	0	1	0	0	0
WS BA WC (39)	*Swartpuntia*	*germsi*	N/A	0	0	0	0	0	1	0	1	0	0	0	0	0	0	0	0	0	0	0	1	1	0	0	0	0	0	0	0	0	1	0	0	0	0	0	0	0	0	0	0	0	0	0	0	0	0	1	0	0	0
WS BA PD (31)	*Tirasiana*	*concentralis*	P29-3	1	0	0	0	0	0	1	0	0	0	0	0	0	0	0	?	0	0	0	0	0	0	1	0	0	0	0	0	0	0	0	0	0	0	0	0	0	0	0	0	0	0	0	0	0	0	0	0	0	0
WS BA PD (31)	*Elasenia*	*aseevae*	P8-7,8	1	0	0	0	0	0	1	0	0	0	0	0	0	1	0	0	0	0	0	0	0	0	0	0	0	0	0	0	0	0	0	0	0	0	0	0	0	0	0	0	0	0	0	0	0	0	0	0	0	0
WS BA PD (31)	*Podolimirus*	*mirus*	P10-4	0	0	1	0	0	0	0	1	0	0	0	0	0	0	0	0	?	0	0	0	0	0	0	0	0	0	0	0	0	0	1	0	0	0	0	0	0	0	0	0	0	0	0	0	0	0	0	0	0	0
WS BA PD (31)	*Medusinites*	*asteroides*	P8-2,4	1	0	0	0	0	0	1	0	0	0	0	0	0	0	0	0	0	0	0	0	0	0	1	0	0	0	0	0	0	0	0	0	0	0	0	0	0	1	0	0	0	0	0	0	0	0	0	0	0	0
WS BA PD (31)	*Valdainia*	*plumosa*	P10-1	0	0	0	0	0	1	0	1	0	0	0	0	0	0	0	0	1	0	0	0	0	0	0	0	0	0	0	0	0	1	0	0	0	0	0	0	0	0	0	0	0	0	0	0	0	0	0	0	0	0
WS BA PD (31)	*Vaveliksia*	*velikanovi*	P12-1	0	0	0	0	0	1	0	1	0	0	0	0	0	0	1	0	0	0	0	0	0	0	0	0	0	0	0	0	0	0	0	0	0	0	0	0	0	0	0	0	0	0	0	0	0	0	0	1	0	0
WS BA PD (32)	*Bronicella*	*podolica*	PXLVIII-1,5,6	1	0	0	0	0	0	1	0	0	0	0	0	0	0	1	0	0	0	0	0	0	0	0	0	0	0	0	0	0	0	0	0	0	0	0	0	0	0	0	0	0	0	0	0	0	0	0	0	0	0
WS BA UR (31)	*Tirasiana*	*coniformis*	P29-2	1	0	0	0	0	0	1	0	0	0	0	0	0	0	0	1	0	0	0	0	0	0	1	0	0	0	0	0	0	0	0	0	0	0	0	0	0	0	0	0	0	0	0	0	0	0	0	0	0	0
WS BA UR (31)	*Tirasiana*	*cocarda*	P29-4	1	0	0	0	0	0	1	0	0	0	0	0	0	0	0	1	0	0	0	0	0	0	1	0	0	0	0	0	0	0	0	0	0	0	0	0	0	0	0	0	0	0	0	0	0	0	0	0	0	0
WS BA UR (31)	*Nemiana*	*simplex*	P5-3	1	0	0	0	0	0	1	0	0	0	0	0	0	0	1	0	0	0	0	0	0	0	0	0	0	0	0	0	0	0	0	0	0	0	0	0	0	0	0	0	0	0	0	0	0	0	0	0	0	0
WS BA UR (31)	*Protodipleurosoma*	*paulus*	P89-1	1	0	0	0	0	0	?	0	1	0	0	0	0	0	0	0	1	0	0	0	0	0	?	0	0	0	0	0	0	0	0	0	0	0	0	0	0	1	0	0	0	0	0	0	0	0	0	0	0	0
WS BA UR (31)	*Medusinites*	sp.	P89-3	1	0	0	0	0	0	1	0	0	0	0	0	0	0	1	0	0	0	0	0	0	0	0	0	0	0	0	0	0	0	0	0	0	0	0	0	0	0	1	0	0	0	0	0	0	0	0	0	0	0
WS BA WC (40)	*Archaeaspis*	*fedonkini*	P1-6-7	0	0	1	0	0	0	0	1	0	0	0	0	0	0	0	0	1	0	0	0	0	0	0	0	0	0	0	0	0	1	0	0	0	0	0	0	1	0	0	0	0	0	0	0	0	0	0	0	0	0
WS BA WC (31)	*Pseudovendia*	sp.	P21-4	0	0	1	0	0	0	0	1	0	0	0	0	0	0	0	0	1	0	0	0	0	0	0	0	0	0	0	0	0	1	0	0	0	0	0	0	1	0	0	0	0	0	0	0	0	0	0	0	0	0
WS BA UR (41)	*Beltanella*	*zilimica*	P1-1-2	1	0	0	0	0	0	1	0	0	0	0	0	0	0	0	1	0	0	0	0	0	0	0	0	0	0	0	0	0	0	0	0	0	0	0	0	0	0	0	0	0	0	0	0	0	0	0	0	0	0
WS BA UR (41)	*Nemiana*	*bakeevi*	P1-3	1	0	0	0	0	0	1	0	0	0	0	0	0	0	0	1	0	0	0	0	0	0	0	0	0	0	0	0	0	0	0	0	0	0	0	0	0	0	0	0	0	0	0	0	0	0	0	0	0	0
WS BA PD (32)	*Tirasiana*	sp.	PXLIX-7	1	0	0	0	0	0	1	0	0	0	0	0	0	0	0	1	0	0	0	0	0	0	1	0	0	0	0	0	0	0	0	0	0	0	0	0	0	0	0	0	0	0	0	0	0	0	0	0	0	0
WS BA FM (42)	*Cyclomedusa*	sp.	F3-1	1	0	0	0	0	0	1	0	0	0	0	0	0	0	0	1	0	0	0	0	0	0	1	0	0	0	0	0	0	0	0	0	0	0	0	0	0	0	0	0	0	0	0	0	0	0	0	0	0	0
WS BA FM (42)	*Cyclomedusa*	sp.	F3-2	1	0	0	0	0	0	1	0	0	0	0	0	0	0	0	1	0	0	0	0	0	0	1	0	?	0	0	0	0	0	0	0	0	0	0	0	0	0	0	0	0	0	0	0	0	0	0	0	0	0
WS BA FM (42)	*Ediacaria*	sp.	F3-3	1	0	0	0	0	0	1	0	0	0	0	0	0	0	0	1	0	0	0	0	0	0	?	0	0	0	0	0	0	0	0	0	0	0	0	0	0	0	0	0	0	0	0	0	0	0	0	0	0	0
WS BA FM (42)	*Beltanella*	sp.	F4	1	0	0	0	0	0	1	0	0	0	0	0	0	0	1	0	0	0	0	0	0	0	0	0	0	0	0	0	0	0	0	0	0	0	0	0	0	0	0	0	0	0	0	0	0	0	0	0	0	0
WS BA FM (42)	*Hiemalora*	sp.	F5-1,2	1	0	0	0	0	0	1	0	0	0	0	0	0	0	1	0	0	0	0	0	0	0	0	0	0	0	0	0	0	0	0	0	0	0	0	0	0	0	1	0	0	0	0	0	0	0	0	0	0	0
WS BA FM (42)	*Nimbia*	sp.	F5-c,d	1	0	0	0	0	0	1	0	0	0	0	0	0	0	0	0	0	0	0	0	0	0	1	0	0	0	0	0	0	0	0	0	0	0	0	0	0	0	0	0	0	0	0	0	0	0	0	0	0	0
WSLAUWN (43)	*Beltanelliformis*	*brunsae*	P74-1,3,5-7;P75-1-8;F8,9	1	0	0	0	0	0	1	0	0	0	0	0	0	0	1	0	0	0	0	0	0	0	?	0	0	0	0	0	0	0	0	0	0	0	0	0	0	0	0	0	0	0	0	0	0	0	0	0	0	0
WSLAUWN (43)	*Ediacaria*	*flindersi*	F7	1	0	0	0	0	0	1	0	0	0	0	0	0	0	0	0	0	0	0	0	0	0	1	0	0	0	0	0	0	0	0	0	0	0	0	0	0	0	0	0	0	0	0	0	0	0	0	0	0	0
WSLAUWN (43)	*Beltanella*	*gilesi*	P73-6	1	0	0	0	0	0	1	0	0	0	0	0	0	0	0	1	0	0	0	0	0	0	0	0	0	0	0	0	0	0	0	0	0	0	0	0	0	0	0	0	0	0	0	0	0	0	0	0	0	0
WSLAUWN (43)	*Charniodiscus*	*arboreus*	F5c	0	0	1	0	0	0	0	0	1	0	0	0	0	0	0	0	1	?	0	0	0	0	0	0	0	0	0	0	0	1	0	0	0	0	0	0	0	0	0	0	0	0	0	0	0	0	0	0	0	0
WSLAUWN (43)	*Charniodiscus*	sp.	F5a,b	1	0	0	0	0	0	1	0	0	0	0	0	0	0	0	0	0	0	0	0	0	0	1	0	0	0	0	0	0	0	0	0	0	0	0	0	0	0	0	0	0	0	0	0	0	0	?	0	0	0
WSLAUWN (43)	*Medusinites*	*asteroides*	P73-7-9	1	0	0	0	0	0	1	0	0	0	0	0	0	0	0	0	0	0	0	0	0	0	1	0	0	0	0	0	0	0	0	0	0	0	0	0	0	0	0	0	0	0	0	0	0	0	0	0	0	0
WSLAUWN (43)	*Cyclomedusa*	*plana*	P73-3	1	0	0	0	0	0	1	0	0	0	0	0	0	0	0	1	0	0	0	0	0	0	1	0	0	0	0	0	0	0	0	0	0	0	0	0	0	0	0	0	0	0	0	0	0	0	0	0	0	0
WSLAUWN (43)	*Cyclomedusa*	sp.	P73-1; F5a	1	0	0	0	0	0	1	0	0	0	0	0	0	0	0	1	0	0	0	0	0	0	1	0	0	0	0	0	0	0	0	0	0	0	0	0	0	0	0	0	0	0	0	0	0	0	0	0	0	0
WSLAUWN (43)	*Nadalina*	*yukonensis*	P73-2	1	0	0	0	0	0	1	0	0	0	0	0	0	0	0	0	0	0	0	0	0	0	1	0	0	0	0	0	0	0	0	0	0	0	0	0	0	0	0	0	0	0	0	0	0	0	0	0	0	0
WSLAUWN (43)	*Rugoconites*	sp.	P73-11	1	0	0	0	0	0	1	0	0	0	0	0	0	0	0	0	0	0	0	0	0	0	0	1	0	0	0	0	0	0	0	0	0	0	0	0	0	0	0	0	0	0	0	0	0	0	0	0	0	0
WSLAUWN (43)	*Spriggia*	*annulata*	P73-10	1	0	0	0	0	0	1	0	0	0	0	0	0	0	0	1	0	0	0	0	0	0	1	0	0	0	0	0	0	0	0	0	0	0	0	0	0	0	0	0	0	0	0	0	0	0	0	0	0	0
WSLAUWN (43)	*Spriggia*	*wadeae*	P73-4	1	0	0	0	0	0	1	0	0	0	0	0	0	0	0	?	0	0	0	0	0	0	1	0	0	0	0	0	0	0	0	0	0	0	0	0	0	0	0	0	0	0	0	0	0	0	0	0	0	0
WSLAUWN (43)	*Tirasiana*	sp.	P74-2,4	1	0	0	0	0	0	1	0	0	0	0	0	0	0	0	1	0	0	0	0	0	0	1	0	0	0	0	0	0	0	0	0	0	0	0	0	0	0	0	0	0	0	0	0	0	0	0	0	0	0
WS SI OU (31)	*Nemiana*	*simplex*	P5-3	1	0	0	0	0	0	1	0	0	0	0	0	0	0	1	0	0	0	0	0	0	0	0	0	0	0	0	0	0	0	0	0	0	0	0	0	0	0	0	0	0	0	0	0	0	0	0	0	0	0
WS SI OU (31)	*Tirasiana*	*disciformis*	P29-1	1	0	0	0	0	0	1	0	0	0	0	0	0	0	0	?	0	0	0	0	0	0	1	0	0	0	0	0	0	0	0	0	0	0	0	0	0	0	0	0	0	0	0	0	0	0	0	0	0	0
WS SI OU (31)	*Ediacaria*	*flindersi*	P1-1,2,5; P2-4; P7-5	1	0	0	0	0	0	1	0	0	0	0	0	0	0	0	1	0	0	0	0	0	0	1	0	0	0	0	0	0	0	0	0	0	0	0	0	0	0	0	0	0	0	0	0	0	0	0	0	0	0
WS SI OU (31)	*Hiemalora*	sp.	P7-4	1	0	0	0	0	0	1	0	0	0	0	0	0	0	1	0	0	0	0	0	0	0	0	0	0	0	0	0	0	0	0	0	0	0	0	0	0	0	1	0	0	0	0	0	0	0	0	0	0	0
WS SI OU (31)	*Charnia*	*masoni*	P12-4; P13-2,3,4	0	0	0	0	0	1	0	1	0	1	0	0	0	0	0	0	1	0	0	0	0	0	0	0	0	0	0	0	0	1	0	0	1	0	0	0	0	0	0	0	0	0	0	0	0	0	0	0	0	0

WS	SI	OU	(44)	*Anabylia*	*impovisa*	N/A	0	0	0	1	0	0	0	0	0	0	1	0	0	0	0	0	0	0	0	0	0	0	1	0	1	0	0	0	0	0	0	0	0	0	0	0	0	0	0	0	0	0	0	0	0	0	0	0	0	0
WS	SI	OU	(44)	*Aspidella*	*costata*	N/A	1	0	0	0	0	0	1	0	0	0	0	0	0	0	0	0	0	0	0	0	0	0	1	0	0	0	0	0	0	0	0	0	0	0	0	0	0	0	0	0	0	0	0	0	0	0	0	0	0	0
WS	SI	OU	(44)	*Aspidella*	*hatyspytia*	N/A	1	0	0	0	0	0	1	0	0	0	0	0	0	0	0	0	0	0	0	0	0	0	1	0	?	0	0	0	0	0	0	0	0	0	0	0	0	1	0	0	0	0	0	0	0	0	0	0	0	0
WS	SI	OU	(44)	*Hiemalora*	*pleiomorphus*	N/A	1	0	0	0	0	0	1	0	0	0	0	0	0	0	1	0	0	0	0	0	0	0	0	0	0	0	0	0	0	0	0	0	0	0	0	0	0	0	1	0	0	0	0	0	0	0	0	0	0	0
WS	SI	OU	(31)	*Khatyspytia*	*grandis*	P13-1	0	0	0	0	0	1	0	1	0	0	0	0	0	0	0	0	0	0	0	0	1	0	0	0	0	0	0	0	0	1	0	0	0	0	0	0	0	0	0	0	0	0	0	0	0	0	1	0	0	0
NA	KL	NM	(45)	*Rangea*	*schneiderboehni*	N/A	0	0	0	0	0	1	0	1	0	1	0	0	0	0	0	0	0	0	0	0	1	0	0	0	0	0	0	0	0	1	0	0	0	1	0	1	0	1	0	0	0	0	0	0	0	0	1	1	0	0
NA	KL	NM	(46)	*Nasepia*	*altae*	F2A-G	0	0	1	0	0	?	0	0	1	0	0	0	0	0	0	0	0	0	0	0	0	1	0	0	0	0	0	0	0	0	0	0	0	0	0	0	0	0	0	0	0	0	0	0	0	0	0	0	0	0
NA	KL	NM	(47)	*Pteridinium*	*simplex*	N/A	0	0	0	0	0	1	0	0	1	0	0	0	0	0	0	0	1	0	0	0	0	0	0	0	0	0	0	0	0	1	0	0	0	0	0	0	0	0	0	0	0	0	0	0	0	0	0	0	0	0
NA	KL	NM	(47)	*Namalia*	*villiersiensis*	N/A	0	0	1	0	0	0	0	0	1	0	0	0	0	0	0	0	1	0	0	0	0	0	0	0	0	0	0	0	0	1	0	0	0	0	0	0	0	0	0	0	0	0	0	0	0	0	0	0	0	0
NA	KL	NM	(48)	*Protechiurus*	*edmondsi*	F1A-D	0	0	0	0	0	1	0	0	1	0	0	0	0	0	1	0	0	0	0	0	0	0	0	0	0	0	0	0	0	0	0	0	0	0	0	0	0	0	0	0	0	0	0	0	0	0	0	0	0	0
NA	KL	NM	(49)	*Swartpuntia*	*germsi*	F4, 6, 9, 10	0	0	0	0	0	1	0	1	0	0	0	0	0	0	0	0	0	0	0	1	1	0	0	0	0	0	0	0	0	0	1	0	0	0	0	0	0	0	0	0	0	0	0	0	0	0	1	0	0	0
NA	KL	NM	(50)	*Paramedusium*	*africanum*	N/A	1	0	0	0	0	0	1	0	0	0	0	0	0	0	0	0	0	0	0	0	0	0	1	0	0	0	0	0	0	0	0	0	0	0	0	0	0	0	0	0	0	1	0	0	0	0	0	0	0	0
NA	KL	NM	(51)	*Ausia*	*fenestrata*	P.1	0	1	0	0	0	0	0	1	0	0	0	0	0	1	0	0	0	0	0	0	0	0	0	0	0	0	0	0	0	0	0	0	0	0	0	0	0	0	0	0	0	0	0	0	0	0	?	0	0	0
NA	KL	NM	(51)	*Kubisia*	*glabra*	P2,3	1	0	0	0	0	0	1	0	0	0	0	0	0	0	1	0	0	0	0	0	0	0	0	0	0	0	0	0	0	0	0	0	0	0	0	0	0	0	0	1	0	0	0	0	0	0	1	0	0	0
NA	KL	NM	(52)	*Hagenetta*	*aarensis*	P1-3	1	0	0	0	0	0	1	0	0	0	0	0	0	0	1	0	0	0	0	0	0	0	0	0	0	0	0	0	0	0	0	0	0	0	0	0	0	0	0	0	0	0	0	0	0	0	0	0	0	0
NA	KL	NM	(53)	*Ernietta*	sp.	F1-3	0	0	1	0	0	0	0	0	1	0	0	0	0	0	0	0	1	0	0	0	0	0	0	0	0	0	0	0	0	1	0	0	0	0	0	0	0	0	0	0	0	0	0	0	0	0	0	0	0	0
NA	KL	NM	(54)	*Erniaster*	*apertus*	P28-1-3, 5-7	0	0	1	0	0	0	0	0	1	0	0	0	0	0	0	0	1	0	0	0	0	0	0	0	0	0	0	0	0	1	0	0	0	0	0	0	?	0	0	0	0	0	0	0	0	0	0	0	0	0
NA	KL	NM	(54)	*Erniocentris*	*centriformis*	P28-4,8,9	1	0	0	0	0	0	1	0	0	0	0	0	0	1	0	1	0	0	0	0	0	0	0	0	0	0	0	0	0	0	0	0	0	0	0	0	0	0	0	0	0	1	0	0	0	0	0	0	0	0
NA	KL	NM	(54)	*Ernionorma*	*peltis*	P29-2,5	0	0	1	0	0	0	0	0	1	0	0	0	0	0	0	0	0	1	0	0	0	0	0	0	0	0	0	0	0	1	0	0	0	0	0	0	0	0	0	0	0	0	0	0	0	0	0	0	0	0
NA	KL	NM	(54)	*Erniobeta*	*forensis*	P39-2-4,10	0	0	1	0	0	0	0	1	0	0	0	0	0	0	0	0	1	0	0	0	0	0	0	0	0	0	0	0	0	0	1	0	0	0	0	0	1	0	0	0	0	0	0	0	0	0	0	0	0	0
NA	KL	NM	(55)	*Velancorina*	*martina*	P2-1-2	0	0	1	0	0	0	0	0	1	0	0	0	0	0	0	0	1	0	0	0	0	0	0	0	0	0	0	0	0	1	0	0	0	0	1	1	0	0	0	0	0	0	0	0	0	0	0	0	0	0
NA	LA	BC	(56)	*Beltanella*	sp.	F6G	1	0	0	0	0	0	1	0	0	0	0	0	0	0	1	0	0	0	0	0	0	0	0	0	0	0	0	0	0	0	0	0	0	0	0	0	0	0	0	0	0	0	0	0	0	0	0	0	0	0
NA	LA	BC	(56)	*Charniodiscus*	sp.	F 6ACDHJ; 7A-D F-I	1	0	0	0	0	0	1	0	0	0	0	0	0	0	0	0	0	0	0	0	0	0	1	0	0	0	0	0	0	0	0	0	0	0	0	0	0	0	0	0	0	0	0	0	0	0	0	0	0	0
NA	LA	BC	(56)	*Irridinitus*	sp.	F6C.E, 7E	1	0	0	0	0	0	1	0	0	0	0	0	0	0	0	1	0	0	0	0	0	0	1	0	1	0	0	0	0	0	0	0	0	0	0	0	0	0	0	0	0	0	0	0	0	0	0	0	0	0
NA	LA	BC	(56)	*Nimbia*	*occlusa*	F6F,G	1	0	0	0	0	0	1	0	0	0	0	0	0	0	0	0	0	0	0	0	0	0	1	0	0	0	0	0	0	0	0	0	0	0	0	0	0	0	0	0	0	0	0	0	0	0	0	0	0	0
NA	LA	BC	(56)	*Protodipleurosoma*	sp.	F6B	1	0	?	0	0	0	1	0	0	0	0	0	0	0	0	0	0	0	0	0	0	0	0	1	0	0	0	0	0	0	0	0	0	0	0	0	0	?	0	0	0	1	0	0	0	0	0	0	0	0
NA	LA	BC	(57)	*Cyclomedusa*	sp.	F2A,B	1	0	0	0	0	0	1	0	0	0	0	0	0	0	0	1	0	0	0	0	0	0	1	0	0	0	0	0	0	0	0	0	0	0	0	0	0	0	0	0	0	0	0	0	0	0	0	0	0	0
NA	LA	GB	(58)	*Nimbia*	sp.	F3-1,2,3	1	0	0	0	0	0	1	0	0	0	0	0	0	0	0	0	0	0	0	0	0	0	1	0	0	0	0	0	0	0	0	0	0	0	0	0	0	0	0	0	0	0	0	0	0	0	0	0	0	0
NA	LA	GB	(58)	*Swartpuntia*	sp.	F4-1-4	0	0	0	0	0	1	0	1	0	0	0	0	0	0	0	0	0	0	0	1	1	0	0	0	0	0	0	0	0	0	?	0	0	0	0	0	0	0	0	0	0	0	0	0	0	0	1	0	0	0
MK	LA	MZ	(59)	*Windermeria*	*aitkeni*	F3.2-3.4, 4	0	0	1	0	0	0	0	0	1	0	0	0	0	0	0	0	1	0	0	0	0	0	0	0	0	0	0	0	0	1	0	0	0	0	0	0	0	0	0	0	0	0	0	0	0	0	0	0	0	0
MK	LA	MZ	(60)	*Beltanella*	*gilesi*	P1-1	1	0	0	0	0	0	1	0	0	0	0	0	0	0	0	1	0	0	0	0	0	0	0	0	0	0	0	0	0	0	0	0	0	0	0	0	0	0	0	0	0	0	0	0	0	0	0	0	0	0
MK	LA	MZ	(60)	*Charniodiscus*	sp.	P1-7	1	0	0	0	0	0	1	0	0	0	0	0	0	0	0	0	0	0	0	0	0	0	1	0	0	0	0	0	0	0	0	0	0	0	0	0	0	0	0	0	0	0	0	0	0	0	?	0	0	0
MK	LA	MZ	(60)	*Cyclomedusa*	*plana*	P1-4	1	0	0	0	0	0	1	0	0	0	0	0	0	0	0	1	0	0	0	0	0	0	?	0	0	0	0	0	0	0	0	0	0	0	0	0	0	0	0	0	0	0	0	0	0	0	0	0	0	0
MK	LA	MZ	(60)	*Cyclomedusa*	sp.	P1-2,6; P2-3,5	1	0	0	0	0	0	1	0	0	0	0	0	0	0	0	1	0	0	0	0	0	0	1	0	0	0	0	0	0	0	0	0	0	0	0	0	0	0	0	0	0	0	0	0	0	0	0	0	0	0
MK	LA	MZ	(60)	*Ediacaria*	sp.	P1-5	1	0	0	0	0	0	1	0	0	0	0	0	0	0	0	1	0	0	0	0	0	0	1	0	0	0	0	0	0	0	0	0	0	0	0	0	0	0	0	0	0	0	0	0	0	0	0	0	0	0
MK	LA	MZ	(60)	*Eoporpita*	sp.	P2-1	1	0	0	0	0	0	1	0	0	0	0	0	0	0	0	1	0	0	0	0	0	0	0	0	1	0	0	0	0	0	0	0	0	0	0	0	0	0	0	0	0	0	0	0	0	0	0	0	0	0
MK	LA	MZ	(60)	*Eoporpita*	sp.	P3-4	1	0	0	0	0	0	1	0	0	0	0	0	0	0	0	?	0	0	0	0	0	0	1	0	0	0	0	0	0	0	0	0	0	0	0	0	0	0	1	0	0	0	0	0	0	0	0	0	0	0
MK	LA	MZ	(60)	*Medusinites*	*asteroides*	P2-6,7	1	0	0	0	0	0	1	0	0	0	0	0	0	0	0	0	0	0	0	0	0	0	1	0	0	0	0	0	0	0	0	0	0	0	0	0	0	0	0	0	0	0	0	0	0	0	0	0	0	0
MK	LA	MZ	(60)	*Pteridinium*	sp.	P2-1	0	0	0	0	0	1	0	0	1	0	0	0	0	0	0	0	1	0	0	0	0	0	0	0	0	0	0	0	0	1	0	0	0	0	0	0	0	0	0	0	0	0	0	0	0	0	0	0	0	0
MK	LA	MZ	(61)	*Sekwia*	*excentrica*	P2-8	1	0	0	0	0	0	1	0	0	0	0	0	0	0	?	0	1	0	0	0	0	0	0	0	0	0	0	0	0	0	0	0	0	0	0	0	0	0	0	0	0	0	0	0	0	0	0	0	0	0
MK	LA	MZ	(61)	*Inkrylovia*	sp.	F3	0	0	0	0	0	1	0	0	1	0	0	0	0	0	0	0	1	0	0	0	0	0	0	0	0	0	0	0	0	1	0	0	0	0	0	0	0	0	0	0	0	0	0	0	0	0	0	0	0	0
MK	LA	MZ	(59)	*Hiemalora*	*stellaris*	F3-1	1	0	0	0	0	0	1	0	0	0	0	0	0	0	1	0	0	0	0	0	0	0	0	0	0	0	0	0	0	0	0	0	0	0	0	0	0	0	1	0	0	0	0	0	0	0	0	0	0	0

Column label abbreviations: AS (Assemblages); CO (Continents); BT (Biotas); Rf (References; see reference list below); See "Materials and Methods" for character abbreviations

Row label abbreviations in column 1: AV (Avalon assemblage); WS (White Sea assemblage); NA (Nama assemblage); MK (Mackenzie Mountains biota)

Row label abbreviations in column 2: AV (Avalon); BA (Baltica); SI (Siberia); AU (Australia); LA (Laurentia); KL (Kalahari)

Row label abbreviations in column 3: NF (Newfoundland); CF (Charnwood Forest); FR (Flinders Ranges); CA (Central Australia); WC (Winter Coast and adjacent area); PD (Podolia); UR (Urals); FM (Finnmark); WN (Wernecke Mountains); OU (Olenëk Uplift); NM (Namibia); BC (British Columbia); GB (Great Basin); MZ (Makenzie Mountains)

Character coding: 1 (present); 0 (absent); ? (uncertain)

List of references

1. LaFlamme, M., Narbonne, G.M., and Anderson, M.M., 2004, Morphometric analysis of the Ediacaran frond Charniodiscus from the Mistaken Point Formation, Newfoundland: Journal of Paleontology, v. 78, p. 827-837.

2. Narbonne, G., Dalrymple, R.W., Flamme, M.L., Gehling, J., and Boyee, W.D., 2005, Life after Snowball: Mistaken Point Biota and the Cambrian of the Avalon: Halifax, Nova Scotia, North American Paleontological Convention Field Trip Guidebook, 100 p.

3. Narbonne, G.M., and Gehling, J.G., 2003, Life after snowball: The oldest complex Ediacaran fossils: Geology, v. 31, p. 27-30.

4. Narbonne, G.M., 2004, Modular Construction of Early Ediacaran Complex Life Forms: Science, v. 305, p. 1141-1144.

5. Gehling, J.G., Narbonne, G.M., and Anderson, M.M., 2000, The first named Ediacaran body fossil, *Aspidella terranovica* : Palaeontology, v. 43, p. 427-456.

6. Brien, S.J.O., and King, A.F., 2004, Ediacaran fossils from the Bonavista Peninsula (Avalon Zone), Newfoundland: preliminary descriptions and implications for regional correlation: Newfoundland Department of Mines and Energy Gelogical Survey, Report, v. 04-1.

7. Clapham, M.E., Narbonne, G.M., Gehling, J.G., Greentree, C., and Anderson, M.M., 2004, *Thectardis avalonensis* : A new Ediacaran fossil from the Mistaken Point Biota, Newfoundland: Journal of Paleontology, v. 78, p. 1031-1036.

8. Anderson, M.M., and Morris, S.C., 1982, A review, with descriptions of four unusual forms, of the soft-bodied fauna of the Conception and St. John's Groups (Late Precambrian), Avalon Peninsula, Newfoundland: Proceedings of the third North American Paleontological Third Convention, v. 1, p. 1-18.

9. Ford, T.D., 1999, The Precambrian fossils of Charnwood Forest: Geology Today, v. 15, p. 230-234.

10. Boynton, H.E., and Ford, T.D., 1995, Ediacaran fossils from the Precambrian (Charnian Supergroup) of Charnwood Forest, Leicestershire, England: Mercian Geologist, v. 13, p. 165-182.

11. Boynton, H.E., and Ford, T.D., 1979, *Pseudovendia charnwoodensis* -- a new Precambrian arthropod from Charnwood Forest, Leicester: Mercian Geologist, v. 7, p. 175-177.

12. Gehling, J.G., Droser, M.L., Jensen, S.R., and Runnegar, B.N., 2005, Ediacara organisms: relating form to function, *in* Briggs, D.E.G., ed., Evolving Form and Function: Fossils and Development: New Haven, Yale Peabody Museum Publications, p. 43-66.

13. Wade, M., 1972, Hydrozoa and Scyphozoa and other medusoids from the Precambrian Ediacara fauna, South Australia: Palaeontology, v. 15, p. 197-225.

14. Glaessner, M.F and W. Mary, 1966, The late Precambrian fossils from Ediacara, South Australia: Palaeontology, v. 9, p. 599-628.

15. Wade, M., 1972, Dickinsonia; polychaete worms from the late Precambrian Ediacara fauna, South Australia: Memoirs of the Queensland Museum, v. 16, p. 171-190.

16. Glaessner, M.F., 1971, The genus *Conomedusites* Glaessner & Wade and the diversification of the Cnidaria: Palaeontologische Zeitschrift, v. 45, p. 7-17.

17. Glaessner, M.F., 1958, New fossils from the base of the Cambrian in South Australia (preliminary account): Transactions of the Royal Society of South Australia, v. 81, p. 185-188.

18. Glaessner, M.F.W., Mary, 1971, *Praecambridium* ; a primitive arthropod: Lethaia, v. 4, p. 77-71.

19. Glaessner, M.F., 1980, *Parvancorina* - an arthropod from the Late Precambrian (Ediacaran) of South Australia: Annalen des, in naturhistorischen Museums In Wien, v. 88, p. 83-90.

20. Wade, M., 1969, Medusae from uppermost Precambrian or Cambrian sandstones, central Australia: Palaeontology, v. 12, p. 351-365.

21. Gehling, J.G., 1988, A cnidarian of actinian-grade from the Ediacaran Pound Subgroup, South Australia: Alcheringa, v. 12, p. 299-314.

22. Gehling, J.G., 1987, Earliest known echinoderm - a new Ediacaran from the Pound Subgroup of South Australia: Alcheringa, v. 11, p. 337-345.
23. Glaessner, M.F., 1976, A new genus of late Precambrian polychaete worms from South Australia: Transactions of the Royal Society of South Australia, v. 100, p. 169-170.
24. Gehling, J.G., and Rigby, J.K., 1996, Long expected sponges from the Neoproterozoic Ediacara fauna of South Australia: Journal of Paleontology, v. 70, p. 185-195.
25. Jenkins, R.J.F., and Gehling, J.G., 1978, A review of the frond-like fossils of the Ediacara assemblage: Record of South Australia Museum, v. 17, p. 347-359.
26. Wade, M., 1971, Bilateral Precambrian chondrophores from the Ediacara fauna, South Australia: Proceedings of the Royal Society of Victoria, v. 84, p. 183-188.
27. Hofmann, H.J., 1988, An alternative interpretation of the Ediacaran (Precambrian) chondrophore *Chondroplon* Wade: Alcheringa, v. 12, p. 315-318.
28. Sun, W., 1986, Precambrian medusoids: The *Cyclomedusa plexus* and *Cyclomedusa* -like pseudofossils: Precambrian Research, v. 31, p. 325-360.
29. Sprigg, R.C., 1949, Early Cambrian "jellyfishes" of Ediacara, South Australia, and Mt. John, Kimberley District, Western Australia: Transaction of the Royal Society of South Australia, v. 73, p. 72-99.
30. Yale Peabody Museum, YPM204511, informally named as *Mandelbrotia* by A. Seilacher.
31. Sokolov, B.S., and Iwanowski, A.B., 1990, The Vendian System, Volume 1: Paleontology: Heidelberg, Springer-Verlag, 1-383 p.
32. Urbanek, A., and Rozanov, A.Y., 1983, Upper Precambrian and Cambrian Palaeontology of the East-European Platform: Warszawa, Publishing House Wydawnictwa Geologiczne, p. 158.
33. Ivantsov, A.Y., 2004, New Proarticulata from the Vendian of the Arkhangel'sk region: Paleontological Journal, v. 38, p. 247-253.
34. Ivantsov, A.Y., Malakhovskaya, Y.E., and Serezhnikova, E.A., 2004, Some Problematic Fossils from the Vendian of the Southeastern White Sea region: Paleontological Journal, v. 38, p. 3-9.
35. Ivantsov, A.Y., and Grazhdankin, D., 1997, A new representative of the Petalonamae from the upper Vendian of the Arkhangelsk Region: Paleontological Journal, v. 31, p. 1-16.
36. Grazhdankin, D., 2000, The Ediacaran genus *Inaria* : a taphonomic/morphodynamic analysis: Neues Jahrbuch fuer Geologie und Palaeontologie. Abhandlungen, v. 216, p. 1-34.
37. Ivanstov, A.Y., 1999, A New representative of Dickinsoniids from the upper Vendian of the Northern Coast of the White Sea (Russia, Arkhangel'sk Region): Zoologicheskii Zhurnal, v. 3, p. 3-11.
38. Fedonkin, M.A., and Waggoner, B.M., 1997, The late Precambrian fossil *Kimberella* is a mollusc-like bilaterian organism: Nature, v. 388, p. 868-871.
39. Grazhdankin, D., 2004, Patterns of distribution in the Ediacaran biotas: facies versus biogeography and evolution: Paleobiology, v. 30, p. 203-221.
40. Ivanstov, A.Y., 2001, *Vendia* and other Precambrian Arthropdos: Zoologicheskii Zhurnal, v. 4, p. 3-10.
41. Bekker, J.R., 1992, Drevnejshaja ediakarskaja biota urala: Izvestija Akademij Nauk, Serija Geologicheskaja, v. 6, p. 16-24.
42. Farmer, J., Vidal, G., Moczydlowska, M., Strauss, H., Ahlberg, P., and Siedlecka, A., 1992, Ediacaran fossils from the Innerelv Member (late Proterozoic) of the Tanafjorden area, northeastern Finnmark: Geological Magazine, v. 129, p. 181-195.
43. Narbonne, G.M., and Hofmann, H.J., 1987, Ediacaran biota of the Wernecke Mountains, Yukon, Canada: Palaeontology, v. 30, p. 647-676.
44. Vodanjuk, S.A., 1989, Ostatki besskeletnykh metazoa iz khatyspytskoj svity Olenekskogo podnjatija,*in* Khomentovskij, V.V., and Sovetov, J.K., eds., Pozdnij dokembrij i rannij paleozoj Sibiri. Akademija Nauk SSSR, Sibirskoe Otdelenie: Novosibirsk, Institut Geologii i Geofiziki, p. 61-74.
45. Jenkins, R.J.F., 1985, The Enigmatic Ediacaran (Late Precambrian) Genus *Rangea* and Related Forms: Paleobiology, v. 11, p. 336-355.
46. Germs, G.J.B., 1973, A reinterpretation of *Rangea schneiderhoehni* and the discovery of a related new fossil from the Nama Group, South West Africa: Lethaia, v. 6, p. 1-9.
47. Grazhdankin, D., and Seilacher, A., 2002, Underground Vendobionta from Namibia: Paleontology, v. 45, p. 57-78.
48. Glaessner, M.F., 1979, An echiurid worm from the Late Precambrian: Lethaia, v. 12, p. 121-124.
49. Narbonne, G.M., Saylor, B.Z., and Grotzinger, J.P., 1997, The youngest Ediacaran fossils from southern Africa: Journal of Paleontology, v. 71, p. 953-967.
50. Gürich, G., 1930, Die bislang altesten Spuren von Organismen in Sudafrika: International Geological Congress. South Africa, 1929 (XV), v. 2, p. 670-680.
51. Hahn, G., and Pflug, H.D., 1985, Polypenartige Organismen aus dem Jung-Praekambrium (Nama-Gruppe) von Namibia. Polyp-like organisms from the upper Precambrian Nama Group of Namibia: Geologica et Palaeontologica, v. 19, p. 1-13.
52. Hahn, G., and Pflug, H.D., 1988, Zweischalige Organismen aus dem Jung-Präkambrium (Vendium) von Namibia (SW-Afrika): Geologica et Palaeontologica, v. 22, p. 1-19.
53. Dzik, J., 1999, Organic membranous skeleton of the Precambrian metazoan from Namibia: geology, v. 27, p. 519-522.
54. Pflug, H.D., 1972, Zur Fauna der Nama-Schichten in Suedwest-Afrika; III, Erniettomorpha, Bau und Systematik. The fauna of the Nama Beds in South-West Africa; 3, Erniettomorpha, structure and systematics: Palaeontographica. Abteilung A: Palaeozoologie-Stratigraphie, v. 139, p. 134-168.
55. Pflug, H.D., 1966, Neue Fossilreste aus den Nama-Schichten in Sudwest-Africa: Palaontologische Zeitschrift, v. 40, p. 14-25.
56. Hofmann, H.J., Mountjoy, E.W., and Teitz, M.W., 1991, Ediacaran fossils and dubiofossils, Miette Group of Mount Fitzwilliam area, British-Columbia: Canadian Journal of Earth Sciences, v. 28, p. 1541-1552.
57. Hofmann, H.J., Mountjoy, E.W., and Teitz, M.W., 1985, Ediacaran fossils from the Miette Group, Rocky Mountains, British Columbia, Canada: Geology, v. 13, p. 819-821.
58. Hagadorn, J.W., and Waggoner, B., 2000, Ediacaran fossils from the southwestern Great Basin, United States: Journal of Paleontology, v. 74, p. 349-359.
59. Narbonne, G.M., 1994, New Ediacaran fossils from the Mackenzie Mountains, northwestern Canada: Journal of Paleontology, v. 68, p. 411-416.
60. Narbonne, G.M., and Aitken, J.D., 1990, Ediacaran fossils from the Sekwi Brook area, Mackenzie Mountains, northwestern Canada: Palaeontology, v. 33, p. 945-980.
61. Hofmann, H.J., 1981, First record of a Late Proterozoic faunal assemblage in the North American Cordillera: Lethaia, v. 14, p. 303-310.

Table 1.5. Mahalanobis distances between the centroids of the three Ediacara assemblages (AV: Avalon; NA: Nama; WS: White Sea), the four biotas in the White Sea assemblage (FR: Flinders Ranges; BA: Baltica; WN: Wernecke; SI: Siberia), and the three biotas representing different paleoenvironments (FR: Flinders Range; NM: Namibia; NF: Newfoundland). Estimates of statistical significance of each distance are shown in parentheses.

Mahalanobis distances between centroids of three Ediacara assemblages		
Assemblage	AV	NA
NA	0.786 (0.005)	
WS	1.162 (<0.0001)	0.045 (0.618)

Mahalanobis distances between centroids of four biotas in the White Sea assemblage			
Biota	FR	BA	WN
BA	0.018 (0.692)		
WN	0.578 (0.046)	0.783 (0.012)	
SI	0.343 (0.229)	0.505 (0.102)	0.030 (0.918)

Mahalanobis distances between centroids of three biotas representing different paleoenvironments		
Biota	FR	NM
NM	0.275 (0.178)	
NF	0.478 (0.020)	0.431 (0.139)

Table 1.6. Classificatory error rates based on the discriminant analysis for the three Ediacara assemblages (AV: Avalon; NA: Nama; WS: White Sea), the four biotas in the White Sea assemblage (FR: Flinders Ranges; BA: Baltica; WN: Wernecke; SI: Siberia), and the three biotas representing different paleoenvironments (FR: Flinders Range; NM: Namibia; NF: Newfoundland). Reported error rates were corrected via jackknife cross-validation.

Classificatory error rates for three Ediacara assemblages					
Assemblage	AV	NA	WS	Average	
Error rate	0.42	1.00	0.35	0.59	
Classificatory error rates for four biotas in the White Sea assemblage					
Continent	FR	BA	WN	SI	Average
Error rate	0.90	0.60	0.31	1.00	0.70
Classificatory error rates for three biotas representing different paleoenvironments					
Biota	FR	NM	NF	Average	
Error rate	0.49	0.50	0.57	0.52	

Chapter 2

Problematic Macrofossils from Ediacaran Successions in the North China and Chaidam Blocks: Implications for Their Evolutionary Roots and Biostratigraphic Significance [1]

Abstract

Upper Neoproterozoic successions in the North China and nearby Chaidam blocks are poorly documented. North China successions typically consist of a diamictite unit overlain by siltstone, sandstone, or slate. Similar successions occur in Chaidam, although a cap carbonate is present atop the diamictite unit. The diamictites in both North China and Chaidam have been variously interpreted as Cryogenian, Ediacaran, or Cambrian glacial deposits. In this paper, we describe problematic macrofossils collected from slate of the upper Zhengmuguan Formation in North China and sandstone of the Zhoujieshan Formation in Chaidam; both fossiliferous formations conformably overlie the aforementioned diamictites. Some of these fossils were previously interpreted as animal traces. Our study of these fossils recognizes four genera and five species—*Helanoichnus helanensis* Yang *in* Yang and Zheng, 1985, *Palaeopascichnus minimus* n. sp., *Palaeopascichnus meniscatus* n. sp., *Horodyskia moniliformis*? Yochelson and Fedonkin, 2000, and *Shaanxilithes* cf. *ningqiangensis* Xing et al., 1984. None of these taxa can be interpreted as animal traces. Instead, they are problematic body fossils of unresolved phylogenetic affinities. The fundamental similarity in the bodyplans of *Horodyskia* and *Palaeopascichnus*, both with serially repeated elements, indicates a possible underlying phylogenetic relationship. Thus, at least some Ediacaran organisms may have a deep root because *Horodyskia* has been previously reported from Mesoproterozoic successions.

Among the four genera reported in this paper, *Palaeopascichnus* Palij, 1976, and *Shaanxilithes* Xing et al., 1984 have been known elsewhere in upper Ediacaran successions, including the Dengying Formation (551–542 Ma) in South China. If these two genera have biostratigraphic significance, then the fossiliferous units in North China and Chaidam may be upper Ediacaran as well. This correlation indicates that the underlying diamictites in North China

[1] Article published by Shen, B, Xiao, S., Dong, L., Zhou, C. and Liu, J. (2007) Problematic macrofossils from Ediacaran successions in the North China and Chaidam blocks: implications for their evolutionary roots and biostratigraphic significance. Journal of Paleontology 81(6): 1396-1411. (Paleontolgical Society)

and Chaidam cannot be of Cambrian age, but their correlation with Ediacaran (e.g., Gaskiers) and Cryogenian glaciations (e.g., Nantuo) remains unclear. As there are no other diamictite intervals in Neoproterozoic successions in the North China and Chaidam blocks, our data suggest that there is only one Neoproterozoic glaciation recorded and preserved in these two blocks.

1. INTRODUCTION

The Ediacaran Period is pivotal to the understanding of a possible Precambrian fuse to the Cambrian explosion and the igniter (e.g., global glaciations) of that evolutionary fuse. The late Ediacaran Period is characterized by classical Ediacara fossils that have been reported from most major continents (Narbonne et al., 2005; Narbonne, 1998), as well as simple trace fossils that have been widely used as direct evidence for the beginning of animal activities (Droser et al., 2002; Dzik, 2005; Fedonkin, 1994). However, recent studies indicate that many previously described trace fossils were incorrectly interpreted as such (Droser et al., 2005a; Jensen, 2003; Jensen et al., 2005; Seilacher et al., 2005; Seilacher et al., 2003). According to a recently compiled list (Jensen et al., 2006), many previously named Ediacaran trace fossil taxa from Russia and China have been reinterpreted as body fossils or as problematic fossils. Thus it is important to reexamine these purported trace fossils. As part of this exercise, in this paper we focus on upper Neoproterozoic (likely Ediacaran) tracelike fossils from the North China and Chaidam blocks that have been previously interpreted as animal traces.

Upper Neoproterozoic outcrops in the North China Block are sporadic, and most occur in the southern and western margins. Typically, upper Neoproterozoic successions in North China consist of a single diamictite unit, unlike other continents such as the Quruqtagh area where up to three Neoproterozoic diamictite units are developed (Xiao et al., 2004). This diamictite unit is overlain by a siliciclastic unit, followed by lower Cambrian deposits. It can be traced along the western and southern margins, and has been suggested to be Cryogenian (or equivalent to the > 635 Ma Nantuo glaciation in South China; (Condon et al., 2005; Zhao et al., 1980a)), Ediacaran (Gao et al., 1980), or Cambrian (Wang et al., 1980a), although chronostratigraphic evidence in support of these correlations is tenuous at best.

The situation is no better in the Chaidam Block of northwestern China, where Neoproterozoic outcrops are few and isolated. Nonetheless, upper Neoproterozoic successions in Chaidam seem to be similar to those in North China; they also consist of a diamictite unit and overlying finer-grained siliciclastics, although a cap carbonate unit occurs atop the diamictite unit. The similar lithostratigraphic sequences have prompted many to correlate the diamictites in North China and Chaidam, although independent tests of this correlation have not been forthcoming.

In both North China and Chaidam, the finer siliciclastic units that overlie the diamictite units contain macroscopic fossils. The initial reports of these fossils were published more than 20 years ago (Wang et al., 1980a; Yang and Zheng, 1985), when such fossils were described under various taxonomic names and were uncritically interpreted as animal traces. In light of recent reevaluation of Neoproterozoic trace fossils (Jensen, 2003), there is a need to clarify the taxonomic confusion and to reassess the trace fossil interpretation of the North China and Chaidam fossils. Thus, the goals of this study are to redescribe previously purported trace fossils and to report two new forms from the upper Neoproterozoic successions in North China and Chaidam. A careful description of these fossils will provide a systematic basis on which we can more objectively assess Ediacaran ichnological diversity and test the biostratigraphic significance of certain Ediacaran fossils (e.g., *Palaeopascichnus* Palij, 1976). In addition, these fossils will help to constrain the age of the underlying diamictites North China and Chaidam; these diamictites, if indeed are of Cambrian or Ediacaran age (Gao et al., 1980; Wang et al., 1980a), would have wider implications for the extent of post-Cryogenian glaciations (Bertrand-Sarfati et al., 1995; Bowring et al., 2003).

2. GEOLOGICAL SETTING

Our samples were collected at two sections, the Suyukou section in the Helanshan area of Ningxia Hui Autonomous Region, northern China, and the Quanjishan Section in the Chaidam Basin of Qinghai Province, northwestern China (Fig. 2.1). The former is located in the western margin of the North China Block, and the latter in the Oulongbuluke microcontinent of the Chaidam Block (Lu, 2002).

2.1. Suyukou section

Upper Neoproterozoic successions occur only on the western and southern margins of the North China Block; much of the rest of the block was exposed above sea level during the late Neoproterozoic (Wang, 1985). The thickness of upper Neoproterozoic successions on the western and southern margin is quite variable, although they always contain a diamictite unit overlain by a siltstone/sandstone/slate unit.

At Suyukou, late Neoproterozoic strata are represented by the Zhengmuguan Formation, which unconformably overlies dolostone of the Mesoproterozoic Wangquankou Group and underlies, also unconformably, phosphorite of the Lower Cambrian Suyukou Formation (Fig. 2.2). The lower member of the Zhengmuguan Formation is a 70 m thick diamictite unit, which is graded into 80 m thick grayish slaty siltstone of the upper member. The lower member is dominated by heterolithic diamictite with cobble- to boulder-sized clasts and mostly calcareous matrix. The 5 m thick transition between the two members is gradual, with the size and abundance of outsized clasts decreasing upsection. No radiometric dates are available to directly constrain the depositional age of the Zhengmuguan Formation, although it is believed to be Neoproterozoic to earliest Cambrian in age on the basis of stratigraphic relationships with the Wangquankou and Suyukou formations.

The fossils reported in this paper were collected in fine-grained slaty siltstone of the uppermost 1 m of the Zhengmuguan Formation, although Yang and Zheng (1985) described five ichnogenera and six ichnospecies from several horizons in the upper member of the Zhengmuguan Formation.

2.2. Quanjishan section

The Quanjishan section is located in northern Chaidam, which was recently recognized as the Oulongbuluke microcontinent (Lu, 2002). Here, Neoproterozoic successions occur in a few sporadic outcrops (Lu, 2002; Wang et al., 1980a). Unlike in the North China Block, upper Neoproterozoic successions in Oulongbuluke are typically more than 1 km thick. The Quanjishan section is one of the best known in this area. At Quanjishan, the Neoproterozoic sequence is represented by the Quanji Group, which overlies amphibolite-gneiss-migmatite of the early Proterozoic Delingha Group and underlies bioturbated dolostone of the Cambrian Xiaogaolu Group. The Quanji Group includes, in ascending order, the Mahuanggou, Kubaimu, Shiyingliang, Hongzaoshan, Heitupo, Hongtiegou, and Zhoujieshan formations (Fig. 2.2). The

450 m thick Mahuanggou Formation consists of conglomerate, cross-bedded quartz sandstone. The 350 m thick Kubaimu Formation is composed of thick-bedded, medium to coarse sandstone, unconformably succeeded by 200 m thick light grey quartzite or quartz sandstone of the Shiyingliang Formation. The 300 m thick Hongzaoshan Formation represents the only carbonate-dominated unit in the Quanji Group, consisting mainly of dolostone with abundant dissolution structures. The Hongzaoshan dolostone is conformably overlain by the 120 m thick Heitupo shale and the <20 m thick Hongtiegou diamictite. The overlying Zhoujieshan Formation begins with a 7 m thick dolostone that may be considered as a cap carbonate conformably overlying the Hongtiegou diamictite (Fig. 2.3.1). The rest of the Zhoujieshan Formation is composed of reddish, fine sandstone and siltstone. No detailed sedimentary analysis of the Quanji Group has been published, although the fossiliferous Zhoujieshan Formation is believed to have deposited in an intertidal environment (Wang et al., 1980a). The only radiometric constraint comes from a 738 ± 28 Ma zircon U–Pb (SHRIMP) date of a basaltic andesite unit in the lower Quanji Group, and thus the base of Quanji Group is estimated to be about 760 Ma (Lu, 2002). Previous authors (Wang et al., 1980a; Xing, 1985) illustrated several fossils from the Zhoujieshan Formation, but systematic description has not been published. We collected additional fossils from more than 10 horizons in the Zhoujieshan Formation, with the lowest occurrence being ~5 m above the cap carbonate unit in the basal Zhoujieshan Formation.

2.3. Interpretation and correlation of diamictites

Diamictites in the Hongtiegou and Zhengmuguan formations have been traditionally interpreted as glacial in origin. Dropstones and striated clasts have been reported to occur in both formations (Wang et al., 1980a; Zheng et al., 1994). In Chaidam, the spatial distribution of the Hongtiegou and equivalent diamictites is poorly documented, but dropstones have been noted in the Hongtiegou diamictite (Fig. 2.3.2), which, like many Neoproterozoic glacial deposits, is immediately overlain by a cap carbonate (Fig. 2.3.1). In the North China Block, the Zhengmuguan and stratigraphically equivalent diamictites—for example, the Luoquan diamictite in Shaanxi and Henan provinces (Guan et al., 1986; Mu, 1981)—can be traced along the southern and western margins. They also contain unambiguous dropstones (Fig. 2.3.3, 2.3.4).

Although the Zhengmuguan and Hongtiegou diamictites in two distinct tectonic units are generally regarded as recording the same glaciation (Wang et al., 1981), their correlation with

other Neoproterozoic glacial deposits is less clear. They have been variously considered as representing the ~635 Ma Nantuo glaciation (Mu, 1981; Zhao et al., 1980b), an Ediacaran glaciation (Gao et al., 1980; Guan et al., 1986; Lu et al., 1985; Wang et al., 1981; Zheng et al., 1994) that may be equivalent to the Hankalchough glaciation in Quruqtagh (Xiao et al., 2004) or the Gaskiers glaciation in Newfoundland (Bowring et al., 2003), or a Cambrian glaciation (Wang et al., 1980a). The fossils described in this paper will be used to test these hypotheses.

3. SYSTEMATIC PALEONTOLOGY

Genus HELANOICHNUS Yang *in* Yang and Zheng, 1985, emended

Type species.—*Helanoichnus helanensis* Yang *in* Yang and Zheng, 1985.

Original diagnosis.—Primitive pascichnia made by soft-bodied organisms feeding along bedding surface. Burrow system can be complex. Inner part of trace consists of spiral or intertwining burrows, whereas outer part consists of circular, elliptical, or sinuous burrows. Inner burrows thinner than outer ones. Burrows 0.5–1.0 mm in diameter. Burrow system covers an area of 5–10 cm^2. Burrow system appears to consist of entangling cords, but burrows separated from each other by certain distance (translated from Yang and Zheng, 1985).

Emended diagnosis.—Cylindrical fossil with no surface ornamentations. Fossils typically preserved as curved or looped ribbons on bedding surface. Ribbon width millimetric but can be variable within a single specimen. Ribbon length typically centimetric in mostly incomplete specimens. Ribbon margin can be smooth or irregular. When intersecting, ribbons show overlapping rather than self-overcrossing relationships. No side branches occur in the ribbons.

Discussion.—This genus was originally interpreted as grazing traces (pascichnia) produced by soft-bodied organisms feeding along bedding surface (Yang and Zheng, 1985). However, most specimens show significant within-specimen variations in their width (Fig. 2.4.2, 2.4.3, 2.4.7), inconsistent with grazing traces, which are expected to have a more or less uniform width along a single trace that corresponds to the width of trace maker (Droser et al., 2005b). The margin of a specimen can be smooth in some parts but irregular in other parts of the ribbon (Fig. 2.4.1). In addition, when two specimens intersect, their relationship appears to be overlapping (Fig. 2.4.4, 2.4.8) rather than self-overcrossing, as would be expected for

intersecting grazing traces. Finally, the ribbons do not form well-organized meanderings as would be expected in animal grazers, particularly sophisticated grazers. These observations suggest that the trace fossil interpretation in general, and the grazing trace interpretation in particular, are questionable. We offer an alternative interpretation that *Helanoichnus* is a body fossil (see below).

HELANOICHNUS HELANENSIS Yang *in* Yang and Zheng, 1985, emended

Figures 2.4.1–2.4.8

Helanoichnus helanensis YANG *in* Yang and Zheng, 1985, p. 14, pl. I, figs. 3–5. [No holotype designated]

Parascalarituba ningxiaensis YANG *in* Yang and Zheng, 1985, p. 15, pl. I, fig. 9. [No holotype designated]

Helminthoida helanshanensis ZHANG *in* Xing et al., 1985, p. 191, pl. 42, fig. 4. [No holotype designated]

Helminthopsis quanjishanensis ZHANG *in* Xing et al., 1985, p. 192, pl. 42, fig. 6. [No holotype designated]

Helminthopsis quanjishanensis ZHANG *in* Xing et al., 1985; Zhang, 1986, p. 83, pl. IV, fig. 3.

Helanoichnus helanensis YANG *in* Yang and Zheng, 1985; Yang et al., 2004, p. 149, pl. 19, fig. 6.

Original diagnosis.—Same as original genus diagnosis by monotypy (Yang and Zheng, 1985).

Emended diagnosis.—Same as emended diagnosis by monotypy.

Description.—Fossils densely clustered on both lower and upper bedding surfaces with significant overlapping but no self-overcrossing (Fig. 2.4.3, 2.4.4, 2.4.8). Most specimens are preserved as curved or looped ribbons (Fig. 2.4.1, 2.4.5, 2.4.8). Ribbons do not branch. They range in length from few millimeters to ~10 cm, and in width from <1 mm to 2.5 mm (Fig. 2.5). Ribbon width can vary substantially along length (Figs. 4.2, 4.7, 5). No surface ornamentations, such as annulations, occur on ribbons. Some specimens extremely short (Fig. 2.4.6), perhaps because of incomplete preservation. In a few specimens where ribbon terminus can be observed, it can be pointed (Fig. 2.4.5, 2.4.7), blunt (Fig. 2.4.1, 2.4.2), or irregular (Fig. 2.4.5). Fossils

distinguished from matrix by finer and more light-colored sediments, and delineated from matrix by reddish or greenish boundary. No organic carbon can be observed on ribbon; this can be due to weathering or cast/mold preservation of the fossils. The Zhengmuguan fossils were collected in a quarry and stratigraphic orientation was not marked at collection, whereas the Quanjishan fossils were collected in situ with known orientations.

Material.—More than 100 specimens on 20 rock slabs.

Type.—The specimen illustrated in plate I, figure 5 of Yang and Zheng (1985) is here designated as a lectotype.

Occurrence.—The upper member of the Zhengmuguan Formation in the Helanshan area, Ningxia Hui Autonomous Region, North China, and the Zhoujieshan Formation, Quanji Group, in the Quanjishan area, Qinghai Province, Chaidam.

Discussion.—The only stated difference between *Helanoichnus helanensis* and *Parascalarituba ningxiaensis*, both of which occur in the upper Zhengmuguan Formation at Suyukou (Yang and Zheng, 1985), lies in the looser and more irregular coiling of the ribbons and somewhat discontinuous "back-fillings" in the latter species. The so-called "back-filling" structures were the reason why *Parascalarituba ningxiaensis* was interpreted as a trace fossil (Yang and Zheng, 1985). Based on our observation, the "back-filling" structures appear to be an artifact of the irregular outer margins of the ribbon. Therefore, *Parascalarituba ningxiaensis* is treated as a synonym of *Helanoichnus helanensis*.

Zhang *in* Xing et al. (1985) described *Helminthoida helanshanensis* from the Zhengmuguan Formation and *Helminthopsis quanjishanensis* from the Zhoujieshan Formation. After a systematic review and revision, Uchman (1995) transferred the type species of *Helminthoida* Schafhäutl, 1851—*H. irregularis* Schafhäutl, 1851—into the genus *Nereites* MacLeay 1839. The emended diagnosis of *Nereites irregularis* (Schäfhautl, 1851) emphasizes the dense and multistory occurrence of this irregularly meandering trace (Uchman, 1995). Neither fossils from our collection nor Zhang's illustration (*in* Xing et al., 1985) show consistent widths or meandering patterns. The taxonomic assignment of the Zhoujieshan material to the genus *Helminthopsis* Heer, 1877, is also questionable. *Helminthopsis* has been diagnosed as a simple, unbranched, elongate, irregularly winding or meandering trace (Han and Pickerill, 1995; Wetzel and Bromley, 1996). However, Zhang's illustration (*in* Xing et al., 1985) of *Helminthopsis quanjishanensis* does not show meandering features characteristic of

Helminthopsis. Instead, *Helminthopsis quanjishanensis* is similar to *Helanoichnus helanensis* in its irregular external margins, lack of internal structures such as back-fillings.

Genus HORODYSKIA Yochelson and Fedonkin, 2000

Type species.—Horodyskia moniliformis Yochelson and Fedonkin, 2000.

Original diagnosis.—Presumed colonial organisms of small, vertically oriented, short wide cones, hemispherical on upper surface, growing from a horizontal tube (Yochelson and Fedonkin, 2000).

Discussion.—This genus was established on the basis of materials from the Mesoproterozoic Belt Supergroup (Fedonkin and Yochelson, 2002; Horodyski, 1982; Yochelson and Fedonkin, 2000). Similar fossils have been reported from the Mesoproterozoic Bangemall Supergroup in Western Australia (Grey and Williams, 1990; Martin, 2004). These fossils have been characterized as a "string of beads" (Grey and Williams, 1990; Martin, 2004), as they consist of a series of millimeter-sized spherical to subspherical objects that may be physically connected (Martin, 2004).

The Zhengmuguan material was originally described under the genus *Neonereites* Seilacher, 1960 and interpreted as strings of fecal pellets (Yang and Zheng, 1985). *Neonereites* is typically preserved as negative epireliefs consisting of serially arranged dimples that are closely spaced without obvious gaps (Häntzschel, 1975). It has been suggested that *Neonereites*, as defined by its type species, may represent a preservational variant of *Nereites*, which is diagnosed as meandering or spiraling, unbranched, predominantly horizontal trails consisting of a medial backfilled tunnel enveloped by an even to lobate zone of reworked sediment (Mangano et al., 2000; Uchman, 1995). Many Ediacaran fossils described as *Neonereites* have been explicitly excluded from this genus (Uchman, 1995). The Zhengmuguan specimens have millimetric gaps between adjacent "beads", and they unlikely represent meandering trails. Thus the Zhengmuguan fossils do not belong to the genus *Neonereites*, and the genus *Horodyskia* may be their alternative taxonomic home.

HORODYSKIA MONILIFORMIS? Yochelson and Fedonkin, 2000

Figure 2.4.9–2.4.12

Neonereites uniserialis SEILACHER, 1960; Yang and Zheng, 1985, p. 13, pl. I, figs. 1, 2.

Description.—Uniserially arranged, millimetric spheres that form straight or curved sequences of centimetric length. Spheres flattened on both upper and lower bedding surfaces. No carbonaceous material present; "beads" composed of sediments finer-grained and lighter-colored than matrix. Number of "beads" in a series ranges from 7 to ~20. Flattened "beads" circular to subcircular in shape and on avarage 0.5–1.2 mm in diameter. "Beads" within same sequence almost identical in size (Fig. 2.6). Adjacent "beads" separated from each other by a gap of ~0.25 mm (Fig. 2.4.9, 2.4.10) to ~1 mm (Fig. 2.4.11, 2.4.12). Gap filled with material identical to matrix.

Material.—About 10 specimens on bedding surface of 3 slabs.

Occurrence.—The uppermost Zhengmuguan Formation in the Helanshan area, Ningxia Hui Autonomous Region, North China.

Discussion.—The "string of beads" from the upper Zhengmuguan Formation was originally described as *Neonereites uniserialis*, and interpreted as fecal pellets (Yang and Zheng, 1985). As discussed above, the assignment to the genus *Neonereites* is not justified. It has been proposed that many Ediacaran *Neonereites*-like fossils can be compared with palaeopascichnids (Jensen et al., 2006; Seilacher et al., 2005; Seilacher et al., 2003). In many cases, this is an appropriate evaluation. At the basic level, both *Neonereites* and *Palaeopascichnus* are characterized by serially arranged elements. In comparison to *Neonereites*, however, *Palaeopascichnus* consists of morphologically more variable elements that are more tightly arranged (see below). The widely spaced, presumably spherical elements of the Zhengmuguan population are more similar to those of *Horodyskia*. Thus, we tentatively place the Zhengmuguan population in *Horodyskia moniliformis* Yochelson and Fedonkin, 2000, the type and only species of *Horodyskia*.

Horodyskia moniliformis from the Mesoproterozoic Belt Supergroup and the Bangemall Supergroup has been interpreted as the oldest tissue-grade colonial eukaryote (Fedonkin and Yochelson, 2002; Yochelson and Fedonkin, 2000). Key evidence in support of this interpretation includes the observations that the sizes of the "beads" are positively correlated with the distances between them and that the "beads" appear to be connected by a stolon (Fedonkin and Yochelson,

2002; Martin, 2004; Yochelson and Fedonkin, 2000). However, neither such a correlation nor the connecting stolon has been observed in the Zhengmuguan specimens, although we cannot determine whether this is because of the relatively few and poorly preserved specimens from the Zhengmuguan Formation. Thus we place the Zhengmuguan material in *Horodyskia moniliformis* with a degree of uncertainty.

Genus PALAEOPASCICHNUS Palij, 1976, emended

Type species.—Palaeopascichnus delicatus Palij, 1976.

Original diagnosis.—"A series of small, parallel, in most cases arcuate, tightly packed furrows (negative epirelief) on siltstone surface. In positive hyporelief, there are respective ridges of similar structures. Ends of furrows indistinct, gradually passing into rock surface or blunt. Some furrows are transversely segmented by contractions. Furrows of one series number from 4 to 10 and over" (from Urbanek and Rozanov, 1983, p. 93).

Emended diagnosis.—Serially arranged segments or units that can be subcircular, elliptical, curved, or crescent in shape. Segments can be variable in shape and size even within a single series, but if they are curved their convex side tends to point in the same direction. Adjacent segments separated by narrow gap, but not laterally connected to form meandering structures. Series straight or sinuous, and sometimes branch, merge, or overgrow on each other. Series typically maintain a constant width, but they may expand in convex direction (the direct in which segments are convex).

Discussion.—Palaeopascichnus is one of the most widespread Ediacaran genera, and it has been reported from Ediacaran rocks in Russia and Newfoundland (Gehling et al., 2000; Narbonne et al., 1987; Sokolov and Iwanowski, 1990; Urbanek and Rozanov, 1983). Similar fossils have been found in the Wonoka Formation and the Ediacara Member in the Flinders Ranges, South Australia (Haines, 2000; Jenkins, 1995). These fossils have dichotomously branching series, but they share the same basic morphology—serially arranged segments—with *Palaeopascichnus* from Russia and Newfoundland, and they likely belong to the same genus (Gehling and Narbonne, 2002). The diagnosis of *Palaeopascichnus* is here emended to accommodate the Australian material.

Palaeopascichnus was originally interpreted as an animal meandering trace (Urbanek and Rozanov, 1983), largely based on its superficial resemblance to meandering traces, or trace made by an organ moving transversely to the direction of animal movement (Fedonkin, 1981; Jensen, 2003). However, as pointed out by several Ediacaran workers (Gehling et al., 2000; Jensen, 2003; Seilacher et al., 2005; Seilacher et al., 2003), the elongated segments of *Palaeopascichnus* are not laterally connected. This observation is confirmed in the Zhengmuguan material and incorporated in the emended diagnosis of *Palaeopascichnus*.

Published *Palaeopascichnus* or *Palaeopascichnus*-like fossils vary in their size, shape, and arrangement of the segments (see terminology in Fig. 2.7; Table 2.1). The segments can be straight (e.g., *P. delicatus* from Newfoundland; Narbonne et al., 1987), curved (e.g., *P. delicatus* from Russia and Newfoundland; Urbanek and Rozanov, 1983; Gehling et al., 2000; and *Palaeopascichnus* from South Australia, Haines, 2000), subcircular to elliptical (e.g., *P. delicatus* from Russia; Jensen, 2003), or crescent (e.g., Zhengmuguan material described in this paper). Typically, the segments are arranged tightly, with a very narrow gap in between (e.g., *P. delicatus* from Russia and Newfoundland, Urbanek and Rozanov, 1983; Sokolov and Iwanowski, 1990; Gehling et al., 2000). The series may be straight (*P. delicatus*, Urbanek and Rozanov, 1983; Sokolov and Iwanowski, 1990; Gehling et al., 2000) or sinuous (*P. sinuosus* Fedonkin, 1981; Sokolov and Iwanowski, 1990). The Wonoka material includes specimens with series that dichotomously branch, merge, or overgrow on each other (Haines, 2000). Typically, the width of the series remains more or less constant during growth, but it may expand to the convex direction (Haines, 2000). Thus, the diagnosis of *Palaeopascichnus* is here emended to incorporate these variations in recently described *Palaeopascichnus* fossils.

Several other Ediacaran genera share the general bodyplan—serially arranged units or segments—with *Palaeopascichnus*. These include *Yelovichnus* Fedonkin, 1985, *Harlaniella* Sokolov, 1972, *Intrites* Fedonkin, 1980, *Gaojiashania* Yang, Zhang, and Yin *in* Lin et al., 1986, and several forms identified as *Neonereites*. Jensen (2003) has shown that the segments in *Yelovichnus gracilis* Fedonkin, 1985, are closed, ovate-shaped loops, which probably represent the deflation and collapse of walled chambers. Other than the shape of the segments, *Yelovichnus* is broadly similar to *Palaeopascichnus*, and the two genera may be phylogenetically related (Jensen, 2003).

Harlaniella podolica Sokolov, 1972 is a twisted ropelike fossil, and has been reported from Russia and Newfoundland (Narbonne et al., 1987; Sokolov, 1972). The orientation of *Harlaniella* segments is oblique to the series axis. *Harlaniella* was originally interpreted as a spiral trace fossil similar to the Phanerozoic *Helicolithus* Azpeitia Moros, 1933 and *Helicorhaphe* Książkiewicz, 1970. Jensen (2003) modeled the morphology of *Harlaniella* and found that it is unlikely a trace fossil. Thus, *Harlaniella* may also be phylogenetically related to *Palaeopascichnus*, sharing with it a basic bodyplan consisting of serially arranged segments.

Another form is *Intrites punctatus* Fedonkin, 1980, which is also found in Russia and Newfoundland (Narbonne et al., 1987; Sokolov and Iwanowski, 1990). *Intrites punctatus* consists of serially arranged segments as well, but the segments are circular to subcircular rings. It is possible that the segments of *Intrites punctatus* were originally tablet-shaped. Their circular to subcircular shape may have resulted from oblique to flat compression of disarticulated and deflated segments. Thus, *Intrites punctatus* may also be related to *Palaeopascichnus*.

As discussed above, some Ediacaran fossils described as *Neonereites* are also characterized by serially arranged units. In particular, *Neonereites renarius* Fedonkin, 1985 (Sokolov and Iwanowski, 1990, pl. 26, fig. 2; pl. 27, fig. 4) from Russia has sub-circular to elliptical discs or rings that are similar to those in *Intrites punctatus*. Again, its basic bodyplan is very similar to *Palaeopascichnus*.

In addition to the Russian and Newfoundland forms discussed above, some Ediacaran species from China are also broadly similar to *Palaeopascichnus*. *Ningxiaichnus* Yang *in* Yang and Zheng, 1985, from the Zhengmuguan Formation at the Suyukou section of North China, was described as consisting of serially arranged, highly arched, U-shaped segments. The opening of the U-shaped segments is not directed in the same direction. Instead, the segments are rather randomly oriented, possibly by taphonomic compression. The shape of the segments is variable within the same specimen, ranging from U-shaped units to almost closed O-rings. Two species of *Ningxiaichnus—N. suyukouensis* Yang *in* Yang and Zheng, 1985 and *N. minimum* Yang *in* Yang and Zheng, 1985—were differentiated on the basis of segment size. Both species are morphologically similar, and probably phylogenetically related, to *Palaeopascichnus*.

Another form from China is *Gaojiashania* from the Ediacaran Dengying Formation at Ningqiang of South China (see Figs. 1 and 2 for location and stratocolumn). *Gaojiashania* consists of closely spaced (and probably articulated) circular rings (Ding et al., 1992; Lin et al.,

1986; Zhang, 1986). However, *Gaojiashania* is significantly larger than most *Palaeopascichnus*, and *Gaojiashania* "series" do not branch or merge. In addition, *Gaojiashania* appears to be weakly biomineralized.

Palaeopascichnus was originally interpreted as an animal meandering trace (Urbanek and Rozanov, 1983). However, as pointed out by earlier workers (Gehling et al., 2000; Jensen, 2003; Seilacher et al., 2005; Seilacher et al., 2003), the repeating elements of *Palaeopascichnus* are not laterally connected to form meandering patterns. It appears that *Palaeopascichnus* is one of a number of Ediacaran body fossils that share a basic bodyplan of serially arranged segments.

PALAEOPASCICHNUS MINIMUS new species

Figure 2.8.1–2.8.5

Diagnosis.—Series, sometimes sinuous, consist of uniserially arranged, isomorphic segments that are <0.2 mm thick, <0.7 mm wide, and slightly curved. Segments separated from each other by gap of 0.1–0.2 mm. Series unbranched and maintain more or less constant width of < 0.8 mm.

Description.—Fossils normally flattened on bedding surface and devoid of carbonaceous material. Series < 10 mm long and may represent incompletely preserved fragments of larger specimens. Series consist of uniserially arranged, curved or crescent segments. Segments in same series identical in size and shape and parallel to one another (Fig. 2.8.1, 2.8.2, 2.8.4, 2.8.5). Each segment about 0.3–0.7 mm wide and < 0.2 mm thick. Gaps between adjacent segments 0.1–0.2 wide, and filled with material identical to the matrix (Fig. 2.8.4, 2.8.5). Specimens slightly curved or rarely sinuous. In strongly bent specimens, segments fan out at convex side of series (Fig. 2.8.3, 2.8.4), suggesting series had some degree of flexibility.

Etymology.—Species epithet derived from the Latin *minimus*, referring to the small segments of this species.

Material.—More than 10 specimens.

Types.—The specimen illustrated in Figure 2.8.2 (field number: ZMG-7; museum catalog number: VPI-4566) is here designated as the holotype, and the specimen illustrated in Figure 2.8.4 (field number: ZMG-7; museum catalog number: VPI-4568) as a paratype. The holotype

and paratype are reposited at the Virginia Polytechnic Institute and State University Geosciences Museum (VPIGM).

Occurrence.—The upper part of the Zhengmuguan Formation at Suyukou in the Helanshan area, Ningxia Hui Autonomous Region, North China.

Discussion.—This species differs from other *Palaeopascichnus* species and *Palaeopascichnus*-like fossils by its much smaller size (Fig. 2.9, Table 2.1). The gaps between segments of *P. minimus* are greater than those of *P. delicatus* and *P. sinuosus*. Most specimens of *P. minimus* are only slightly curved, similar to *P. delicatus*. One specimen shows significant sinuosity with the segments diverging at the convex side (Fig. 2.8.3). We interpret the sinuosity as evidence for the flexibility of series. Thus, sinuous series may be a taphonomic feature.

PALAEOPASCICHNUS MENISCATUS new species

Figure 2.8.6, 2.8.7

Diagnosis.—Series strongly curved, consisting of uniserially arranged and closely spaced segments. Strongly crescent segments are in close contact axially, but their sharp, lateral edges are free and point in the same direction.

Description.—Strongly curved fossils flattened on both bedding surfaces and not associated with carbonaceous material. Series 1.5–3 mm in width, and can be >100 mm in length. Segments 1 mm in greatest thickness.

Etymology.—Species epithet derived from the Greek *meniskos*, referring to the crescent segments of this species.

Material.—About 10 specimens collected from the upper part of the Zhengmuguan Formation at Suyukou, Ningxia Hui Autonomous Region, North China.

Types.—The specimen illustrated in Figure 2.8.7 is designated as the holotype (field number: ZMG–16; museum catalog number: VPI-4571). The holotype is reposited at the Virginia Polytechnic Institute and State University Geosciences Museum (VPIGM).

Occurrence.—The uppermost Zhengmuguan Formation at Suyukou, Helanshan area, Ningxia Hui Autonomous Region, North China.

Discussion.—The segments of *Palaeopascichnus meniscatus* are strongly crescent and closely spaced, distinct from those of other *Palaeopascichnus* species, which are either straight,

slightly curved, or sub-circular (Table 2.1). Because the segments are flattened, it is uncertain whether they were originally funnel-shaped or crescent-shaped.

Genus SHAANXILITHES Xing, Yue, and Zhang *in* Xing et al., 1984, emended

Type species.—*Shaanxilithes ningqiangensis* Xing, Yue, and Zhang *in* Xing et al., 1984.

Original diagnosis.—Ribbon-shaped impression with constant width. Specimens mostly fragmentary. Width ranges from 1 to 6 mm or more. Observed length ranges from 25 to 60 mm. Closely spaced transverse annulations visible on impressions. Ribbon-shaped impressions do not have well-defined lateral boundaries. Thin annulations parallel to one another. Nineteen to thirty nine annuli per centimeter length of ribbon-shaped impressions (translated from Xing et al., 1984, p. 182).

Emended diagnosis.—Ribbon-shaped body fossils with millimetric width, centimetric length, clearly defined lateral margins, and numerous, closely spaced annulations. Ribbons may represent originally cylindrical tubes. No branching observed.

Discussion.—Annulated, ribbon-shaped fossils from the middle Dengying Formation in southern Shaanxi were first assigned to *Sabellidites* Yanichevsky, 1926 and interpreted as body fossils (Chen et al., 1975). Later, these fossils were redescribed as *Shaanxilithes* and reinterpreted as trace fossils (Xing et al., 1984). Annulated ribbon-shaped fossils collected from the Zhengmuguan and Zhoujieshan formations are very similar to those from the middle Dengying Formation. The Zhengmuguan fossils were originally described as *Taenioichnus* Yang *in* Yang and Zheng, 1985, and interpreted as animal traces (Yang and Zheng, 1985). Subsequently, *Taenioichnus* was synonymized with *Shaanxilithes*, and both were interpreted as trace fossils (Li et al., 1997), although neither were listed in the most recent monographic study of Chinese trace fossils (Yang et al., 2004). The Zhoujieshan fossils were poorly illustrated in the literature as *Sabellidites*-like trace fossils (Wang et al., 1980b).

We agree with previous authors that *Shaanxilithes* is broadly similar to *Sabellidites*, which has been interpreted as a pogonophoran tube fossil (Sokolov, 1967; Sokolov, 1968). However, *Sabellidites* is characterized by annulated, organic tubes (Sokolov, 1967; Sokolov, 1968) (Sun et al., 1986), whereas the tubular nature of *Shaanxilithes* remains to be confirmed in more specimens (e.g., twisted specimen of *Taenioichnus*; Yang and Zheng, 1985). Specimens of

Shaanxilithes typically do not contain much carbonaceous material, let alone coherent organic tube walls. Moreover, it has been shown that *Sabellidites* tube walls consist of interwoven, submicrometer-sized filaments (Ivantsov, 1990; Moczydlowska, 2003; Urbanek and Mierzejewska, 1977), a feature that does not occur in *Shaanxilithes*.

Recently, Hua et al. (2004) presented further evidence that *Shaanxilithes* is a body fossil rather than an animal trace. Observations in support of a body fossil interpretation include twisted and folded specimens (Yang and Zheng, 1985, pl. 1, fig. 8), overlapping rather than self-overcrossing relationships among densely packed specimens (Hua et al., 2004), and deformation of annulations arrangement caused by bending (i.e., annulations converge at concave side and diverge at convex side of bent specimens; Fig. 2.8.10, 2.8.11). Thus, the diagnosis of *Shaanxilithes* is here emended to accommodate these observations. Furthermore, the original diagnosis states that *Shaanxilithes* does not have well-defined lateral boundaries, whereas our own observation of material from the middle Dengying Formation at the type locality suggests that the fossils do have well-defined margins subtly distinguishable from the matrix.

SHAANXILITHES cf. NINGQIANGENSIS Xing, Yue, and Zhang *in* Xing et al., 1984

Figure 2.8.8–2.8.12

cf. *Sabellidites* YANICHEVSKY, 1926; M. Chen, X. Chen, and Lao, 1975, p. 186, pl. 1, figs. 8, 9.
cf. *Shaanxilithes ningqiangensis* XING, YUE, and ZHANG *in* Xing et al., 1984, p. 182, pl. 28, figs. 19, 20.
Taenioichnus zhengmuguanensis YANG *in* Yang and Zheng 1985, p. 16, pl. I, fig. 8.
cf. *Shaanxilithes erodus* ZHANG, 1986, p. 83, pl. IV, figs. 11, 13b.
cf. *Shaanxilithes* sp. Li, Yang, and Li, 1997, p. 73, pl. 5, fig. 2.
cf. *Shaanxilithes* sp. Hua, Chen, and Zhang, 2004, pl. I, figs. 1–6.

Original diagnosis.—Same as original genus diagnosis by monotypy (Xing et al., 1984).

Emended Diagnosis.—Same as emended diagnosis by monotypy.

Description.—Ribbons flattened as part and counterpart on both bedding surfaces. Fossils from Zhengmuguan Formation composed of light grey clay minerals with little contrast to grey matrix, whereas those from Zhoujieshan Formation weathered to a light grey color in sharp

contrast to reddish to greenish matrix. Fossils normally less than 5 mm in width, up to several centimeters in length, and clearly delineated from the surrounding matrix by an outer boundary. Some ribbons maintain constant width along their length and have a smooth outer boundary (Fig. 2.8.8), whereas others show significant variations in width and have an irregular outer boundary (Fig. 2.8.9, 2.8.11, 2.8.12), possibly due to poor preservation. One to two annuli per millimeter of length (Fig. 2.8.9–2.8.11). Annulations poorly preserved in most specimens from Zhoujieshan Formation (Fig. 2.8.10–2.8.12) because of relatively coarse grain size. No branching observed.

Material.—More than 50 specimens collected from the Zhoujieshan Formation, Qinghai Province, and several poorly preserved specimens collected from the Zhengmuguan Formation at Suyukou, Ningxia Hui Autonomous Region. Yang and Zheng (1985) reported a very well-preserved specimen from the Zhengmuguan Formation in Ningxia Hui Autonomous Region (*Taenioichnus zhengmuguanensis* Yang *in* Yang and Zheng, 1985, pl. 1, fig. 8).

Occurrence.—The uppermost Zhengmuguan Formation in the Helanshan area, Ningxia Hui Autonomous Region, North China; the Zhoujieshan Formation, Quanji Group in the Quanjishan area, Qinghai Province; the Gaojiashan Member of the middle Dengying Formation in the Ningqiang area, Shaanxi Province; the Taozicong Formation in Qingzhen county, Guizhou Province; and the Jiucheng Member of the middle Dengying Formation (formerly lower Yuhucun Formation) in eastern Yunnan, South China (Hua et al., 2004).

Discussion.—Material from the Zhengmuguan and Zhoujieshan formations is not well preserved. In particularly, the annulations are not as regularly disposed and the margin is not as smoothly delineated as in the type material from the middle Dengying Formation of southern Shaanxi. It is likely that the poor preservation is due to the relatively coarse grains of the host rocks, particularly in the Zhoujieshan Formation. Thus, we place the current material in an open nomenclature.

Given the poor preservation in the Zhengmuguan and Zhoujieshan formations, it is also entirely possible that the lack of ornamentation or annulations in *Helanoichnus* may be due to poor preservation. As such, *Helanoichnus helanensis* and *Shaanxilithes* cf. *ningqiangensis* might be synonymous; they are similar other than the presence/absence of annulations. At present, however, these two species are kept separate pending further investigation.

Two species of *Shaanxilithes* have been established: *S. ningqiangensis* and *S. erodus*. The difference between these two species lies in the seriated or irregular margin of the latter. As

discussed above, the irregular margin is likely a preservation artifact. Thus *S. erodus* may be considered as a junior synonym of *S. ningqiangensis*.

4. TAPHONOMY

The preservation style of the Zhengmuguan and Zhoujieshan assemblages are quite similar. At both localities, fossils are typically preserved on both bedding surfaces as flattened clay-silt veneers; no significant amount of carbonaceous matter is currently present in these fossils. They are often densely packed, with a large number of specimens superposed on each other.

The clay-silt veneer is only about 100 μm thick and composed of material much finer-grained than the matrix, as shown in thin sections perpendicular to bedding plane (Fig. 2.10.1, 2.10.2). Electron microprobe analysis shows that the fossil material has greater Al/Si ratios than the matrix, indicating that aluminum-rich clay minerals are present in the fossils (Fig. 2.10.3).

We are uncertain whether the lack of carbonaceous matter in both assemblages is primary or secondary. Because these fossils were collected from outcrops in relatively arid areas, it is possible that weathering oxidation on the long exposed surface has removed carbonaceous material that used to exist in these fossils. However, even the specimens collected from relatively fresh outcrops of the Zhengmuguan Formation at Suyukou show no trace of carbonaceous matter. If the lack of carbonaceous matter is primary, then the Zhengmuguan and Zhoujieshan fossils can only be interpreted as agglutinated tests or as casts and molds by aluminum-rich clay minerals, and their taphonomy may be understood using the Ediacara preservational models (Narbonne et al., 2005). This interpretation is worth considering particularly for understanding the taphonomy of *Palaeopascichnus* and *Horodyskia*; these two genera also occur in other Ediacaran successions where they are not known to be preserved with organic walls. For *Shaanxilithes* and possibly *Helanoichnus*, however, the lack of carbonaceous material is more likely due to secondary weathering. At least one specimen of *Shaanxilithes* cf. *ningqiangensis* (described as *Taenioichnus zhengmuguanensis*, Yang and Zheng, 1985, pl. 1, fig. 8) from the relatively fresh outcrop of the Zhengmuguan Formation at Suyukou shows twisted and folded tubular walls. Furthermore, specimens of *Shaanxilithes ningqiangensis* from the middle Dengying Formation at Ningqiang, southern Shaanxi, have a shining film reminiscent of Burgess

Shale fossils. Thus, it is possible that clay minerals may have played a role in the preservation of *Shaanxilithes ningqiangensis* and the Burgess Shale taphonomic models (Butterfield, 1990; Orr et al., 1998) may be applicable.

The color contrast between the fossils and matrix is largely due to differences in grain size and composition. In addition, weathering may have also enhanced the color contrast. For example, the Zhengmuguan fossils, collected from relatively fresh outcrops, have a much more subtle contrast than the Zhoujieshan fossils collected from long exposed outcrops. Presumably, the reddish color in the Zhoujieshan sandstone is due to weathering and oxidation of iron-rich minerals in the matrix (but not in the fossils), thus enhancing the color contrast.

5. INTERPRETATIONS AND AFFINITIES

5.1. *Helanoichnus helanensis*

This species is dominant in the Zhengmuguan assemblage and common in the Zhoujieshan assemblage. We reconstruct *Helanoichnus helanensis* as a cylindrical tubular organism that was flattened because of compression. *Helanoichnus helanensis* curves or coils in a way very similar to *Grypania spiralis* (Walcott, 1899) Walter et al., 1976, but it is rarely folded or twisted, indicating that it was probably a turgid cylindrical tube at the time of burial (Kumar, 1995; Walter et al., 1990).

The paleoecology and phylogenetic affinity of *Helanoichnus helanensis* are less clear. Given the lack of any holdfast structures, it is unlikely that *Helanoichnus helanensis* was an erect benthic organism. More likely, it was a flat-lying benthic organism—much like the Mesoproterozoic *Grypania spiralis* (Kumar, 1995; Walter et al., 1990). It does not have any features that would suggest a phylogenetic affinity with animal, fungi, algae, protist, or bacteria, although its simple morphology seems to be consistent with siphonous algae (e.g., the green alga *Valonia* Agardh, 1823), large protists, or colonial bacteria (e.g., cyanobacterial colonies of *Nostoc* Vaucher *in* Bornet and Flahault, 1888).

5.2. *Horodyskia*

Horodyskia has been interpreted as a tissue-grade colonial eukaryote, with its serially arranged “beads” connected by horizontal stolons (Fedonkin and Yochelson, 2002; Yochelson

and Fedonkin, 2000). The discovery of a strand connecting neighboring "beads" (Martin, 2004) lends further support to this morphological interpretation. Fedonkin and Yolchelson (2002) also speculate that *Horodyskia* was an epibenthic or shallow infaunal and a photosynthetic or chemosynthetic organism, which grew by amalgamation of smaller and closely spaced "beads" to make larger and widely spaced ones. Our specimens from the Zhengmuguan Formation at Suyukou are strongly flattened, and they do not allow an unambiguous test of Fedonkin and Yolchelson's morphological and paleoecological interpretations.

5.3. *Palaeopascichnus*

This genus is characterized by serially arranged segments. The segments are morphologically variable, ranging from straight, curved, circular, elliptical, to crescent, although part of this variation may be due to taphonomy (e.g., a circular segment may be preserved in different shapes depending on whether it is compressed vertically, horizontally, or obliquely). It is likely that the segments were walled chambers that were articulated in life.

Palaeopascichnus was probably a benthic organism, and it appears to be a flat-lying benthic organism. It does not have a specialized holdfast, which would be expected for macroscopic, fan-shaped organisms that were erect benthic organisms. Dichotomous branching (e.g., in the Wonoka material reported by Haines, 2000) is common but not unique to erect benthic organisms. Similarly, an overlapping relationship (Haines, 2000) is consistent with erect benthic organisms felled by water currents and procumbent benthic organisms overgrowing on each other. Merged series (e.g., Haines, 2000, fig. 6b) and mutual avoidance in densely packed specimens, however, are more consistent with a procumbent than erect lifestyle. Regardless, the consistent curvature of segments within the same series suggests directional growth through serial addition of new segments.

If all described *Palaeopascichnus* populations shared the same trophic strategy, then they were unlikely photosynthetic, because presumably in-situ preservation of *Palaeopascichnus* occurs in deepwater (below photic zone) Ediacaran successions in Newfoundland (Gehling et al., 2000)(Gehling et al., 2000). Zhuravlev (1993) and Seilacher et al. (2003) interpreted *Palaeopascichnus* as a xenophyophore protist. Modern xenophyophores are deep sea, epibenthic or infaunal, rhizopodial protists with a multinucleate plasmodium (granellare) within a branching tubular test system that consists of stercomare (fecal pellets material) and xenophyae

(agglutinated material) (Levin, 1994; Tendal, 1972; Tendal et al., 1982). They typically have intracellular barite crystals (Gooday and Nott, 1982; Hopwood et al., 1997). Molecular phylogenetic analysis based on small subunit rRNA indicates that xenophyophores are probably foraminifers (Pawlowski et al., 2003). Whereas the general morphology of *Palaeopascichnus* is broadly similar to some epibenthic xenophyophores—for example, *Stannophyllum* Haeckel, 1889, some of the key xenophyophore features such as a branching tubular system and intracellular barite crystals have not been verified in *Palaeopascichnus*. Thus, a xenophyophore interpretation is possible, but the concentric zonations in *Stannophyllum* seem to be distinct from the loosely articulated segments of *Palaeopascichnus*.

However *Palaeopascichnus* is related to living eukaryotes, its fundamental bodyplan appears to be similar to that of *Horodyskia*; both genera are characterized by serially repeated segments or units. They differ only in the morphology and spacing of the segments. This observation may lead to a deeper understanding of serially modular Ediacaran organisms, as *Horodyskia* can be traced to the Mesoproterozoic successions (Fedonkin and Yochelson, 2002; Grey and Williams, 1990; Horodyski, 1982; Martin, 2004; Yochelson and Fedonkin, 2000). It is worth considering the possibility that the colonial, modular origin of Ediacaran organisms may have begun in the Mesoproterozoic.

5.4. *Shaanxilithes*

Ribbons of *Shaanxilithes* are characterized by a well-defined peripheral boundary and closely spaced annulations. One specimen from the Zhengmuguan Formation shows evidence of twisting (Yang and Zheng, 1985, pl. 1, fig. 8), indicating that the organism was likely ribbon-shaped at burial, although it may have been cylindrical in life. There are a number of Precambrian and Cambrian annulated ribbon-shaped fossils, including *Sabellidites*, *Sinosabellites* W. Zheng, 1980, *Protoarenicola* G. Wang, 1982, *Pararenicola* G. Wang, 1982, and *Sinospongia* M. Chen *in* M. Chen and Xiao, 1992. These fossils have been interpreted as animals or possible animals (Chen and Xiao, 1992; Sokolov, 1967; Sun et al., 1986), although the animal interpretation for the latter four genera has been questioned (Dong et al., In press; Qian et al., 2000; Xiao et al., 2002). *Shaanxilithes* have been analogously interpreted as an animal (Chen et al., 1975) or animal trace (Xing et al., 1984), and these interpretations have also

been challenged (Hua et al., 2004). Because of the lack of any diagnostic features, the phylogenetic affinity of *Shaanxilithes* remains problematic.

6. IMPLICATIONS FOR REGIONAL CORRELATION

Due to the lack of direct radiometric dates, the depositional age of the Zhengmuguan and Zhoujieshan formations is poorly constrained. The macroscopic fossils described here, although they may be phylogenetically problematic, can be used to facilitate regional and global correlation of these two formations. *Helanoichnus helanensis* and *Shaanxilithes ningqiangensis* also occur in Ediacaran successions in South China (Hua et al., 2004; Zhang, 1986). Both species occur in the middle Gaojiashan Member of the middle Dengying Formation in the Ningqiang area, southern Shaanxi. The Gaojiashan Member is correlated—on the basis of the common occurrence of *Sinotubulites* M. Chen et al., 1981—with the Shibantan Member of the middle Dengying Formation in the Yangtze Gorge area (Fig. 2.2) (Chen, 1999; Hua et al., 2005; Hua et al., 2003). In the Yangtze Gorges area, the Dengying Formation is constrained between 551 and 542 Ma, based on direct dating and correlation with Ediacaran–Cambrian successions in Oman (Amthor et al., 2003; Condon et al., 2005). Thus it is likely that the fossiliferous upper Zhengmuguan Formation and the Zhoujieshan Formation are chronostratigraphically equivalent to the middle Dengying Formation. Consistent with this correlation is the occurrence of *Palaeopascichnus* in the upper Zhengmuguan Formation. *Palaeopascichnus* is widely known from middle-upper Ediacaran strata (e.g., the Ust Pinegia Formation in White Sea, Russian, Grazhdankin, 2004; Pound Quartzite and Wonoka Formation, South Australia, Glaessner, 1969 and Haines, 2000; Fermuse Formation, Newfoundland, Narbonne et al., 1987 and Gehling et al., 2000). Of course, the paleontological data from the Zhengmuguan and Zhoujieshan formations indicate that *Horodyskia* has a long stratigraphic duration and is biostratigraphically less useful.

If our biostratigraphic correlation is correct, then the paleontological data from the upper Zhengmuguan Formation and the Zhoujieshan Formation also provide a minimum age for the underlying diamictites of the lower Zhengmuguan Formation and the Hongtiegou Formation. These diamictites have been variously considered to be Cryogenian, Ediacaran, or Cambrian. Based on our biostratigraphic correlation, they are unlikely of Cambrian age. They have to be either Cryogenian or Ediacaran in age, possibly correlating with the Nantuo (Condon et al.,

2005), Gaskiers (Bowring et al., 2003), or Hankalchough glaciation (Xiao et al., 2004). More chronostratigraphic data are needed to distinguish these possibilities. Nonetheless, because the Zhengmuguan and Hongtiegou formations (or their equivalents) represent the only Neoproterozoic diamictite interval in the North China and Chaidam blocks respectively, our data suggest that only one Neoproterozoic glaciation is recorded and preserved in these two blocks.

7. CONCLUSIONS

Five problematic fossil taxa—*Helanoichnus helanensis* Yang *in* Yang and Zheng, 1985, *Horodyskia moniliformis*? Yochelson and Fedonkin, 2000, *Palaeopascichnus minimus* n. sp., *Palaeopascichnus meniscatus* n. sp., and *Shaanxilithes* cf. *ningqiangensis* Xing, Yue, and Zhang *in* Xing et al., 1984—have been recognized from the slate of the upper Zhengmuguan Formation in the Helanshan area of the North China Block and the Zhoujieshan Formation of the Chaidam Block. All five taxa are interpreted as body fossils, not trace fossils. Three of the four described genera—*Helanoichnus*, *Palaeopascichnus*, and *Shaanxilithes*—appear to be restricted to the Ediacaran Period, and help to correlate the fossiliferous upper Zhengmuguan Formation and the Zhoujieshan Formation, in the North China and Chaidam blocks, respectively, with the middle Dengying Formation in South China, which has been dated between 551 and 542 Ma. This correlation indicates that the underlying diamictites in the lower Zhengmuguan Formation and the Hongtiegou Formation must be Cryogenian or Ediacaran in age.

The occurrence of *Horodyskia* in Ediacaran successions, if further confirmed by future investigation, suggests that at least some Ediacaran elements may have a deep root traceable into the Mesoproterozoic. Furthermore, the fundamental similarity in the bodyplans of *Horodyskia* and *Palaeopascichnus*, both were macroscopic organisms with serially repeated segments, may be indicative of an underlying phylogenetic relationship. It is worth considering whether such modular organisms had any role in the origin of colonial eukaryotes or even the colonial origin of metazoans (Dewel, 2000). If so, then there may indeed have been a long fuse leading to the Cambrian explosion.

REFERENCES

Agardh, C.A., 1823. Species algarum. Berling, Lund, Vol. 1: 169-531.

Amthor, J.E., Grotzinger, J.P., Schröder, S., Bowring, S.A., Ramezani, J., Martin, M.W. and Matter, A., 2003. Extinction of *Cloudina* and *Namacalathus* at the Precambrian-Cambrian boundary in Oman. Geology, 31: 431-434.

Azpeitia Moros, F., 1933. Datos para el estudio paleontológica del Flysch de la Costa Cantábrica y de algunos otros puntos de España. Boletin del Instituto Geológico y Minero de España, 53: 1-65.

Bertrand-Sarfati, J., Moussine-Pouchkine, A., Amard, B. and Ait Kaci Ahmed, A., 1995. First Ediacaran fauna found in western Africa and evidence for an Early Cambrian glaciation. Geology, 23: 133-136.

Bornet, E. and Flahault, C., 1888. Revision des Nostocacées hétérocystées. Annales des Sciences Naturelles Botanique et Biologie Vegetale, VII: 177-262.

Bowring, S., Myrow, P., Landing, E., Ramezani, J. and Grotzinger, J., 2003. Geochronological constraints on terminal Neoproterozoic events and the rise of metazoans. Geophysical Research Abstracts, 5: 13219.

Butterfield, N.J., 1990. Organic preservation of non-mineralizing organisms and the taphonomy of the Burgess Shale. Paleobiology, 16: 272-286.

Chen, M.-E., Chen, X.-G. and Lao, Q.-Y., 1975. An introduction to the metazoa fossil from the upper Sinian system in southern Shensi and it's stratigraphic significance. Scientia Geologica Sinica, 2: 181-190.

Chen, M. and Xiao, Z., 1992. Macrofossil biota from upper Doushantuo Formation in eastern Yangtze Gorges, China. Acta Palaeontologica Sinica, 31(5): 513-529.

Chen, Z., 1999. Late Sinian metazoan Tubular fossils from western Hubei and Southern Shaanxi, China. Ph.D Dissertation Thesis, Nanjing, 128 pp.

Condon, D., Zhu, M., Bowring, S., Wang, W., Yang, A. and Jin, Y., 2005. U-Pb Ages from the Neoproterozoic Doushantuo Formation, China. Science, 308: 95-98.

Dewel, R.A., 2000. Colonial origin for Eumetazoa: Major morphological transitions and the origin of bilaterian complexity. Journal of Morphology, 243: 35-74.

Ding, L., Li, Y. and Chen, H., 1992. Discovery of *Micrhystridium regulare* from Sinian -- Cambrian boundary strata in Yichang, Hubei, and its stratigraphic significance. Acta Micropalaeontologica Sinica, 9: 303-309.

Dong, L., Xiao, S., Shen, B., Yuan, X., Yan, X. and Peng, Y., In press. Restudy of the worm-like carbonaceous compression fossils *Protoarenicola*, *Pararenicola*, and *Sinosabellidites* from early Neoproterozoic successions in North China. Palaeogeography, Palaeoclimatology, Palaeoecology.

Droser, M.L., Gehling, J.G. and Jensen, S., 2005a. Ediacaran trace fossils: "Tubey" or not to be. GSA Annual Meeting Abstracts with Programs, 37(7): 484.

Droser, M.L., Gehling, J.G. and Jensen, S., 2005b. Ediacaran trace fossils: true and false. In: D.E.G. Briggs (Editor), Evolving Form and Function: Fossils and Development. Yale Peabody Museum Publications, New Haven, pp. 125-138.

Droser, M.L., Jensen, S. and Gehling, J.G., 2002. Trace fossils and substrates of the terminal Proterozoic-Cambrian transition: implications for the record of early bilaterians and sediment mixing. Proceedings National Academy of Sciences, USA, 99: 12572-12576.

Dzik, J., 2005. Behavioral and anatomical unity of the earliest burrowing animals and the cause of the “Cambrian explosion”. Paleobiology, 31: 503-521.

Fedonkin, M.A., 1981. Belomorskaya biota venda. Trudy Akademii Nauk SSSR, 342: 1-100.

Fedonkin, M.A., 1994. Vendian body fossils and trace fossils. In: S. Bengtson (Editor), Early Life on Earth. Columbia University Press, New York, pp. 370-388.

Fedonkin, M.A. and Yochelson, E.L., 2002. Middle Proterozoic (1.5 Ga) *Horodyskia moniliformis* Yochelson and Fedonkin, the oldest known tissue-grade colonial eucaryote. Smithsonian Contributions to Paleobiology, 94: 1-29.

Gao, Z., Peng, C., Li, Y., Qian, J. and Zhu, S., 1980. The Sinian System and its glacial deposits in Quruqtagh, Xinjiang. In: Tianjin Institute of Geology and Mineral Resources (Editor), Research in Precambrian Geology, Sinian Suberathem in China. Tianjin Science and Technology Press, Tianjin, pp. 186-213.

Gehling, J.G. and Narbonne, G.M., 2002. Zonation of the terminal Proterozoic (Ediacarian). International Palaeontological Congress, Geological Society of Australia Abstracts, 68: 63-64.

Gehling, J.G., Narbonne, G.M. and Anderson, M.M., 2000. The first named Ediacaran body fossil, *Aspidella terranovica*. Palaeontology, 43: 427-456.

Glaessner, M.F., 1969. Trace fossils from the Precambrian and basal Cambrian. Lethaia, 2: 369-393.

Gooday, A.J. and Nott, J.A., 1982. Intracellular barite crystals in two xenophyophores, Aschemonella ramuliformis and Galatheammina sp. (Protozoa: Rhizopoda) with comments on the taxonomy of A. ramuliformis. Journal of the Marine Biological Association of the United Kingdom, 62: 595-605.

Grazhdankin, D., 2004. Patterns of distribution in the Ediacaran biotas: facies versus biogeography and evolution. Paleobiology, 30: 203-221.

Grey, K. and Williams, I.R., 1990. Problematic bedding-plane markings from the Middle Proterozoic Manganese Subgroup, Bangemall Basin, Western Australia. Precambrian Research, 46: 307-328.

Guan, B., Wu, R., Hambrey, M.J. and Geng, W., 1986. Glacial sediments and erosional pavements near the Cambrian- Precambrian boundary in western Henan Province, China. Journal of the Geological Society, London, 143: 311-323.

Haeckel, E., 1899. Report on the deep-sea Keratosa collected by H.M.S. Challenger during the years 1873–76. Reports of The Scientific Results of The Voyage of The Challenger. Zoology, 32: 1-92.

Haines, P.W., 2000. Problematic fossils in the late Neoproterozoic Wonoka Formation, South Australia. Precambrian Research, 100: 97-108.

Han, Y. and Pickerill, R.K., 1995. Taxonomic review of the ichnogenus Helminthopsis Heer 1977 with a statistical analysis of selected ichnospecies. Ichnos, 4: 83-118.

Häntzschel, W., 1975. Treatise on Invertebrate Paleontology: Part W Miscellanea supplement 1 Trace fossils and Problematica. Geological Society of America and University of Kansas, Boulder, Colorado, 269 pp.

Heer, O., 1877. Flora Fossilis Helvetiae. Die Vorweltliche Flora der Schweiz. J. Würster, Zürich, 182 pp.

Hopwood, J.D., Mann, S. and Gooday, A.J., 1997. The crystallography and possible origin of barium sulphate in deep sea rhizopod protists (Xenophyophorea). Journal of Marine Biology Association, United Kingdom, 77: 969-987.

Horodyski, R.J., 1982. Problematic bedding-plane markings from the middle Proterozoic Appekunny argillite, Belt Supergroup, northwestern Montana. Journal of Paleontology, 56: 882-889.

Hua, H., Chen, Z., Yuan, X., Zhang, L. and Xiao, S., 2005. Skeletogenesis and asexual reproduction in the earliest biomineralizing animal *Cloudina*. Geology, 33: 277-280.

Hua, H., Chen, Z. and Zhang, L., 2004. *Shaanxilithes* from lower Taozichong Formation, Guizhou Province and its geological and paleobiological significance. Journal of Stratigraphy, 28: 265-269.

Hua, H., Pratt, B.R. and Zhang, L., 2003. Borings in *Cloudina* Shells: Complex Predator-Prey Dynamics in the Terminal Neoproterozoic. Palaios, 18: 454–459.

Ivantsov, A.Y., 1990. New data on the ultrastructure of sabelliditids (Pogonophora?). Paleontologicheskii Zhurnal, 24: 125-128.

Jenkins, R.J.F., 1995. The problems and potential of using animal fossils and trace fossils in terminal Proterozoic biostratigraphy. Precambrian Research, 73: 51-69.

Jensen, S., 2003. The Proterozoic and Earliest Cambrian trace fossil record: patterns, problems and perspectives. Integrative and Comparative Biology, 43: 219-228.

Jensen, S., Droser, M.L. and Gehling, J.G., 2005. Trace fossil preservation and the early evolution of animals. Palaeogeography, Palaeoclimatology, Palaeoecology, 220: 19-29.

Jensen, S., Droser, M.L. and Gehling, J.G., 2006. A critical look at the Ediacaran trace fossil record. In: S. Xiao and A.J. Kaufman (Editors), Neoproterozoic Geobiology and Paleobiology. Springer, Dordrecht, Netherlands, pp. 116-159.

Ksiazkiewicz, M., 1970. Observations on the ichnofauna of the Polish Carpathians. In: P. Crimes and J.C. Harper (Editors), Trace Fossils. Seel House Press, Liverpool, pp. 283-322.

Kumar, S., 1995. Megafossils from the Mesoproterozoic Rohtas Formation (the Vindhyan Supergroup), Katni area, central India. Precambrian Research, 72: 171-184.

Levin, L.A., 1994. Paleoecology and ecology of xenophyophores. Palaios, 9: 32-41.

Li, R., Yang, S. and Li, W., 1997. Trace Fossils from Sinian-Cambrian Boundary Strata in China. Geological Publishing House, Beijing, 99 pp.

Lin, S., Zhang, Y., Zhang, L., Tao, X. and Wang, M., 1986. Body and trace fossils of metazoa and algal macrofossils from the upper Sinian Gaojiashan Formation in southern Shaanxi. Geology of Shaanxi, 4: 9-17.

Lu, S., 2002. The Precambrian geology of Northern Tibet. Geological Publishing House, Beijing, 125 pp.

Lu, S., Ma, G., Gao, Z. and Lin, W., 1985. Sinian ice ages and glacial sedimentary facies-areas in China. Precambrian Research, 29: 53-63.

Mangano, M.G., Buatois, L.A., Maples, C.G. and West, R.R., 2000. A new ichnospecies of Nereites from Carboniferous tidal-flat facies of eastern Kansas, USA; implications for the Nereites-Neonereites debate. Journal of Paleontology, 74: 149-157.

Martin, D.M., 2004. Depositional environment and taphonomy of the 'strings of beads': Mesoproterozoic multicellular fossils in the Bangemall Supergroup, Western Australia. Australian Journal of Earth Sciences, 51: 555-561.

Moczydlowska, M., 2003. Earliest Cambrian putative bacterial nanofossils. Memoirs of the Association of Australasian Palaeontologists, 29: 1-11.

Mu, Y., 1981. Luoquan tillite of the Sinian System in China. In: M.J. Hambrey and W.B. Harland (Editors), Pre-Pleistocene Glacial Record, IGCP 38. Cambridge University Press, Cambridge, pp. 402-413.

Narbonne, G., Dalrymple, R.W., Flamme, M.L., Gehling, J. and Boyee, W.D., 2005. Life after Snowball: Mistaken Point Biota and the Cambrian of the Avalon. North American Paleontological Convention Field Trip Guidebook, Halifax, Nova Scotia, 100 pp.

Narbonne, G.M., 1998. The Ediacara Biota: A terminal Neoproterozoic experiment in the evolution of life. GSA Today, 8: 1-6.

Narbonne, G.M., Myrow, P.M., Landing, E. and Anderson, M.M., 1987. A candidate stratotype for the Precambrian-Cambrian boundary, Fortune Head, Burin Peninsula, southeastern Newfoundland. Canadian Journal of Earth Sciences, 24: 1277-1293.

Orr, P.J., Briggs, D.E.G. and Kearns, S.L., 1998. Cambrian Burgess Shale Animals Replicated in Clay Minerals. Science, 281: 1173-1175.

Palij, V.M., 1976. Remains of non-skeletal fauna and trace fossils from upper Precambrian and Lower Cambrian deposits of Podolia. In: V.A. Ryabenko (Editor), Paleontology and Stratigraphy of the upper Precambrian and lower Paleozoic of the south-western part of the East European Platform. Naukova Dumka, Kiev, pp. 63-77.

Pawlowski, J., Holzmann, M., Fahrni, J. and Richardson, S.L., 2003. Small subunit ribosomal DNA suggests that the xenophyophorean Syringammina corbicula is a foraminiferan. Journal of Eukaryotic Microbiology, 50: 483-487.

Qian, M., Yuan, X., Wang, Y. and Yang, Y., 2000. New material of metaphytes from the Neoproterozoic Jinshanzhai Formation in Huaibei, North Anhui, China. Acta Palaeontologica Sinica, 39: 516-520.

Schäfhautl, K.E., 1851. Geognostische Untersuchungen des Südbayrischen Alpendebirgers. Literarisch-Artistische Anstalt, München, 208 pp.

Seilacher, A., Buatois, L.A. and Mángano, M.G., 2005. Trace fossils in the Ediacaran–Cambrian transition: Behavioral diversification, ecological turnover and environmental shift. Palaeogeography, Palaeoclimatology, Palaeoecology, 227: 323-356.

Seilacher, A., Grazhdankin, D. and Legouta, A., 2003. Ediacaran biota: The dawn of animal life in the shadow of giant protists. Paleontological Research, 7: 43-54.

Sokolov, B.S., 1967. Drevneyshiye pognofory [The oldest Pogonophora]. Doklady Akademii Nauk SSSR, 177: 201-204.

Sokolov, B.S., 1968. Vendian and Early Cambrian Sabellitida (Pogonophora) of the SSSR. Proceedings of the International Paleontological Union , 23 rd International Geologyical Congress: 79-86.

Sokolov, B.S., 1972. Vendskiy etap v istorii Zemli [The Vendian Period in Earth history], Mezhdunarodnyj geologicheskij kongress XXIV sessiya. Daldadov sovetskikh geologov. Problema 7. Paleontologiya. Nauka, Moscow, pp. 114-124.

Sokolov, B.S. and Iwanowski, A.B., 1990. The Vendian System, Volume 1: Paleontology. Springer-Verlag, Heidelberg, 1-383 pp.

Sun, W., Wang, G. and Zhou, B., 1986. Macroscopic worm-like body fossils from the Upper Precambrian (900-700Ma), Huainan district, Anhui, China and their stratigraphic and evolutionary significance. Precambrian Research, 31: 377-403.

Tendal, O.S., 1972. A monograph of the Xenophyophoria (Rhizopodea, Protozoa). Galathea Report, 12: 7-99.

Tendal, O.S., Swinbanks, D.D. and Shirayama, Y., 1982. A new infaunal xenophyophore (Xenophyophoria, Protozoa) with notes on its ecology and possible trace fossil analogues. Oceanologica Acta, 5: 325-329.

Uchman, A., 1995. Taxonomy and palaeoecology of flysch trace fossils: the Marnoso-arenacea Formation and associated facies (Miocene, Northern Apennines, Italy). Beringeria, 15: 1-115.

Urbanek, A. and Mierzejewska, G., 1977. The fine structure of zooidal tubes in Sabelliditida and Pogonophora with reference to their affinity. Acta Palaeontologica Polonica, 22: 223-240.

Urbanek, A. and Rozanov, A.Y. (Editors), 1983. Upper Precambrian and Cambrian Palaeontology of the East-European Platform. Publishing House Wydawnictwa Geologiczne, Warszawa, 158 pp.

Walcott, C.D., 1899. Pre-Cambrian fossiliferous formations. Bulletin of the Geological Society of America, 10: 199-244 (pls. 122–128).

Walter, M.R., Du, R. and Horodyski, R.J., 1990. Coiled carbonaceous megafossils from the middle Proterozoic of Jixian (Tianjin) and Montana. American Journal of Science, 290-A: 133-148.

Walter, M.R., Oehler, J.H. and Oehler, D.Z., 1976. Megascopic algae 1300 million years old from the Belt Supergroup, Montana: A reinterpretation of Walcott's Helminthoidichnites. Journal of Paleontology, 50: 872–881.

Wang, G., 1982. Late Precambrian Annelida and Pogonophora from the Huainan of Anhui Province. Bulletin of the Tianjin Institute of Geology and Mineral Resources, 6: 9-22.

Wang, H., 1985. Atlas of the Palaeogeography of China. Cartographic Publishing House, Beijing, 85 pp.

Wang, Y., Chen, Y., Wang, R., Chen, X. and Wei, X., 1980a. Stratigraphic types and characteristics of Sinian in Hunan, Guizhou and Guangsi. In: Tianjin Institute of Geology and Mineral Resources (Editor), Research in Precambrian Geology: Sinian Suberathem in China. Tianjin Science and Technology Press, Tianjin, pp. 146-163.

Wang, Y., Lu, S., Gao, Z., Lin, W. and Ma, G., 1981. Sinian tillites of China. In: M.J. Hambrey and W.B. Harland (Editors), Pre-Pleistocene Glacial Record, IGCP 38. Cambridge University Press, Cambridge, pp. 386-401.

Wang, Y., Zhuang, Q., Shi, C., Liu, J. and Zheng, L., 1980b. Quanji Group along the northern border of Chaidamu Basin. In: Tianjin Institute of Geology and Mineral Resources (Editor), Research on Precambrian Geology Sinian Suberathem in China, Tianjin, pp. 214-230.

Wetzel, A. and Bromley, R., 1996. Re-evaluation of the ichnogenus Helminthopsis - a new look at the type material. Palaeontology, 30: 1-19.

Xiao, S., Bao, H., Wang, H., Kaufman, A.J., Zhou, C., Li, G., Yuan, X. and Ling, H., 2004. The Neoproterozoic Quruqtagh Group in eastern Chinese Tianshan: Evidence for a post-Marinoan glaciation. Precambrian Research, 130: 1-26.

Xiao, S., Yuan, X., Steiner, M. and Knoll, A.H., 2002. Macroscopic carbonaceous compressions in a terminal Proterozoic shale: A systematic reassessment of the Miaohe biota, South China. Journal of Paleontology, 76: 345-374.

Xing, Y., Ding, Q., Luo, H., He, T. and Wang, Y., 1984. The Sinian-Cambrian boundary of China. Bulletin of the Institute of Geology, Chinese Academy of Geological Sciences: 1-262.

Xing, Y., Ding, Q., Lin, W., Yan, Y., Zhang, L., 1985. Metazoans and trace fossils. In: Y. Xing, Duan, C., Liang, Y,, Cao, R. (Editor), Late Precambrian palaeontology of China. Geological Publishing House, Beijing.

Yang, S., Zhang, J. and Yang, M., 2004. Trace Fossils of China. Science Press, Beijing, 353 pp.

Yang, S. and Zheng, Z., 1985. The Sinian trace fossils from Zhengmuguan Formation of Helanshan Mountain, Ningxia. Earth Science - Journal of Wuhan College of Geology, 10.

Yanichevsky, M.E., 1926. Ob ostatkakh trubchatykh chervej iz kembrijskoj Sinej Gliny [On remains of tube-dwelling worms from the Cambrian Blue Clay]. Ezhegodnik Vsesoyuznogo Paleontologicheskogo Obshchestva, 4: 99-111.

Yochelson, E.L. and Fedonkin, M.A., 2000. A new tissue-grade organism 1.5 billion years old from Montana. Proceedings of the Biological Society of Washington, 113: 843-847.

Zhang, L., 1986. A discovery and preliminary study of the late stage of late Gaojiashan biota from Sinian in Ningqiang County, Shaanxi. Bulletin of the Xi'an Institute of Geology and Mineral Resources, Chinese Academy of Geological Sciences, 13: 67-88.

Zhao, X., Zhang, L., Zou, X., Wang, S. and Hu, Y., 1980a. Sinian tillites in Northwest China and their stratigraphic significance. In: Tianjin Institute of Geology and Mineral Resources (Editor), Research on Precambrian Geology Sinian Suberathem in China. Tianjin Science and Technology Press, Tianjin, pp. 164-185.

Zhao, Z., Xing, Y., Ma, G., Yu, W. and Wang, Z., 1980b. The Sinian System of eastern Yangtze Gorges, Hubei. In: Tianjin Institute of Geology and Mineral Resources (Editor), Research

in Precambrian Geology: Sinian Suberathem in China. Tianjin Science and Technology Press, Tianjin, pp. 31-55.

Zheng, W., 1980. A new occurence of fossil group *Chuaria* from the Sinian System in north Anhui and its geological meaning. Bulletin of the Tianjin Institute of Geology and Mineral Resources, 1: 49-69.

Zheng, Z., Li, Y., Lu, S. and Li, H., 1994. Lithology, sedimentology and genesis of the Zhengmuguan Formation of Ningxia, China. In: M. Deynoux et al. (Editors), Earth's Glacial Record. Cambridge University Press, Cambridge, pp. 101-108.

Zhuravlev, A.Y., 1993. Were Ediacaran vendobionta multicellulars? Neues Jahrbuch fuer Geologie und Palaeontologie. Abhandlungen, 190: 299-314.

Figure 2.1—Geographic map, showing the location of the North China Block, South China Block, Tarim Block, and Chaidam Block. White dot denotes the Suyukou locality in the western margin of the North China Block. Star denotes the Quanjishan section in the Oulongbuluke microcontinent (Lu, 2002) lying on the northern margin of the Chaidam Block.

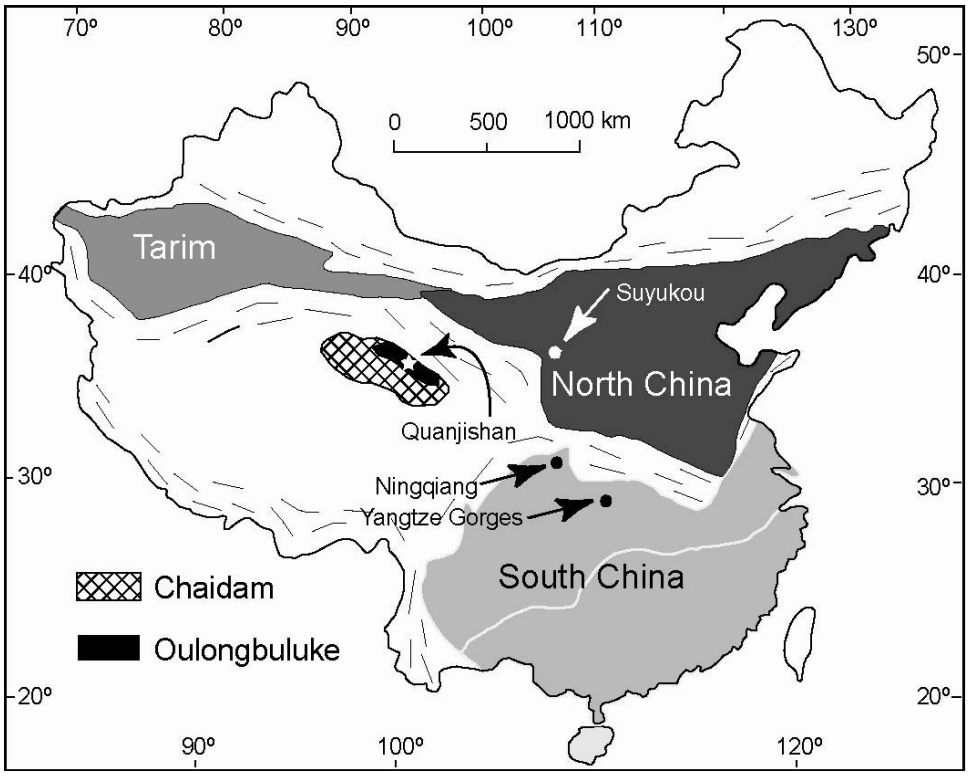

Figure 2.2 —Stratigraphic columns of upper Neoproterozoic successions in (from left to right) the Helanshan area, North China; Quanjishan area, Chaidam; Ningqiang area, South China; and Yangtze Gorge area, South China. See Figure 1 for locality information. WQK: Wangquankou Gr.; SYK: Suyukou Fm.; MHG: Mahuanggou Fm.; KBM: Kubaimu Fm.; SYL: Shiyingliang Fm.; HZS: Hongzaoshan Fm.; HTP: Heitupo Fm.; HTG: Hongtiegou Fm.; ZJS: Zhoujieshan Fm.; XGL: Xiaogaolu Gr.; GJB: Guojiaba Fm.; SJT: Shuijintuo Fm.

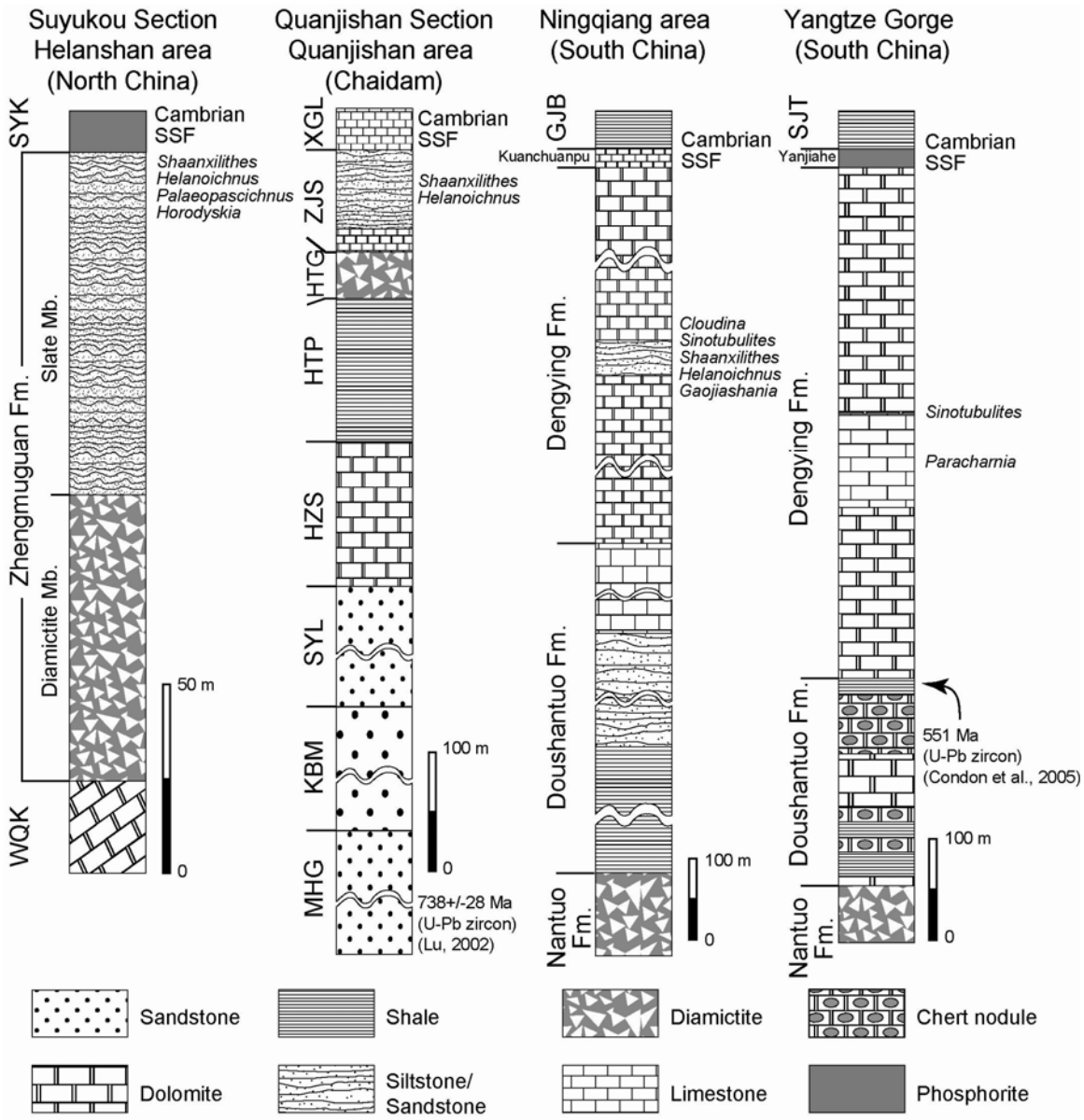

Figure 2.3—Field photographs of the Quanjishan and Suyukou sections. *1*, Field photograph of the Quanjishan section. Black and white arrows point to the fossiliferous Zhoujieshan sandstone and the basal Zhoujieshan cap-carbonate atop the Hongtiegou diamictite, respectively. Geologist in ellipse for scale. *2*, Dropstone in the Hongtiegou diamictite, Quanjishan section. Coin next to dropstone about 2 cm in diameter. *3*, Dropstone in the Luoquan diamictite (equivalent to the lower Zhengmuguan diamictite), Luonan section, central Shaanxi Province, North China Block. Dropstone about 7 cm in maximum diameter. *4*, Dropstone in the Zhengmuguan diamictite, Suyukou section, Ningxia Hui Autonomous Region. Marker pen about 15 cm in length.

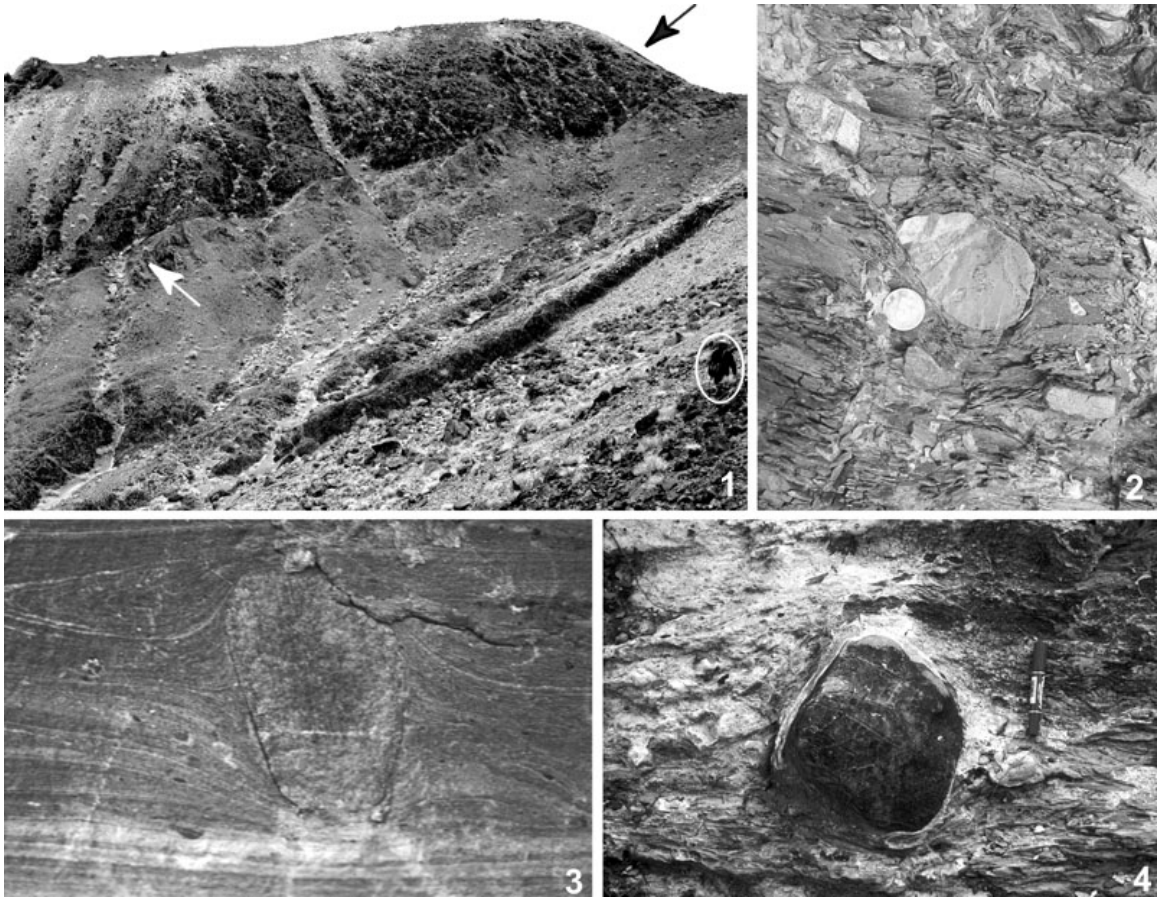

Figure 2.4—*Helanoichnus helanensis* Yang *in* Yang and Zheng, 1985, from the Zhengmuguan (*1–6*) and Zhoujieshan formations (*7*, *8*), and *Horodyskia moniliformis*? Yochelson and Fedonkin, 2000, from the Zhengmuguan Formation (*9–12*). *1*, ZMG-15 (museum number VPI-4554); *2*, ZMG-15 (museum number VPI-4555). Note variation in the ribbon width; *3*, ZMG-7 (museum number VPI-4556); *4*, ZMG-10 (museum number VPI-4557). Arrow points to the overlapping relationship between two specimens; *5*, ZMG-18 (museum number VPI-4558). This coiled specimen has a tapering end (arrow); *6*, ZMG-4 (museum number VPI-4559). A small fragment(?) with a tapering end; *7*, ZJS-36 (museum number VPI-4560); 8, ZJS-35 (museum number VPI-4561). The east-west oriented specimen overlaps the southeast-northwest oriented specimen (arrow). *9–12*, Arrows point to examples of "beads" (presumably compressed spheres) that are uniserially arranged. *9*, ZMG-1 (museum number VPI-4562), *10*, ZMG-1 (museum number VPI-4563), *11*, ZMG-7 (museum number VPI-4564), *12*, ZMG-7 (museum number VPI-4565). Scale bars represent 2 mm if not otherwise noted. In this and all other fossil illustrations, all photographs were taken under a reflected light microscope except otherwise noted. Illustrated fossils are reposited at the Virginia Polytechnic Institute and State University Geosciences Museum (VPIGM). The filed number (ZMG: Zhengmuguan; ZJS: Zhoujieshan) and museum number (VPI-) of each illustrated fossils are given.

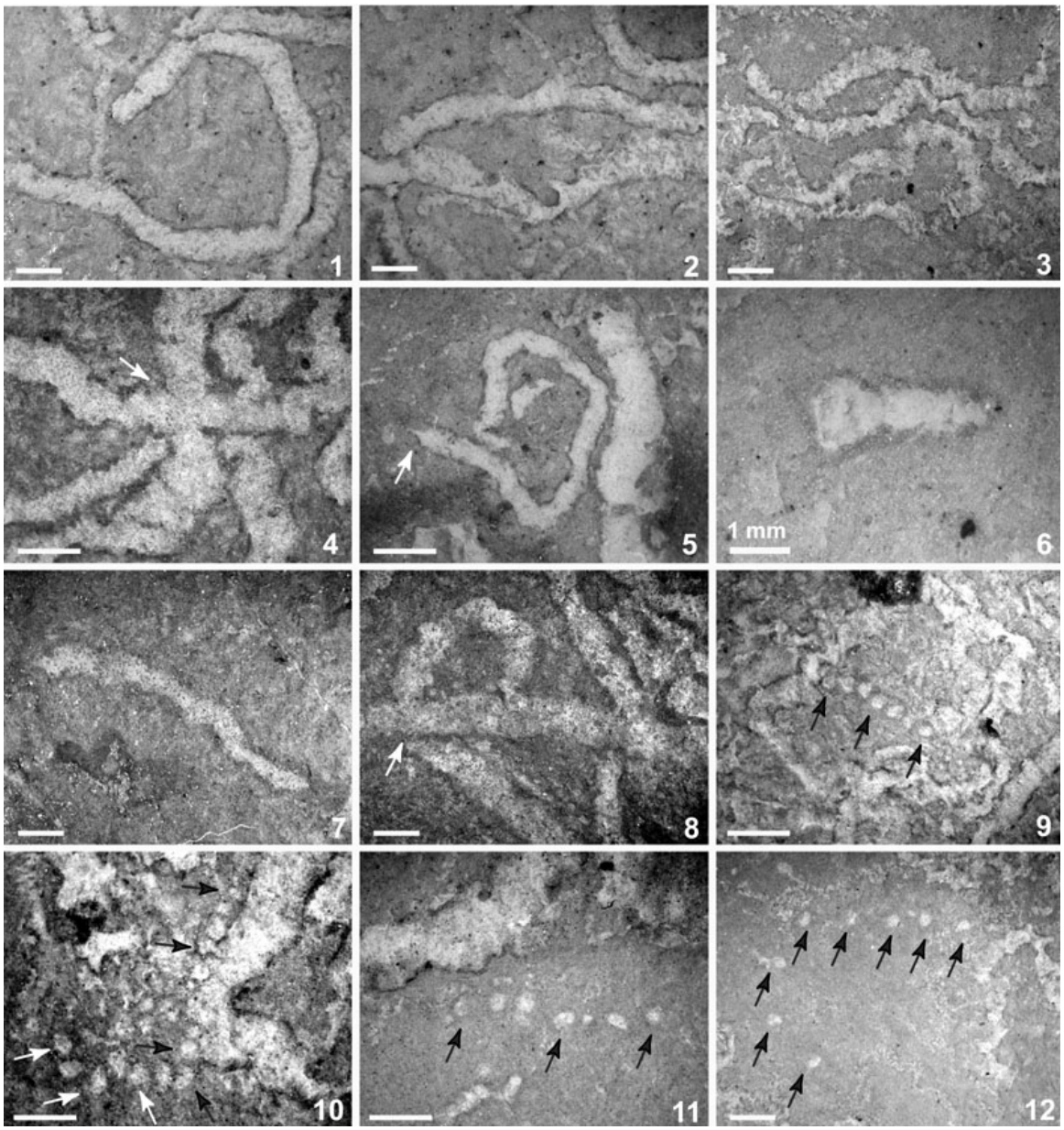
1
2
3
4
5
1 mm
6
7
8
9
10
11
12

Figure 2.5—Measurements of 25 *Helanoichnus helanensis* specimens from the Zhengmuguan Formation. Multiple measurements of the width were randomly taken along the length of each specimen. Bars represent the 25th and 75th percentiles, caps represent the range, and transverse line in box represents the 50th percentile (medium) of the measurements.

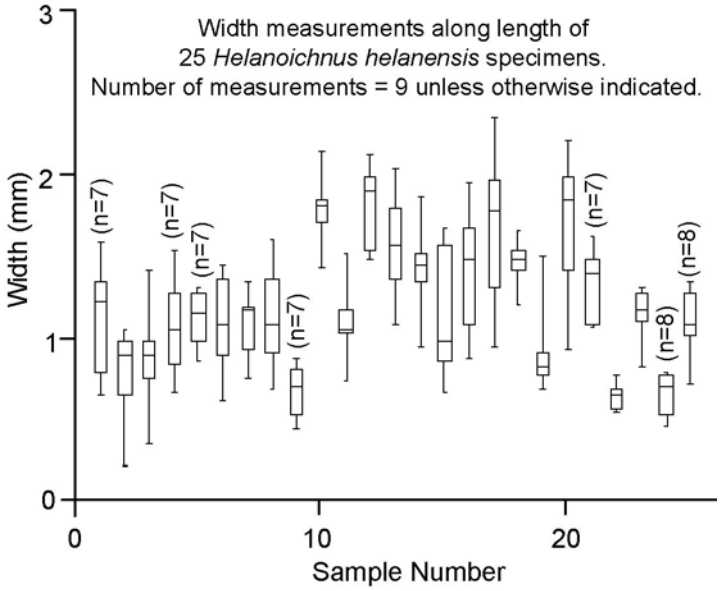

Figure 2.6—Measurements of 5 *Horodyskia moniliformis*? specimens from the Zhengmuguan Formation. The diameter of each "bead" in the same series was measured and plotted. Bars represent the 25th and 75th percentiles, caps represent the range, and transverse line in the box represents the 50th percentile (medium).

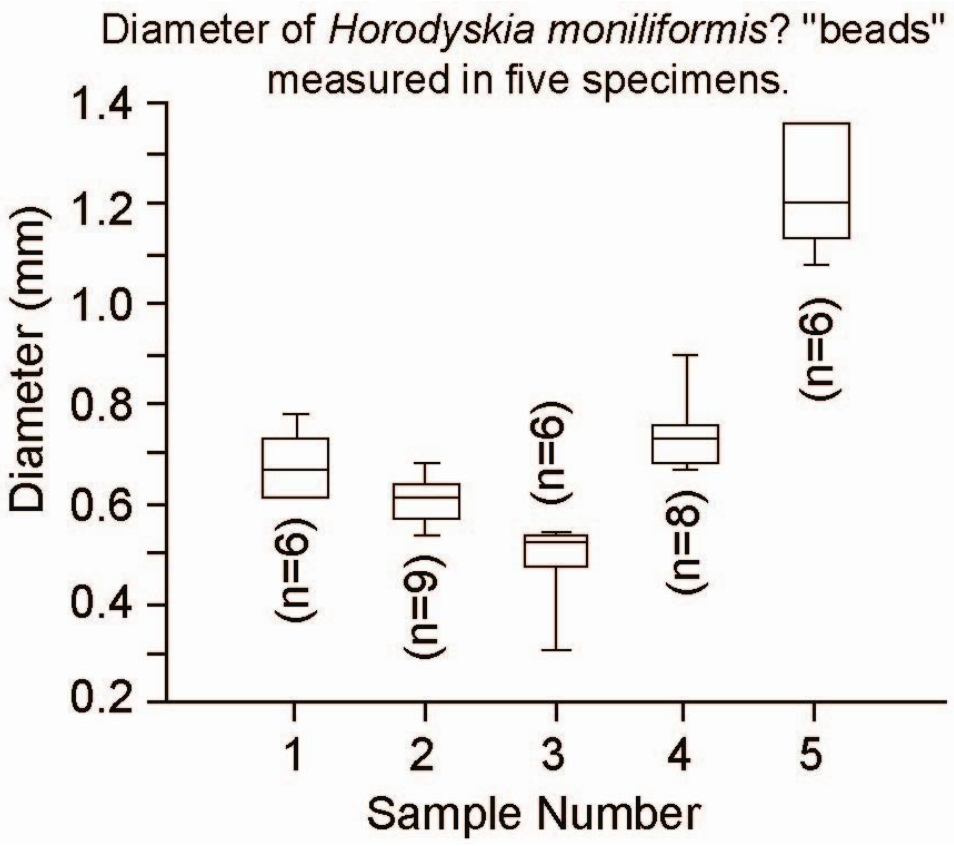

Figure 2.7—Cartoon showing the descriptive terminology of *Palaeopascichnus* Palij, 1976. A *Palaeopascichnus* specimen consists of a series of segments. Dimensions of series are defined by series length and series width, whereas segments are described by segment width and segment thickness.

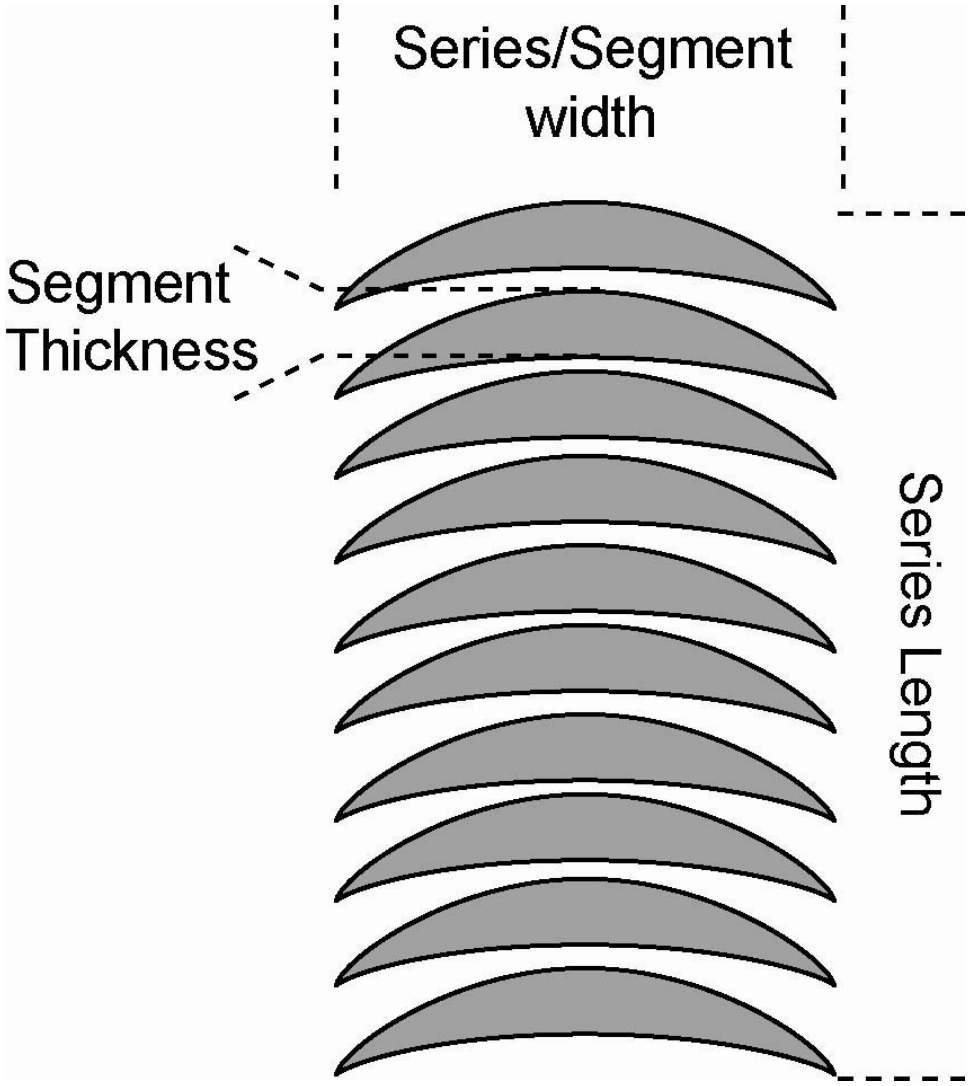

Figure 2.8—*Palaeopascichnus minimus* n. sp. (*1–5*); *Palaeopascichnus meniscatus* n. sp. (*6–7*); and *Shaanxilithes* cf. *ningqiangensis* Xing, Yue, and Zhang *in* Xing et al., 1984 (*8–12*). *1*, ZMG-7. Two specimens (museum numbers VPI-4566 and VPI-4567) of *Palaeopascichnus minimus* n. sp. located within a looped specimen of *Helanoichnus helanensis*; *2*, ZMG-7 (museum number VPI-4566, holotype). A magnified view of the upper left part of *1*; *3*, ZMG-7 (museum number VPI-4568; paratype). A curved specimen of *P. minimus*. Arrow points to the displacement of segments due to bending; *4*, ZMG-5 (museum number VPI-4569). Arrow points to the displacement of segments due to bending; *5*, ZMG-5 (museum number VPI-4570). *6*, ZMG-16 (museum number VPI-4571). Sinuous specimens of *Palaeopascichnus meniscatus* n. sp. from the Zhengmuguan Formation. *7*, Magnified view of the lower left part of *6* (outlined), showing part of the holotype specimen (museum number VPI-4571); *8*, ZMG-15 (museum number VPI-4573), ribbons of *Shaanxilithes* cf. *ningqiangensis* with relatively constant width. Arrow points to an indentation; *9*, ZMG-19 (museum number VPI-4574), poorly preserved specimens with irregular margins; *10*, ZJS-44 (museum number VPI-4575), specimens with relatively constant width. Arrow points to a false branching where two overlapping specimens are located at slightly different horizons; *11*, ZJS-12 (museum number VPI-4576). Arrow denotes divergence of annulations due to bending; *12*, ZJS-30 (museum number VPI-4577). Note the irregular margins of this specimen. Scale bars represent 1 mm in *2*, *4*, *5*; 5 mm in *6*; and 2 mm in all other figures.

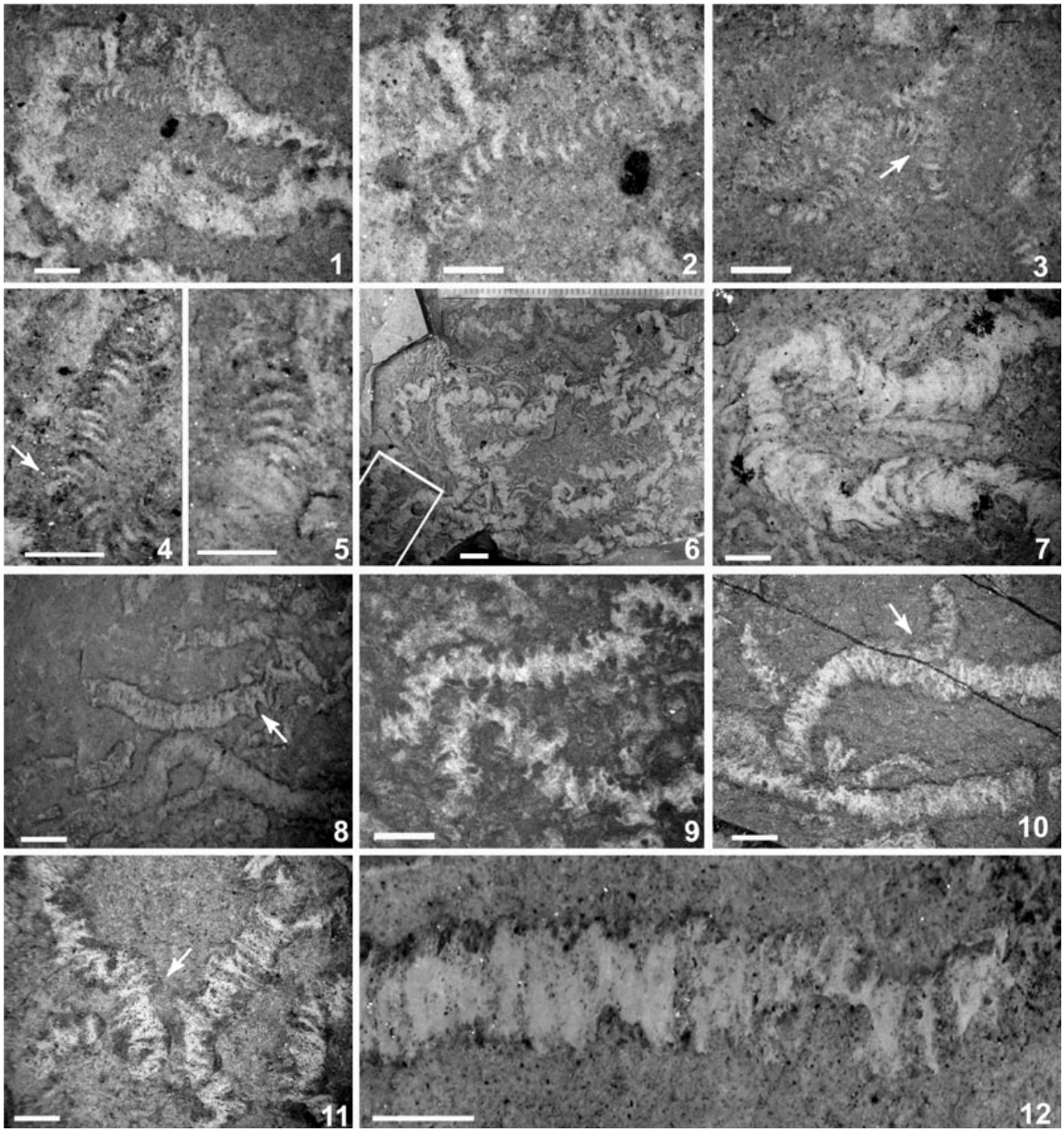
1
2
3
4
5
6
7
8
9
10
11
12

Figure 2.9—Log plot, showing the correlation between segment width and segment thickness of *Palaeopascichnus*. *Palaeopascichnus minimus* n. sp., *Palaeopascichnus meniscatus* n. sp., and *Palaeopascichnus* specimens from Eastern Europe Platform (Sokolov and Iwanowski, 1990; Urbanek and Rozanov, 1983), Newfoundland (Narbonne et al., 1987; Gehling et al., 2000) and Australia (Glaessner, 1969; Haines, 1990).

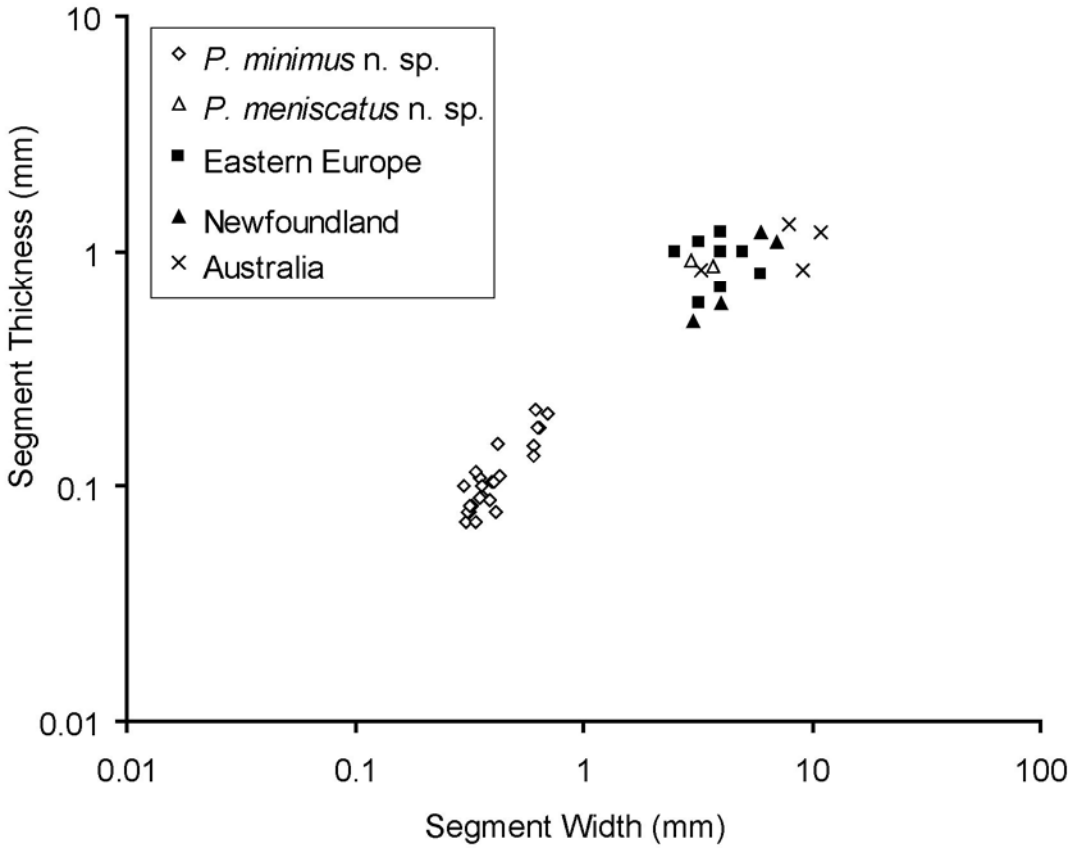

Figure 2.10— Thin sections and elemental geochemistry of *Helanoichnus helanensis* from the Zhoujieshan Formation and Zhengmuguan Formation Thin sections of *Helanoichnus helanensis* from the Zhoujieshan Formation (*1*) and Zhengmuguan Formation (*2*). Fossils were identified on bedding surface and were then embedded in epoxy for thin sectioning. Sections were made perpendicular to the bedding plane, and cut along the length of the fossils. *1*, Photomicrograph under reflected light. The fossil is represented by light-colored clay veneer at the top (arrows). *2*, Photomicrograph under transmitted, nonpolarized light. The fossil is represented by the dark-colored clay layer at the top (arrows). *3*, Al/Si versus Mg/Si plot (as determined by EDS) of a *Helanoichnus helanensis* fossil from the Zhoujieshan Formation and its surrounding matrix. Al/Si ratio of the fossil is greater than that of the matrix. Scale bars in *1* and *2* represent 0.25 and 0.5 mm, respectively. Thin section number: 1, ZJS-30; 2, ZJS-ts.

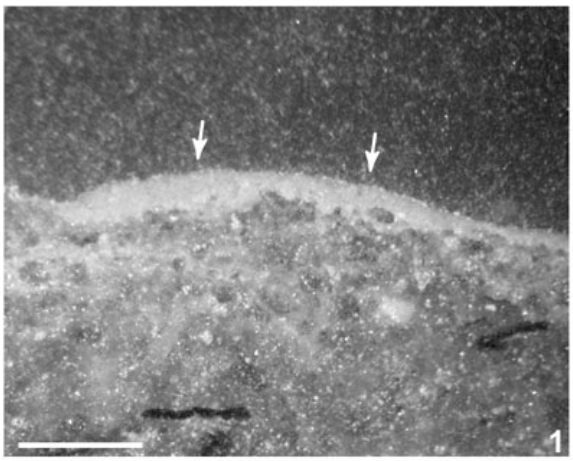
1

2

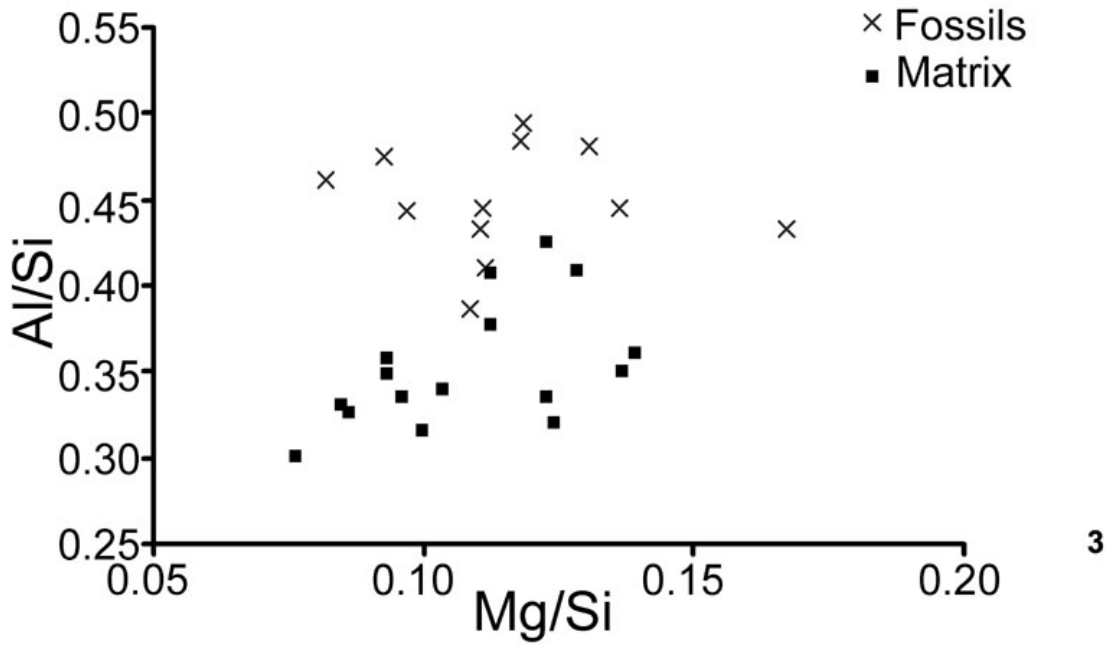
× Fossils
▪ Matrix
0.55
0.50
0.45
0.40
0.35
0.30
0.25
Al/Si
0.05
0.10
0.15
0.20
Mg/Si

3

TABLE 2.*1*—Comparison of *Palaeopascichnus* species and *Palaeopascichnus*-like fossils.

Genus		*Palaeopascichnus*					*Yelovichnus*	*Harlaniella*	*Intrites*	*Gaojiashania*	*Horodyskia*	*Neonereites*
species		*delicatus*	*sinuosus*	*minimus*	*meniscatus*	*P.* sp.						
Locality		1, 2, 3	1	4	4	3, 6	1, 3	2, 3, 6	1, 3	6	4, 7, 8	1, 3, 6
Formation		A, B, C, D	B	E	E	F, G, H	B, D	C, G, H	B, D	I	E, J, K	B, D, G
Age		Ediacaran	Ediacaran	Ediacaran	Ediacaran	Ediacaran	Ediacaran	Ediacaran	Ediacaran	Ediacaran	Mesoprot. Ediacaran	Ediacaran
Series Size	Width (mm)	1: 2~6 2: 3~4 3: 5~10	1: ~5	4: <0.7	4: 1.5~3	6F: >10 6G: 10~20 3H: 3~4	1: 8~15 3: >24	2: ~1.2 3: ~2 5: ~3	1: 5~10 3: 4~8	6: 7~9	4: 0.25 7: 2~10 8: 0.5~4	1: 4~7 3: ~6 6: 5~7
	Length (mm)	1: 15~30 2: 2.4~30 3: ~40	1: >170	4: <10	4: >100	6F: >100 6G: >50 3H: >10	1: >20 3: >100	1: ~20 3: ~25–40 6: >100	1: 35 3: 24	6: 50~120	4: 6~15 7: Variable 8: 10~70	1: 17~45 3: >50 6: >30
Serial Shape	Straight	1, 2		4				3	1, 3	6	8	1
	Curved	1, 2, 3		4		6F, 6G, 3H	1. 3	2, 6		6	4, 7, 8	1, 3, 6
	Sinuous		1		4						4, 7, 8	
	Constant width	2		4	4?	3H	1	2, 6	1?	6	7	
	Expanding width	1		4		6F	1			6		
	Branching	3?				6F	3?	3?				
	Merging					6F						
	Overlap					6F		6?				
Segment Size	Width (mm)	1: 2~6 2: 3~4 3: 5~10	1: ~5	4: <0.7	4: 1.5~3	6F: >10 6G: 10~20 3H: 3~4	1: 8~15 3: >24	2: ~1.2 3: ~2 6: 3	1: 5~10 3: 4~8	6: 7~9	4: 0.5~1.2 7: 2~10 8: 0.5~4	1: 4~7 3: ~6 6: 5~7
	Thickness (mm)	1: 0.6~1 2: 1~1.5 3: 1~3	1: 1~1.5	4: <0.2	4: <1	6F: 1 6G: 1~2 3H: <1	1: 1~3 3: ~3	2: <1 3: 0.5 6: <1	1: 5~9 3: 4	6: 1~2	Same as width	1: 3~4 3: 2~4 6: 3~6
	Ratio	1: 4~10 2: 2~3 3: 3~5	1: 3~5	4: ~3.5	4: 2~4	6F: 2.5~10 6G: 5~10 3H: >3~4	1: 2.6~20 3: >8	2: 3~6 3: 4 6: >3	1: 1 3: 1~2	6: 5~9	4: ~1 7: ~1 8: ~1	1: 1.2~2 3: 1.5~2 6: 1~2
	Number	1: >8 2: 4~10 3: ~20	1: >20	4: >20	4: >20	All >20	1: >20 3: >20	2: >20 3: >20 6: >20	1: 4 3: 4	6: >20	4: 7~20 7: 5~29 8: 3~30	1: 4~>10 3: >15 6: >7
Segment Shape and Arrangement	Straight	1, 2, 3	1	4		6G, 3H		2, 3, 6				3, 6
	Curved	1, 2, 3	1	4		6F, 6G, 3H	1, 3					3
	Crescent				4	6F						
	Circular	1							1, 3	6	4, 7, 8	3?, 6
	Ovate								1		7	1, 3 , 6
	Ring	1					1		1, 3			1
	Tightly	1,2,3	1		4	6G, 3H	1, 3	2, 3, 6	1, 3	6		1, 3, 6
	Loosely			4		6F						
	Parallel	1,2	1?	4		All	1	3, 6		6	4, 7, 8	1?
References and measured specimens (following locality and, when needed formation)		1: a (pl. 22, fig. 1) b (Fig. 5b) 2: c (pl.50, figs. 4-7) 3: d (pl. 1, fig. 3)	1: a (pl. 22, fig. 6)	4: This paper (Fig. 8.1-8.5)	4: This paper (Fig.8.6, 8.7)	6F: e (figs.6, 7) 6G: f (fig. 5c-d) 3H: g (fig. 6b)	1: a (pl. 27, fig. 2) b (fig. 5a) 3: d (pl. 1, fig. 1)	2: c (pl. 50, figs.1-3) 3: g (fig. 6a) 6: k (pl. 2, fig. m)	1: a (pl. 26, fig. 7) 3: d (pl. 1, fig. 1)	5: l (pl. 1, figs. 13, 14) m (pl. 2, figs. 2, 3, 6)	4: This paper (Fig. 4.9-4.12) 7: h (figs. 2, 5, 10) 8: i (figs. 3, 4, 6, 7)	1: a (pl. 26, fig. 2; pl. 27, fig. 4) 3: d (pl. 1, fig. 4) 6: k (pl. 2, fig. n)

Localities: (1) White Sea, Russian; (2) Podolia Basin; (3) Newfoundland; (4) North China; (5) South Australia; (6) South China; (7) Montana, USA; (8) Western Australia.

Formations: A: Mogilev; B: Ust Pinega; C: Kaninov; D: Fermuse; E: Zhengmuguan; F: Wonoka; G: Pound Quartzite; H: Chapel Island; I: Dengying Formation; J: Stag Arrow; K: Appekunny

References: a: Sokolov and Iwanowski, 1990; b: Jensen, 2003; c: Urbanek and Rozanov, 1983; d: Gehling et al., 2000; e: Haines, 2000; f: Glaessner, 1969; g: Narbonne et al., 1987; h: Grey and Williams, 1990; i: Fedonkin and Yochelson, 2002; k: Jenkins, 1995; l: Lin et al., 1986; m: Zhang, 1986

Chapter 3

Stratification and Mixing of a Post-glacial Neoproterozoic Ocean: Evidence from Carbon and Sulfur Isotopes in a Cap Dolostone from Northwest China[1]

Abstract

To improve our knowledge about the geochemical and environmental aftermath of Neoproterozoic global glaciations, we analyzed stable isotopes ($\delta^{13}C$, $\delta^{18}O$, $\delta^{34}S$) and elemental concentrations (Ca, Mg, S, Sr, Fe, and Mn) of the ~10-m-thick Zhamoketi cap dolostone atop the Tereeken diamictite in the Quruqtagh area, eastern Chinese Tianshan. Available chemostratigraphic data suggest that the Tereeken diamictite (between 727 Ma and 615 Ma) is probably equivalent to the Marinoan glaciation. Our new data indicate that organic and carbonate carbon isotopes of the ~10-m-thick Zhamoketi cap dolostone show little stratigraphic variations, averaging –28.2‰ and –4.6‰, respectively. In contrast, sulfur isotopes show significant stratigraphic variations. Carbonate associated sulfate (CAS) abundance decreases rapidly in the basal cap dolostone and $\delta^{34}S_{CAS}$ composition varies between +9‰ and +15‰ in the lower 2.5 m. In the overlying interval, CAS abundance remains low while $\delta^{34}S_{CAS}$ rises ~5‰ and varies more widely between +10‰ and +21‰. The range of $\delta^{34}S_{py}$ of the cap dolostone overlaps with that of $\delta^{34}S_{CAS}$, but direct comparison shows that $\delta^{34}S_{py}$ is typically greater than $\delta^{34}S_{CAS}$ measured from the same samples. Hypotheses to explain the observations must account for both the remarkable sulfur isotope enrichment of pyrites and the inverse fractionation. We propose that CAS and pyrite were derived from two isotopically distinct reservoirs in a chemically stratified basin or a basin with a sulfate minimum zone. In this model, CAS was derived from shallow, oxidized surface waters with moderate sulfate concentration and depleted in ^{34}S due to the post-glacial influx of sulfur from continental weathering. In contrast, pyrite was derived from anoxic bottom waters (or a sulfate minimum zone) with low sulfate concentration and ^{34}S enrichment due to long-term synglacial sulfate reduction. The rapid shift in CAS abundance and sulfur isotope composition within the

[1] Article published by Shen, B., Xiao, S., Bao, H., Kaufman, A. J. and Zhou, C., (2008). Stratification and mixing of the post-glacial Neoproterozoic ocean: Evidence from carbon and sulfur isotopes in a cap dolostone from northwest China. Earth and Planetary Science Letter, 265: 209-228. (Elseiver)

cap dolostone is interpreted to reflect the mixing of the two reservoirs after initial deglaciation. Comparison with other post-Marinoan cap carbonates shows significant spatial heterogeneity in $\delta^{34}S_{CAS}$, which together with strong temporal variation in $\delta^{34}S_{CAS}$, points to generally low sulfate concentrations in post-Marinoan oceans.

Keywords: Neoproterozoic, Quruqtagh, cap dolostone, sulfur isotope, carbon isotope, stratification

1. INTRODUCTION

Neoproterozoic glacial deposits and immediately overlying carbonates are globally distributed (Evans, 2000; Hoffman and Schrag, 2002), recording severe climatic oscillations. In the snowball Earth model, the world ocean may have been frozen at the equator to a significant depth during glaciation, but rapid warming and extreme oceanic alkalinity during deglaciation resulted in the cap dolostone (Hoffman et al., 1998). The best candidate for such an event is the Marinoan glaciation, which terminated about 635 Ma (Condon et al., 2005; Hoffmann et al., 2004). Most Marinoan glacial deposits are overlain by cap dolostones with characteristic negative $\delta^{13}C_{carb}$ and enigmatic sedimentary features (Corsetti and Lorentz, 2006; Halverson, 2006; Halverson et al., 2005; Hoffman et al., 2007; Hoffman and Schrag, 2002; James et al., 2001; Jiang et al., 2003; Jiang et al., 2006; Shields et al., 2007). Collectively, these geochemical and sedimentary features hold the key to understand the aftermath of Marinoan deglaciation.

Current debates on the geochemistry of post-Marinoan oceans have focused primarily on carbon cycle perturbations (Halverson, 2006; Halverson et al., 2005; Hoffman and Schrag, 2002; Jiang et al., 2003; Kennedy et al., 2001a), but recent $\delta^{34}S$ studies of sulfides and CAS are providing new insights from the viewpoint of oxidized and reduced reservoirs (Fike et al., 2006; Goldberg et al., 2005; Gorjan et al., 2000; Hurtgen et al., 2004; Hurtgen et al., 2002; Hurtgen et al., 2006; Kaufman et al., 2007). However, systematic studies of carbon and sulfur isotope fractionation in cap dolostones are generally lacking, and these would likely place important constraints on the biological and physical processes operating in the post-glacial world.

In this study, we carried out high resolution analysis of both carbon and sulfur isotopes in oxidized and reduced phases, along with several major and trace element concentrations, from the ~10 m thick Zhamoketi cap dolostone. This unit directly overlies the Tereeken diamictite in the Quruqtagh area, eastern Chinese Tianshan, which has been interpreted to be Marinoan in age. Together with previously published data (Xiao et al., 2004), the high resolution geochemical data reported here provide evidence for chemical stratification and subsequent overturn in the Quruqtagh basin and perhaps the world ocean in the aftermath of a widespread Neoproterozoic glaciation.

2. GEOLOGICAL BACKGROUND

The Quruqtagh area belongs to the southeast branch of Chinese Tianshan, and is geologically part of the northern Tarim Block (Gao et al., 1980; Zhang et al., 2007). Neoproterozoic successions in the Quruqtagh area (Fig. 1) were first described as the Quruqtagh Series (Norin, 1937), and later as the Quruqtagh Group (Gao et al., 1993; Gao and Zhu, 1984).

The Quruqtagh Group overlies early Neoproterozoic stromatolitic carbonates, and disconformably underlies basal Cambrian phosphorites/cherts (Yao et al., 2005). It is divided into the Bayisi, Zhaobishan, Altungol, Tereeken, Zhamoketi, Yukkengol, Shuiquan, and Hankalchough formations (Fig. 2a). The >250-m-thick Bayisi Formation consists of phyllite-slate grade metasediments and metavolcaniclastics. Four units of greenish gray diamictite, each ranging from a few to >100 m in thickness and separated by quartz and polylithic metawackes, occur in the Bayisi Formation. Outsized clasts, mostly derived from older metamorphic and igneous rocks, occur in the diamictite. A volcanic unit in the basal Bayisi Formation gives a SHRIMP zircon U–Pb age of 755±15 (1σ) Ma (Xu et al., 2005) and another near the topmost Bayisi Formation has been dated as 727±8 (1σ) Ma (unpublished data). The Bayisi Formation is succeeded by the 100–300-m-thick Zhaobishan Formation, which consists of metawackes, metarenites, calcareous siltstones, and slates. The overlying Altungol Formation consists of metamorphosed diamictites, metavolcanics, and marbles characterized by $\delta^{13}C_{carb}$ values between +2‰ and +10‰ (Xiao et al., 2004). The ~200-m-thick Tereeken Formation

consists of at least five diamictite intervals separated by finely laminated siltstones and mudstones, with abundant dropstones and striated clasts (Fig. 3a) in the diamictites (Gao and Zhu, 1984; Xiao et al., 2004). The siltstone/mudstone intervals may represent interludes of less extensive glacial cover (Leather et al., 2002) and bioproductivity resumption.

The Tereeken Formation is sharply succeeded by a ~10-m-thick cap dolostone in the basal Zhamoketi Formation (Fig. 3b), which is characterized by $\delta^{13}C_{carb}$ values between –4‰ and –6‰ (Xiao et al., 2004). The rest of the Zhamoketi Formation and the overlying Yukkengol Formation consist of ~1200 m of meter-scale cycles of sandstone and siltstone, which are interpreted as deep-water turbidites. The Zhamoketi and Yukkengol formations are demarcated by basaltic and andesitic volcanic rocks. Further upsection is the Shuiquan Formation that consists of <100 m carbonate characterized by a large $\delta^{13}C_{carb}$ shift from –9‰ to nearly 0‰. This shift may be equivalent to the upper part of the Shuram anomaly (Fike et al., 2006). The uppermost Quruqtagh Group is represented by the ~400-m-thick Hankalchough Formation, which consists of light gray diamictite with abundant dropstones and striated clasts (Zhao et al., 1980). A 1–5-m-thick dolostone unit succeeding the Hankalchough diamictite and characterized by variably negative $\delta^{13}C_{carb}$ values is regarded as the Hankalchough cap carbonate. The Hankalchough Formation is overlain disconformably by phosphorites/cherts of the Xishanblaq Formation where basal Cambrian *Micrhystridium*-like acritarchs and small shelly fossils have been reported (Yao et al., 2005).

A glacial origin for diamictites in the Bayisi, Altungol, Tereeken, and Hankalchough formations has been proposed (Gao and Zhu, 1984), although the most convincing glacial evidence comes from the Tereeken and Hankalchoug diamictites, where abundant striated clasts (Fig. 3a) and dropstones are present (Gao and Zhu, 1984; Xiao et al., 2004). Although radiometric ages provide only loose constraints on the Tereeken glaciation (< 727±8 Ma), the stratigraphic association of the 727±8 Ma age and the Bayisi diamictite suggests that the Bayisi and Tereeken formations probably record the Sturtian and Marinoan glaciations, respectively. This is consistent with $\delta^{13}C$ chemostratigraphic evidence (Xiao et al., 2004), including (1) the $\delta^{13}C$ stratigraphic pattern of the Zhamoketi cap dolostone, which is more akin to post-Marinoan than to

post-Sturtian cap carbonates; and (2) highly positive $\delta^{13}C$ values (up to 10‰) in the Altungol Formation, which may be equivalent to the positive $\delta^{13}C$ excursion between the Sturtian and Marinoan glaciations (Halverson et al., 2005). This correlation implies that the Tereeken glaciation may have terminated about 635 Ma (Condon et al., 2005; Hoffmann et al., 2004).

The focus of this study is the Zhamoketi cap dolostone. Sixty-three samples, at an average spacing of 10–20 cm, were collected at the Yukkengol section (Fig.1). Here, the Zhamoketi cap dolostone consists of 10-meter-thick pink-colored dolostone or limy dolostone (Fig. 3b). The Zhamoketi cap dolostone can be divided into three lithostratigraphic units (Fig. 2). The lower unit A consists of ~1.2-m-thick thin-bedded calcitic dolomicrosparite. The middle unit B is composed of a 1.5-m-thick macropeloidal dolostone (Fig. 3c) that is lithologically similar to macropeloidal dolostones in the Ravensthroat cap carbonate in the Mackenzie Mountains (James et al., 2001), Bwipe cap carbonate in the Volta Basin (Nédélec et al., 2007), and Doushantuo cap carbonate in South China (personal observation). The macropeloids, 0.5–4 mm in diameter, are aggregates of very small peloids. They are cemented by blocky calcite (Fig. 3c; calcite cement representing <10% rock volume). The upper unit C consists of 7-m-thick homogeneous dolomicrosparite (Fig. 3d) and siliciclastic components increase upsection. The Zhamoketi cap carbonate contains a small amount of pyrites, which are disseminated randomly in dolomicrosparite matrix (Fig. 3e–f).

The Zhamoketi cap dolostone was probably deposited below storm wave base. Tepee-like structures, interpreted as giant wave ripples (Allen and Hoffman, 2005), are not present in the Zhamoketi cap dolostone. Nor are other sedimentary structures such as cross stratification, sheet cracks, and tube-forming stromatolites (Corsetti and Grotzinger, 2005) that would indicate sedimentation in the euphotic zone. The lack of enigmatic sedimentary features characteristic of many other post-Marinoan cap dolostones is probably due to the deep-water settings of the Zhamoketi cap dolostone.

3. METHODS

3.1. Carbon and oxygen isotopes

$\delta^{13}C_{carb}$ and $\delta^{18}O$ data of the Zhamoketi cap dolostone at Yukkengol were previously published by Xiao et al. (2004), although their stratigraphic resolution was on the order of 50 cm. To increase the stratigraphic resolution, we analyzed additional $\delta^{13}C_{carb}$ and $\delta^{18}O$ data from Yukkengol section 1 described in figure 7a of Xiao et al. (2004). $\delta^{13}C_{carb}$ and $\delta^{18}O$ were measured on drilled microsamples, following procedures described in Xiao et al. (2004). Isotopic results are expressed in the standard δ notation as per mil (‰) deviations from VPDB. Uncertainties determined by multiple measurements of a laboratory standard carbonate (calibrated to NBS-19) were better than 0.05‰ (1σ) for both $\delta^{13}C_{carb}$ and $\delta^{18}O$.

For $\delta^{13}C_{org}$ analysis, 1–2 grams of rock chips were first leached with 15% HCl and 10% HF for 15 min, and washed with deionized water three times to remove surface weathering. Washed chips were dried and crushed to 80 mesh. Sample powders were then acidified three times with 6 M HCl to dissolve carbonate. Insoluble residue was centrifuged and washed with deionized water more than three times, and was then dried in an oven at 60°C. $\delta^{13}C_{org}$ values were determined on decalcified residues by combustion at 850°C for 2 h with CuO as an oxidant in evacuated and sealed Vycor tubing. CO_2 derived from the combustion was quantified and packaged for mass spectrometric analysis. Results are reported as per mil (‰) deviations from VPDB. Uncertainties based on multiple analyses of a standard carbonate are better than 0.3‰ (1σ).

3.2. Sulfur isotopes

Sulfur isotopes compositions were determined on co-existing sulfide and trace sulfate isolated from the same samples where $\delta^{13}C_{carb}$ and $\delta^{18}O$ were measured. Extraction of carbonate associated sulfate (CAS) followed the procedure of Goldberg et al. (2005). 50–100 grams of rock chips were leached with 3 M HCl to remove surface weathering, washed and dried prior to being crushed to 80 mesh. Powders were weighed, leached in 10% NaCl solution for 24 hours, and then washed three times with deionized water to remove soluble sulfate. Leached powders were transferred into a 500 ml flask with 50 ml of deionized water, and then dissolved in the flask following a stepwise acidification procedure in which HCl acid was added successively 3 or 4 times. In the first treatment, 20 ml of 10 M HCl was added, and the flask was gently shaken to allow

reaction for 20 to 30 minutes. This step was repeated 2 or 3 times until carbonate was quantitatively dissolved, and final solution was allowed to sit for ~2 hours. Insoluble residues were removed by filtration with 1 μm filter paper, carefully washed, dried, and weighed. The volume of supernatant was measured, and then distributed in four 50 ml centrifuge tubes, one of which was used for elemental analysis. Barite was precipitated by adding 1–2 ml of saturated $BaCl_2$ solution to the three remaining tubes and allowing reaction for 48 hours. All processed samples precipitated sufficient barite for $\delta^{34}S_{CAS}$ analysis.

Disseminated pyrite was extracted following the chromium reduction method (Canfield et al., 1986; Goldberg et al., 2005). 5–7 grams of fresh rock samples was crushed to 80 mesh and powders were reacted with 50 ml of 1 M $CrCl_2$ and 20 ml of 10 M HCl in an N_2 atmosphere. H_2S produced from pyrite reduction by $CrCl_2$ was bubbled through a 1 M zinc acetate trap where it was precipitated as ZnS, which was then converted to Ag_2S by ion exchange with $AgNO_3$. The Ag_2S was centrifuged, washed three times using deionized water, and dried at 60°C. Twenty-three out of 63 processed samples did not yield a sufficient quantity of Ag_2S for analysis.

Sulfur isotopes were measured in the geochemistry laboratory at University of Maryland. Prepared samples (~100 μg $BaSO_4$ or Ag_2S) were accurately weighed and folded into small tin cups. A Eurovector elemental analyzer (EA) was used for on-line combustion at 1030^{o}C and separation of SO_2 on-line to a GV Isoprime mass spectrometer for $^{34}S/^{32}S$ analyses, following the procedures of Grassineau et al. (2001). Isotopic results are expressed in the δ notation as per mil (‰) deviations from VCDT. Uncertainties determined by multiple analyses of a standard barite (NBS 127) are better than 0.3‰ (1σ).

3.3. Elemental geochemistry

Major and trace elemental contents of Ca, Mg, Fe, Mn, Sr, and S were analyzed on an Inductively Coupled Plasma Atomic Emission Spectrometer (ICP–AES) in the Virginia Tech Soil Testing Laboratory. Solutions from the CAS extraction procedure that did not react with $BaCl_2$ were used for elemental analysis. Elemental concentrations were corrected for insoluble residue (by subtracting insoluble residue from sample powder mass), and CAS concentrations were calculated from sulfur abundances. Analytical

precision is better than 5% for sulfur and 3% for other elements when they are above the detection limit.

4. RESULTS

4.1. Carbon and oxygen isotopes

The high resolution $\delta^{13}C_{carb}$ and $\delta^{18}O$ data (Table 3.1; Fig. 4a–b) confirm the stratigraphic pattern reported by Xiao et al. (2004). With the exception of the two lowermost samples, which might have experienced some degree of diagenetic alteration (as indicated by their $\delta^{18}O$ values <–15‰ and close contact to underlying diamictite), $\delta^{13}C_{carb}$ values show little variation. Above the basal samples values start around –4‰ and then fall to near –6‰ at 0.3 m before returning within the macropeloidal unit (unit B) to a plateau value of ca. –4‰. Oxygen isotopes are similarly stable with most values ranging between –8 and –11‰, but do co-vary with carbon isotopes (Fig. 5a).

$\delta^{13}C_{org}$ values (Fig. 4a) range from –29.7 to –24.7‰ (n=53, mean=–28.2‰, SD=1‰), again showing very little variation. Fractionations between carbonate and organic carbon are remarkably stable throughout the cap dolostone. Excluding the two lowermost samples, $\Delta\delta^{13}C$ values ($=\delta^{13}C_{carb} - \delta^{13}C_{org}$) range from +25.2‰ to +20.2‰ (n=50, mean=+23.8‰, SD=1‰), consistent with carbon isotope fractionation by oxygenic photoautotrophs.

4.2. Sulfur isotopes

In contrast to carbon isotopes, $\delta^{34}S_{CAS}$ values show wide variations between +9.1‰ and +20.6‰ (Table 3.1; Fig. 4c; n=63, mean=13.4‰, SD=2.9‰). Closer inspection of the stratigraphic profile reveals a 3–5‰ positive shift and increase in variability at ~2.5 m; this is apparent from statistical analysis (below 2.5 m: n=29, range=9.1–14.6‰, mean=11.9‰, SD=1.4‰; above 2.5 m: n =34, range=9.7–20.6‰, mean=+14.7‰, SD=3.1‰). The variability can also be evaluated by examining the absolute difference between successive samples (Fig. 4d; below 2.5 m: mean=1.7‰; above 2.5 m: mean=3.6‰). In contrast, there are no stratigraphic patterns in the mean,

range, or variability of $\delta^{34}S_{py}$ values, which vary widely between +11.8‰ and +19.5‰ throughout the cap dolostone (Table 3.1; Fig. 4e; n=40, mean=15.8‰, SD=1.5‰).

The isotopic difference between CAS and pyrite ($\Delta\delta^{34}S_{CAS-py}=\delta^{34}S_{CAS} - \delta^{34}S_{py}$) ranges from –9.4‰ to +6.6‰ (Fig. 4f; n=40, mean=–3.0‰, SD=3.0‰), demonstrating that bulk pyrite is remarkably enriched in ^{34}S relative to trace sulfate of the same samples. In 36 out of the 40 samples, bulk pyrite $\delta^{34}S_{py}$ values are greater than $\delta^{34}S_{CAS}$ values.

4.3. Elemental geochemistry

No persistent stratigraphic trends are apparent in Mn concentrations (3700–6500 ppm), but Fe concentrations (2800–8800 ppm) appear to increase in the upper 3 m of the cap dolostone (Fig. 4h). In addition, Sr (210–930 ppm) and CAS concentrations (100–1100 ppm) decrease in the lowest meter (Fig. 4g–h), whereas Mg/Ca ratios increase (Fig. 4i) in the lowest 2 m, suggesting a transition from calcitic dolomite to stoichiometric dolomite with decreasing Sr and CAS concentrations.

5. VALIDITY OF CAS CONCENTRATION, $\delta^{34}S_{CAS}$, AND $\delta^{34}S_{PY}$ DATA

5.1. Pyrite oxidation during laboratory preparation or outcrop weathering

It is conceivable that the extraction of CAS may be contaminated by pyrite oxidation during laboratory preparation or outcrop weathering. However, pyrite concentration in the Zhamoketi cap dolostone is very low. We estimate on the basis of Ag_2S yield that Zhamoketi samples typically contain <20 ppm pyrite (or <10 ppm pyrite sulfur, compared with 30–430 ppm CAS sulfur). In fact, more than a third of processed samples did not yield measurable amount of Ag_2S (<0.1 mg). Controlled experiment by one of us (AJK) has shown that laboratory oxidation of pyrite does occur, but its effect on CAS and $\delta^{34}S_{CAS}$ measurements is negligible when pyrite concentration is low compared to CAS abundance. Outcrop weathering of pyrite would produce sulfate on rock surface or in fractures. But the sample powders were pretreated with 10% NaCl solution, which should remove soluble sulfate derived from outcrop weathering of pyrite.

With regard to the Quruqtagh data reported in this paper, the following consideration argues against significant contamination from pyrite oxidation. Such

contamination would lead to a positive correlation between CAS concentrations and $\delta^{34}S_{CAS}$ values insofar as pyrite in these samples has greater ^{34}S abundance than CAS, but our data show a weak negative correlation between CAS concentration and $\delta^{34}S_{CAS}$ (Fig. 5b). Neither is there a positive correlation between Fe and CAS concentrations (Fig. 5c) or between Fe concentration and $\delta^{34}S_{CAS}$ (Fig. 5e), as might be expected if both sulfate and Fe oxyhydroxide from *in-situ* pyrite oxidation were retained in the rock and later liberated in CAS extraction. The lack of these expected geochemical correlations also indicate that the low pyrite concentrations in the Zhamoketi cap dolostone can not be due to significant oxidative loss of originally abundant pyrite.

5.2. Diagenetic alteration of CAS concentration and $\delta^{34}S_{CAS}$

It is also a concern that $\delta^{34}S_{CAS}$ may have been altered during late diagenesis. CAS can be lost from or added to carbonates during post-burial diagenesis. Lyons et al. (2004, 2005) have shown that, despite CAS concentrations decreasing from 3500 to 500 ppm in aragonite–calcite inversion during meteoric diagenesis, $\delta^{34}S_{CAS}$ values remained within 1 to 2‰ of the coeval seawater value. Thus, it is reasonable to assume that $\delta^{34}S_{CAS}$ is largely buffered against diagenetic alteration at least during aragonite stabilization.

The effect of dolomitization on CAS concentration and $\delta^{34}S_{CAS}$ has not been completely understood (Lyons et al., 2005). Hurtgen et al. (2006) reported that CAS concentrations of Neoproterozoic dolostones seem to be greater than limestones (contrary to our own observation, Fig. 5d). Hurtgen et al.'s data can be interpreted in two ways. Primary dolomites can have high CAS concentrations if they are precipitated in evaporitic environments and can retain high CAS concentrations due to their greater stability to reduce diagenetic CAS loss. Alternatively, secondary dolomites might incorporate additional sulfate from pore-water during dolomitization. The former interpretation implies that primary dolomites are better proxies for sea water $\delta^{34}S$. The latter interpretation predicts that $\delta^{34}S_{CAS}$ of dolostones be slightly greater than coeval seawater sulfate, because bacterial sulfate reduction in sediments could drive $\delta^{34}S_{\text{pore water sulfate}}$ to be greater than $\delta^{34}S_{\text{seawater sulfate}}$, particularly when sulfate reduction rate is high and diffusion of sulfate into sediment is not facilitated by bioturbation. Indeed, this prediction is consistent with the observation that $\delta^{34}S_{CAS}$ values of dolostones are

consistently 3–5‰ greater than interbedded gypsum beds in the Mesoproterozoic Bylot Supergroup (Kah et al., 2004), although this difference between dolostone and gypsum is relatively small compared to stratigraphic variation of $\delta^{34}S_{CAS}$ values.

In the Zhamoketi cap dolostone, there is evidence suggesting that, although CAS concentrations might have altered, the broad secular trends of CAS concentrations are still useful in qualitatively constraining sulfate concentrations in Neoproterozoic oceans. The weak negative correlation between Mg/Ca ratio and CAS concentration (Fig. 5d) indicates possible CAS loss during dolomitization, inconsistent with previous observations that Neoproterozoic dolomites have greater CAS concentrations than limestones (Hurtgen et al., 2006). Regardless, Zhamoketi CAS concentrations (100–1100 ppm; n=63, mean=308 ppm, SD=194 ppm; Fig. 4g) are comparable to or slightly greater than other Neoproterozoic or Mesoproterozoic carbonates (Gellatly and Lyons, 2005; Hurtgen et al., 2005; Hurtgen et al., 2004; Kah et al., 2004; Kaufman et al., 2007) but significantly lower than Cenozoic values (Burdett et al., 1989; Staudt and Schoonen, 1995). The broad consistency of CAS concentrations in Precambrian carbonates, including dolostones and limestones, suggests that large-scale secular trends in CAS concentration and $\delta^{34}S_{CAS}$ are not completely obliterated by dolomitization and confirms the proposition that sulfate concentrations in Proterozoic oceans were generally lower than in Cenozoic oceans (Pavlov et al., 2003).

Although more studies are needed to understand the effect of dolomitization on $\delta^{34}S_{CAS}$, geochemical data from the Zhamoketi cap dolostone seem to suggest that $\delta^{34}S_{CAS}$ values were not strongly altered during dolomitization. The correlations between $\delta^{34}S_{CAS}$ values and Mg/Ca ratios (Fig. 5f) and between $\delta^{34}S_{CAS}$ values and CAS concentrations (Fig. 5b) are both very weak, suggesting no systematic alteration of $\delta^{34}S_{CAS}$ signature during dolomitization or CAS loss.

5.3. Using $\delta^{34}S_{CAS}$ as a proxy for seawater sulfate

CAS is structurally incorporated in the lattice of carbonate minerals, replacing the CO_3^{2-} anions (Pingitore et al., 1995). It has been widely used as a proxy for seawater sulfate $\delta^{34}S$ compositions, especially in Precambrian successions where evaporite rocks are rare (Bottrell and Newton, 2006; Gellatly and Lyons, 2005; Hurtgen et al., 2004;

Hurtgen et al., 2002; Hurtgen et al., 2006; Kah et al., 2004; Kampschulte et al., 2001; Kampschulte and Strauss, 2004). Comparisons between sulfur isotope compositions of CAS and co-occurring evaporites reveal only small differences (<5‰) (Burdett et al., 1989; Kah et al., 2004; Kampschulte and Strauss, 2004; Lyons et al., 2004), supporting the use of CAS as a reasonable $\delta^{34}S$ proxy as long as carbonate precipitates are equilibrated with seawater and their diagenetic history is carefully evaluated.

The Zhamoketi cap dolostone was probably deposited below storm wave base. Microsparites and peloids (constituents of macropeloids) in the cap dolostone were likely precipitated in surface water and then settled to the ocean bottom. Diagenetic cements precipitated from pore-water are volumetrically small (<10%; Fig. 3c). Thus, we regard the Zhamoketi $\delta^{34}S_{CAS}$ values as a reasonable proxy for surface seawater $\delta^{34}S$.

5.4. Evaluation of $\delta^{34}S_{py}$ values

The chromium reduction method has been used widely in pyrite extraction (Canfield et al., 1986). The extraction procedure does not introduce any significant isotopic fractionation (Newton et al., 1995). Our experiment with pure pyrite also shows that the procedure did not introduce significant fractionation ($\delta^{34}S_{Ag2S}$=+2.6‰ vs. $\delta^{34}S_{py}$=+1.9‰).

Pyrites exist in the Zhamoketi cap dolostone as disseminated subeuhedral crystals <10 μm in size (Fig. 3e–f). Their distribution is not associated with any microveins or other hydrothermal activities. Certainly, the formation of disseminated pyrites in the Zhamoketi cap dolostone occurred in an anoxic environment where bacterial sulfate reduction took place and reactive iron supply was available. They could have formed during early diagenesis below water-sediment interface or syngenetically in bottom water (e.g., in a sulfate minimum zone). Thus, their $\delta^{34}S_{py}$ values could reflect the isotopic signatures of local environments. Nonetheless, their $\delta^{34}S_{py}$ values are still useful in understanding the sulfur cycle even if they formed in a semi-closed system below the water-sediment interface. In such a system, sulfur isotope fractionation should be limited and $\delta^{34}S_{py}$ values of bulk samples should approach $\delta^{34}S$ of seawater. Many Zhamoketi samples, however, are characterized by $\delta^{34}S_{py}$ values greater than co-occurring $\delta^{34}S_{CAS}$ values (i.e., negative $\Delta\delta^{34}S_{CAS-py}$ values), posing a challenge in their interpretation.

6. IMPLICATIONS FOR SULFUR CYCLING IN THE QURUQTAGH BASIN

In our interpretation, we focus on two important features of the $\delta^{34}S$ of the Zhamoketi cap dolostone: the strong stratigraphic variation in $\delta^{34}S$ (in sharp contrast to the stable $\delta^{13}C$ values) and the negative $\Delta\delta^{34}S_{CAS-py}$ values. The rapid stratigraphic variation in $\delta^{34}S_{CAS}$ and $\delta^{34}S_{sulfide}$ of Proterozoic carbonates, along with generally low CAS concentrations, has been interpreted as evidence for a relatively small sulfate reservoir (Gellatly and Lyons, 2005; Hurtgen et al., 2005; Kah et al., 2004; Lyons et al., 2006; Pavlov et al., 2003). This is also a reasonable interpretation for the Zhamoketi cap dolostone. With a generally small sulfate reservoir, the isotopic signature would be more susceptible to local perturbations (e.g., weathering input and upwelling), and there would be frequent development of spatial and depth heterogeneity. All these would contribute to the rapid stratigraphic variation in $\delta^{34}S_{CAS}$ values. The stratigraphic and spatial variations imply that $\delta^{34}S_{CAS}$ and $\delta^{34}S_{py}$ profiles are less useful in chemostratigraphic correlation than $\delta^{13}C$ data.

The negative $\Delta\delta^{34}S_{CAS-py}$ values (Fig. 4f) are puzzling. The formation of sedimentary pyrites is directly related to bacterial sulfate reduction. Experimental data show that the isotopic effect of bacterial sulfate reduction ranges from 2‰ to 42‰ (Detmers et al., 2001). Additional fractionation beyond 42‰ is associated with the disproportionation of intermediate sulfur species (Canfield and Thamdrup, 1994). Thus, sedimentary pyrites are generally expected to be isotopically lighter than contemporaneous seawater sulfate. However, many Mesoproterozoic and Neoproterozoic successions are characterized by highly variable $\delta^{34}S_{py}$ values, some of which exceed the $\delta^{34}S_{CAS}$ values of contemporaneous carbonate (Canfield, 1998; Gorjan et al., 2000; Hurtgen et al., 2002; Liu et al., 2006; Lyons et al., 2006; Ross et al., 1995; Strauss, 2002). $\delta^{34}S_{py}$ values approaching contemporaneous $\delta^{34}S_{CAS}$ values have been interpreted as resulting from bacterial sulfate reduction in sulfate-limited environments (e.g., closed system below water-sediment interface; Strauss, 2002). However, $\delta^{34}S_{py}$ values exceeding contemporaneous $\delta^{34}S_{CAS}$ values were largely ignored by previous authors, because they cannot be easily explained by traditional models where pore-water sulfate

for pyrite formation is derived from a homogenous seawater sulfate reservoir. Although the instantaneous sulfide product from bacterial sulfate reduction in a nearly closed system could be isotopically heavier than seawater sulfate, the cumulative sulfide product is not expected to be isotopically heavier than seawater sulfate. The $\delta^{34}S_{py}$ and $\delta^{34}S_{CAS}$ data reported in this paper and from many other Proterozoic successions were from bulk analyses, and the isotopic values are supposed to reflect cumulative rather than instantaneous products. Thus, the negative $\Delta\delta^{34}S_{CAS-py}$ values of the Zhamoketi cap dolostone remain enigmatic.

In order to explain the negative $\Delta\delta^{34}S_{CAS-py}$ values, we hypothesize that Zhamoketi CAS and pyrite were derived from isotopically distinct sulfur reservoirs. In searching for possible processes involved in the sulfur cycling of the post-glacial Quruqtagh basin, we consider the following two models, both of which are related to the generally low sulfate concentrations and isotopic heterogeneity.

6.1. Oceanic stratification model

During the Marinoan glaciation, glaciers existed in tropical oceans (Evans, 2000), and the polar regions were likely completely frozen. As a result, the global ocean conveyor system was probably slowed down, regardless whether the tropical oceans were completely frozen or remained open (Hyde et al., 2000). With reduced polar down-welling, oxygen and sulfate fluxes to the bottom ocean would be reduced. Continuing respiration and bacterial sulfate reduction in the bottom ocean, fueled by a large reservoir of dissolved organic carbon (Rothman et al., 2003) and synglacial bioproductivity, would progressively deplete the oxygen and sulfate levels in the bottom ocean. With sufficient reactive iron input (as indicated by the high Fe concentration in the Zhamoketi cap dolostone), isotopically light H_2S would be removed from the bottom ocean, raising the $\delta^{34}S_{sulfate}$ of residual sulfate reservoir. In the mean time, significant amount of isotopically light DIC (dissolved inorganic carbon) would be produced. Thus, the bottom ocean relic from the Tereeken glaciation would be characterized by anoxia, low sulfate concentration, high $\delta^{34}S_{sulfate}$, and low $\delta^{13}C_{DIC}$ (Fig. 6a).

Upon deglaciation, warm meltwater formed a plume on cold relict bottom water, maintaining physical and chemical stratification for $>10^3$ years (Hoffman et al., 2007;

Shields, 2005). The geochemistry of the meltwater plume (or surface water) would be dominated by oxidative weathering of pyrite, evaporite, organic carbon, and silicate minerals. Due to accelerated post-glacial weathering, significant amount of sulfate and DIC would be delivered to oxygenated surface waters, where sulfate reduction is prohibited. Using modern weathering fluxes as a guide ($\delta^{34}S_{weathering}$=+6‰, $\delta^{13}C_{weathering}$=–5‰) (Kah et al., 2004; Kump, 1991), the post-glacial meltwater plume would be generally characterized by moderate sulfate concentration, low $\delta^{34}S_{sulfate}$, and low $\delta^{13}C_{DIC}$ (Fig. 6b).

If the Zhamoketi cap dolostone was deposited below storm wave base, as indicated by the lack of wave affected sedimentary structures, then it deposited below the pycnocline that separates the meltwater plume and bottom water. We hypothesize that, in a stratified basin, the Zhamoketi carbonate and CAS were derived from surface water, recording low $\delta^{34}S_{CAS}$, low $\delta^{13}C_{carb}$, and moderate CAS concentrations. Petrographic observations are consistent with this hypothesis. Zhamoketi microsparites and peloids likely formed in the surface water probably as pelagic carbonate; benthic carbonate such as cements is volumetrically insignificant (Fig. 3c). As the $\delta^{34}S_{CAS}$ values have not been strongly altered by diagenesis (see above discussion), we infer that either the Zhamoketi cap carbonate was precipitated as primary dolomite or its $\delta^{34}S_{CAS}$ values were buffered against secondary dolomitization.

In contrast, sulfur available for pyrite formation was derived from anoxic bottom water characterized by high $\delta^{34}S$ values due to long-term synglacial sulfate reduction. $\delta^{34}S_{py}$ can thus approach and exceed $\delta^{34}S_{CAS}$ derived from surface water, particularly if pyrite formation occurred in a semi-closed system below the water-sediment interface.

Calculation based on a Rayleigh distillation model shows that about 30–85% depletion of the bottom water sulfate reservoir by sulfate reduction is required to produce the observed sulfur isotope signature of the Zhamoketi cap dolostone (Fig. 7). This is calculated as follows. If bottom water sulfate was the ultimate sulfur source of Zhamoketi pyrite, the observed average $\delta^{34}S_{py}$ value of 15.8‰ requires a bottom water $\delta^{34}S_{sulfate}$ value of 50.8‰ assuming a cumulative isotopic fractionation of 35‰ by sulfate reduction bacteria (SRB)—a conservative assumption because the cumulative fractionation was likely much less than 35‰ due to sulfate limitation. This indicates 30–85% syn-glacial

depletion of bottom water sulfate by SRB, depending on pre-glacial $\delta^{34}S_{sulfate}$ value (e.g. +30‰; Shields et al., 2007) and the instantaneous isotopic fractionation factor by SRB. In comparison, the observed average $\delta^{34}S_{CAS}$ value is +13.4‰, requiring that weathering influx ($\delta^{34}S_{weathering}$=+6‰) contributed roughly 50–70% of surface water sulfate reservoir depending on pre-glacial $\delta^{34}S_{sulfate}$ value (Fig. 7).

The stratification model brings up two questions. First, what drove the sulfur isotope distillation of the bottom ocean? Presumably, organic carbon for bacterial sulfate reduction was supplied by a large DOC reservoir (Rothman et al., 2003) and possible syn-glacial bioproduction (Corsetti and Kaufman, 2003). Syn-glacial bioproduction may have occurred in potentially open tropic oceans (Hyde et al., 2000) or during intermittently thawing periods (as suggested by the siltstones interbedded with diamictites of the Zhamoketi Formation). However, syn-glacial sulfate replenishment to the deep ocean was minimal because of reduced polar down-welling. These factors, together with the low sulfate concentrations in Proterozoic oceans to being with, make it theoretically possible to deplete deep water sulfate by 30–85% if the basin was stratified. Another question relates to the low pyrite concentrations in the Zhamoketi cap dolostone. Why pyrite concentrations are low if 30–85% deep water sulfate was consumed by sulfate reduction bacteria? Reactive iron does not appear to have imposed a limitation on pyrite formation, because iron concentrations are generally high. We argue that low pyrite concentrations are related to the generally low sulfate availability in Proterozoic oceans. In addition, the rapid sedimentation rate of the cap carbonate (Hoffman et al., 1998) may have also played a role in diluting pyrite concentrations.

It is uncertain how long the basin stratification lasted. However, there is evidence for some degree of mixing at about 2.5 m. Below 2.5 m, $\delta^{34}S_{CAS}$ values are consistently lower than $\delta^{34}S_{py}$ values, a pattern that could be explained by the stratification model described above. Above 2.5 m, however, the overall range of $\delta^{34}S_{CAS}$ values encompass the $\delta^{34}S_{py}$ range although individual samples have $\delta^{34}S_{CAS} < \delta^{34}S_{py}$. We interpret the overlapping $\delta^{34}S_{CAS}$ and $\delta^{34}S_{py}$ ranges as evidence for partial mixing of surface and bottom waters (Fig. 6c). After mixing, sulfate concentration would decrease while $\delta^{34}S$ increases in surface water. This is consistent with the stratigraphic increase in average $\delta^{34}S_{CAS}$ at about 2.5 m. The decrease in CAS, however, occurs lower in stratigraphy (~1

m), and it is uncertain whether the stratigraphic offset is geochronologically significant because of the uncertainty in sedimentation rate. $\delta^{34}S_{py}$ values, on the other hand, would not be affected as much as $\delta^{34}S_{CAS}$ by the mixing if sulfur source for pyrite formation was consistently derived from anoxic deep waters.

If partial mixing occurred around 2.5 m, why wasn't the $\delta^{13}C_{carb}$ signature disturbed at the same level? Negative $\delta^{13}C_{carb}$ values of cap dolostones atop Marinoan glacial deposits have been interpreted in terms of post-glacial overturn of a ^{12}C-enriched deep ocean (Grotzinger and Knoll, 1995; Kaufman et al., 1991; Knoll et al., 1996; Knoll et al., 1986), Rayleigh distillation of a large atmospheric CO_2 reservoir (Hoffman et al., 1998), release of isotopically light gas hydrates (Jiang et al., 2003; Kennedy et al., 2001b), catastrophic temperature rise and kinetic isotopic effect associated with rapid carbonate sedimentation (Higgins and Schrag, 2003). Perhaps all of these processes may have contributed to the $\delta^{13}C_{carb}$ pattern. But if both the meltwater plume and bottom water are characterized by similarly negative $\delta^{13}C_{carb}$ values, the partial mixing at 2.5 m would not have significant impact on the $\delta^{13}C_{carb}$ values of the cap dolostone. This is particularly true if the surface ocean represented a high alkalinity source and had a stronger buffer against disturbance than the sulfur system. Even so, the negative stratigraphic trend of $\delta^{13}C_{carb}$ in many Marinoan cap dolostones (Kennedy et al., 1998; Zhou and Xiao, 2007) may record an oceanic mixing between surface and bottom waters (Grotzinger and Knoll, 1995; Kaufman et al., 1991; Knoll et al., 1996).

Because of the uniqueness of Neoproterozoic global glaciations, a modern analog to the stratification model would not be expected. Nonetheless, the euxinic fjord at Framvaren of southern Norway may shed some light on the stratification model. Pyrite in the bottom sediments of the Framvaren fjord is enriched in ^{34}S, reaching $\delta^{34}S_{py}$ values around –12‰, compared with values around –35‰ near and above the chemocline (Sælen et al., 1993). This enrichment was interpreted as a result of intense bacterial reduction in the bottom water whose exchange with the open ocean is limited by shallow sills and a surface lid of low-salinity meltwater. Of course, despite their negative $\Delta\delta^{34}S_{sulfate-py}$ values, Framvaren pyrites are not as ^{34}S-enriched as Zhamoketi pyrites. However, with (1) a smaller sulfate reservoir in the Neoproterozoic ocean, (2) prolonged syn-glacial bacterial sulfate reduction, (3) sufficient reactive iron to titrate sulfide from

the bottom water, and (4) continuing post-glacial stratification, the residual sulfate and hence pyrite derived from in the Zhamoketi bottom water would be much more ^{34}S-enriched than the Framvaren fjord.

A similar stratification model has been proposed by Holser (1977) to explain superheavy $\delta^{34}S_{py}$ values at the Neoproterozoic–Cambrian, middle–late Devonian, and early–middle Triassic transitions. In Holser's model, oceanic stratification in more or less restricted basins is induced by brine formation in evaporitic environments. Evaporitic brines stored in deep basins are subjected to isotopic distillation by sulfate reduction bacteria, driving the sulfur isotope of residual sulfate to greater values. Catastrophic overturn of deep water brines would introduce ^{34}S-enriched sulfate into the surface water, leading to the precipitation of ^{34}S-enriched pyrites. A general theme of these models is chemical stratification, the isolation of a ^{34}S-enriched sulfate pool in the bottom water, and subsequent oceanic overturn resulting in the observed sulfur isotopic patterns.

6.2. Sulfate minimum zone model

Inspired by Logan et al. (1995), we also consider an alternative model in which the ^{34}S-enriched sulfate pool is not isolated in the bottom water, but in a sulfate minimum zone (SMZ). Indeed, the SMZ model has been used to explain the generally heavy $\delta^{34}S_{sulfide}$ values that exceed corresponding $\delta^{34}S_{sulfate}$ values in Neoproterozoic rocks (Li et al., 1999; Logan et al., 1995). In this model, no oceanic stagnation is required. The oceanic conveyor system would operate as in modern oceans, delivering oxygen and sulfate to the deep ocean. However, because of the generally low sulfate concentration in Neoproterozoic oceans, sulfate could be overwhelmed by settling organic carbon, creating a SMZ analogous to the oxygen minimum zone in the modern ocean (Logan et al., 1995). In this SMZ, intense bacterial sulfate reduction would deplete sulfate and drive $\delta^{34}S_{sulfate}$ to greater values (Fig. 8a). The SMZ would be likely below the storm wave base. Where the SMZ encroached the continental shelf or slope, its ^{34}S-enriched sulfate pool would become the source of pore water sulfate reduction, leading to the formation of ^{34}S-enriched pyrite. Alternatively, pyrite formation could also occur syngenetically in the anoxic SMZ. Thus, at least the lowermost 2.5 m of the Zhamoketi cap dolostone represent deposition at or beneath the SMZ, with carbonate and CAS derived from

surface water, and sulfur for pyrite formation from the SMZ. Above 2.5 m, partial decay of the SMZ may be responsible for the slight change in $\Delta\delta^{34}S_{CAS-py}$ values (Fig. 8b).

These models should be tested with more geochemical data from other cap dolostones. Unfortunately, high-resolution paired $\delta^{34}S_{CAS}$ and $\delta^{34}S_{py}$ analyses of carbonates equivalent to the Zhamoketi cap dolostone are still sporadic and systematic $\delta^{34}S_{CAS}$ data are only available for the Maieberg Formation in Namibia (Hurtgen et al., 2002; Hurtgen et al., 2006), Noonday Dolomite in Death Valley (Hurtgen et al., 2004), Jbeliat cap carbonate in the Taoudéni Basin (Shields et al., 2007), and the Doushantuo cap dolostone in South China (Goldberg et al., 2005; Zhang et al., 2003). Although their thickness varies significantly (Hoffman et al., 2007), several Marinoan cap dolostones are characterized by a 3–15‰ positive $\delta^{34}S_{CAS}$ shift in the lowermost part (arrows in Fig. 9), similar to the positive shift (~5‰) in the basal Zhamoketi cap dolostone. However, systematic and concurrent $\delta^{34}S_{py}$ analyses have not been carried out for these successions and a comparative study between the Zhamoketi and other Ediacaran cap dolostones is premature.

Nonetheless, available $\delta^{34}S_{CAS}$ data from basal Ediacaran cap carbonates show strong spatial and stratigraphic variations (Fig. 9), in sharp contrast to the consistently negative $\delta^{13}C_{carb}$ values (Kennedy et al., 1998; Zhou and Xiao, 2007). The variations speak to the generally small sulfate reservoir in post-glacial oceans and the volatility of the $\delta^{34}S_{sulfate}$ signatures that were subject to local disturbance including riverine and upwelling input. In light of this, it is not surprising that there may have been a significant onshore-offshore $\delta^{34}S_{sulfate}$ gradient (Hurtgen et al., 2006). As would be expected, $\delta^{34}S_{CAS}$ values of the Zhamoketi cap dolostone (+9.1‰ to +20.6‰), which was deposited in relatively deep water environment below storm wave base, would be more akin to those of open shelf sections (section MS-3: +15.2‰ to +24.1‰; section MS-8: +15.5‰ to +44.8‰) than restricted shelf sections (MS-1: +19.3‰ to +47.0‰) of the Maieberg Formation in Namibia (Hurtgen et al., 2006).

7. CONCLUSIONS

Systematic sulfur isotope analysis of the basal Ediacaran Zhamoketi cap dolostone shows that $\delta^{34}S_{py}$ values are within ±10‰ of corresponding $\delta^{34}S_{CAS}$ values, and in most samples $\delta^{34}S_{py}$ is greater than corresponding $\delta^{34}S_{CAS}$. The negative $\Delta\delta^{34}S_{CAS-py}$ values, calculated from $\delta^{34}S_{CAS}$ and $\delta^{34}S_{py}$ analyses of bulk samples, are inconsistent with derivation of sulfate and sulfide from the same sulfur reservoir. Instead, CAS and pyrite were likely derived from two isotopically distinct reservoirs in a chemically stratified basin. In this model, CAS is hypothesized to have been derived from oxic surface water with moderate sulfate concentration, lower $\delta^{34}S_{sulfate}$ (due to post-glacial, oxidative weathering of pyrite), and lower $\delta^{13}C_{DIC}$. In contrast, sulfur for pyrite formation may have come from anoxic bottom water that was relict from the Marinoan glaciation and was characterized by lower sulfate concentration, higher $\delta^{34}S_{sulfate}$ (due to limited sulfate supply, continuing sulfate reduction, and pyrite precipitation during the Marinoan glaciation), and lower $\delta^{13}C_{DIC}$ (due to production of alkalinity associated with sulfate reduction). Alternatively, the Quruqtagh basin was not chemically stratified, but pyrites were formed in a sulfate minimum zone. In either case, it appears that oceanic mixing occurred about 2.5 m, where $\delta^{34}S_{CAS}$ and $\delta^{34}S_{py}$ values begin to converge.

The spatial heterogeneity and temporal variations in $\delta^{34}S_{CAS}$ and $\delta^{34}S_{py}$, as well as the possibility for the bottom water sulfate reservoir to be isotopically distilled during stratification, indicate relatively low sulfate concentration in post-glacial oceans. Because of the heterogeneity, care must be taken when applying $\delta^{34}S$ data in chemostratigraphic correlation of Proterozoic successions.

REFERENCES

Allen, P.A. and Hoffman, P.F., 2005. Extreme winds and waves in the aftermath of a Neoproterozoic glaciation. Nature, 433: 123-127.

Bottrell, S.H. and Newton, R.J., 2006. Reconstruction of changes in global sulfur cycling from marine sulfate isotopes. Earth Science Reviews, 75: 59-83.

Burdett, J., Authur, M. and Richardson, M., 1989. A Neogene seawater sulfur isotope age curve from calcareous pelagic microfossils. Earth and Planetary Science Letters, 94: 189-198.

Canfield, D.E., 1998. A new model for Proterozoic ocean chemistry. Nature, 396: 450-453.

Canfield, D.E., Raiswell, R., Westrich, J.T., Reaves, C.M. and Berner, R.A., 1986. The use of chromium reduction in the analysis of reduced inorganic sulfur in sediments and shales. Chemical Geology, 54: 149-155.

Canfield, D.E. and Thamdrup, B., 1994. The production of ^{34}S-depleted sulfide during bacterial disproportionation of elemental sulfur. Science, 266: 1973-1975.

Condon, D., Zhu, M., Bowring, S., Wang, W., Yang, A. and Jin, Y., 2005. U-Pb Ages from the Neoproterozoic Doushantuo Formation, China. Science, 308: 95-98.

Corsetti, F.A. and Grotzinger, J.P., 2005. Origin and significance of tube structures in Neoproterozoic post-glacial cap carbonates: Example from Noonday Dolomite, Death Valley, United States. Palaios, 20: 348–362.

Corsetti, F.A. and Kaufman, A.J., 2003. Stratigraphic investigations of carbon isotope anomalies and Neoproterozoic ice ages in Death Valley, California. Geological Society of America Bulletin, 115: 916–932.

Corsetti, F.A. and Lorentz, N.J., 2006. On Neoproterozoic cap carbonate as chronostratigraphic markers. In: S. Xiao and A.J. Kaufman (Editors), Neoproterozoic geobiology and paleobiology. Springer, Dordrecht, Netherlands, pp. 273-294.

Detmers, J., Brüchert, V., Habicht, K.S. and Kuever, J., 2001. Diversity of sulfur isotope fractionations by sulfate-reducing prokaryotes. Applied and Environmental Microbiology, 67: 888-894.

Evans, D.A.D., 2000. Stratigraphic, geochronological, and paleomagnetic constraints upon the Neoproterozoic climatic paradox. American Journal of Science, 300: 347-433.

Fike, D.A., Grotzinger, J.P., Pratt, L.M. and Summons, R.E., 2006. Oxidation of the Ediacaran ocean. Nature, 444: 744-747.

Gao, Z., Chen, J., Lu, S., Peng, C. and Qin, Z., 1993. The Precambrian Geology in Northern Xinjiang (Precambrian Geology No. 6). Geological Publishing House, Beijing, 171 pp.

Gao, Z., Peng, C., Li, Y., Qian, J. and Zhu, S., 1980. The Sinian System and its glacial deposits in Quruqtagh, Xinjiang. In: Tianjin Institute of Geology and Mineral Resources (Editor), Research in Precambrian Geology, Sinian Suberathem in China. Tianjin Science and Technology Press, Tianjin, pp. 186-213.

Gao, Z. and Zhu, S., 1984. Precambrian Geology in Xinjiang, China. Xinjiang People's Publishing House, Urumuqi, China, 151 pp.

Gellatly, A.M. and Lyons, T.W., 2005. Trace sulfate in mid-Proterozoic carbonates and the sulfur isotope record of biospheric evolution. Geochimica et Cosmochimica Acta, 69: 3813-3829.

Goldberg, T., Poulton, S.W. and Strauss, H., 2005. Sulphur and oxygen isotope signatures of late Neoproterozoic to early Cambrian sulphate, Yangtze Platform,

China: Diagenetic constraints and seawater evolution. Precambrian Research, 137: 223-241.

Gorjan, P., Veevers, J.J. and Walter, M.R., 2000. Neoproterozoic sulfur-isotope variation in Australia and global implications. Precambrian Research, 100: 151-179.

Grassineau, N.V., Mattey, D.P. and Lowry, D., 2001. Sulfur isotope analysis of sulfide and sulfate minerals by continuous flow-isotope ratio mass spectrometry. Analytical Chemistry, 73: 220-225.

Grotzinger, J.P. and Knoll, A.H., 1995. Anomalous carbonate precipitates: Is the Precambrian the key to the Permian? Palaios, 10: 578-596.

Halverson, G.P., 2006. A Neoproterozoic chronology. In: S. Xiao and A.J. Kaufman (Editors), Neoproterozoic geobiology and paleobiology. Springer, Dordrecht, Netherlands, pp. 232-271.

Halverson, G.P., Hoffman, P.F., Schrag, D.P., Maloof, A.C. and Rice, A.H.N., 2005. Toward a Neoproterozoic composite carbon-isotope record. Geological Society of America Bulletin, 117: 1181-1207.

Higgins, J.A. and Schrag, D.P., 2003. Aftermath of a snowball Earth. Geochemistry, Geophysics, Geosystems (G^3), 4: Article Number 1028, DOI 10.1029/2002GC000403.

Hoffman, P.F., Halverson, G.P., Domack, E.W., Husson, J.M., Higgins, J.A. and Schrag, D.P., 2007. Are basal Ediacaran (635 Ma) post-glacial "cap dolostones" diachronous? Earth and Planetary Science Letters, 258: 114-131.

Hoffman, P.F., Kaufman, A.J., Halverson, G.P. and Schrag, D.P., 1998. A Neoproterozoic snowball Earth. Science, 281: 1342-1346.

Hoffman, P.F. and Schrag, D.P., 2002. The snowball Earth hypothesis: Testing the limits of global change. Terra Nova, 14: 129-155.

Hoffmann, K.-H., Condon, D.J., Bowring, S.A. and Crowley, J.L., 2004. U-Pb zircon date from the Neoproterozoic Ghaub Formation, Namibia: Constraints on Marinoan glaciation. Geology, 32: 817-820.

Holser, W.T., 1977. Catastrophic chemical events in the history of the ocean. Nature, 267: 403-408.

Hurtgen, M.T., Arthur, M.A. and Halverson, G.P., 2005. Neoproterozoic sulfur isotopes, the evolution of microbial sulfur species, and the burial efficiency of sulfide as sedimentary pyrite. Geology, 33: 41-44.

Hurtgen, M.T., Arthur, M.A. and Prave, A.R., 2004. The sulfur isotope composition of carbonate-associated sulfate in Mesoproterozoic to Neoproterozoic carbonates from Death Valley, California. In: J.P. Amend, K.J. Edwards and T.W. Lyons (Editors), Sulfur Biogeochemistry-Past and Present: Geological Society of America Special Paper, pp. 177-194.

Hurtgen, M.T., Arthur, M.A., Suits, N.S. and Kaufman, A.J., 2002. The sulfur isotopic composition of Neoproterozoic seawater sulfate: implications for a snowball Earth? Earth and Planetary Science Letters, 203: 413-429.

Hurtgen, M.T., Halverson, G.P., Arthur, M.A. and Hoffman, P.F., 2006. Sulfur cycling in the aftermath of a 635-Ma snowball glaciation: Evidence for a syn-glacial sulfidic deep ocean. Earth and Planetary Science Letters, 245: 551-570.

Hyde, W.T., Crowley, T.J., Baum, S.K. and Peltier, W.R., 2000. Neoproterozoic "snowball Earth" simulations with a coupled climate/ice-sheet model. Nature, 405: 425-429.

James, N.P., Narbonne, G.M. and Kyser, T.K., 2001. Late Neoproterozoic cap carbonates: Mackenzie Mountains, Northwestern Canada: Precipitation and global glaciation meltdown. Canadian Journal of Earth Sciences, 38: 1229-1262.

Jiang, G., Kennedy, M.J. and Christie-Blick, N., 2003. Stable isotopic evidence for methane seeps in Neoproterozoic postglacial cap carbonates. Nature, 426: 822-826.

Jiang, G., Kennedy, M.J., Christie-Blick, N., Wu, H. and Zhang, S., 2006. Stratigraphy, Sedimentary Structures, and Textures of the Late Neoproterozoic Doushantuo Cap Carbonate in South China. Journal of Sedimentary Research, 76: 978-995.

Kah, L.C., Lyons, T.W. and Frank, T.D., 2004. Low marine sulphate and protracted oxygenation of the Proterozoic biosphere. Nature, 431: 834-838.

Kampschulte, A., Bruckschen, P. and Strauss, H., 2001. The sulphur isotopic composition of trace sulphates in Carboniferous brachiopods: implications for coeval seawater, correlation with other geochemical cycles and isotope stratigraphy. Chemical Geology, 205: 149-173.

Kampschulte, A. and Strauss, H., 2004. The sulfur isotopic evolution of Phanerozoic seawater based on the analysis of structurally substituted sulfate in carbonates. Chemical Geology, 204: 255-286.

Kaufman, A.J., Corsetti, F.A. and Varni, M.A., 2007. The effect of rising atmospheric oxygen on carbon and sulfur isotope anomalies in the Neoproterozoic Johnnie Formation, Death Valley, USA. Chemical Geology, 237: 47-63.

Kaufman, A.J., Hayes, J.M., Knoll, A.H. and Germs, G.J.B., 1991. Isotopic compositions of carbonates and organic carbon from upper Proterozoic successions in Namibia: stratigraphic variation and the effects of diagenesis and metamorphism. Precambrian Research, 49: 301-327.

Kennedy, M.J., Christie-Blick, N. and Prave, A.R., 2001a. Carbon isotopic composition of Neoproterozoic glacial carbonates as a test of paleoceanographic models for snowball Earth phenomena. Geology, 29: 1135-1138.

Kennedy, M.J., Christie-Blick, N. and Sohl, L.E., 2001b. Are Proterozoic cap carbonates and isotopic excursions a record of gas hydrate destabilization following Earth's coldest intervals? Geology, 29: 443-446.

Kennedy, M.J., Runnegar, B., Prave, A.R., Hoffmann, K.-H. and Arthur, M.A., 1998. Two or four Neoproterozoic glaciations? Geology, 26: 1059-1063.

Knoll, A.H., Bambach, R.K., Canfield, D.E. and Grotzinger, J.P., 1996. Comparative earth history and Late Permian mass extinction. Science, 273: 452-457.

Knoll, A.H., Hayes, J.M., Kaufman, A.J., Swett, K. and Lambert, I.B., 1986. Secular variation in carbon isotope ratios from Upper Proterozoic successions of Svalbard and East Greenland. Nature, 321: 832-838.

Kump, L.R., 1991. Interpreting carbon-isotope excursions: Strangelove oceans. Geology, 19: 299-302.

Leather, J., Allen, P.A., Brasier, M.D. and Cozzi, A., 2002. Neoproterozoic snowball Earth under scrutiny: Evidence from the Fiq glaciation of Oman. Geology, 30: 891-894.

Li, R., Chen, J., Zhang, S., Lei, J., Shen, Y. and Chen, X., 1999. Spatial and temporal variations in carbon and sulfur isotopic compositions of Sinian sedimentary rocks in the Yangtze platform, South China. Precambrian Research, 97: 59-75.

Liu, T.-B., Maynard, J.B. and Alten, J., 2006. Superheavy S isotopes from glacier-associated sediments of the Neoproterozoic of south China: Oceanic anoxia or sulfate limitation? In: S.E. Kesler and H. Ohmoto (Editors), Evolution of Early Earth's Atmosphere, Hydrosphere, and Biosphere—Constraints from Ore Deposits: Geological Society of America Memoir 198. Geological Society of America, Boulder, Colorado, pp. 205-222.

Logan, G.A., Hayes, J.M., Hieshima, G.B. and Summons, R.E., 1995. Terminal Proterozoic reorganization of biogeochemical cycles. Nature, 376: 53-57.

Lyons, T.W., Gellatly, A.M., McGoldrick, P.J. and Kah, L.C., 2006. Proterozoic sedimentary exhalative (SEDEX) deposits and links to evolving global ocean chemistry. In: S.E. Kesler and H. Ohmoto (Editors), Evolution of Early Earth's Atmosphere, Hydrosphere, and Biosphere—Constraints from Ore Deposits: Geological Society of America Memoir 198. Geological Society of America, Boulder, Colorado, pp. 169-184.

Lyons, T.W., Hurtgen, M.T. and Gill, B.C., 2005. New insight into the utility of carbonate-associated sulfate. Geochimica et Cosmochimica Acta, 69: A128.

Lyons, T.W., Walter, L.M., Gellatly, A.M., Martini, A.M. and Blake, R.E., 2004. Sites of anomalous organic remineralization in the carbonate sediment of South Florida, USA: The sulfur cycle and carbonate-associated sulfate. In: J.P. Amend, K.J. Edwards and T.W. Lyons (Editors), Sulfur Biogeochemistry: Past and Present (GSA Special Paper 379). Geological Society of America, Boulder, Colorado, pp. 161–176.

Nédélec, A., Affaton, P., France-Lanord, C., Charrière, A. and Alvaro, J., 2007. Sedimentology and chemostratigraphy of the Bwipe Neoproterozoic cap dolostones (Ghana, Volta Basin): A record of microbial activity in a peritidal environment. Comptes Rendus Geoscience 339: 223-239.

Newton, R.J., Bottrell, S.H., Dean, S.P., Hatfield, D. and Raiswell, R., 1995. An evaluation of the use of the chromous chloride reduction method for isotopic analyses of pyrite in rocks and sediment. Chemical Geology, 125: 317-320.

Norin, E., 1937. Reports from the Scientific Expedition to the Northwestern Provinces of China under the Leadership of Dr. Sven Hedin, III. Geology, 1. Geology of Western Quruqtagh, Eastern Tien-Shan. Bokförlags Aktiebolaget Thule, Stockholm, 194 pp.

Pavlov, A.A., Hurtgen, M.T., Kasting, J.F. and Arthur, M.A., 2003. Methane-rich Proterozoic atmosphere? Geology, 31: 87-90.

Pingitore, N.E., Jr., Meitzner, G. and Love, K.M., 1995. Identification of sulfate in natural carbonates by x-ray absorption spectroscopy. Geochimica et Cosmochimica Acta, 59: 2477-2483.

Ross, G.M., Bloch, J.D. and Krouse, H.R., 1995. Neoproterozoic strata of the southern Canadian Cordillera and the isotopic evolution of seawater sulfate. Precambrian Research, 73: 71-99.

Rothman, D.H., Hayes, J.M. and Summons, R.E., 2003. Dynamics of the Neoproterozoic carbon cycle Proceedings of the National Academy of Sciences of the United States of America, 100: 8124-8129.

Sælen, G., Raiswell, R., Talbot, M.R., Skei, J.M. and Bottrell, S.H., 1993. Heavy sedimentary sulfur isotopes as indicators of super-anoxic bottom-water conditions. Geology, 21: 1091-1094.

Shields, G.A., 2005. Neoproterozoic cap carbonates: a critical appraisal of existing models and the plumeworld hypothesis. Terra Nova, 17: 299-310.

Shields, G.A., Deynoux, M., Strauss, H., Paquet, H. and Nahon, D., 2007. Barite-bearing cap dolostones of the Taoudéni Basin, northwest Africa: Sedimentary and isotopic evidence for methane seepage after a Neoproterozoic glaciation Precambrian Research, 153: 209-235.

Staudt, W.J. and Schoonen, M.A.A., 1995. Sulfate incorporation into sedimentary carbonates. In: M.A. Vairavamurthy and M.A.A. Schoonen (Editors), Geochemical Transformations of Sedimentary Sulfur American Chemical Society, pp. 332–345.

Strauss, H., 2002. The isotopic composition of Precambrian sulphides: Seawater chemistry and biological evolution. In: W. Altermann and P.L. Corcoran (Editors), Precambrian Sedimentary Environments: A Modern Approach to Ancient

Depositional Systems (Special Publication Number 33 of the International Association of Sedimentologists). Blackwell Science, Oxford, pp. 67-105.

Xiao, S., Bao, H., Wang, H., Kaufman, A.J., Zhou, C., Li, G., Yuan, X. and Ling, H., 2004. The Neoproterozoic Quruqtagh Group in eastern Chinese Tianshan: Evidence for a post-Marinoan glaciation. Precambrian Research, 130: 1-26.

Xu, B., Jian, P., Zheng, H., Zou, H., Zhang, L. and Liu, D., 2005. U–Pb zircon geochronology and geochemistry of Neoproterozoic volcanic rocks in the Tarim Block of northwest China: implications for the breakup of Rodinia supercontinent and Neoproterozoic glaciations. Precambrian Research, 136: 107-123.

Yao, J., Xiao, S., Yin, L., Li, G. and Yuan, X., 2005. Basal Cambrian microfossils from the Yurtus and Xishanblaq formations (Tarim, north-west China): Systematic revision and biostratigraphic correlation of *Micrhystridium*-like acritarchs from China. Palaeontology, 48: 687-708.

Zhang, C.-L., Li, X.-H., Li, Z.-X., Lu, S.-N., Ye, H.-M. and Li, H.-M., 2007. Neoproterozoic ultramafic-mafic-carbonatite complex and granitoids in Quruqtagh of northeastern Tarim Block, western China: Geochronology, geochemistry and tectonic implications. Precambrian Research, 152: 149–169.

Zhang, T., Chu, X., Zhang, Q., Feng, L. and Huo, w., 2003. Variations of sulfur and carbon isotopes in seawater during the Doushantuo stage in late Neoproterozoic. Chinese Science Bulletin, 48: 1375-1380.

Zhao, X., Zhang, L., Zou, X., Wang, S. and Hu, Y., 1980. Sinian tillites in Northwest China and their stratigraphic significance. In: Tianjin Institute of Geology and

Mineral Resources (Editor), Research on Precambrian Geology Sinian Suberathem in China. Tianjin Science and Technology Press, Tianjin, pp. 164-185.

Zhou, C. and Xiao, S., 2007. Ediacaran $\delta^{13}C$ chemostratigraphy of South China. Chemical Geology, 237: 107-126.

Fig. 3.1. Geographic location of the Tarim Block and Quruqtagh area. (a) Geographic location of the Tarim Block. Rectangle indicates area shown in b. (b) Geological map of the Quruqtagh area. Arrow points to location of the Yukkengol section.

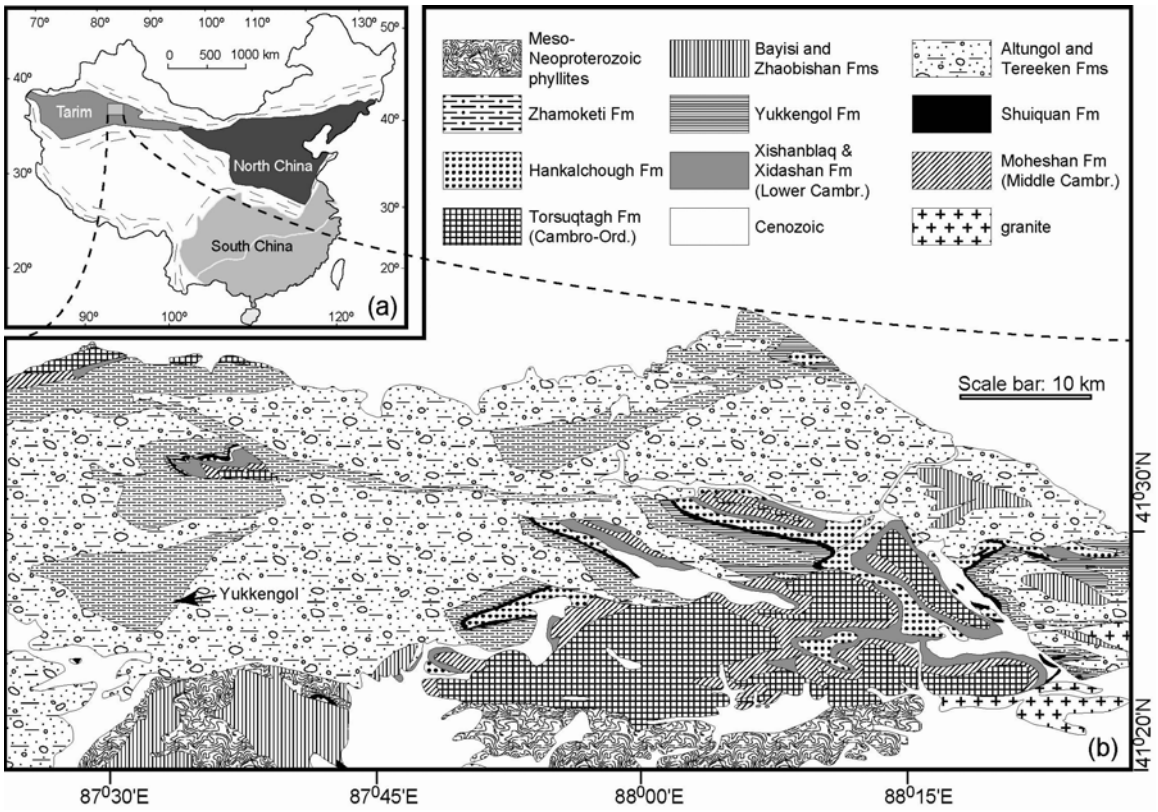

Fig. 3.2. (a) Stratigraphic column of Neoproterozoic Quruqtagh Group. (b) Detailed stratigraphic column of the Zhamoketi cap carbonate at the Yukkengol section.

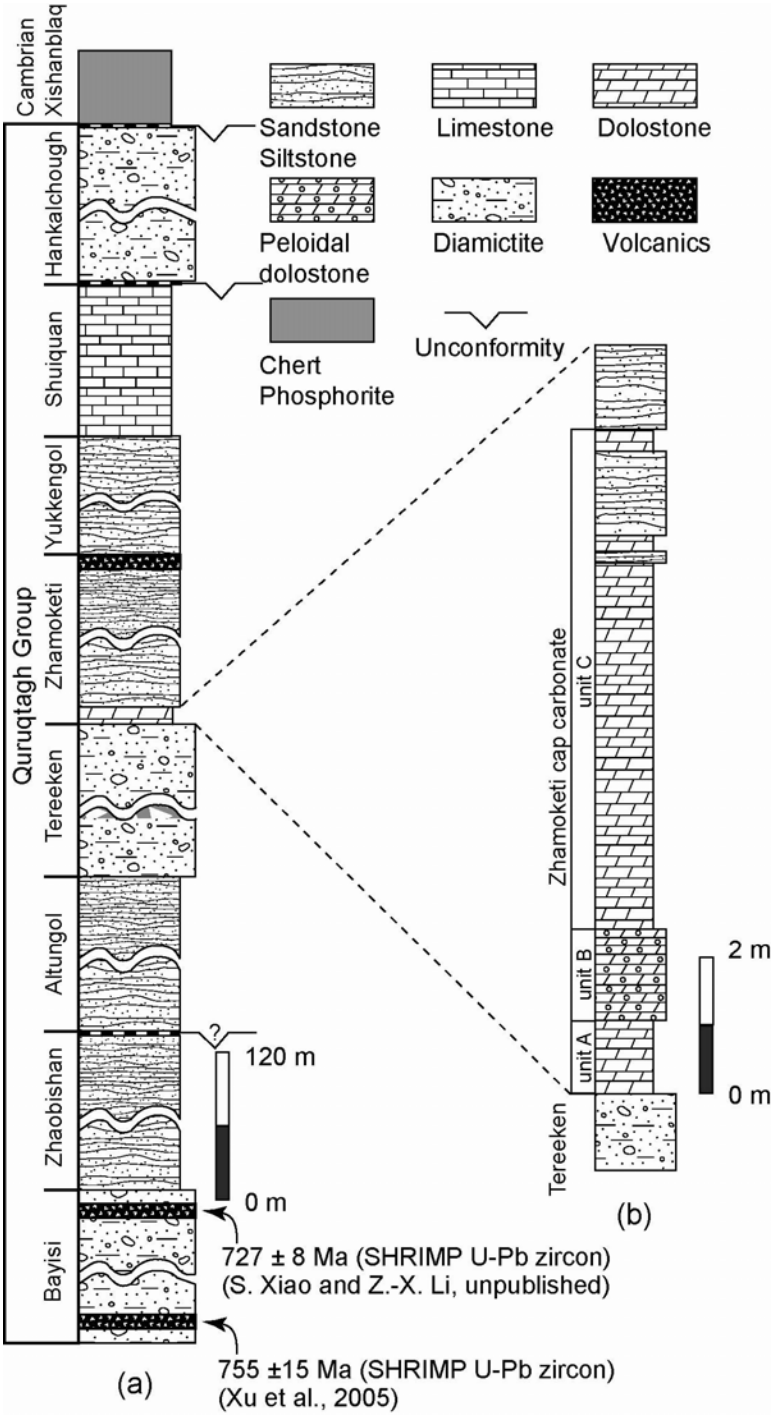

Fig. 3.3. Field photograph and SEM photomicrography of the Zhamoketi cap carbonate. (a) Striated clast in the Tereeken diamictite. (b) Field photograph showing the sharp contact between Tereeken diamictite and pinkish Zhamoketi cap dolostone at the Yukkengol section. (c) Photomicrograph of macropeloids in the Zhamoketi cap dolostone (unit B; delta-27, 136x11). (d) Photomicrograph of dolomicrite/dolomicrosparite in the Zhamoketi cap dolostone (delta-51, 141.8x11.7). (e–f) Back scattered electron micrographs of disseminated pyrites (bright color) in the Zhamoketi cap dolostone (delta-11).

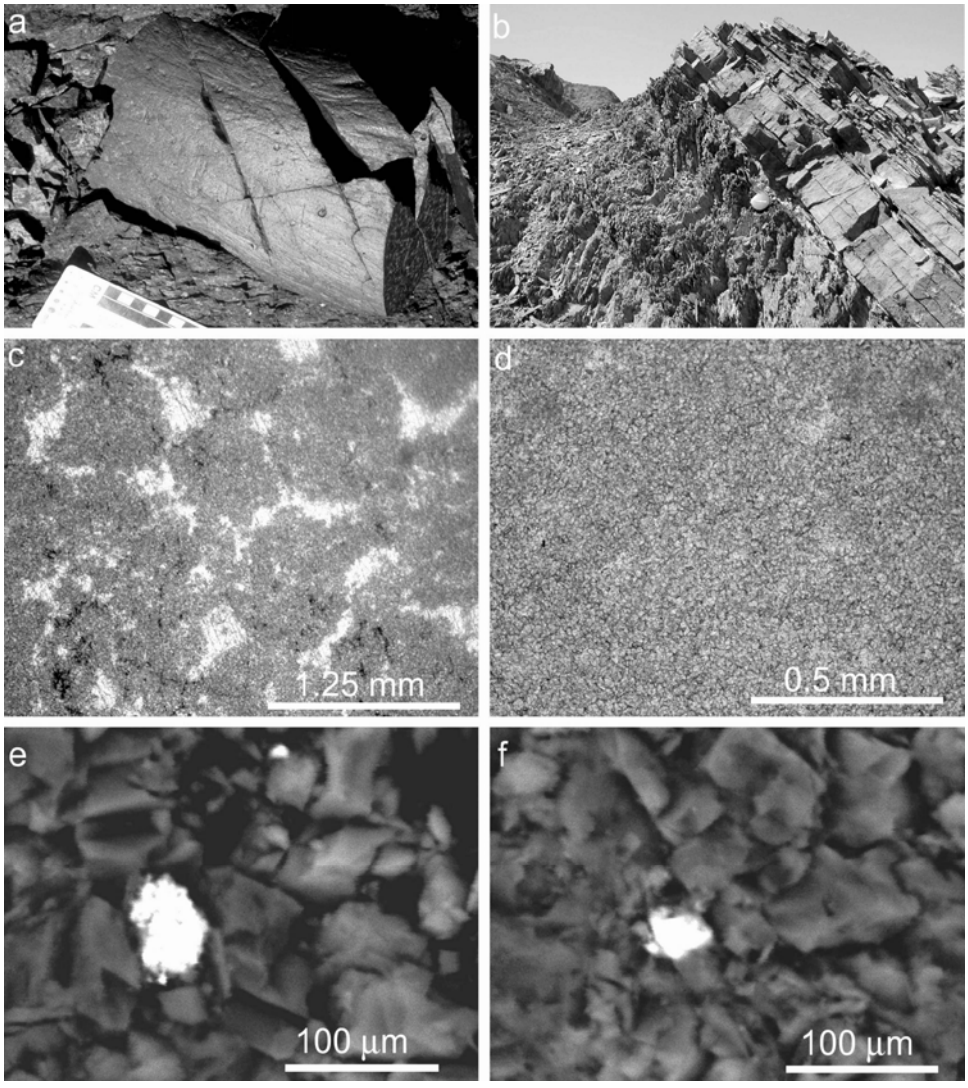

Fig. 3.4. Isotopic and elemental geochemistry profiles of the Zhamoketi cap dolostone at the Yukkengol section. Between sample $\delta^{34}S_{CAS}$ difference is calculated as the absolute difference in $\delta^{34}S_{CAS}$ between successive samples. $\Delta\delta^{13}C = \delta^{13}C_{carb} - \delta^{13}C_{org}$; $\Delta\delta^{34}S = \delta^{34}S_{CAS} - \delta^{34}S_{py}$.

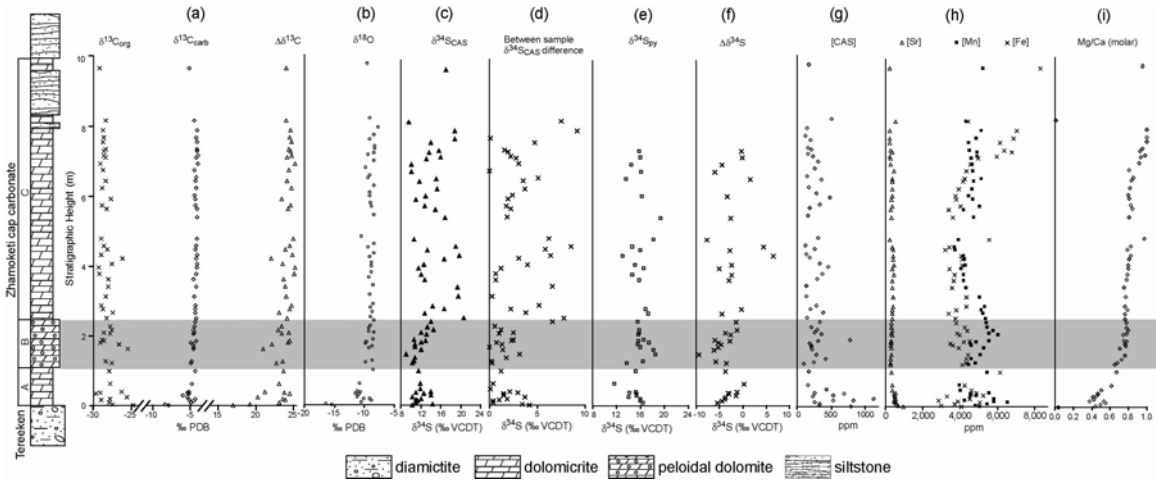

Fig. 3.5. Isotope and elemental cross-plots.

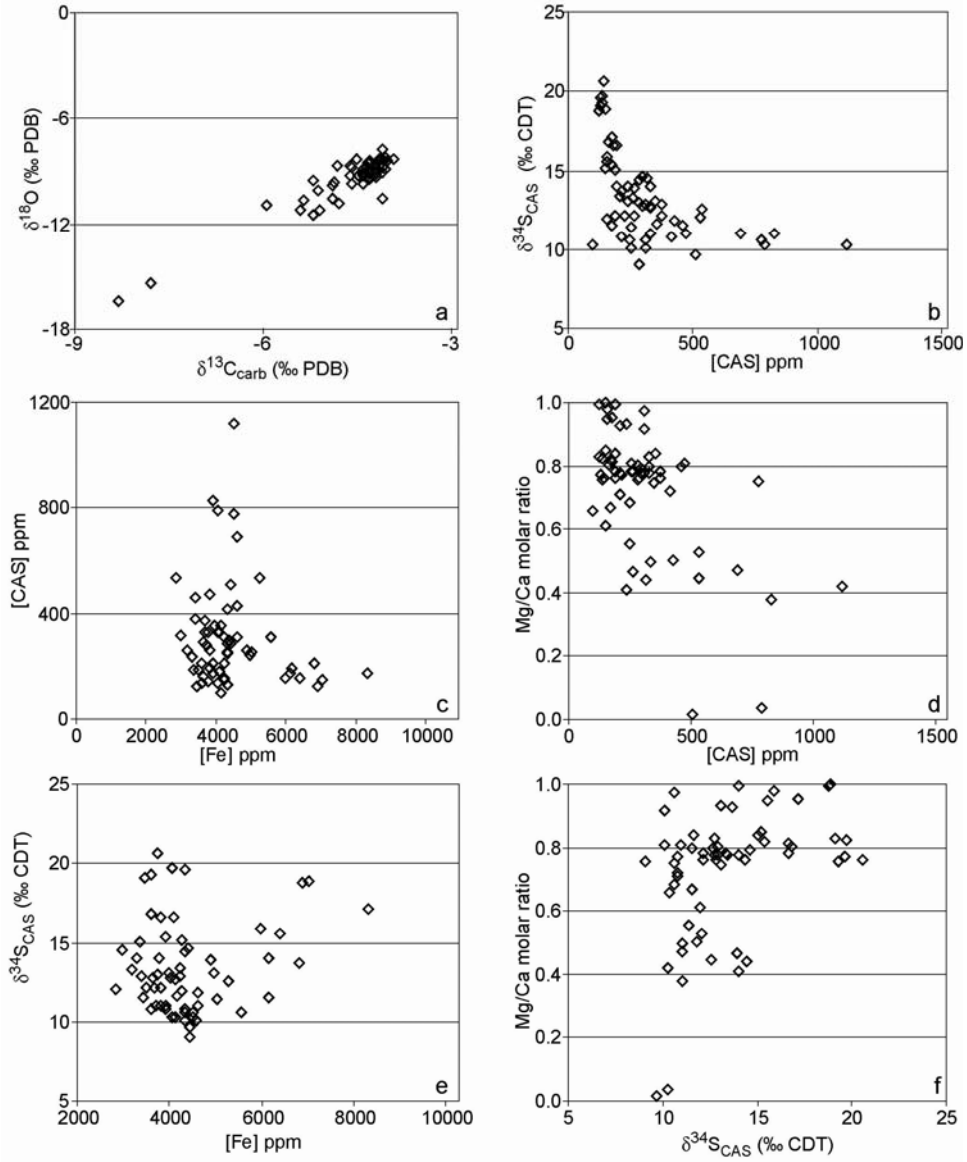

Fig. 3.6. Basin stratification model. (a) During the Tereeken glaciation, basin was covered by ice sheet and bacterial sulfate reduction was active in bottom water, leading to lower SO_4^{2-} concentrations and higher $\delta^{34}S_{sulfate}$ values. (b) During early deglaciation (Zhamoketi cap carbonate unit A and B), meltwater plume maintained basin stratification. Weathering input led to moderate SO_4^{2-} concentrations and low $\delta^{34}S_{sulfate}$ values in surface water. It is hypothesized that cap carbonate and CAS were derived from surface water, whereas sulfur source for pyrite formation came from bottom water. (c) During late deglaciation (Zhamoketi cap carbonate unit C), partial mixing led to higher $\delta^{34}S_{sulfate}$ and lower sulfate concentration in surface water.

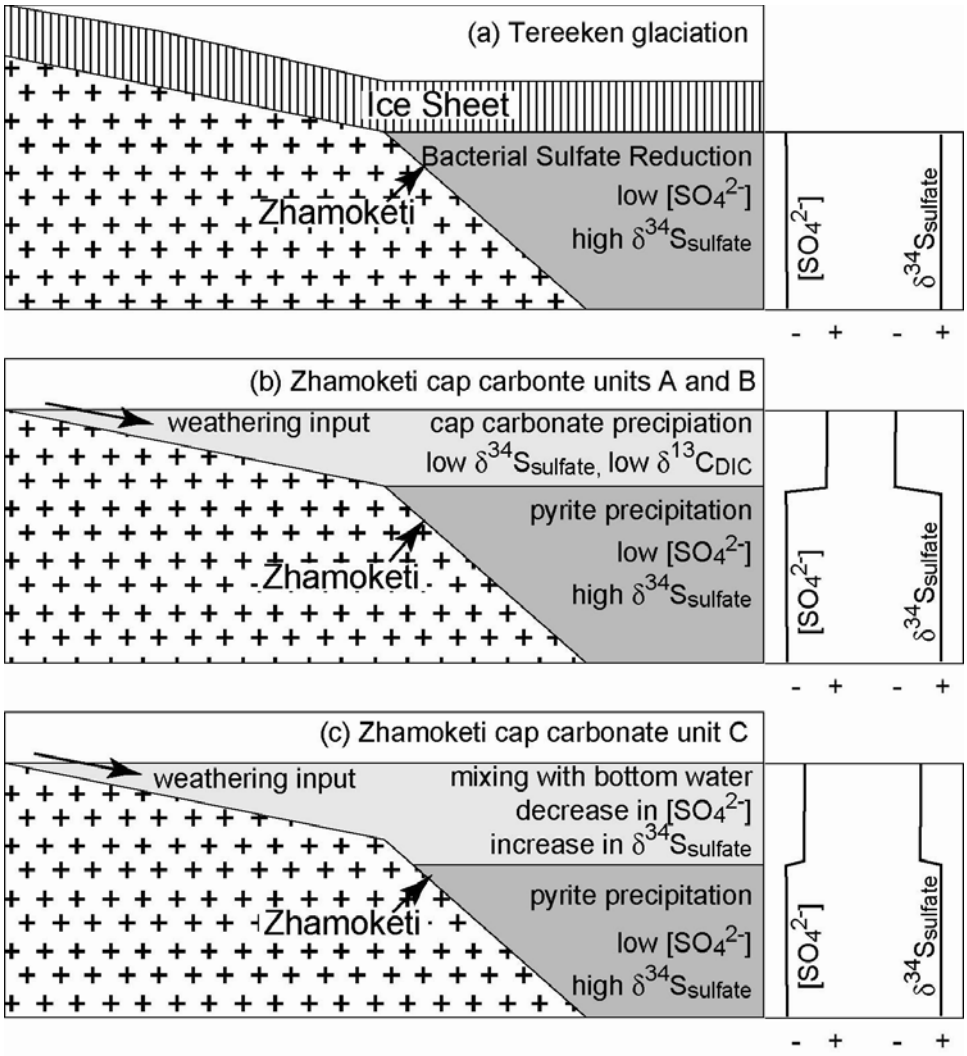

Fig. 3.7. Mass balance calculation of basin stratification model. (a) Schematic diagram showing $\delta^{34}S_{sulfate}$ evolution in the surface water (thin grey lines) and bottom water (thick solid lines) during and after the Tereeken glaciation. (b) Post-glacial weathering flux to surface water (thin grey lines) and synglacial distillation of bottom water by sulfate reduction (thick solid lines) necessary to explain observed sulfur isotopes (average $\delta^{34}S_{CAS}$=+13.4‰; average $\delta^{34}S_{py}$=+15.8‰; dotted lines) of the Zhamoketi cap dolostone based on the basin stratification model. As a sensitivity test, calculation was made assuming an initial pre-glacial $\delta^{34}S_{sulfate}$ value of +20‰ and +30‰, and a fractionation factor (α) of 0.945, 0.965, and 0.985.

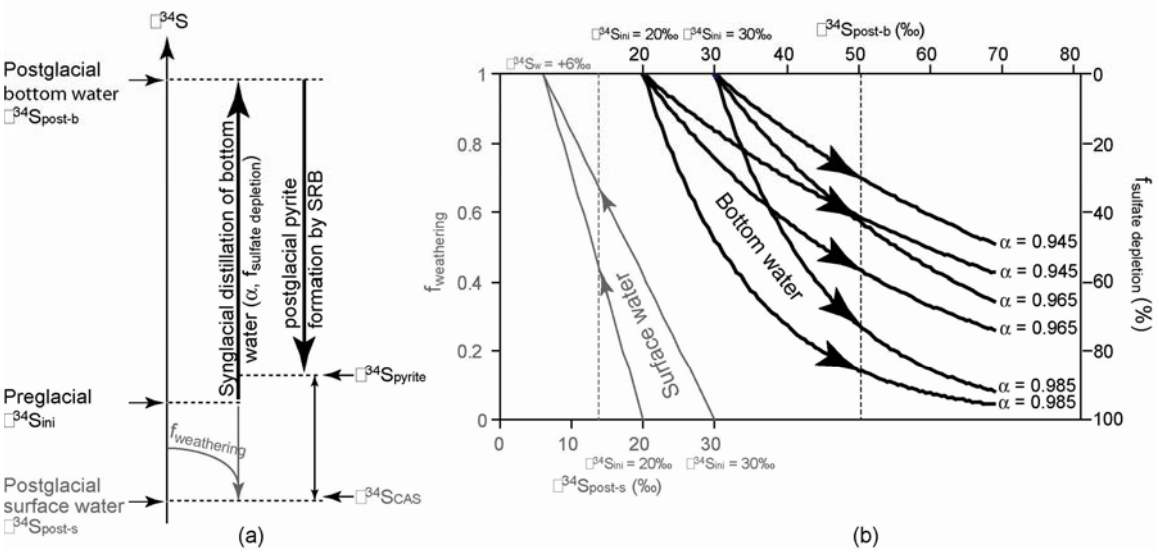

Fig. 3.8. Sulfate minimum zone model. (a) A sulfate minimum zone was formed due to slow sinking rate of organic carbon (Logan et al., 1995). Isotopic distillation in the sulfate minimum zone led to low SO_4^{2-} concentrations and elevated $\delta^{34}S_{sulfate}$ values. It is hypothesized that carbonate and CAS in Zhamoketi cap dolostone units A–B were derived from surface water, whereas sulfur for pyrite formation came from the sulfate minimum zone. (b) Attenuation of the sulfate minimum zone led to partial mixing and increased $\delta^{34}S_{sulfate}$ values in surface water during the precipitation of Zhamoketi cap carbonate unit C.

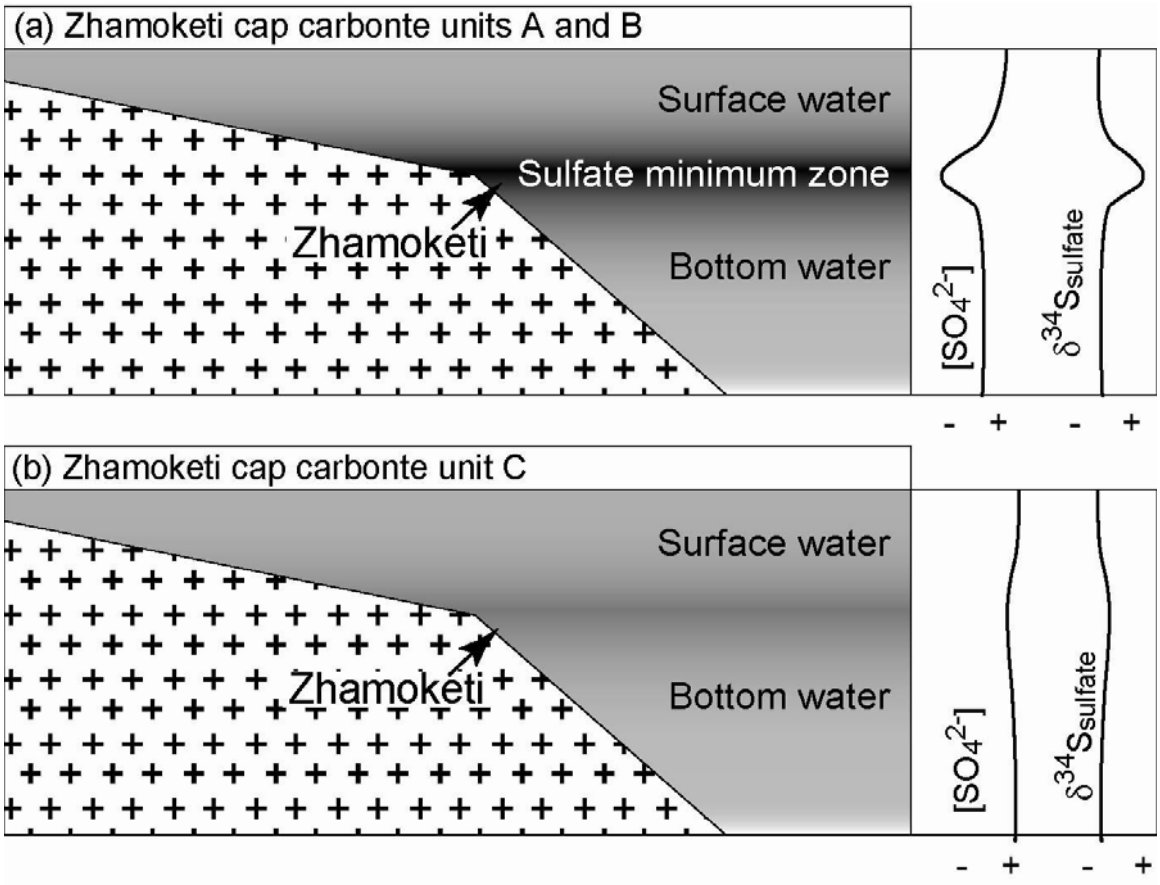

Fig. 3.9. Comparison of $\delta^{34}S_{CAS}$ profiles of supposedly equivalent cap carbonate following the Marinoan glaciation. (a–c) Keiberg cap dolostone, Namibia (Hurtgen et al., 2006). Section S1, restricted shelf. Sections S3 and S8, open shelf.. (d) Noonday cap carbonate, Death Valley (Hurtgen et al., 2004). (e) Nuccaleena cap dolostone, South Australia (Hurtgen et al., 2005). (f) Doushantuo cap dolostone, South China (Zhang et al., 2003). (g) Zhamoketi cap dolostone, Quruqtagh (this paper). Arrows indicates positive $\delta^{34}S_{CAS}$ shift in basal cap carbonates.

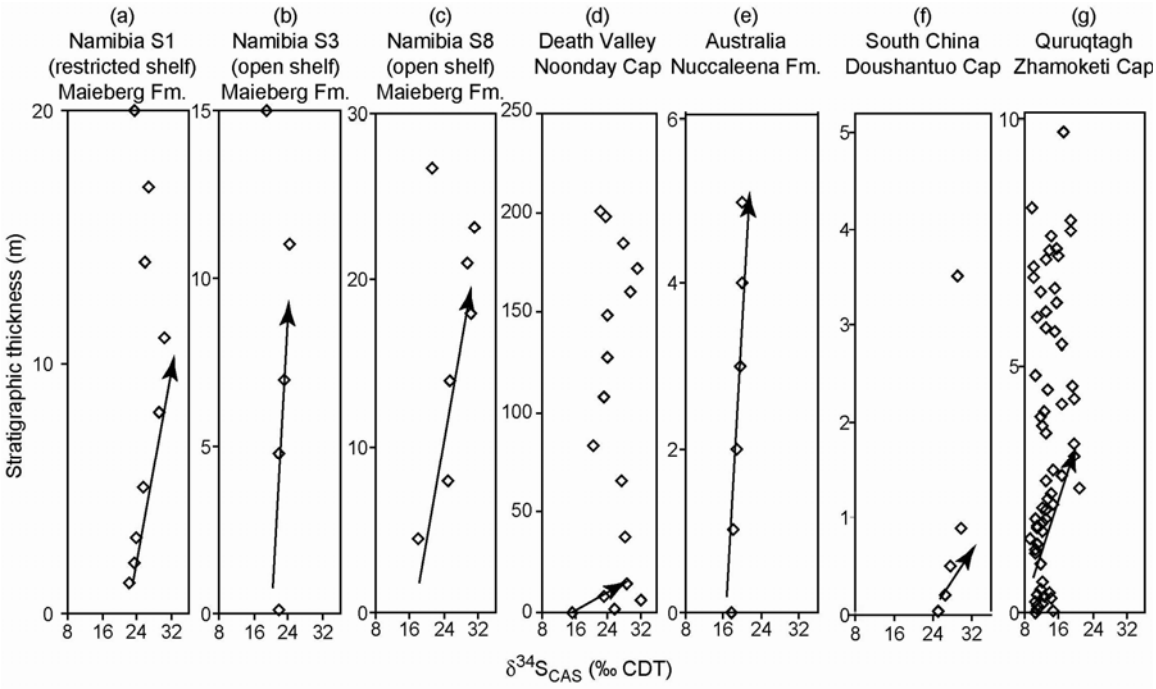

Table 3.1: Geochemical data of the Zhamoketi cap carbonate at the Yukkengol.

Sample Number	Height (m)	$\delta^{13}C_{carb}$ ‰	$\delta^{13}C_{org}$ ‰	$\Delta\delta^{13}C$ ‰	$\delta^{18}O$ ‰	$\delta^{34}S_{CAS}$ ‰	$\delta^{34}S_{py}$ ‰	$\Delta\delta^{34}S$ ‰	Fe ppm	Mn ppm	Sr ppm	CAS ppm	Mg/Ca molar
Δ-10	0.00	-7.8	-24.7	16.9	-15.4	10.3	ns.	na.	4055	5064	930	791	0.04
Δ-11	0.03	-8.3	-27.4	19.1	-16.4	14.5	ns.	na.	2981	4836	657	315	0.44
Δ-12	0.09	-4.9	-28.0	23.1	-10.5	11.1	16.4	-5.4	3709	5481	593	332	0.50
Δ-13	0.12	-4.6	na.	na.	-8.8	11.4	16.0	-4.6	5046	6540	502	253	0.55
Δ-14	0.16	-5.1	-29.0	23.9	-10.1	11.0	ns.	na.	3913	5815	532	829	0.38
Δ-15	0.18	-4.3	-27.8	23.5	-9.0	12.1	15.9	-3.9	2845	4237	456	533	0.53
Δ-16	0.23	-5.4	-25.6	20.2	-11.2	10.3	14.1	-3.8	4513	5828	561	1116	0.42
Δ-17	0.30	-5.9	na.	na.	-10.9	14.0	15.4	-1.3	3302	4590	505	237	0.41
Δ-18	0.33	-5.2	-29.7	24.5	-11.5	12.5	15.5	-2.9	5270	4899	482	535	0.45
Δ-19	0.37	-5.3	-29.1	23.8	-10.6	11.0	14.2	-3.2	4629	4560	449	690	0.47
Δ-20	0.39	-5.1	-26.3	21.2	-11.2	14.0	15.2	-1.3	4888	5570	521	264	0.46
Δ-21	0.48	na.	na.	na.	na.	11.8	ns.	na.	4626	4040	375	430	0.50
Δ-22	0.62	-4.8	-27.9	23.1	-10.8	12.0	11.8	0.2	4262	3999	360	154	0.61
Δ-23	1.00	-4.3	-28.0	23.7	-8.5	11.6	15.3	-3.7	6145	5476	312	173	0.67
Δ-24	1.22	-4.9	-27.6	22.7	-9.8	10.3	13.9	-3.5	4134	4488	281	97	0.66
Δ-25	1.27	-4.8	-28.4	23.5	-8.7	10.6	16.5	-5.9	4350	4836	279	249	0.68
Δ-26	1.38	na.	na.	na.	na.	10.8	ns.	na.	4340	4619	267	414	0.72
Δ-27	1.50	na.	na.	na.	na.	9.1	18.5	-9.4	4435	5101	304	285	0.76
Δ-28	1.63	-4.5	-25.5	21.0	-9.2	12.2	18.3	-6.1	na.	na.	na.	225	na.
Δ-29	1.70	-4.6	na.	na.	-8.7	10.8	16.0	-5.2	3939	5276	320	211	0.71
Δ-30	1.77	-4.6	-26.7	22.1	-9.7	10.8	15.5	-4.7	3603	4629	286	214	0.77
Δ-31	1.82	-4.9	-29.2	24.3	-9.6	12.1	17.4	-5.3	3506	4586	326	188	0.76
Δ-32	1.88	-4.2	-28.7	24.5	-8.5	12.9	15.7	-2.8	4223	4874	291	308	0.78
Δ-33	1.90	na.	-28.9	na.	na.	10.6	16.5	-5.9	4520	5551	333	777	0.75
Δ-34	2.08	-4.5	-27.9	23.4	-8.3	13.1	15.7	-2.6	3983	6079	352	352	0.75
Δ-35	2.12	-4.4	-28.7	24.3	-9.2	12.1	15.9	-3.8	3826	5561	335	262	0.78
Δ-36	2.20	-4.6	-27.6	23.0	-9.3	14.6	15.8	-1.2	4396	5798	365	296	0.79
Δ-37	2.29	-4.4	-27.9	23.5	-8.9	13.4	ns.	na.	4238	5484	333	208	0.78
Δ-38	2.43	-4.3	na.	na.	-8.4	14.0	15.5	-1.5	3781	5446	333	328	0.78
Δ-39	2.54	-4.2	-28.3	24.1	-8.9	20.6	ns.	na.	3760	5386	366	145	0.76
Δ-40	2.68	-4.4	-27.5	23.1	-8.7	12.9	17.4	-4.5	3409	5233	355	378	0.76
Δ-41	2.79	-4.3	-28.8	24.5	-8.9	16.6	17.0	-0.3	3813	5181	357	191	0.78
Δ-42	2.89	-4.3	-29.1	24.7	-8.5	14.4	ns.	na.	4329	5335	415	288	0.76

Δ-43	3.16	-4.4	-28.4	24.0	-9.1	19.6	ns.	na.	4350	5057	395	130	0.77
Δ-44	3.44	-4.2	-28.1	23.9	-8.5	19.3	ns.	na.	3591	4356	359	136	0.75
Δ-45	3.64	-4.5	-28.1	23.6	-9.2	12.8	15.8	-3.0	3656	4230	379	295	0.78
Δ-46	3.80	-4.2	-29.3	25.1	-8.8	12.2	14.6	-2.5	3688	4198	449	374	0.78
Δ-47	3.98	-4.1	-29.3	25.2	-8.8	11.5	16.6	-5.0	3419	4050	381	458	0.80
Δ-48	4.08	-4.1	-27.6	23.5	-8.8	12.7	15.1	-2.4	4116	4293	443	329	0.80
Δ-49	4.25	-4.2	-26.2	22.0	-9.1	16.7	ns.	na.	4112	4253	406	181	0.81
Δ-50	4.34	-4.1	-29.0	24.9	-8.3	19.7	13.1	6.6	4077	4225	396	138	0.82
Δ-51	4.51	-4.3	-28.2	23.9	-9.3	13.3	16.0	-2.7	3193	3747	389	260	0.78
Δ-52	4.60	-4.2	-28.6	24.5	-8.4	19.1	14.6	4.5	3460	3697	359	127	0.83
Δ-53	4.82	-4.1	-29.0	24.9	-10.5	10.6	18.3	-7.7	5555	3951	247	308	0.97
Δ-54	5.45	-4.1	na.	na.	-8.4	16.8	19.5	-2.6	3619	4766	307	164	0.81
Δ-55	5.68	-4.1	-28.4	24.3	-8.8	15.0	ns.	na.	3379	4194	267	189	0.84
Δ-56	5.78	-4.3	-28.9	24.6	-8.9	12.7	ns.	na.	4043	5086	344	329	0.83
Δ-57	5.97	-4.3	-27.7	23.4	-9.1	11.0	ns.	na.	3803	4718	302	475	0.81
Δ-58	6.08	-4.4	na.	na.	-9.1	13.0	16.2	-3.3	3742	4490	344	282	0.80
Δ-59	6.27	-4.1	-28.9	24.7	-8.4	15.4	ns.	na.	3933	4681	376	172	0.82
Δ-60	6.49	-4.3	-28.4	24.1	-9.4	11.7	ns.	na.	4159	4753	366	352	0.84
Δ-61	6.58	-4.2	na.	na.	-9.0	15.2	13.7	1.5	4261	5176	379	152	0.85
Δ-62	6.79	-4.4	-28.7	24.3	-9.7	10.1	16.1	-6.0	4329	4698	451	254	0.81
Δ-63	6.99	-4.0	-29.1	25.1	-8.4	10.1	14.6	-4.5	4586	4678	266	312	0.91
Δ-64	7.15	-4.2	-28.4	24.2	-9.3	13.1	ns.	na.	4956	4609	264	240	0.93
Δ-65	7.21	-3.9	-28.7	24.7	-8.3	15.9	16.0	-0.1	5988	4947	234	158	0.98
Δ-66	7.34	-4.1	-28.7	24.5	-8.3	13.7	ns.	na.	6805	4919	340	213	0.93
Δ-67	7.39	-4.1	-28.4	24.4	-8.2	15.6	15.9	-0.3	6397	4522	267	158	0.95
Δ-68	7.61	-4.1	-28.8	24.7	-9.0	14.1	ns.	na.	6173	4478	207	192	1.00
Δ-69	7.73	-4.2	-28.7	24.5	-8.4	18.8	ns.	na.	6896	4883	216	124	1.00
Δ-70	7.95	-4.1	-28.7	24.6	-7.7	18.9	ns.	na.	7042	5137	227	148	1.00
Δ-71	8.22	-4.4	-28.4	24.0	-9.0	9.7	ns.	na.	4432	4342	547	509	0.01
Δ-72	9.75	-5.2	-29.2	24.0	-9.5	17.1	ns.	na.	8337	5240	233	176	0.95

Footnote: ns: no sufficient yield; na: not analyzed; CAS: carbonate associated sulfate; $\Delta\delta^{13}C = \delta^{13}C_{carb} - \delta^{13}C_{org}$; $\Delta\delta^{34}S = \delta^{34}S_{CAS} - \delta^{34}S_{py}$.

Chapter 4

The Neoproterozoic Quanji Group in the Chaidam Basin, carbon and sulfur isotopes of a cap carbonate associated with an Ediacaran glaciation

Abstract

The Neoproterozoic Quanji Group in the Oulongbluq microcontinent (Chaidam Block, northwest China) consists of, in ascending order, the Mahuanggou, Kubaimu, Shiyingliang, Hongzaoshan, Heitupo, Hongtiegou and Zhoujieshan formations. It is dominated by siliciclastic deposits, with two carbonate units, one in the Hongzaoshan Formation and the other in the basal Zhoujieshan Formation. The 4-m-thick dolostone in the basal Zhoujieshan Formation directly overlies the glaciogenic Hongtiegou diamictite. It has been shown by previous investigators that this diamictite-cap carbonate pair is likely of Ediacaran age. In this study, we measure $\delta^{13}C_{carb}$ and $\delta^{18}O_{carb}$ of carbonate samples from the upper Hongzaoshan and basal Zhoujieshan formations. We also analyzed $\delta^{34}S_{CAS}$, $\delta^{34}S_{py}$, and trace element compositions (Fe, Mn, Sr, and S) of the Zhoujieshan cap dolostone. $\delta^{13}C$ values of the Hongzaoshan dolostone range from –6‰ to 0‰. The Zhoujieshan cap dolostone shows positive $\delta^{13}C$ values (0 –1.7‰), representing a case where a cap carbonate is not characterized by negative $\delta^{13}C$ values. Thus, the generalization that cap carbonates overlying Neoproterozoic glaciation are always characterized by negative $\delta^{13}C$ values may not applicable to Ediacaran glaciations. $\delta^{34}S_{CAS}$ of the Zhoujieshan cap dolostone shows rapid stratigraphic variations from +13.9 to +24.1‰, probably due to relatively low oceanic sulfate concentrations. $\delta^{34}S_{py}$ values of the Zhoujieshan cap dolostone do not covary with $\delta^{34}S_{CAS}$ values. Instead, they show a steady stratigraphic trend from +12.9‰ to +26.4‰. Thus, the $\delta^{34}S_{CAS}$ and $\delta^{34}S_{py}$ trends are decoupled from each other, and the high $\delta^{34}S_{py}$ values in the upper part of the Zhoujieshan cap dolostone result in inverse sulfur isotope fractionations ($\delta^{34}S_{CAS} < \delta^{34}S_{py}$). The decoupling of $\delta^{34}S_{CAS}$ and $\delta^{34}S_{py}$ trends suggests that CAS and pyrite were derived from different sulfur pools, which were probably isolated from each other by the postglacial basin stratification. The early diagensis origin of pyrite in more or less closed

pore waters may have also contributed to the high the $\delta^{34}S_{py}$ values and inverse fractionation.

Keywords: Neoproterozoic; Ediacaran; Glaciation; Carbon isotopes; Sulfur isotopes; Northwest China

1. INTRODUCTION

Available geochronological data require at least four Neoproterozoic glaciations (Hoffman and Schrag, 2002). These are, in chronological order, the Kaigas (Frimmel et al., 1996), Sturtian (Allen et al., 2002; Fanning and Link, 2004; Kendall et al., 2006), Marinoan (Condon et al., 2005; Hoffmann et al., 2004; Zhou et al., 2004), and Gaskiers glaciations (Bowring et al., 2003). However, previous attention was focused on Cryogenian glaciations, the Ediacaran glaciations are pooly understood. So far, only the cap carbonates overlying the Gaskiers in Newfoundland (Myrow and Kaufman, 1999), Hankalchough in northwest China (Xiao et al., 2004) and Egan in Australia (Corkeron, 2007) have been reported. The chemostratigraphic patterns of the cap carbonate overlying Ediacaran glaciations are quite variable (Corkeron, 2007; Myrow and Kaufman, 1999; Xiao et al., 2004). Therefore, there is a need to acquire more chemostratigraphic data for cap carbonates associated with Ediacaran glaciations. The Zhoujieshan cap dolostone that overlies the Hongtiegou glaciation in the Chaidam basin, northwest China offers an opportunity. Previous investigators suggest that the Hongtiegou glaciation may represent an Ediacaran glaciation that can be regionally correlated with the Hankalchough glaciation in the Quruqtagh area (Lu et al., 1985; Wang et al., 1981).

In this paper, we first review the lithostratigraphy, and then report geochemistry data for the carbonate rocks in the Quanji Groups. Particular attention is focused on the Zhoujieshan cap dolostone that directly overlies the Hongtiegou diamictite. In addition to $\delta^{13}C$ and $\delta^{18}O$, we also measured $\delta^{34}S_{CAS}$, $\delta^{34}S_{py}$ and trace elemental concentrations (Fe, Mn, Sr, S) of the Zhoujieshan cap dolostone.

2. REGIONAL GEOLOGY

The Neoproterozoic succession in the Chaidam Basin is represented by the Quanji Group, which sporadically crops out at a few isolated localities. The stratigraphy of the Quanji Group was first described by Zhu (1957), and refined by Wang et al. (1980). Previous field investigations recognized one glacial interval— the Hongtiegou diamictite— in the Quanji Group (Sun, 1959; Wang and Chen, 1983). Because of the lack of direct radiometric dates and paleontological constraints, the age and correlation of the Hongtiegou diamictite remain uncertain. It has been variously correlated with the ~635 Ma Nantuo glaciation in South China (Zhao et al., 1980), the Ediacaran Hankalchough glaciation in the Quruqtagh area (Lu et al., 1985; Wang et al., 1981), or regarded as a Cambrian glaciation (Wang et al., 1980). Recent paleontological study exclude a Cambrian age for the Hongtiegou diamictite, because Ediacaran fossils *Shaanxilithes* and *Helanoichnus* have been discovered from sandstone of the overlying Zhoujieshan Formation (Shen et al., 2007).

The Quanjishan area is located in northwestern Qinghai province, northwest China. Geographically, the Quanjishan area lies on the northern margin of the Chaidam Basin, and is adjacent to the southern slope of the Qilian Mountain Range.

Geologically, the Quanjishan area belongs to the Oulongbluq microcontinent (Fig. 4.1) (Lu, 2002). The Oulongbluq microcontinent is one of the four minor tectonic units recognized between the Tarim and North China blocks. These four microcontinents are, from northeast to southwest, the Alashan, Qilian, Oulongbluq and Chaidam, and are interpreted as microcontinents to the east of Tarim Block during Neoproterozoic to early Paleozoic (Lu, 2002). They collided with one another to form a larger block during late Silurian to early Devonian (Lu, 2002). The Oulongbluq microcontinent was approximately 500 km in length, and extended in a northwest-to-southeast direction. It borders the Qilian and Chaidam microcontinents by the Zongwulong fault and the Shaliuhe–Yukahe eclogite zone, respectively.

3. LITHO- AND BIOSTRATIGRAPHY OF THE QUANJI GROUP

The Oulongbluq basement is composed of the early Palaeoproterozoic Deringha gneisses, late Palaeoproterozoic Dakendaban schist, and Mesoproterozoic Wandonggou schist. Unmetamorphosed Neoproterozoic sedimentary sequence, the Quanji Group, unconformably overlies the Oulongbluq metamorphic basement, and disconformably underlies early Paleozoic strata. The Neoproterozoic Quanji Group sporadically crops out at a few localities in the Oulongbluq, Shihuigou, Quanjishan and Dayangtougou areas, but is best exposed in the Quanjishan area (Fig. 4.1, 4.3a). Here, the Quanji Group is represented by a ~1.5 km-thick siliciclastic-dominated succession that was probably deposited in a Neoproterozoic intra-continental aulacogen (Lu, 2002). In the Quanjishan area, it unconformably overlies the late Palaeoproterozoic Dakendaban Group and underlies the early Cambrian Xiaogaolu Group (Wang et al., 1980). The Quanji Group is divided into 7 formations, in stratigraphic order, the Mahuanggou, Kubaimu, Shiyingliang, Hongzaoshan, Heitupo, Hongtiegou and Zhoujieshan formations (Fig. 4.2a) (Wang et al., 1980). Below we summarize the litho- and biostratigraphy of the Quanji Group in the Quanjishan area.

3.1. The Mahuanggou Formation

The Mahuanggou Formation is about 450 m-thick, and unconformably overlies the late Palaeoproterozoic biotite, plagioclase schist of the Dakendaban Group. The lower Mahuanggou Formation is composed of greenish-gray to purplish-gray thick cross-bedded conglomerates. Clasts in conglomerate are well rounded and moderately to poorly sorted, and are mostly composed of quartzite with minor volcanics and gneisses. Conglomerates gradually grade into cross-bedded arkosic sandstone in the upper Mahuanggou Formation. The Mahuanggou Formation represents fluvial deposits on the Oulongbluq metamorphic basement.

3.2. The Kubaimu Formation

The Kubaimu Formation overlie the Mahuanggou Formation, and is about 350 m-thick, and is characterized by a fining upward sequence. It is divided into three lithological members. The lower member is dominated by conglomerate intercalated with quartzarenite. Clasts are well rounded and sorted, and mainly source from quartzarenite,

metavolcanic tuff, and porphyritic granite. Subaerial exposure structures (e.g. mudcrack casts) are common in quartzarenite of the lower member. The middle member consists of light red quartzarenite with rare clasts, whereas the upper member is composed of medium to fine grained quartzarenite with well-developed cross-bedding, symmetrical and asymmetrical ripple marks.

3.3. The Shiyingliang Formation

The Shiyingliang Formation disconformably overlies the Kubaimu Formation, and is about 200 m-thick in the Quanjishan area. The disconformity between the Kubaimu and Shiyingliang formations is not obvious in the Quanjishan area, but a prominent erosional surface is observed in the Oulongbluq area (Wang et al., 1980). The Shiyingliang Formation begins with a 30 m-thick greenish-gray basaltic andesite with lapilli stone. Another 8 m-thick yellowish-green basaltic and andesitic volcanic unit occurs ~30 m above the basal volcanic unit. A 738±26 Ma SHRIMP zircon U–Pb age has been obtained from the lower volcanic unit (Lu, 2002). The rest of the Shiyingliang Formation consists of light grey, thin to thick-bedded quartzite intercalated with yellowish-green thin-bedded siltstone. Cross-beddings are well-developed throughout the entire formation. Subaerial exposure structures (e.g. mudcrack casts) abundantly occur in the lower Shiyingliang Formation. The Shiyingliang Formation may represent a transgressive sequence.

3.4. The Hongzaoshan Formation

The transition from the Shiyingliang to Hongzaoshan Formation is gradational. The beginning of the Hongzaoshan Formation is marked by the first occurrence of purplish, thin to medium-bedded tuffaceous sandstone (Fig. 4.3b). Mudcrack casts (Fig. 4.3c) and halite pseudomorphs (Fig. 4.3d) are common in tuffaceous sandstone of lower Hongzaoshan Formation. In addition, cross-beds and ripple marks are common in the lower Hongzaoshan Formation. The purple sandstones grade into fine laminated dolostone with thin chert beds. A 3 m-thick greenish volcanic unit with lapilli (Fig. 4.3e) occurs within laminated dolomite. The laminated dolomite is succeeded by ~230 m-thick dark-gray to light-gray stromatolitic dolostone (Fig. 4.3f), dolorudite (Fig. 4.3h), and

laminated dolomicrite (Fig. 4.3g). Some dolostone is partially silicified or recrystallized. Stromatolites are identified as *Cryptozoon*, *Conophyton*, and *Katavia* (Wang et al., 1980). The Hongzaoshan Formation represents a peritidal to shallow subtidal environment.

3.5. The Heitupo Formation

The Heitupo Formation in the Quanjishan area is about 120 m thick. The transition between the Hongzaoshan Formation and the overlying Heitupo Formation appears to be gradational. The lowest 10 meters of the Heitupo Formation is composed of yellowish-green, thin to medium-bedded dolomicrite that grades into grayish siltstone. Several layers of hematite occur within dolomicrite with maximum thickness of 30 cm. The upper part of the Heitupo Formation is composed of dark-gray carbonaceous shale with sandstone concretions (Fig. 4.3i). Tooth-shaped fossils identified as Scolecodonts (but probably representing fragments of *Cochlectina*) were reported from the Heitupo Formation (Wang et al., 1980). Because *Cochlectina* occurrs in the Ediacaran Kotlin and Rovno Series in the East European Platform (Burzin, 1995), its occurrence in the Heitupo Formation indicates an Ediacaran age.

3.6. The Hongtiegou Formation

The Hongtiegou Formation is 18 m-thick in the Quanjishan area, but has the maximal thickness of 75 m in the Shihuigou area. The Hongtiegou Formation consists of green, yellow and purplish-red massive diamictite (Fig. 4.4a–d). The transition from the Heitupo shale to Hongtiegou diamictite is gradual. In the Quanjishan area, the basal Hongtiegou Formation is marked by the presence of pebbles in a greenish muddy/silty matrix. Both clast size and abundance increase upsection. Most clasts are derived from the underlying Hongzaoshan dolostone, although some are from older sandstone, conglomerate, and metamorphic rocks. Clasts are angular and poorly sorted (Fig. 4.4d). The largest clast observed in the measured section is ~30 cm in diameter (Fig. 4.4b), but some giant boulders more than 2 m in diameter have been reported from other localities (Wang et al., 1980). Dropstones (Fig. 4.4c), and striated clasts (Pl. I, fig. 8 (Wang and Chen, 1983)) in the Hongtiegou Formation indicate a glacial origin

3.7. The Zhoujieshan Formation

The Zhoujieshan Formation begins with a 4-6 m-thick yellow to pink dolostone overlying the Hongtiegou diamictite (Fig. 4.4a). The dolostone is regarded as the Zhoujieshan cap dolostone to the underlying Hongtiegou diamictite. In the Quanjishan area, the Zhoujieshan cap dolostone is lithologically divided into three units (Fig. 4.2b). The lower unit is about 0.5 m-thick, and contains abundant siliciclastic and dolomitic clasts (Fig. 4.4e). The middle unit is ~2.1 m thick, and consists of dolomicrite and dolomicrosparite with well-developed sheet-cracks filled with chert (Fig. 4.4f). The upper 1.2-m-thick unit is characterized by red dolomitic sandstone (Fig. 4.4g), with well rounded and moderately sorted quartz grains.

The upper 50 m of the Zhoujieshan Formation is composed of red thin-laminated siltstone/fine sandstone, which conformably overlies the Zhoujieshan cap dolostone and disconformably underlies the lower Cambrian Xiaogaolu Group that yields echinoderm fragments and hyolith fossils. Abundant ribbon-shaped fossils have been discovered from the Zhoujieshan sandstone. The first occurrence of these fossils, based on our field collection, is only 5 m above the Zhoujieshan cap dolostone. These ribbon-shaped fossils were traditionally interpreted as trace fossils or *Sabelliditedes*–like tubular fossils (Wang et al., 1980; Xing et al., 1984). These fossils have been identified as *Shaanxilithes* (Fig. 4.4h) and *Helanoichnus*, and both genera are interpreted as body fossils of unknown phylogenetic affinity (Shen et al., 2007). *Shaanxilithes* is a common member in upper Ediacaran successions in South China (Hua et al., 2004; Hua et al., 2000) and North China (Li et al., 1997; Shen et al., 2007). *Helanoichnus* is also known from Ediacaran rocks in North China (Yang and Zheng, 1985). Thus, the occurrence of *Shaanxilithes* and *Helanoichnus* in the Zhoujieshan Formation indicates a late Ediacaran age.

4. METHODS

We investigated two sections in the Quanjishan area (labeled as section A and B in Fig. 4.1). At section A, we collected samples of the Zhoujieshan cap dolostone and the upper most 100 m of the Hongzaoshan dolostone. At section B, the Zhoujieshan cap dolostone and the top 150 m of the Hongzaoshan Formation were sampled. Sampling intervals were 1–4 m for the Hongzaoshan Formation and 0.1–0.5 m for the Zhoujieshan

cap dolostone. We measured the carbon and oxygen isotopic composition of all carbonate samples. In addition, we measured the sulfur isotopic composition of carbonate associated sulfate (CAS) and pyrite, as well as trace element concentrations (S, Fe, Mn, Sr), of the Zhoujieshan cap dolostone at section B.

4.1. Carbon and oxygen isotopes

Carbon and oxygen isotopes were analyzed in two laboratories. Samples from section A were prepared and analyzed in Nanjing Institute of Soil Science, Chinese Academy of Science. Small chips were cleaned and powdered. 5-mg powder was allowed to react with concentrated H_3PO_4 at 50 °C for 12 h, and CO_2 was extracted using traditional off-line technique. Carbon and oxygen isotope ratios were measured on a Finnigan MAT 251 mass spectrometer. Analytical precision is 0.1‰ for $\delta^{13}C$, and 0.3‰ for $\delta^{18}O$.

Samples from section B were prepared at Virginia Tech, and analyzed on a Micromass Isoprime dual-inlet gas source stable isotope mass spectrometer at University of Maryland, which is equipped with a peripheral Multiprep system for on-line carbonate reaction. Fresh carbonate samples were cut to make mirroring thin and thick sections. Powders were microdrilled from thick sections using a 1 mm drill bit. Microdrilling was guided by the petrographic observations of thin sections to avoid microveins and diagenetically altered areas. Analytical precision (1σ) is better than 0.1‰ for $\delta^{13}C$, and 0.3‰ for $\delta^{18}O$. Both $\delta^{13}C$ and $\delta^{18}O$ are reported as ‰ deviation from VPDB.

4.2. Sulfur isotope

Sulfur isotopic compositions were determined on co-existing disseminated pyrite and carbonate associated sulfate (CAS) extracted from the same samples where carbon and oxygen isotopes were measured. The procedure for CAS extraction followed Shen et al. (Shen et al., in press). 50~100 grams of rock chips were washed by 3 M HCl to remove surface weathering products. Fresh samples were then crushed to 80 mesh, and leached with 10% NaCl for 24 hours to remove soluble non-CAS sulfate. Pretreated samples were then dissolved following a stepwise acidification procedure (Shen et al., in press). In the first treatment, each sample was immersed in 50 ml deionized water and 20 ml of 10 M HCl. It normally took about 30 to 60 min for the reaction to be complete. In subsequent

treatments, 25 ml 10 M HCl was added each time until carbonate component was quantitatively dissolved and no CO_2 bubbles were generated. After ~2 hours, insoluble residue (mostly detrital component) was removed using 1 μ filter paper. Insoluble residue was carefully washed, dried, and weighed in order to quantify carbonate content (carbonate %). The volume of supernatant was measured and then distributed into 50 ml centrifuge tubes, one of which was used for elemental analysis. 1–5 ml of $BaCl_2$ saturated aqueous solution was added to other tubes to precipitate sulfate as barite.

Disseminated pyrite was extracted using a modified chromium reduction method (Canfield et al., 1986; Goldberg et al., 2005; Shen et al., in press) . 5~7 g of sample powder (80 mesh) was reacted with 20 ml of 10 M HCl and 50 ml of 1 M $CrCl_2$ under a N_2 atmosphere. H_2S produced from pyrite reduction was bubbled through a 1 M zinc acetate trap to be precipitated as ZnS, which was later transferred into Ag_2S by reacting with $AgNO_3$ solution. Ag_2S was centrifuged, carefully washed using deionized water, and dried at 60 °C.

Sulfur isotopes were measured in the geochemistry laboratory at the University of Maryland. A Eurovector elemental analyzer (EA) was used for on-line combustion of barite and silver sulfide. The separation of SO_2 to a GV Isoprime mass spectrometer for $^{34}S/^{32}S$ analyses followed the procedures described in Grassineau et al. (Grassineau et al., 2001). Barite and silver sulfide (~100 μg) were accurately weighed and folded into small tin cups with similar amount of V_2O_5. They were sequentially dropped with a pulsed O_2 purge of 12 ml into a catalytic combustion furnace operating at 1030^{o}C. The frosted quartz reaction tube was packed with granular tungstic oxide on alumina ($WO_3 + Al_2O_3$) and high purity reduced copper wire for quantitative oxidation and O_2 resorption. Water is removed from the combustion products with a 10-cm magnesium perchlorate column, and the SO_2 was separated from other gases with a 0.8 m PTFE GC column packed with Porapak 50–80 mesh heated to 90^{o}C. The cycle time for these analyses was 210 seconds with reference gas injection as a 30-s pulse beginning at 20 seconds. Sample SO_2 pulses begin at 110 seconds and return to baseline values between 150 and 180 seconds, depending on sample size and column conditions. The effluent from the EA was introduced in a flow of He (80–120 ml/min) to the IRMS through a SGE splitter valve that controls the variable open split. Timed pulses of SO_2 reference gas (99.9% purity, ~

3nA) were introduced at the beginning of the run using an injector connected to the IRMS with a fixed open ratio split. The isotope ratios of reference and sample peaks were determined by monitoring ion beam intensities relative to background values. Isotope ratios are determined by comparing integrated peak areas of m/z 66 and 64 for the reference and sample SO_2 pulses, relative to the baseline of ~1 x 10^{-11}A. Isotopic results are expressed in the δ notation as per mil (‰) deviations from the VCDT standard. One sigma uncertainties of these measurements (± 0.3‰ or better) were determined by multiple analyses of a standard barite (NBS 127) interspersed with the samples.

4.3. Elemental geochemistry

Trace elements (Fe, Mn, Sr, and S) were analyzed on an Inductively Coupled Plasma Atomic Emission Spectrometer (ICP–AES) in the Soil Testing Laboratory at Virginia Polytechnic Institute and State University. Solutions from CAS extraction were used for elemental analysis. Element concentrations were corrected for insoluble residue. CAS concentration was calculated from sulfur concentration. Analytical precision for elemental analyses was better than 5% as determined by repeated analyses of a standard solution with known concentration.

5. RESULTS

5.1. $\delta^{13}C$ and $\delta^{18}O$

$\delta^{13}C$ and $\delta^{18}O$ in both sections are listed in Table 4.1. The $\delta^{13}C$ profiles of the Hongzaoshan Formation differ between the two measured sections. The $\delta^{13}C$ profile of section A shows a positive trend from –5‰ to 0‰ (Fig. 4.5a). In contrast, there is no stratigraphic trend in section B, where $\delta^{13}C$ values are between –1‰ and 0‰. $\delta^{18}O$ values of the Hongzaoshan Formation are between –4.7‰ and –14.5‰ in section A, and between –5.1‰ and –11.4‰ at section B. $\delta^{13}C$ values of the Zhoujieshan cap dolostone are similar between the two measured sections, with values between +0.5‰ and +1.5‰ for section A, and between 0‰ and +1.7‰ for section B (Fig. 4.5a, 4.6a). $\delta^{18}O$ values of

the Zhoujieshan cap dolostone are less variable than $\delta^{18}O$ of the Hongzaoshan Formation, ranging from –3.6‰ to –7.7‰ (Fig. 4.5, 4.6a).

5.2. $\delta^{34}S_{CAS}$ and $\delta^{34}S_{py}$

$\delta^{34}S_{CAS}$ and $\delta^{34}S_{py}$ values of the Zhoujieshan cap dolostone at section B are summarized in Table 4.2, and plotted in Fig. 4.6b. $\delta^{34}S_{CAS}$ values vary between +13.9‰ and +24.1‰, and do not show any stratigraphic trends. $\delta^{34}S_{py}$ profile displays a persistent positive stratigraphic trend from +12.9‰ to +26.4‰. The isotopic difference between CAS and pyrite ($\Delta^{34}S_{CAS-py}$) varies from –0.5‰ to +7.0‰ in the lower 2.3 m section, and decreases to negative values between –4.8‰ and –11.2‰ in the upper 1.5 m interval.

5.3. Elemental geochemistry

Trace element (Fe, Mn, Sr and S) concentrations of the Zhoujieshan cap dolostone at section B are summarized in Table 4.2, and plotted in Fig 6c, 6d. CAS concentration ([CAS]) varies between 53 and 783 ppm (mean = 299 ppm; SD = 185 ppm), and shows a weak increasing trend (Fig. 4.6c). [Mn] does not show any stratigraphic trend, and ranges from 1203 to 2720 ppm (mean = 1668 ppm; SD = 480 ppm) (Fig. 4.6d). [Fe] slightly increases upsection, and varies between 3995 to 10969 ppm (mean = 6440 ppm; SD = 1935 ppm) (Fig. 4.6d). Carbonate content (carbonate %) shows a decreasing trend (Fig. 4.6e), consistent with petrographic observation that detrital component increases upsection.

6. DISCUSSIONS

6.1. Diagenetic alteration of $\delta^{13}C$ values

It is possible that the carbon isotope composition of the Quanji Group has been modified as a result of diagenetic alteration. Since diagenetic alteration tends to reduce $\delta^{13}C$ values, the measured $\delta^{13}C$ values may represent minimal estimates of the sedimentary values of the Quanji Group. Because $\delta^{18}O$ and Mn/Sr are also altered during meteoric diagenesis, they are commonly used in diagenetic evaluation (Kaufman and Knoll, 1995). It has been suggested that samples with Mn/Sr <10 and $\delta^{18}O$ > –5‰ can be

regarded as least altered, and their $\delta^{13}C$ values may approximate the primary sedimentary values (Kaufman and Knoll, 1995). Using these criteria, most $\delta^{13}C$ values of the Hongzaoshan Formation have been diagenetically altered. Samples from the Zhoujieshan cap dolostone have $\delta^{18}O$ values around –5‰ (Fig. 4.7a) and Mn/Sr ratios mostly less than 10 (Fig. 4.7b), suggesting less significant diagenetic alteration of $\delta^{13}C$ values.

The difference in $\delta^{13}C$ values of the Hongzaoshan dolostone between section A and B may be a diagenetic artifact. Alternatively, it may be derived from different sample preparation methods. Petrographic observation reveals some degree of recrystallization and silicification in the Hongzaoshan dolostone. Microdrilling can help avoid diagenetically altered areas, and focus on dolomicrite and dolomicrosparite lithologies. Bulk samples, on the other hand, do not distinguish such diagenetic details. In addition, the average of bulk sample $\delta^{18}O$ (–8.5‰) is about 2‰ lighter than $\delta^{18}O$ of microdrilled samples (–6.6‰), suggesting that bulk samples probably incorporate more diagenetic components. A third possibility is that the Hongzaoshan Formation at the two measured sections are not entirely correlatable, probably due to basal truncation of section B.

6.2. Fidelity of sulfur isotope signatures

Two sulfur components of the Zhoujieshan cap dolostone are considered in this study: carbonate associated sulfate (CAS) and disseminated pyrite. CAS is trace amount of sulfate that substitutes CO_3^{2-} within the carbonate lattice (Pingitore et al., 1995), and has been widely used as a useful proxy for seawater $\delta^{34}S_{sulfate}$ (Bottrell and Newton, 2006; Kampschulte et al., 2001; Kampschulte and Strauss, 2004). CAS extracted from modern foraminifera tests yields an average $\delta^{34}S$ value of +20.6‰, which is comparable to $\delta^{34}S$ of modern seawater sulfate (Burdett et al., 1989).

However, possible diagenetic alteration in $\delta^{34}S_{CAS}$ should be considered, particular for old samples. During diagenesis (e.g. dolomitization), CAS can be expelled from precursor carbonate minerals (e.g. aragonite, high-Mg calcite), and pore water sulfate can be incorporated into carbonate minerals. It has been shown that CAS loss during aragonite-calcite inversion in Cenozoic sediments has minimum effect on $\delta^{34}S_{CAS}$ values (Gellatly and Lyons, 2005; Lyons et al., 2004). The effect of dolomitization in $\delta^{34}S_{CAS}$ is less well understood, although direct comparison of $\delta^{34}S$ interbedded evaporites and

dolostones did reveal some difference (Kah et al., 2004; Mazumdar and Strauss, 2006). $\delta^{34}S_{CAS}$ of dolostone is about 4‰ higher than coeval evaporite (Kah et al., 2004). The isotopic difference suggests that, during diagenesis, carbonate incorporates pore water sulfate that is heavier than ambient seawater due to bacterial sulfate reduction. Thus, our $\delta^{34}S_{CAS}$ values of dolostone may represent a maximum estimate for seawater $\delta^{34}S_{sulfate}$.

It is also possible that $\delta^{34}S_{CAS}$ values could be affected by the contamination of non-CAS sulfate. For example, pyrite might be oxidized to sulfate on outcrop exposure or during CAS extraction procedure. In our analysis, sample powders were first treated with 10% NaCl solution for 24 hours and washed using deionized water to remove non-CAS sulfates. NaCl solution greatly enhances the solubility of non-CAS sulfate, such as gypsum and sulfate derived from post-depositional oxidation of pyrite. The potential pyrite oxidation during acidification is likely minimum, because most of samples have low pyrite content. In addition, laboratory experiment shows that soaking pure pyrite in 25% HCl (6.8 M) under oxic conditions for 24 hours does not yield a measurable amount of sulfate (Goldberg et al., 2005).

The application of chromium reduction method has been widely used to extract pyrite sulfur (Canfield et al., 1986). The extraction procedure does not introduce significant isotopic fractionation. We have conducted control experiments to reduce pure pyrite to Ag_2S, and found no significant fractionation ($\delta^{34}S_{py}$ = +1.9‰ vs. $\delta^{34}S_{Ag2S}$ = +2.6‰).

Pyrites in the Zhoujieshan cap dolostone are probably deposited from porewater during early diagenesis. In the Zhoujieshan cap dolostone, most pyrites are <20μ subeuhedral crystals. They are randomly distributed within dolomicrite/dolomicriosparite matrix, and are not associated with microveins. These observations imply that disseminated pyrites in the Zhoujieshan cap dolostone were not formed during late diagenesis. Nor could have they directly precipitated from seawater. Instead, they were likely precipitated from porewater during early diagensis.

6.3. Age of the Hongtiegou glaciation

The only geochronological constraint for the Hongtiegou diamictite is a SHRIMP zircon U–Pb age of 738 ± 28 Ma from the basal Shiyingliang Formation (Lu, 2002). This age is consistent with a Cryogenian (Zhao et al., 1980), an Ediacaran (Lu et al., 1985;

Wang et al., 1981), or a Cambrian age (Wang and Chen, 1983; Wang et al., 1980) for the Hongtiegou diamictite.

In this study, we provide additional carbon isotope data that may have potential implications for chemostratigraphic correlation. $\delta^{13}C$ of the Zhoujieshan cap dolostone does not resemble any Sturtian or Marinoan cap carbonates, which are characterized by consistently negative values. Thus, either the Zhoujieshan cap dolostone was deposited in a localized environment, or the Hongtiegou glaciation is not correlated with the Sturtian or Marinoan glaciation. Unlike the Cryogenian glaciations, the cap carbonate of the Ediacaran glaciations shows much wider ranges of $\delta^{13}C$ values. For example, $\delta^{13}C$ of the Gaskiers cap carbonate is exclusively negative (Myrow and Kaufman, 1999), whereas some Egan cap carbonate samples from Australia have positive $\delta^{13}C$ values (Corkeron, 2007).. $\delta^{13}C$ of Hankalchough cap carbonate shows a wide range of spatial variation, ranging from 0‰ to –18‰ (Xiao et al., 2004). Thus, the positive $\delta^{13}C$ values of the Zhoujieshan cap dolostone are more consistent with an Ediacaran cap carbonate.

$\delta^{13}C$ profiles of the Hongzaoshan Formation are different between section A and B. There are several possible explanations. Such difference may be a diagenetic artifact, may have resulted from different sample preparation methods, or may indicate the two measured sections are not entirely correlatable. On the basis of $\delta^{18}O$ values as a criterion for diagenesis evaluation, the $\delta^{13}C$ profile of section B is more robust than that of section A, in which the mean $\delta^{18}O$ value is about 2‰ lower than that of section A.

Alternatively, it is also possible that the two measured sections are not correlatable. The upper part of of the Hongzaoshan Formation in section A is probably cut by fault, accordingly the upper most part of the Hongzaoshan Formation might be sampled in this section. Therefore, the Hongzaoshan Formatin in section B can only be correlated with the upper part of section A. If this is the case, a 5‰ increase in $\delta^{13}C$ observed in section A probably can be correlated with the Shuiquan Formation that underlies the Ediacaran Hankalchough diamictite in the Quruqtagh area or the upper Shuram excursion in Oman (Fike et al., 2006; Xiao et al., 2004). This correlation also suggests that the Hongtiegou diamictite is of Ediacaran age, and the Shuram excursion predates the Hongtiegou or Halkalchough glaciations in northwest China. .

Paleontological evidence from the Zhoujieshan and Heitupo formations is also consistent with an Ediacaran age of the Hongtiegou glaciation. The presence of the late Ediacaran fossils *Helanoichnus* and *Shaanxilithes* in the Zhoujieshan sandstone excludes a Cambrian age for the underlying Hongtiegou diamictite (Shen et al., 2007). The first occurrence of these late Ediacaran fossils in the Zhoujieshan sandstone is only 5 m above the Zhoujieshan cap dolostone. Given the gradational transition from the Zhoujieshan cap dolostone to the Zhoujieshan sandstone, the Zhoujieshan cap dolostone and underlying Hongtiegou diamictite are likely of Ediacaran age. We infer that the possible occurrence of the Ediacaran fossil *Cochleatina* in the Heitupo Formation also constraints the overlying Hongtiegou diamictite to be of Ediacaran age (Burzin, 1995; Wang et al., 1980).

Sedimentary evidence for Ediacaran glaciation has been reported from several regions in China, including the Zhengmuguan and Luoquan diamictite in North China, and the Hankalchough glaciation in Quruqtagh (Guan et al., 1986; Li, 1980; Xiao et al., 2004). In addition, the Gaskiers diamictite in Newfoundland (Bowring et al., 2003), the Squantum 'tillite' member in the Boston basin (Thompson and Bowring, 2000), the Mortensnes diamictite in northern Norway (Halverson et al., 2005), the Moelv diamictite in south Norway (Bingen et al., 2005), and the Landrigan tillite and its equivalents in Australia (Corkeron, 2007).

Available radiometric dates are not sufficient to unambiguously support the synchroneity of all these Ediacaran diamictite. However, chemostratigraphic data is consistent with a short-lived glaciation without the long-lived Shuram negative $\delta^{13}C$ excursion (Guerroué et al., 2006).

6.4. Geochemical cycle after the Hongtiegou glaciation

The Zhoujieshan cap dolostone represents carbonate deposition immediately after the Hongtiegou glaciation and records geochemical signatures in the wake of an Ediacaran glaciation. In our interpretation, we focus on two important geochemical features of the Zhoujieshan cap dolostone: the unusual positive $\delta^{13}C$ values and decoupled $\delta^{34}S_{CAS}$ and $\delta^{34}S_{py}$ values.

6.4.1. Interpretation of $\delta^{13}C$ in the Zhoujieshan cap dolostone

The Zhoujieshan cap dolostone has unusual positive $\delta^{13}C$ values (Fig. 4.5, 4.6a) that are different from $\delta^{13}C$ of most other Neoproterozoic cap carbonates (Halverson, 2006; Jiang et al., 2006). Sturtian and Marinoan cap carbonates show characteristic negative $\delta^{13}C$ values, and cap carbonate of the Ediacaran Gaskiers glaciation in Newfoundland has negative $\delta^{13}C$ values as well (Myrow and Kaufman, 1999). To account for the negative $\delta^{13}C$ values, influx of ^{12}C enriched alkalinity is required. The possible sources of ^{12}C enriched alkalinity that may account for the global negative $\delta^{13}C$ values in the Marinoan cap carbonates includes (1) methane hydrate (Jiang et al., 2003; Kennedy et al., 2001), (2) dissolved inorganic carbon derived from remineralization of organic matter in deep ocean (Grotzinger and Knoll, 1995; Knoll et al., 1996), or (3) oxidation of fossil organic carbon through oxidative weathering of organic rich shales (Kaufman et al., 2007).

The observed positive $\delta^{13}C$ values in the Zhoujieshan cap dolostones implies that the aforementioned ^{12}C enriched alkalinities are insignificant comparing with oceanic inorganic carbon pool. Actually, above models were proposed to explain $\delta^{13}C$ values of the cap carbonates overlying the Marinoan glaciation, which is believed to be synchronous and have world-wide distribution. However, the Ediacaran glaciations are probably not globally distributed, and their synchroneity is questionable. Therefore, previous models for the Marinoan cap carbonate may not be applied to an Ediacaran cap carbonate. Instead, the Zhoujieshan cap dolostone might have been precipitated from a normal marine condition.

Alternatively, models for the Marinoan cap carbonate might be applied to the Zhoujieshan cap dolostone. Positive $\delta^{13}C$ values in the Zhoujieshan cap dolostone imply that ^{12}C enriched alkalinity was either locally shut off or buffered by dissolved inorganic carbon in the Oulongbluq basin. The observed positive $\delta^{13}C$ values in the Zhoujieshcan cap dolostone are not global, but a localized signature.

6.4.2. Interpretation of sulfur isotopes

$\delta^{34}S_{CAS}$ and $\delta^{34}S_{py}$ are decoupled in the Zhoujieshan cap dolostone. $\Delta^{34}S_{CAS}$ varies between +13.9‰ and +24.1‰, whereas $\delta^{34}S_{py}$ steadily increases from +12.9‰ to +26.4‰ within the 3.8-m thick cap dolostone. The decoupling of $\delta^{34}S_{CAS}$ and $\delta^{34}S_{py}$ values is also apparent from the variable isotopic fractionations between CAS and pyrite

($\Delta^{34}S = \delta^{34}S_{CAS} - \delta^{34}S_{py}$). In the lower 2.3 m of the cap dolostone, $\Delta^{34}S_{CAS-py}$ varies between –0.5‰ and +7.0‰, whereas in the upper cap dolostone, $\Delta^{34}S_{CAS-py}$ becomes negative, ranging from –4.8‰ to –11.2‰ (Fig. 4.6b).

The rapid stratigraphic variation in $\delta^{34}S_{CAS}$ suggests a generally small sulfate reservoir after the Hongtiegou glaciation. A small reservoir size means that the isotopic signature is more susceptible to local perturbations. For example, rapid variations in $\delta^{34}S_{CAS}$ in Mesoproterozoic successions have been interpreted as evidence for low sulfate concentration in Mesoproterozoic ocean (Kah et al., 2004). Extremely rapid stratigraphic variations in $\delta^{34}S_{CAS}$ is one of the common features in Marinoan cap carbonates (Shen et al., in press), and have been interpreted as evidence for low sulfate concentration after the Marinoan glaciation (Hurtgen et al., 2002). Although sulfate concentration may have been greater in mid-Ediacaran oceans than in Cryogenian oceans (Fike et al., 2006), it may have still been significantly below the modern seawater sulfate concentration of 28 mM.

In the upper unit, $\delta^{34}S_{CAS}$ values of the dolomitic sandstone become less variable (between +14.3‰ and +16.8‰), while CAS concentrations increase (between 331 ppm and 783 ppm) (Fig. 4.7d). Increase of CAS concentration probably was due to enhanced terrestrial input. The negative correlation between $\delta^{34}S_{CAS}$ and CAS concentration implies that $\delta^{34}S$ of terrestrial sulfate was lighter than that of seawater sulfate.

$\Delta^{34}S$ of terrestrial sulfate is controlled by the proportional mixing between two sulfur sources: (1) dissolution of evaporitic sulfate and minor amount of CAS released from carbonate weathering and (2) oxidation of sulfides, mostly pyrite. Typically, $\delta^{34}S_{py}$ is lighter than $\delta^{34}S_{evaporite}$, although some interglacial pyrites have extremely high $\delta^{34}S$ values (Gorjan et al., 2000; Li et al., 1999). The negative correlation between CAS concentration and $\delta^{34}S_{CAS}$ suggests the influx of light terrigenous sulfate was mainly derived from pyrite oxidation (Fig. 4.7c).

The interpretation of $\delta^{34}S_{py}$ is more complex. Coupling of sulfate and sulfide via bacteria sulfate reduction (BSR) predicts the covariation between these two components. In a steady state open system where fractionation between sulfate and sulfide remains constant, $\delta^{34}S_{py}$ and $\delta^{34}S_{sulfate}$ are expected to covary linearly. In a closed system, depletion of seawater sulfate is associated with elevation of $\delta^{34}S$ of residual sulfate and

concurrent increase in $\delta^{34}S_{py}$. Under either case, the coupling of sulfate and sulfide via BSR predicts a positive correlation between $\delta^{34}S_{CAS}$ and $\delta^{34}S_{py}$ and positive $\Delta^{34}S_{CAS-py}$ values. However, the lack of positive correlation between $\delta^{34}S_{py}$ and $\delta^{34}S_{CAS}$ in the Zhoujieshan cap dolostone suggests that sulfate and sulfide were decoupled in the postglacial Oulongbluq basin. In other words, they were not derived from a same sulfur pool.

In addition, the inverse fractionation between sulfate and pyrite in the upper Zhoujieshan cap dolostone also indicates that CAS and pyrite did not come from the same reservoir. In a normal marine environment, sedimentary pyrites are derived from the reaction of active Fe^{2+} and H_2S that is produced by BSR of seawater sulfate. Since sulfur reduction bacteria (SRB) preferentially reduces $^{32}SO_4^{2-}$ to sulfide, $\delta^{34}S_{py}$ is always lower than contemporaneous $\delta^{34}S_{sulfate}$ (Shen and Buick, 2004). Although instantaneous $\delta^{34}S_{py}$ can become higher and may exceed the original $\delta^{34}S_{sulfate}$ value, the cumulative $\delta^{34}S_{py}$ is always lower than that of $\delta^{34}S_{sulfate.}$ Our analysis is based on bulk samples and should reflect cumulative $\delta^{34}S_{py}$ values. Thus the observed negative $\Delta^{34}S_{CAS-py}$ suggests that pyrite and CAS were derived from separated sulfur pools.

Different sulfur sources for CAS and pyrite sulfur pool have been reported from the Zhamoketi cap dolostone overlying the Marinoan Tereeken diamictite in the Quruqtagh area (Shen et al., in press), and may represent a common phenomenon on the Marinoan glaciation. The sulfur pools may have been isolated from each other by postglacial basin stratification. In a stratified basin, CAS was derived from surface water and pyrite was precipitated from bottom water. A similar stratification model can be applied to the Zhoujieshan cap dolostone. The steady increase of $\delta^{34}S_{py}$ by ~13‰ in the 3.8-m Zhoujieshan cap dolostone can be interpreted as evidence for Rayleigh distillation of bottom water in a closed system. However, stratification model is inconsistent with sedimentary evidence of the Zhoujieshan cap dolostone. For example, the stratification model requires that the Zhoujieshan cap dolostone be deposited in a deep water environment below the pycnocline, sedimentary evidence seems to suggest that the Quanji Group was deposited in a relatively shallow-water environment with subaerial exposure and cross-stratification at some horizons.

Decoupling of CAS and pyrite sulfur isotopes would also be affected by temporal separation of CAS and pyrite sulfur sources could have also caused the decoupling of $\delta^{34}S_{CAS}$ and $\delta^{34}S_{py}$, i.e. there was an offset between CAS and pyrite formation. Although pyrite sulfur was ultimately derived from seawater, from which CAS was derived, $\delta^{34}S_{CAS}$ and $\delta^{34}S_{py}$ record $\delta^{34}S$ of seawater sulfate at different time. In the Zhoujieshan cap dolostone, authigenic pyrite was precipitated from porewater, whose initial $\delta^{34}S$ value was equivalent to that of seawater sulfate. Since bacterial sulfate reduction preferentially reduced $^{32}SO_4^{2-}$ into pyrite, the remaining porewater sulfate became heavy. The remaining heavy porewater sulfate could mix with overlying seawater sulfate, making porewater sulfate heavier than the initial seawater sulfate. Thus the later formed pyrite in porewater would have heavier sulfur isotope than the earlier ones, and $\delta^{34}S_{py}$ profile can show a steady increase trend.

7. CONCLUSIONS

The Neoproterozoic Quanji Group in the Oulongbluq microcontinent is a siliciclastic-dominated sequence with two carbonate units, the Hongzaoshan dolostone and the Zhoujieshan cap dolostone. One glacial deposit, the Hongtiegou diamictite, was recognized in the Quanji Group. Paleontological and chemostratigraphic data imply that the Hongtiegou glaciation might be Ediacaran in age. The Zhoujieshan cap dolostone atop the Hongtiegou diamictite has distinct positive $\delta^{13}C$ values that are different from most other Neoproterozoic cap carbonate, but similar to the Egan dolostone of Ediacaran age in Australia. $\delta^{34}S_{CAS}$ and $\delta^{34}S_{py}$ of the Zhoujieshan cap dolostone are decoupled from each other. $\delta^{34}S_{CAS}$ shows rapid stratigraphic variations ranging from +13.9‰ to +24.1‰, suggesting low sulfate concentration after the Hongtiegou glaciation. Although seawater sulfate concentration was thought to have increased during Ediacaran Period, $\delta^{34}S_{CAS}$ was still more susceptible to local perturbations in the Ediacaran ocean than in modern ocean. $\delta^{34}S_{py}$ does not covary with $\delta^{34}S_{CAS}$, but shows a steady increase from +12.9‰ to +26.4‰. In addition, inverse fractionation ($\Delta^{34}S_{CAS-py} < 0$) was observed in the upper unit of the Zhoujieshan cap dolostone. The decoupling of $\delta^{34}S_{CAS}$ and $\delta^{34}S_{py}$ implies that CAS and pyrite were derived from different sulfur sources. CAS was probably derived from

surface water, whereas pyrite was precipitated from bottom water of the postglacial stratified Oulongbluq basin. The steady increase of $\delta^{34}S_{py}$ can be interpreted as Rayleigh fractionation in a close bottom water system.

References

Allen, P.A., Bowring, S., Leather, J., Brasier, M., Cozzi, A., Grotzinger, J.P., McCarron, G. and Amthor, J.J., 2002. Chronology of Neoproterozic glaciations: New insights from Oman. International Sedimentological Congress, 16th,: Abstract Volume: Johannesburg, South Africa: 7-8.

Bingen, B., Griffin, W.L., Torsvik, T.H. and Saeed, A., 2005. Timing of Late Neoproterozoic glaciation on Baltica constrained by detrital zircon geochronology in the Hedmark Group, south-east Norway. Terra Nova, 17: 250-258.

Bottrell, S.H. and Newton, R.J., 2006. Reconstruction of changes in global sulfur cycling from marine sulfate isotopes. Earth Science Reviews, 75: 59-83.

Bowring, S., Myrow, P., Landing, E., Ramezani, J. and Grotzinger, J., 2003. Geochronological constraints on terminal Neoproterozoic events and the rise of metazoans. Geophysical Research Abstracts, 5: 13219.

Burdett, J., Authur, M. and Richardson, M., 1989. A Neogene seawater sulfur isotope age curve from calcareous pelagic microfossils. Earth and Planetary Science Letters, 94: 189-198.

Burzin, M.B., 1995. Late Vendian helicoid filamentous microfossils. Paleontological Journal, 29: 1-34.

Canfield, D.E., Raiswell, R., Westrich, J.T., Reaves, C.M. and Berner, R.A., 1986. The use of chromium reduction in the analysis of reduced inorganic sulfur in sediments and shales. Chemical Geology, 54: 149-155.

Condon, D., Zhu, M., Bowring, S., Wang, W., Yang, A. and Jin, Y., 2005. U-Pb Ages from the Neoproterozoic Doushantuo Formation, China. Science, 308: 95-98.

Corkeron, M., 2007. 'Cap carbonates' and Neoproterozoic glacigenic successions from the Kimberley region, north-west Australia Sedimentology, 54: 871-903.

Fanning, C.M. and Link, P.K., 2004. U-Pb SHRIMP ages of Neoproterozoic (Sturtian) glaciogenic Pocatello Formation, southeastern Idaho. Geology, 32: 881-884.

Fike, D.A., Grotzinger, J.P., Pratt, L.M. and Summons, R.E., 2006. Oxidation of the Ediacaran ocean. Nature, 444: 744-747.

Frimmel, H.E., Kloetzli, U.S. and Siegfried, P.R., 1996. New Pb-Pb single zircon age constraints on the timing of Neoproterozoic glaciation and continental break-up in Namibia. Journal of Geology, 104: 459-469.

Gellatly, A.M. and Lyons, T.W., 2005. Trace sulfate in mid-Proterozoic carbonates and the sulfur isotope record of biospheric evolution. Geochimica et Cosmochimica Acta, 69: 3813-3829.

Goldberg, T., Poulton, S.W. and Strauss, H., 2005. Sulphur and oxygen isotope signatures of late Neoproterozoic to early Cambrian sulphate, Yangtze Platform, China: Diagenetic constraints and seawater evolution. Precambrian Research, 137: 223-241.

Gorjan, P., Veevers, J.J. and Walter, M.R., 2000. Neoproterozoic sulfur-isotope variation in Australia and global implications. Precambrian Research, 100: 151-179.

Grassineau, N.V., Mattey, D.P. and Lowry, D., 2001. Sulfur isotope analysis of sulfide and sulfate minerals by continuous flow-isotope ratio mass spectrometry. Analytical Chemistry, 73: 220-225.

Grotzinger, J.P. and Knoll, A.H., 1995. Anomalous carbonate precipitates: Is the Precambrian the key to the Permian? Palaios, 10: 578-596.

Guan, B., Wu, R., Hambrey, M.J. and Geng, W., 1986. Glacial sediments and erosional pavements near the Cambrian- Precambrian boundary in western Henan Province, China. Journal of the Geological Society, London, 143: 311-323.

Guerroué, E.L., Allen, P.A. and Cozzi, A., 2006. Chemostratigraphic and sedimentological framework of the largest negative carbon isotopic excursion in Earth history: The Neoproterozoic Shuram Formation (Nafun Group, Oman). Precambrian Research, 146: 68-92.

Halverson, G.P., 2006. A Neoproterozoic chronology. In: S. Xiao and A.J. Kaufman (Editors), Neoproterozoic geobiology and paleobiology. Springer, Dordrecht, Netherlands, pp. 232-271.

Halverson, G.P., Hoffman, P.F., Schrag, D.P., Maloof, A.C. and Rice, A.H.N., 2005. Toward a Neoproterozoic composite carbon-isotope record. Geological Society of America Bulletin, 117: 1181-1207.

Hoffman, P.F. and Schrag, D.P., 2002. The snowball Earth hypothesis: Testing the limits of global change. Terra Nova, 14: 129-155.

Hoffmann, K.-H., Condon, D.J., Bowring, S.A. and Crowley, J.L., 2004. U-Pb zircon date from the Neoproterozoic Ghaub Formation, Namibia: Constraints on Marinoan glaciation. Geology, 32: 817-820.

Hua, H., Chen, Z. and Zhang, L., 2004. *Shaanxilithes* from lower Taozichong Formation, Guizhou Province and its geological and paleobiological significance. Journal of Stratigraphy, 28: 265-269.

Hua, H., Zhang, L., Zhang, Z. and Wang, J., 2000. Fossil evidence of latest Neoproterozoic Gaojiashan biota and their characteristics. Acta Palaeontologica Sinica, 39: 507-515.

Hurtgen, M.T., Arthur, M.A., Suits, N.S. and Kaufman, A.J., 2002. The sulfur isotopic composition of Neoproterozoic seawater sulfate: implications for a snowball Earth? Earth and Planetary Science Letters, 203: 413-429.

Jiang, G., Kennedy, M.J. and Christie-Blick, N., 2003. Stable isotopic evidence for methane seeps in Neoproterozoic postglacial cap carbonates. Nature, 426: 822-826.

Jiang, G., Kennedy, M.J., Christie-Blick, N., Wu, H. and Zhang, S., 2006. Stratigraphy, Sedimentary Structures, and Textures of the Late Neoproterozoic Doushantuo Cap Carbonate in South China. Journal of Sedimentary Research, 76: 978-995.

Kah, L.C., Lyons, T.W. and Frank, T.D., 2004. Low marine sulphate and protracted oxygenation of the Proterozoic biosphere. Nature, 431: 834-838.

Kampschulte, A., Bruckschen, P. and Strauss, H., 2001. The sulphur isotopic composition of trace sulphates in Carboniferous brachiopods: implications for coeval seawater, correlation with other geochemical cycles and isotope stratigraphy. Chemical Geology, 205: 149-173.

Kampschulte, A. and Strauss, H., 2004. The sulfur isotopic evolution of Phanerozoic seawater based on the analysis of structurally substituted sulfate in carbonates. Chemical Geology, 204: 255-286.

Kaufman, A.J., Corsetti, F.A. and Varni, M.A., 2007. The effect of rising atmospheric oxygen on carbon and sulfur isotope anomalies in the Neoproterozoic Johnnie Formation, Death Valley, USA. Chemical Geology, 237: 47-63.

Kaufman, A.J. and Knoll, A.H., 1995. Neoproterozoic variations in the C-isotope composition of sea water: Stratigraphic and biogeochemical implications. Precambrian Research, 73: 27-49.

Kendall, B., Creaser, R.A. and Selby, D., 2006. Re-Os geochronology of postglacial black shales in Australia: Constraints on the timing of "Sturtian" glaciation. Geology, 34: 729-732.

Kennedy, M.J., Christie-Blick, N. and Sohl, L.E., 2001. Are Proterozoic cap carbonates and isotopic excursions a record of gas hydrate destabilization following Earth's coldest intervals? Geology, 29: 443-446.

Knoll, A.H., Bambach, R.K., Canfield, D.E. and Grotzinger, J.P., 1996. Comparative earth history and Late Permian mass extinction. Science, 273: 452-457.

Li, Q., 1980. Sinian Subearthem in the Minor Qinling Range in Shaanxi province. In: T.I.o.G.a.M. Resources (Editor), Research in Precambrian Geology, Sinian Suberathem in China. Tianjin Science and Technology Press, Tianjin, pp. 314-331.

Li, R., Chen, J., Zhang, S., Lei, J., Shen, Y. and Chen, X., 1999. Spatial and temporal variations in carbon and sulfur isotopic compositions of Sinian sedimentary rocks in the Yangtze platform, South China. Precambrian Research, 97: 59-75.

Li, R., Yang, S. and Li, W., 1997. Trace Fossils from Sinian-Cambrian Boundary Strata in China. Geological Publishing House, Beijing, 99 pp.

Lu, S., 2002. The Precambrian geology of Northern Tibet. Geological Publishing House, Beijing, 125 pp.

Lu, S., Ma, G., Gao, Z. and Lin, W., 1985. Sinian ice ages and glacial sedimentary facies-areas in China. Precambrian Research, 29: 53-63.

Lyons, T.W., Walter, L.M., Gellatly, A.M., Martini, A.M. and Blake, R.E., 2004. Sites of anomalous organic remineralization in the carbonate sediment of South Florida,

USA: The sulfur cycle and carbonate-associated sulfate. In: J.P. Amend, K.J. Edwards and T.W. Lyons (Editors), Sulfur Biogeochemistry: Past and Present (GSA Special Paper 379). Geological Society of America, Boulder, Colorado, pp. 161–176.

Mazumdar, A. and Strauss, H., 2006. Sulfur and strontium isotopic compositions of carbonate and evaporite rocks from the late Neoproterozoic–early Cambrian Bilara Group (Nagaur-Ganganagar Basin, India): Constraints on intrabasinal correlation and global sulfur cycle. Precambrian Research, 149: 217-230.

Myrow, P.M. and Kaufman, A.J., 1999. A newly discovered cap carbonate above Varanger-age glacial deposits in Newfoundland, Canada Journal of Sedimentary Research, 69: 784-793.

Pingitore, N.E., Jr., Meitzner, G. and Love, K.M., 1995. Identification of sulfate in natural carbonates by x-ray absorption spectroscopy. Geochimica et Cosmochimica Acta, 59: 2477-2483.

Shen, B., Xiao, S., Bao, H., Kaufman, A.J., Zhou, C. and Wang, H., in press. Stratification and mixing of the post-glacial Neoproterozoic ocean: Evidence from carbon and sulfur isotopes in a cap dolostone from northwest China. Earth and Planetary Science Letters.

Shen, B., Xiao, S., Dong, L., Zhou, C. and Liu, J., 2007. Problematic macrofossils from Ediacaran successions in the North China and Chaidam blocks: implications for there evolutionary root and biostratigraphic significance. Journal of Paleontology, 81: 1396-1411.

Shen, Y. and Buick, R., 2004. The antiquity of microbial sulfate reduction. Earth-Science Reviews, 64: 243-272.

Sun, D., 1959. Tertiary stratigraphy and tectonic characters in the northern Tarim Basin. Science Press, Beijing.

Thompson, M.D. and Bowring, S.A., 2000. Age of the Squantum 'tillite', Boston basin, Massachusetts: U-Pb zircon constraints on terminal Neoproterozoic glaciation. American Journal of Science, 300: 630-655.

Wang, Y. and Chen, J., 1983. The petrographic characteristics and the age of Hongtiegou tillites from Xiaogaolu Group in Qinghai Province. Precambrian Research, 1: 145-162.

Wang, Y., Lu, S., Gao, Z., Lin, W. and Ma, G., 1981. Sinian tillites of China. In: M.J. Hambrey and W.B. Harland (Editors), Pre-Pleistocene Glacial Record, IGCP 38. Cambridge University Press, Cambridge, pp. 386-401.

Wang, Y., Zhuang, Q., Shi, C., Liu, J. and Zheng, L., 1980. Quanji Group along the northern border of Chaidamu Basin. In: Tianjin Institute of Geology and Mineral Resources (Editor), Research on Precambrian Geology Sinian Suberathem in China, Tianjin, pp. 214-230.

Xiao, S., Bao, H., Wang, H., Kaufman, A.J., Zhou, C., Li, G., Yuan, X. and Ling, H., 2004. The Neoproterozoic Quruqtagh Group in eastern Chinese Tianshan: Evidence for a post-Marinoan glaciation. Precambrian Research, 130: 1-26.

Xing, Y., Ding, Q., Luo, H., He, T. and Wang, Y., 1984. The Sinian-Cambrian boundary of China. Bulletin of the Institute of Geology, Chinese Academy of Geological Sciences: 1-262.

Yang, S. and Zheng, Z., 1985. The Sinian trace fossils from Zhengmuguan Formation of Helanshan Mountain, Ningxia. Earth Science - Journal of Wuhan College of Geology, 10.

Zhao, X., Zhang, L., Zou, X., Wang, S. and Hu, Y., 1980. Sinian tillites in Northwest China and their stratigraphic significance. In: Tianjin Institute of Geology and Mineral Resources (Editor), Research on Precambrian Geology Sinian Suberathem in China. Tianjin Science and Technology Press, Tianjin, pp. 164-185.

Zhou, C., Tucker, R., Xiao, S., Peng, Z., Yuan, X. and Chen, Z., 2004. New constraints on the ages of Neoproterozoic glaciations in South China. Geology, 32: 437-440.

Zhu, X., 1957. The major geological questions of the Tarim Basin. Knowledge of Geology, Volume 6 & 7.

Figure 4.1: Geological map and localities of Quanji Group in the Chaidam Basin. (a) outcrops of the Quanji Group in the northern Chaidam Basin. Inset the geographic location of the Oulongbluq microcontinent. TA: Tarim; NC: North China; SC: South China; OU: Oulongbluq microcontinent. (b) Geological map of the Quanjishan area. Sections A and B are marked.

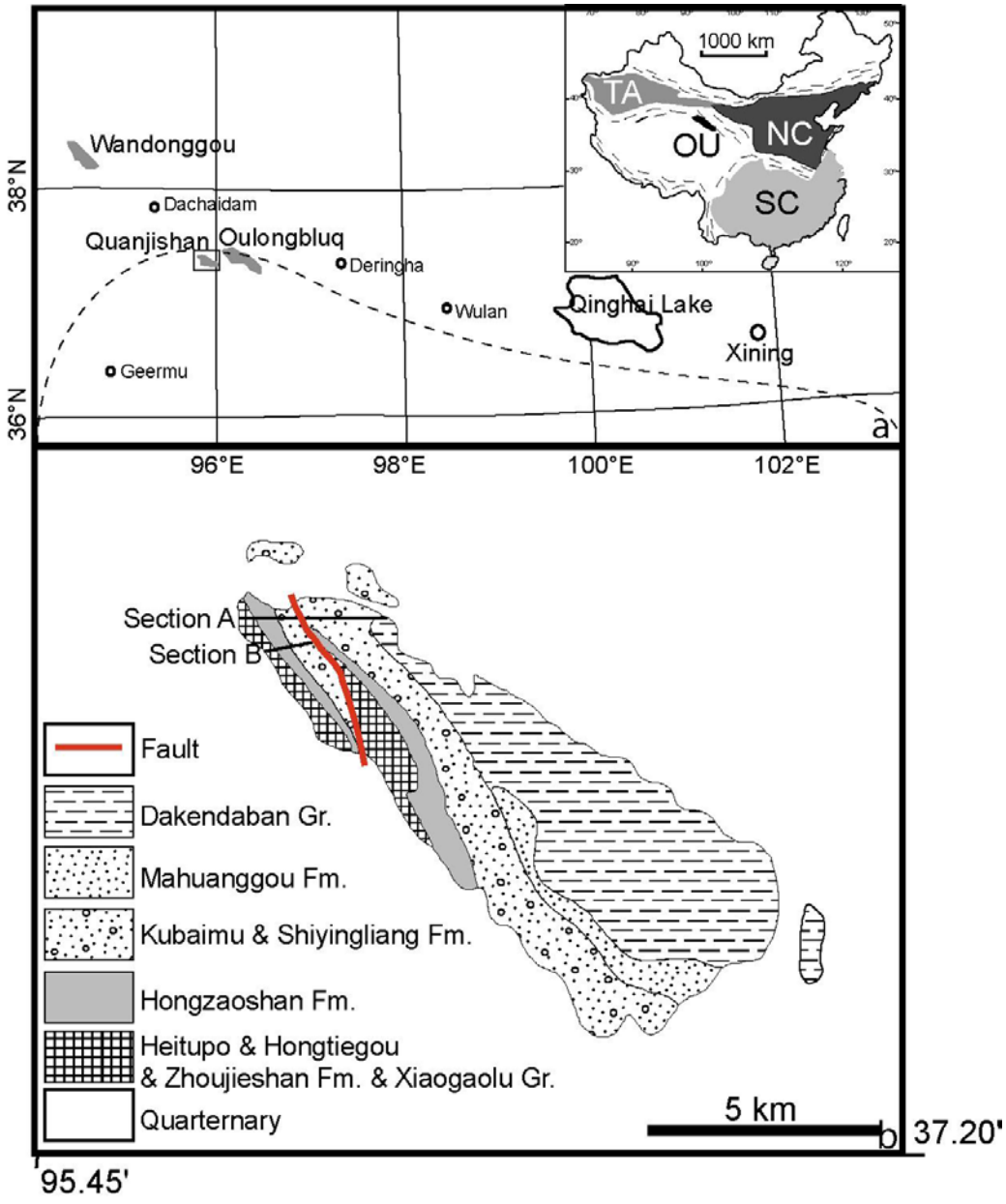

Figure 4.2: Stratigraphic columns of the Quanji Group and the Zhoujieshan cap dolostone. (a) Stratigraphic column of the Quanji Group. HTG: Hongtiegou Fm., ZJS: Zhoujieshan Fm. XGL: Xiaogaolu Gr. (b) Stratigraphic column of the Zhoujieshan cap dolostone at section B in the Quanjishan area.

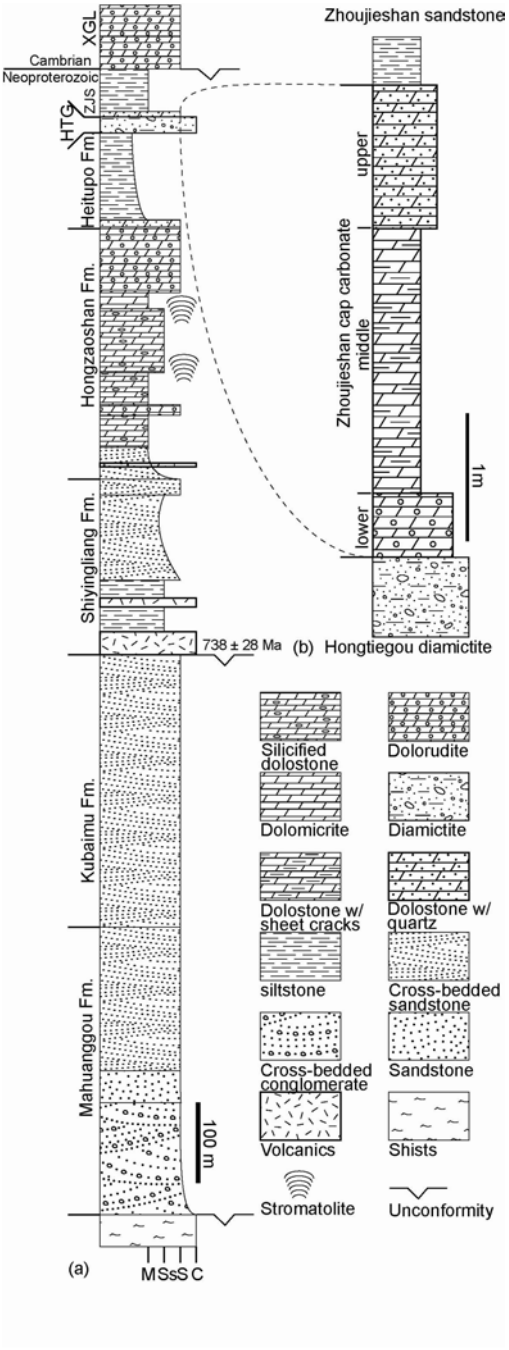

Figure 4.3: Field photographs of the lower Quanji Group. (a) Field photograph of the Quanji Group at section A in the Quanjishan area. DKD: Dakendaban Gr.; KBM: Kubaimu Fm.; SYL: Shiyingliang Fm.; HZS: Hongzaoshan Fm.; HTP: Heitupo Fm.; HTG: Hongtiegou Fm.; ZJS: Zhoujieshan Fm. (b) Purplish red thin-bedded tuffaceous sandstone of the lower Hongzaoshan Formation. (c) Mudcrack cast in the lower Hongzaoshan Formation. (d) Halite pseudomorphs in the lower Hongzaoshan Formation. (e) Volcaniclastic rock with lapilli in the lower Hongzaoshan Formation. (f) Silicified stromatolite in the Hongzaoshan Formation. (g) Thin-laminated dolostone of the Hongzaoshan Formation. (h) Dolorudite in the Hongzaoshan Formation. (i) Dark gray siltstone/shale with sandstone concretion of the Heitupo Formation. Coins in e, g, h, and i are about 1.5 cm in diameter, in b, c, and d are about 2 cm in diameter, and marker pen in f is about 14 cm.

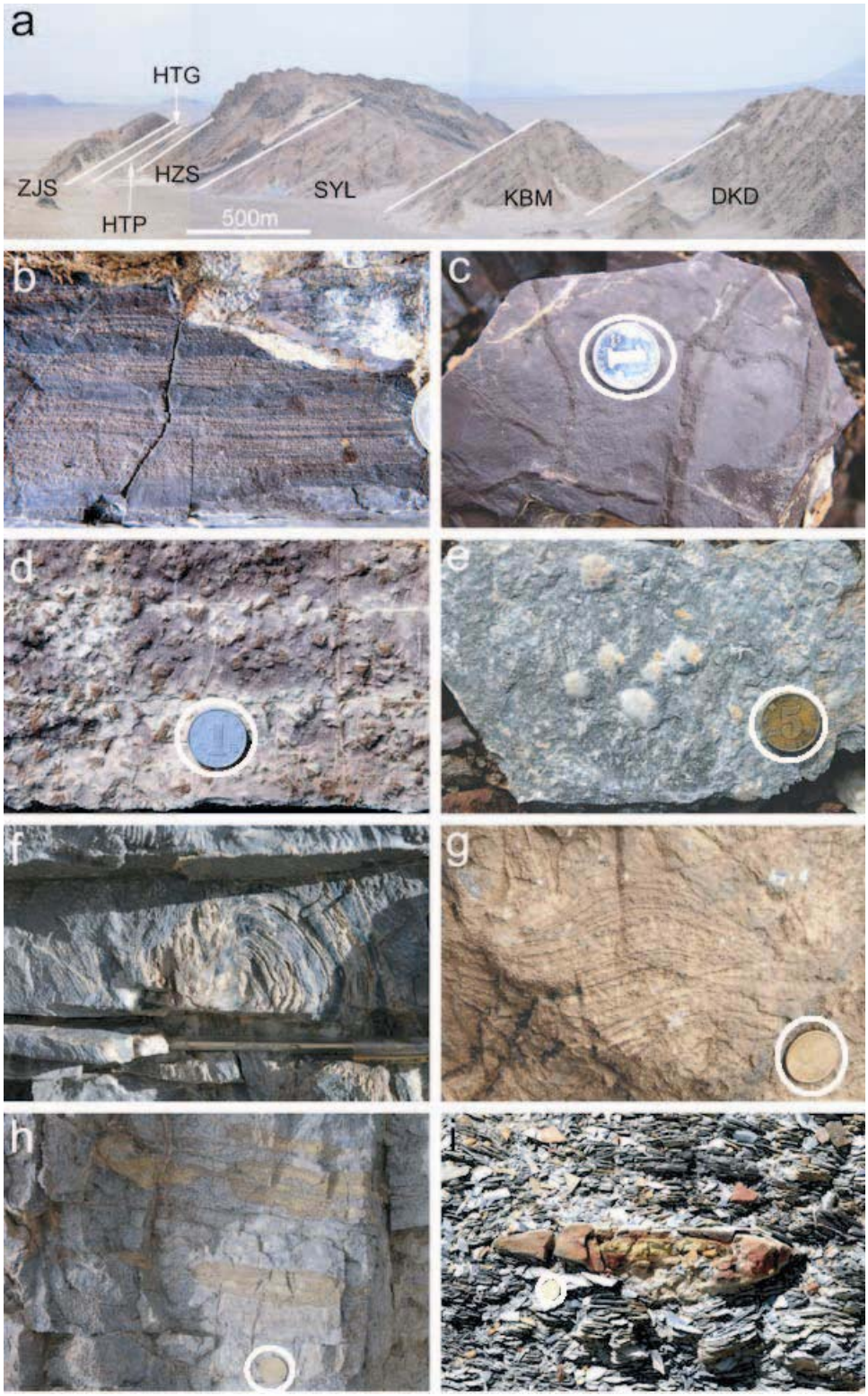
a
HTG
HZS
ZJS
HTP
SYL
KBM
DKD
500m
b
c
d
e
f
g
h
i

Figure 4.4: Field photographs of the upper Quanji Group. (a) Field photograph for the Heitupo (HTP), Hongtiegou (HTG), Zhoujieshan (ZJS) formations, and Xiaogaolu Group (XGL) at section A. White arrow indicates the Zhoujieshan cap dolostone. (b) Out-sized clasts in the Hongtiegou diamictite. (c) Dropstone in the Hongtiegou diamictite. (d) The Hongtiegou diamictite. Note the poorly sorted clasts within greenish matrix.. (e) Field photography of the lower unit of the Zhoujieshan cap dolostone with dolomitic and siliciclastic clasts. (f) Dolostone with sheet cracks in the middle +Zhoujieshan cap dolostone. (g) Red dolomitic sandstone in the upper Zhoujieshan cap dolostone. (f) *Shaanxilithes* from the Zhoujieshan sandstone. Coins in c and g are about 1.5 cm in diameter, in e and f are about 2 cm in diameter, hammer in b is about 30 cm long, marker pen in d is about 14 cm, and scale bar in h in millimetric units.

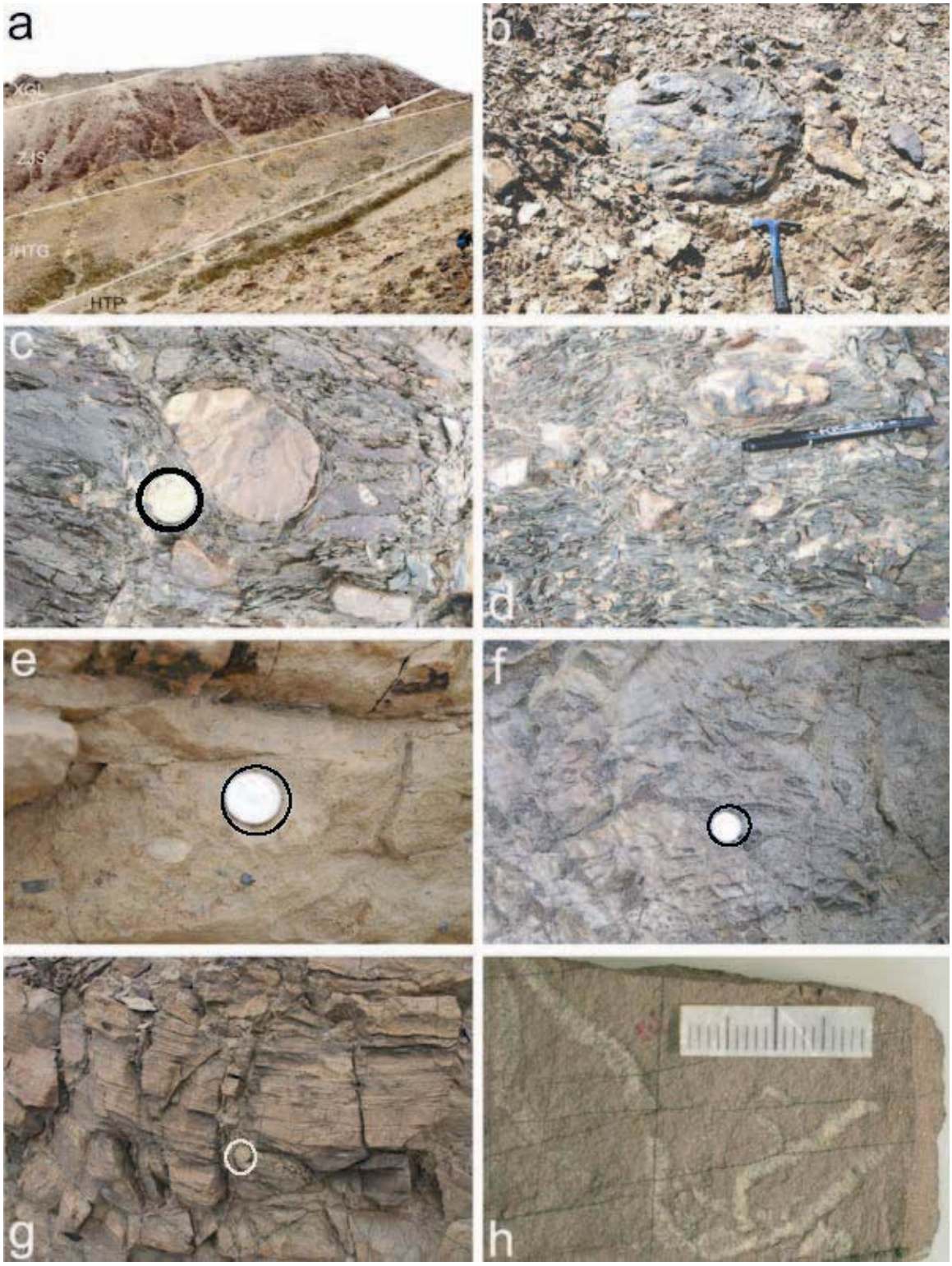
a
Xcl
Zjs
HTG
HTP
b
c
d
e
f
g
h

Figure 4.5: Carbon and oxygen isotope profiles of the Hongzaoshan Formation and the Zhoujieshan cap dolostone. (a) Carbon and oxygen isotope profiles of the Hongzaoshan Formation and the Zhoujieshan cap dolostone at section A. (b) Carbon and oxygen isotope profiles of the Hongzaoshan Formation at section B. Samples from section A and section B were analyzed in bulk and microdrilled samples, respectively.

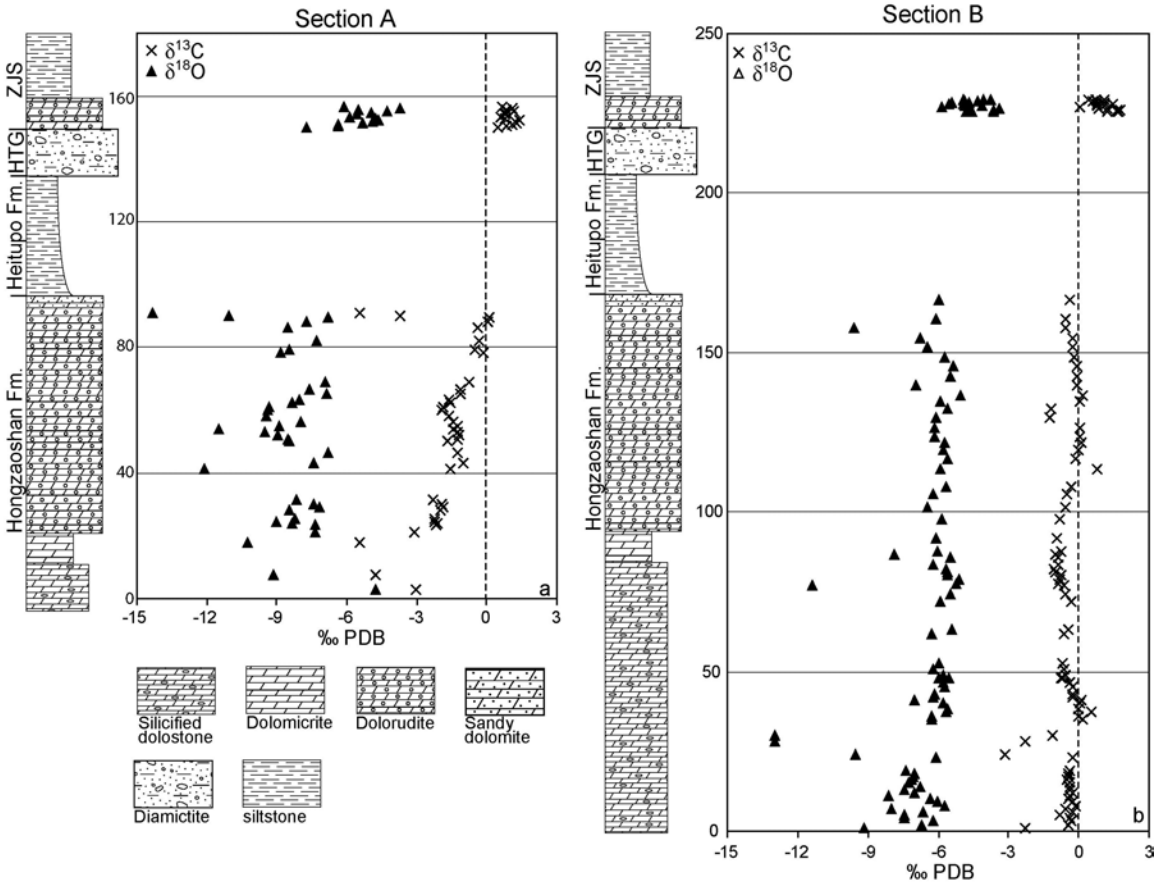

Figure 4.6: Isotopic and elemental geochemistry profiles of the Zhoujieshan cap dolostone at section B. (a) $\delta^{13}C$ and $\delta^{18}O$; (b) $\delta^{34}S_{CAS}$, $\delta^{34}S_{py}$ and $\Delta^{34}S_{CAS-py}$ (= $\delta^{34}S_{CAS}$– $\delta^{34}S_{py}$); (c) CAS concentration; (d) Fe and Mn concentrations; (e) Carbonate content (carbonate%).

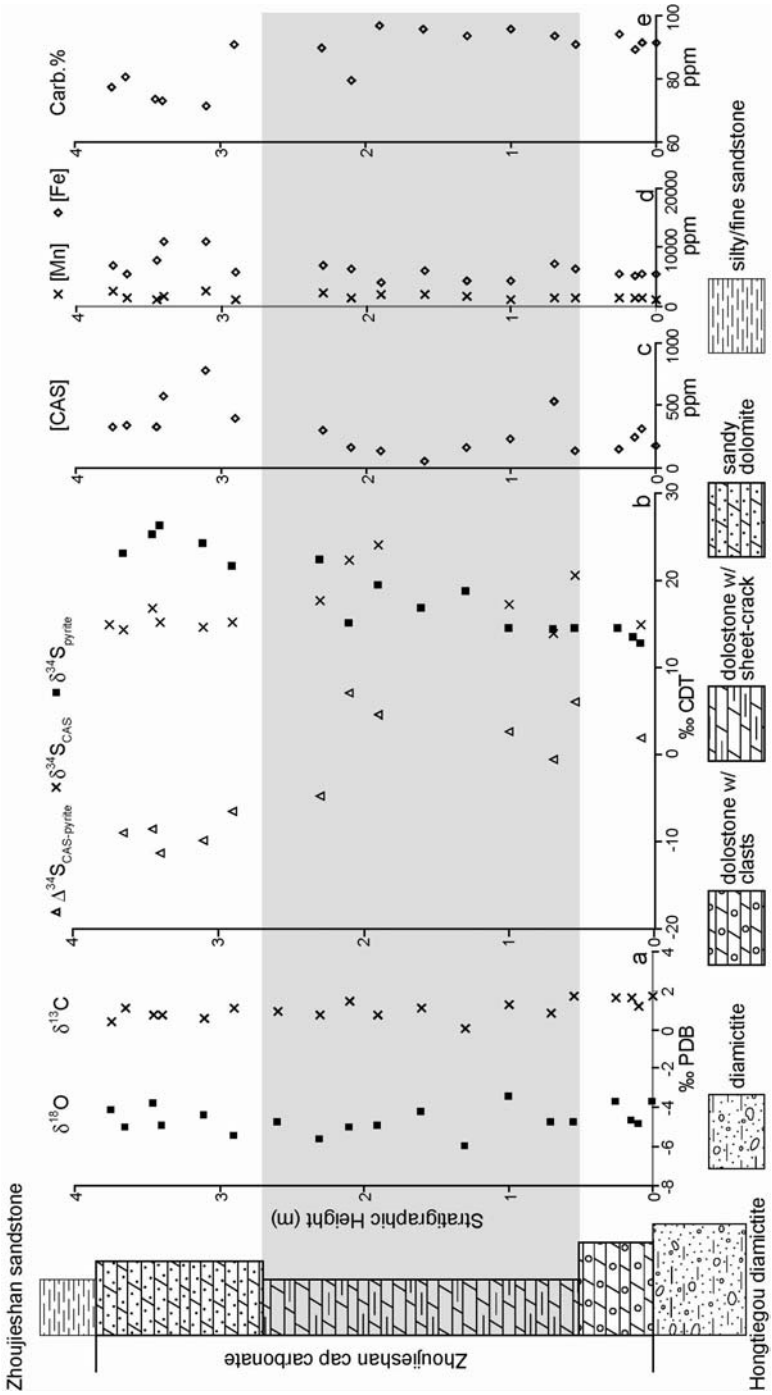

Figure 4.7: Isotope and elemental crossplots. (a) $\delta^{13}C$–$\delta^{18}O$ crossplot. Dashed line represents $\delta^{18}O$ = –5‰. (b) $\delta^{13}C$–[Mn]/[Sr] crossplot. (c) $\delta^{34}S_{CAS}$–[CAS] crossplot. (d) Carbonate%–[CAS] crossplot. ZCD: Zhoujieshan cap dolostone; HZS: Hongzaoshan dolostone.

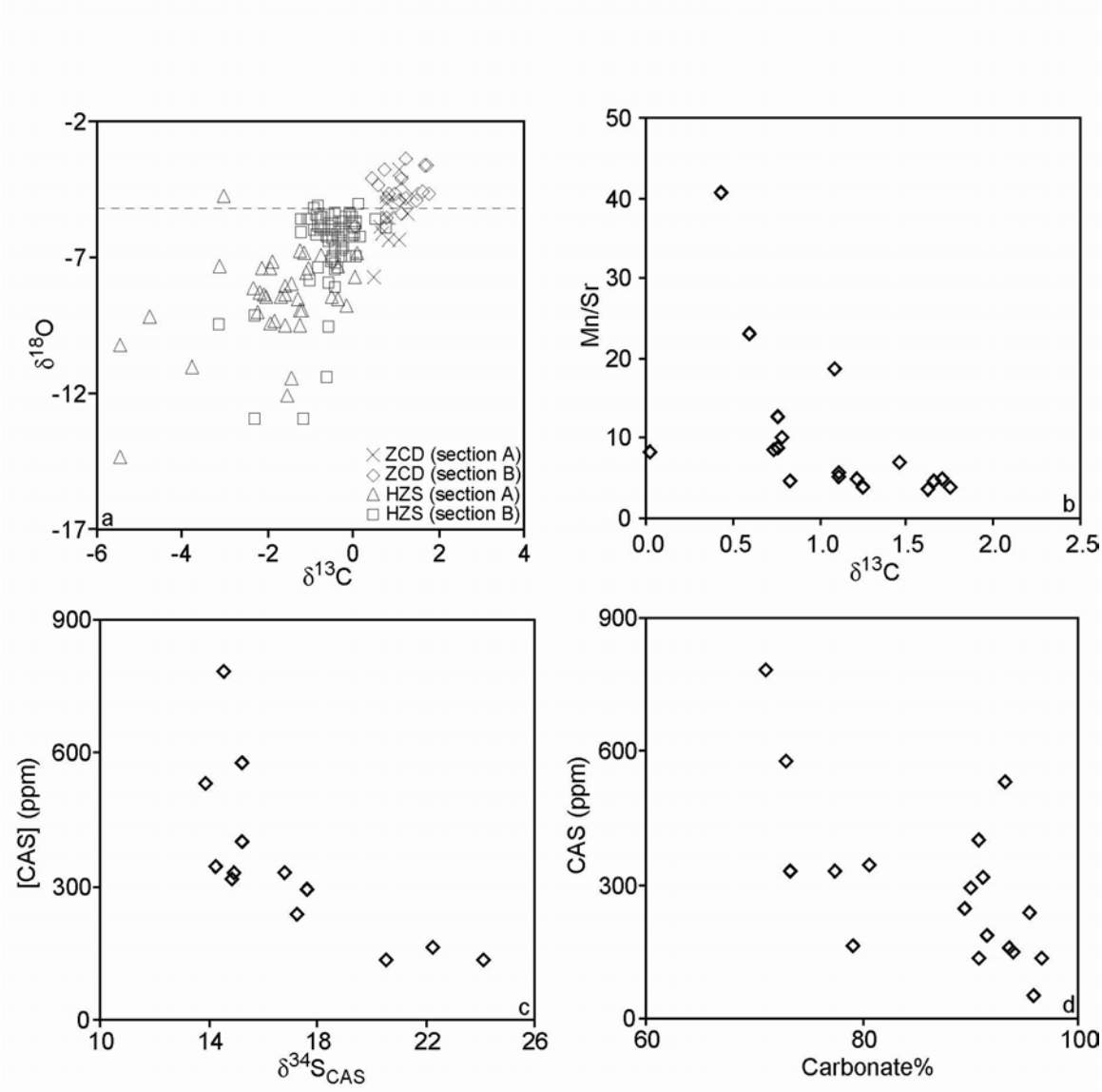

Table 4.1. $\delta^{13}C$ and $\delta^{18}O$ data of the Quanjishan carbonate samples from section A and the Hongzaoshan dolostone from section B in the Quanjishan area. (na. not analyzed).

Sample number	Depth (m)	$\delta^{13}C$ (‰)	$\delta^{18}O$ (‰)
Hongzaoshan dolostone at section A			
QDQ–30	3.0	-3.1	-4.7
QDQ–31	7.5	-4.7	-9.2
QDQ–32	18.0	-5.4	-10.3
QDQ–33	20.9	-3.1	-7.3
QDQ–34	23.3	-2.2	-7.4
QDQ–35	23.8	-2.1	-8.4
QDQ–36	24.4	-2.2	-9.0
QDQ–37	25.5	-2.2	-8.3
QDQ–38	28.0	-2.0	-8.5
QDQ–39	29.1	-1.9	-7.2
QDQ–40	29.8	-1.9	-7.4
QDQ–41	31.2	-2.3	-8.1
QDQ–45	41.4	-1.6	-12.1
QDQ–45-1	43.0	-1.0	-7.4
QDQ–46	46.5	-1.2	-6.8
QDQ–51	50.0	-1.7	-8.4
QDQ–52	50.8	-1.3	-8.6
QDQ–53	51.8	-1.2	-9.0
QDQ–54	52.8	-1.2	-9.5
QDQ–55	54.1	-1.5	-11.5
QDQ–56	54.8	-1.3	-8.9
QDQ–57	56.4	-1.4	-8.0
QDQ–58	57.9	-1.6	-9.5
QDQ–59	60.1	-1.9	-9.4
QDQ–60	61.0	-1.8	-9.3
QDQ–61	62.4	-1.6	-8.3
QDQ–62	63.3	-1.6	-8.0
QDQ–63	65.3	-1.1	-6.8
QDQ–64	66.4	-1.1	-7.6
QDQ–65	69.0	-0.8	-6.9
QDQ–66	78.2	-0.1	-8.8
QDQ–67	79.2	-0.5	-8.5
QDQ–68	82.2	-0.4	-7.3
QDQ–70	86.2	-0.4	-8.5
QDQ–71	88.2	0.1	-7.8
QDQ–72	89.5	0.1	-6.8
QDQ–74	90.0	-3.8	-11.0
QDQ–75	91.0	-5.5	-14.3
Zhoujieshan cap carbonate at section A			
QDQ–79a	150.0	0.5	-7.7
QDQ–79	150.5	0.8	-6.3
QDQ–80	151.0	1.1	-6.4
QDQ–81	151.5	1.3	-5.4
QDQ–82	152.0	1.2	-4.9
QDQ–83	152.5	1.4	-4.6

QDQ–84	153.0	0.8	-4.8
QDQ–85	153.5	0.6	-5.9
QDQ–86	154.0	0.8	-5.6
QDQ–87	154.5	0.8	-5.0
QDQ–88	155.0	1.1	-4.3
QDQ–89	155.5	0.8	-5.5
QDQ–90	156.0	1.1	-3.8
QDQ–91	156.5	0.7	-6.1
Hongzaoshan dolostone at section B			
QJS–105	0	na.	na.
QJS–106	1	–2.3	–9.1
QJS–107	2	–0.4	–6.7
QJS–108	3	–0.3	–6.2
QJS–109	4	–0.4	–7.4
QJS–110	5	–0.8	–7.4
QJS–111	6	–0.2	–6.7
QJS–112	7	–0.5	–8.0
QJS–113	8	–0.2	–5.7
QJS–114	9	–0.2	–6.0
QJS–115	10	–0.4	–6.3
QJS–116	11	–0.4	–8.1
QJS–117	12	–0.3	–7.0
QJS–118	13	–0.4	–7.5
QJS–119	14	–0.4	–6.8
QJS–120	15	–0.4	–7.3
QJS–121	16	–0.5	–7.2
QJS–122	17	–0.5	–7.1
QJS–123	18	–0.4	–7.0
QJS–124	19	–0.4	–7.4
QJS–125	20	na.	na.
QJS–126	21	na.	na.
QJS–127	22	na.	na.
QJS–128	23	–0.3	–6.1
QJS–101	24	–3.2	–9.5
QJS–102	26	na.	na.
QJS–103	28	–2.3	–13.0
QJS–104	30	–1.1	–13.0
QJS–129	33	na.	na.
QJS–130	34	na.	na.
QJS–131	35	0.2	–6.3
QJS–132	36	0	–6.2
QJS–133	37.5	0.5	–5.6
QJS–134	38.5	0	–5.6
QJS–135	40	0.1	–5.8
QJS–136	41	0.1	–7.0
QJS–137	42	–0.2	–6.2
QJS–138	43	–0.2	–6.1
QJS–139	45	–0.2	–5.7
QJS–140	46.5	–0.4	–5.8
QJS–141	48	–0.7	–5.5

QJS–142	48.1	–0.8	–5.9
QJS–143	49.1	–0.6	–5.8
QJS–144	50.6	–0.6	–6.2
QJS–145	52.6	–0.7	–6.0
QJS–146	54.6	na.	na.
QJS–147	55.6	na.	na.
QJS–148	57.6	na.	na.
QJS–149	59.6	na.	na.
QJS–150	61.6	–0.6	–6.3
QJS–151	63.1	–0.4	–5.4
QJS–152	65.1	na.	na.
QJS–153	67.1	na.	na.
QJS–154	69.1	na.	na.
QJS–155	72.1	–0.3	–5.9
QJS–156	74.1	–0.6	–5.5
QJS–157	76.1	na.	na.
QJS–158	77.1	–0.6	–11.4
QJS–159	77.6	–0.9	–5.3
QJS–160	79.1	–0.8	–5.1
QJS–161	80.1	–0.8	–5.6
QJS–162	81.1	–1.0	–5.6
QJS–163	82.1	–1.1	–5.6
QJS–164	83.6	–0.8	–6.2
QJS–165	84.6	na.	na.
QJS–166	85.6	–0.9	–5.5
QJS–167	86.6	–1.0	–7.9
QJS–168	87.6	–0.7	–6.0
QJS–169	89.6	na.	na.
QJS–170	91.6	–0.9	–6.1
QJS–171	93.6	na.	na.
QJS–172	95.6	na.	na.
QJS–173	97.6	–0.8	–5.9
QJS–174	99.6	na.	na.
QJS–175	101.6	–0.6	–6.5
QJS–176	103.6	na.	na.
QJS–177	105.6	–0.5	–6.2
QJS–178	108.1	–0.3	–5.7
QJS–179	111.1	na.	na.
QJS–180	113.6	0.8	–5.9
QJS–181	116.6	–0.2	–5.6
QJS–182	119.6	0	–5.8
QJS–183	121.6	0.1	–5.7
QJS–184	123.6	0.1	–6.2
QJS–185	126.6	0.1	–6.2
QJS–186	129.6	–1.2	–6.1
QJS–187	132.6	–1.2	–5.6
QJS–188	134.6	0	–5.9
QJS–189	136.6	0.2	–5.1
QJS–190	139.6	–0.1	–7.0
QJS–191	142.6	0	–5.5

QJS–192	145.6	–0.1	–5.4
QJS–193	148.6	–0.2	–5.7
QJS–194	151.6	–0.2	–6.4
QJS–195	154.6	–0.3	–6.8
QJS–196	157.6	–0.5	–9.6
QJS–197	160.6	–0.6	–6.1
QJS–198	165.6	na.	na.
QJS–199	166.6	–0.4	–6.0

Table 4.2. Geochemical data of the Zhoujieshan cap carbonate at section B in the Quanjishan area. ns. no sufficient yield; na. not analyzed.

Number	*Height (m)*	*Fe (ppm)*	*Mn (ppm)*	*Sr (ppm)*	*CAS (ppm)*	*Mg/Ca*	*Carb.%*	$\delta^{13}C$	$\delta^{18}O$	$\delta^{34}S_{CAS}$	$\delta^{34}S_{Pyrite}$	$\Delta^{34}S$
QJS–19	3.75	6839	2603	64	331	0.99	77	0.4	–4.1	14.9	ns.	na.
QJS–18	3.65	5433	1325	71	347	1.02	81	1.1	–4.9	14.3	23.2	–8.9
QJS–17	3.45	7694	1244	146	333	0.99	73	0.7	–3.7	16.8	25.4	–8.6
QJS–16	3.40	10969	1746	137	580	0.93	73	0.8	–4.9	15.2	26.4	–11.2
QJS–15	3.10	10960	2720	118	783	0.93	71	0.6	–4.3	14.6	24.3	–9.8
QJS–14	2.90	5850	1281	226	403	0.99	91	1.1	–5.4	15.2	21.7	–6.5
QJS–13	2.60	na.	na.	na.	na.	na.	na.	1.0	–4.7	ns.	ns.	na.
QJS–12	2.30	7008	2401	274	295	0.96	90	0.8	–5.5	17.6	22.4	–4.8
QJS–11	2.10	6470	1458	210	161	1.00	79	1.5	–4.9	22.2	15.2	7.0
QJS–10	1.90	3995	1958	195	134	1.03	97	0.8	–4.9	24.1	19.6	4.5
QJS–9	1.60	6188	1968	388	53	1.01	96	1.1	–4.1	ns.	16.9	na.
QJS–8	1.30	4264	1755	215	159	1.01	94	0.0	–5.9	ns.	18.8	na.
QJS–7	1.00	4475	1203	301	237	1.01	96	1.2	–3.4	17.2	14.6	2.6
QJS–6	0.70	7369	1501	329	530	1.00	93	0.8	–4.6	13.9	14.4	–0.5
QJS–5	0.55	6484	1420	371	134	1.01	91	1.7	–4.6	20.6	14.6	6.0
QJS–4	0.25	5575	1371	301	148	1.01	94	1.7	–3.6	ns.	14.5	na.
QJS–3	0.15	5157	1321	358	246	0.99	89	1.6	–4.6	ns.	13.6	na.
QJS–2	0.10	5607	1508	304	317	1.01	91	1.2	–4.8	14.9	12.9	2.0
QJS–1	0.00	5591	1249	255	185	0.99	92	1.7	–3.6	ns.	ns.	na.